University of Nottingham
UK | CHINA | MALAYSIA

EVALUATION OF SYNTHETIC AND BIO-BASED ADDITIVES AS OXIDATION STABILITY ENHANCERS IN PALM BIODIESEL

LAU CHI HOU, BSc. (Hons)

THESIS SUBMITTED TO THE UNIVERSITY OF NOTTINGHAM MALAYSIA FOR THE DEGREE OF DOCTOR OF PHILOSOPHY

SEPTEMBER 2024

Abstract

Study on the antioxidants' efficiency on biodiesel becomes crucial as the research for greener fuel continues. Set against this background, this thesis aims to evaluate the effects of synthetic and bio-based additives in palm biodiesel through a comprehensive assessment of fuel stability properties, oxidation kinetics and thermodynamics of doped fuels, and long-term storage stability. Synthetic additives were found to be more effective compared to their bio-based counterparts in terms of oxidation stability index (OSI), however, butylated hydroxyanisole (BHA) and tert-butyl hydroquinone (TBHQ) showed contradictory OSI results from Rancimat and PetroOXY test methods. Similar findings were observed in the long-term storage study which highlighted that TBHQ was the best additive followed by BHA and α-T being inefficient in long term storage of palm biodiesel. In addition, kinetics modelling utilising regression analyses coupled with error functions for doped palm biodiesels determined that BHA, BHT, TBHQ, and α-T adhered to the first order kinetic model judging from the high R and R^2 values and low χ^2 values obtained. The increase in E_a for DPOME showed that the performance of all additives was great, while positive $\Delta H^{\ddagger}$, negative $\Delta S^{\ddagger}$ and positive $\Delta G^{\ddagger}$ values suggested that all oxidation reactions were endothermic, non-spontaneous and endergonic. The gas chromatography-mass spectrometry (GC-MS) analyses revealed that 3-octyl-oxiraneoctanoic acid ME, and 17-octadecynoic acid ME were the major oxidation products of palm biodiesel. ANN models were also developed to predict fuel stability properties, and the accuracy of the models was in the order of Rancimat IP > PetroOXY IP >

kinematic viscosity > acid value > iodine value**.** Developed models highlighted the potential of ANN in reducing cost and time needed for analysis**.** Comprehensive evaluation of additives in palm biodiesel were carried out.

Acknowledgements

I would like to express my gratitude for the guidance and support provided by my supervisors, Prof Gan Suyin, Prof Ng Hoon Kiat and Dr Lee Lai Yee from University of Nottingham Malaysia as well as Dr Harrison Lau Lik Nang from the Malaysia Palm Oil Board (MPOB). Their support enables me to understand more about the things I lack and strive me to work harder. I am also thankful to my parents for supporting me on my new journey as a student, and my brother whom I share the same vision as rival in this research field. Special thanks to Ms. Yamashita Emiri and Ms. Mogami Nanaka for giving me the motivation and energy to push forward for the entire period of study. The Ministry of Higher Education (MOHE), Malaysia is gratefully acknowledged for the financial support towards this project under the Fundamental Research Grant Scheme FRGS/1/2020/TK02/UNIM/01/1. MPOB is also acknowledged for the provision of technical and facilities support.

List of Publications

Lau, C.H., Gan, S., Lau, H.L.N., Lee, L.Y., Thangalazhy-Gopakumar, S., Ng, H.K. Insights into the effectiveness of synthetic and natural additives in improving biodiesel oxidation stability, Sustainable Energy Technologies and Assessments 52 Part D, August 2022, 102296. doi: 10.1016/j.seta.2022.102296.

Lau, C.H., Lau, H.L.N., Ng, H.K., Thangalazhy-Gopakumar, S., Lee, L.Y., Gan, S. Evaluation of synthetic and bio-based additives on the oxidation stability of palm biodiesel: Parametric, kinetics and thermodynamics studies, Sustainable Energy Technologies and Assessments 64, April 2022, 103738. doi: 10.1016/j.seta.2024.103738.

Lau, C.H., Lau, H.L.N., Ng, H.K., Thangalazhy-Gopakumar, S., Lee, L.Y., Gan, S. Evaluation of oxidation stability for palm biodiesel with additives using Fourier transform infrared spectroscopy, gas chromatography-mass spectrometry and high-performance liquid chromatography, Results in Engineering 22, June 2024, 102165. doi: 10.1016/j.rineng.2024.102165.

Lau, C.H., Gan, S., Lau, H.L.N., Lee, L.Y., Thangalazhy-Gopakumar, S. A perspective on the influencing factors in the use of antioxidants for biodiesel oxidation stability enhancement. *In*: Kim, J., Chen, Z. (eds) Trends in Environmental Sustainability and Green Energy. Springer Proceedings in Earth and Environmental Sciences. Springer, Cham., 2023, 93–106. doi: 10.1007/978-3-031-27803-7_9.

Lau, C.H., Lau, H.L.N., Ng, H.K., Thangalazhy-Gopakumar, S., Lee, L.Y., Gan, S. Modelling of oxidation stability and related properties for palm biodiesel with additives using artificial neural net-work approach, Accepted for publication in Springer Proceedings in Earth and Environmental Sciences.

Table of Contents

List of Figures

List of Tables

List of Abbreviations

ASTM D445	Standard Test Method for Kinematic Viscosity of Transparent and Opaque Liquids (and Calculation of Dynamic Viscosity)
ASTM D664	Standard Test method for Acid Number of Petroleum Products by Potentiometric Titration
ATSM D6751	Standard Specification for Biodiesel Fuel Blend Stock (B100) for Middle Distillate Fuels
ASTM D7545	Standard Test Method for Oxidation Stability of Middle Distillate Fuels - Rapid Small Scale Oxidation Test (RSSOT)
B5	5 % biodiesel and 95 % diesel
B7	7 % biodiesel and 93 % diesel
B10	10 % biodiesel and 90 % diesel
B20	20 % biodiesel and 80 % diesel
B30	30 % biodiesel and 70 % diesel
B100	100 % biodiesel
BHA	Butylated hydroxyanisole
BHT	Butylated hydroxytoluene
DPPH	2,2-diphenyl-1-picrylhydrazyl
EN 14103	Fat and oil derivates - Fatty acid methyl ester (FAME) - Determination of ester and linolenic acid methyl ester content
EN 14104	Fat and oil derivates - Fatty acid methyl ester (FAME) - Determination of acid value
EN 14111	Fat and oil derivates - Fatty acid methyl ester (FAME) -

	Determination of iodine value
EN 14214	European Standard Specification for Biodiesel
EN 15751	Automotive fuels - Fatty acid methyl ester (FAME) fuel and blends with diesel fuel - Determination of oxidation stability by accelerated oxidation method
EN 16091	Liquid petroleum products - Middle distillates and fatty acid methyl ester (FAME) fuels and blends - Deermination of oxidation stability by rapid small scale oxidation method
EN ISO 3104	Petroleum products - Transparent and opaque liquids - Determination of kinematic viscosity and calculation of dynamic viscosity
ISO 3105	Glass capillary kinematic viscometer - Specifications and operating instructions
ISO 7536 - ASTM D 525- IP 40	Standard Test Method for Oxidation Stability of Gasoline (Induction Period Method)
FAC	Fatty acid composition
FTIR	Fourier transform infrared spectroscopy
GA	Gallic acid
GAE	Gallic acid equivalent
GC	Gas chromatography
GC-FID	Gas chromatography-flame ionization detector
GC-MS	Gas chromatography-mass spectrometry
HPLC	High performance liquid chromatography

I_2	Iodine
IP	Induction period
ISO 3105	Glass capillary kinematic viscometer - Specifications and operating instructions
ISO 7536 - ASTM D 525- IP 40	Standard Test Method for Oxidation Stability of Gasoline (Induction Period Method)
KOH	Potassium hydroxide
KOME	Karanja oil methyl ester
MPOB	Malaysian Palm Oil Board
NO_x	Nitrogen oxides
OSI	Oxidation stability index
PDA	N,N'-disec-butyl-p-phenylenediamine
PDSC	Pressure differential scanning calorimetry
PG	Propyl gallate
PY	Pyrogallol
RBDPO	Refined, bleached, deodorized palm oil
TBHQ	Tert-butylhydroquinone
TPC	Total phenolic content
UV	Ultraviolet

List of Units

°C	degree Celsius
°C/min	degree Celcius per minute
% (mol/mol)	mol to mol percentage
µg/ml	microgram per millilitre
µL	microlitre/microlitres
Mm	micrometre/micrometres
g I_2/100 g	grams of iodine per 100 gram
H	hour/hours
kHz	Kilohertz
kPa	Kilopascal
L	litre/litres
L/h	litre per hour
M	Metre
Mg	milligram/milligrams
mg KOH/g	milligrams of potassium hydroxide per gram
mg/g	milligram per gram
mg/kg	milligram per kilogram
mg/mL	milligram per millilitre
Min	minute/minutes
mm^2/s	millimetres square per second
nm	Nanometer
Ppm	parts per million
S	second/seconds

1. Introduction

1.1 Background

The growing concern on the depletion of finite, non-renewable fossil fuels as well as their adverse impacts on the environment has been the main driving force for the development of biofuels such as biodiesel. Biodiesel which is made up of long-chain fatty acid esters is typically derived from vegetable and animal fats. It possesses better degradability, higher flashpoint, negligible sulphur content and good lubricity in comparison to fossil diesel (Knothe and Razon, 2017). Biodiesel combustion generally produces lesser hydrocarbons, carbon monoxide and particular matter, but higher nitrogen oxides (NO_x) (Xue *et al.*, 2011; Rajendran, 2020; Elsayed *et al*., 2024). Biodiesel can be considered as a carbon neutral fuel provided the feedstock used is grown in a sustainable manner. Plants draw in carbon dioxide from the atmosphere to carry out photosynthesis for their growth. When these plants are used as biodiesel feedstock, the carbon uptake from the prior photosynthesis is subsequently released into the atmosphere. Thus, this creates a loop in which carbon is recycled in the atmosphere (Deng *et al.*, 2012; Singh *et al.*, 2020).

Aghbashlo *et al.* (2021) documented increased usage in vegetable oil as biodiesel feedstock since 2014, a trend which would continue until 2026. Nonetheless, second-generation feedstock such as non-edible and waste feedstocks have also garnered attention over the past decades due to the food-fuel competition (Goh *et al*., 2022). For instance, Jahirul *et al.* (2015) concluded that beauty leaf

(*Calophyllum inophyllum*) was able to meet ATSM D6751 and EN 14214 biodiesel standards requirements despite having poorer cold flow properties and free fatty acids content as compared to palm oil methyl ester (POME). Additionally, *Jatropha curcas* L. was reported to have good potential as an alternative second-generation feedstock for biodiesel production with the potential to reduce greenhouse gas emissions compared to conventional fossil fuels (Neupane *et al.*, 2021). With the great debate on securing land and food prior to the development of renewable fuel, it is noted that algae-based third-generation feedstock is gaining more interests from researchers (Singh *et al.*, 2019; Maroušek *et al.*, 2023).

Over the past decades, the production of biodiesel has been widely researched, and multiple approaches haves been proposed to enhance the quality and usage of these alternative fuels. Direct use of vegetable oil and blending with existing fossil diesel were the first ideas to be suggested, but due to their disadvantages, microemulsion was suggested as another physical approach. Soon after that, chemical approach for biodiesel production such as transesterification was introduced to chemically alter natural fats and oils to better suit the fuel industry (Tabatabaei *et al.*, 2019). As of now, transesterification is the most widely used method for biodiesel production.

In the context of Malaysia, it is not surprising that palm oil is the feedstock used for biodiesel production. As one of the largest palm oil producers in the world, second only to Indonesia, palm oil production represents a major source of income

for Malaysia. Over the years, oil palm plantations in Malaysia have surged from 54,000 hectares post-independence in the 1960s to 5.39 million hectares in 2014 (Awalludin *et al.*, 2015). The total oil palm plantations coverage was recorded at 5.65 million hectares in 2023 (MPOB, 2023). This translates to a staggering 18.55 million tonnes of crude palm oil produced in 2023 alone. In 2023, Malaysia also exported 15.13 million tonnes of palm oil (MPOB, 2023).

The Malaysian government has established mandates on the use of palm biodiesel blends. Biodiesel blends are abbreviated with B, followed by the volume percentage of biodiesel present in the blend. For example, B5 biodiesel consist of 5 % biodiesel and 95 % of fossil diesel. In 2011, B5 palm biodiesel was introduced to the diesel transportation sector. By 2015, the level of palm biodiesel blend in diesel was upgraded to B7. Back in 2020, the implementation of B30 was aimed to be completed before 2025 (Reuters, 2020). However, the original plan was disrupted due to the Covid-19 outbreak, which also delayed the complete implementation of B20 within the transportation sector to January 2022 (Bernama, 2021). Currently, B10 palm biodiesel is adopted in the transportation sector nationwide with the exceptions of Langkawi and Labuan which have adopted B20 (Ho, 2020; Reuters, 2024) while B7 palm biodiesel is used in the industrial sector (Reuters, 2020).

The fossil fuel consumption for Malaysia has consistently stayed above 95 % since the 1990s. The consumption figures fluctuated between 95 to 98 % until 2016. However, since the introduction of B5 palm biodiesel in 2011, the figure

declined from 97.39 % to 93.61 % in 2019, which aligned with the constant upgrades of biodiesel mandates over the past decade (Ritchie and Roser, 2020). Furthermore, in 2009, Malaysia made a commitment to reduce its carbon emission intensity by 40 % compared to 2005 level by 2020. By 2015, Malaysia had already achieved 33 % carbon emission intensity reduction, and made a bolder pledge to increase its carbon emission intensity reduction to 45 % from its 2005 baseline by 2030 to address climate change and global warming (Bernama, 2016). In line with this, the National Automotive Policy 2020 has outlined measures to enhance the use of palm biodiesel including empowering technical research activities on biodiesel applications in the automotive sector (National Automotive Policy 2020).

This study will evaluate the effects of a wide range of additives as oxidation stability enhancers in palm biodiesel to identify the most effective ones and gain a deeper understanding of palm biodiesel oxidation stability, especially under long-term storage. Through the kinetics and thermodynamics study, the rate and nature of the oxidation process such as spontaneity and endothermicity will be elucidated. Identification of oxidation byproducts under long-term storage will enable oxidation pathways to be formulated, thus adding to the fundamental knowledge in this area. The need for such a study is both crucial and timely considering Malaysia's plan to increase the research and adoption of palm biodiesel blends in both the transportation and industrial sectors.

1.2 Problem statement

In contrast with fossil diesel fuels, biodiesels are more prone to oxidative degradation due to their unsaturated and polyunsaturated methyl esters (Ginanjar *et al.*, 2024). The presence of unsaturation in the alkyl esters increases the susceptibility of biodiesel to oxidation, thus making the storage of biodiesel a challenge, which in turn poses a problem for wide-scale adoption of biodiesel as a renewable source of energy. While this may not be a problem for the transportation sector due to the high turnover rate of biodiesel in petrol station, its implication in industrial sector where biodiesel is expected to be stored for a long period of time is much more serious. A main solution to increase the storage stability of biodiesel is through the doping of fuel with additives to delay the oxidation process that occurs naturally through exposure to air, metal and light (Christensen and McCormick, 2014).

To address the poorer oxidation stability of biodiesel, the effects of synthetic additives such as butylated hydroxyanisol (BHA), butylated hydroxytoluene (BHT) and tert-butylhydroquinone (TBHQ), pyrogallol (PY) and propyl gallate (PG) have been studied (Borsato *et al*., 2014a; Rashed *et al.*, 2015; Fazal *et al.*, 2017; Kleinberg et al., 2019; Nogales-Delgado *et al.*, 2019; Nogales-Delgado *et al.*, 2020). While the oxidation process occurs naturally and cannot be fully thwarted, the addition of these additives into the fuel is able to delay the oxidation process at least until they are full exhausted (García *et al.*, 2017; Uğuz *et al.*, 2019). However, synthetic additives pose multiple health risks including skin allergies, gastrointestinal tract problems, and cancer (Lourenço *et al.*, 2019). For example,

BHA had reported to have genotoxicity and endocrine-distrupting effects (Ji *et al*., 2023). As such, natural or bio-based additives have been proposed as safer alternatives. In recent years, an increasing number of studies on biodiesel doped with bio-based additives have been carried out. Such studies include curcumin and β-carotene (de Sousa *et al.*, 2014), as well as quercetin (de Sousa *et al.*, 2019). Despite the surge of studies on both synthetic and bio-based additives, comparative studies covering a wide range of additives across the two categories are not widely available. Furthermore, contradictory findings regarding the relative effectiveness of synthetic and bio-based additives have been reported, whereby same antioxidants showed different antioxidation capabilities even when added in the same concentration (Agarwal and Khurana, 2013; Yang *et al*.'s 2017). For palm biodiesel specifically, a comparative evaluation of different additives is lacking. Additionally, the oxidation kinetics and thermodynamics of palm biodiesel with additives, as well as fuel stability and palm biodiesel oxidation pathways over long-term storage remains largely unexplored. To date as well, the prediction of fuel oxidation stability properties via artificial neural network (ANN) modelling has not been attempted since most ANN modelling studies in this area focused on biodiesel production. This research aims to address these gaps in knowledge and ultimately identify the most effective additive for palm biodiesel through a combination of comparative fuel oxidation stability assessment, kinetics and thermodynamics studies, ANN modelling and long-term storage stability study.

1.3 Aim and objectives

The aim of this study is to evaluate synthetic and bio-based additives as oxidation stability enhancers in palm biodiesel. The specific project objectives are listed as below.

1. To assess the influence of synthetic and bio-based additives on the oxidation stability of palm biodiesel.
2. To appraise the oxidation kinetics and thermodynamics of palm biodiesel with synthetic and bio-based additives.
3. To evaluate the long-term storage stability of palm biodiesel with synthetic and bio-based additives.
4. To formulate the oxidation pathways of palm biodiesel under long-term storage with and without synthetic and bio-based additives.
5. To develop predictive models of oxidation stability properties for palm biodiesel with synthetic and bio-based additives using artificial neural network (ANN).

1.4 Research scope and activities

The scope of study can be divided into four phases described as follows.

1. Comparative assessment of the oxidation stability of palm biodiesel with additives

Characterisation of palm biodiesel is firstly carried out to determine the oxidation

stability index (OSI) and other related physicochemical properties such as acid value, iodine value and kinematic viscosity. Synthetic additives including propyl gallate (PG), pyrogallol (PY), butylated hydroxyanisol (BHA), butylated hydroxytoluene (BHT) and tert-butylhydrooquinone (TBHQ) as well as bio-based additives comprising α-tocopherol (α-T), curcumin and quercetin at different concentration levels are assessed for their effectiveness in maintaining the oxidation stability of palm biodiesel. This step serves to determine the best performing additive from both the synthetic and bio-based categories that will be the focus for the subsequent studies.

2. Oxidation kinetics and thermodynamics studies of palm biodiesel with additives

In this phase, palm biodiesel doped with selected synthetic and bio-based antioxidants are subjected to the oxidative stability tests at different temperatures to appraise the kinetics and thermodynamics of the oxidation process. The rate constants, activation energies and pre-exponential factors are assessed using the Arrhenius equation from the experimentally obtained induction periods. Thermodynamic principles as well as the Eyring equation are used to determine the enthalpy, entropy and Gibbs free energy of oxidation.

3. Long-term storage stability studies of palm biodiesel with additives

In Phase 3, palm biodiesel doped with best performing synthetic and bio-based additives at different concentration levels are evaluated under long-term storage. 100 ppm and 500 ppm are selected based on previous experiments and literature.

Fuel sampling is carried out fortnightly for a total duration of 6 months. In addition to oxidation stability, other physicochemical properties such as acid value, iodine value, kinematic viscosity and water content are determined for the doped fuels. The sample are also analysed via gas chromatography-mass spectrometry (GC-MS), gas chromatography-flame ionization detector (GC-FID), high performance liquid chromatography (HPLC) and Fourier transform infrared spectroscopy (FTIR) to identify intermediates, oxidation products and byproducts. The oxidation pathways of palm biodiesel are then proposed to gain an understanding of the fuel oxidation process and the role of additives.

4. Modelling of oxidation stability properties for palm biodiesel with additives using artificial neural network (ANN)

In the final phase, artificial neural network (ANN) models are developed with the aid of MATLAB (version R2023b) software. Prediction models for the effects of additives on the oxidation stability of palm biodiesel are developed using acquired oxidation stability data from the previous phase. These models are then evaluated based on error functions to determine the viability of this approach to predict the fuel properties.

Figure 1.1 shows the flowchart of the phases along with their associated objectives and research activities.

Phase 1 (*Objective 1*: To assess the influence of synthetic and bio-based additives on the oxidation stability of palm biodiesel)
– Characterisation of palm biodiesel in terms of vitamin E content, oxidation stability index (OSI) using Rancimat and PetroOXY, acid value, iodine value and kinematic viscosity.
– Determination of oxidation stability related properties of doped palm biodiesel.
Independent variables: Additive type (BHT, BHA, TBHQ, PG, PY, quercetin, α-T and curcumin), concentration (250, 500, 750, 1000 ppm).
Dependent variables: OSI, acid value (AV), iodine value (IV), kinematic viscosity, vitamin E content, DPPH free radical scavenging activity, fatty acid content (FAC)

↓

Phase 2 (*Objective 2*: To appraise the oxidation kinetics and thermodynamics of palm biodiesel with synthetic and bio-based additives)
– Regression and error functions analyses of conductivity against time data for zeroth, first and second order kinetic models.
– Determination of rate constant (k), activation energy (E_a), enthalpy change ($\Delta H^{\ddagger}$), entropy change ($\Delta S^{\ddagger}$) and Gibbs free energy ($\Delta G^{\ddagger}$) using Arrhenius, Eyring and thermodynamic equations.
Independent variables: Best performing antioxidants based on Phase 1, temperature (100, 110, 120, 130 °C).
Dependent variables: Conductivity, time.

↓

Phase 3 (Objective *3*: To evaluate the long-term storage stability of palm biodiesel with synthetic and bio-based additives)
– Determination of oxidation stability related properties of doped palm biodiesel over a duration of 6 months.
Independent variables: Best performing antioxidants based on Phase 2, concentration (100, 500 ppm).
Dependent variables: OSI, AV, IV, kinematic viscosity, water content, vitamin E content
(*Objective 4*: To formulate the oxidation pathways of palm biodiesel under long-term storage with and without synthetic and bio-based additives)
– Studying the role of additives in oxidation stability, as well as identification of oxidation intermediates and/or byproducts using gas chromatography-mass spectrometry (GC-MS), high performance liquid chromatography (HPLC) and Fourier transform infrared spectroscopy (FTIR).

↓

Phase 4 (*Objective 5*: To develop predictive models of oxidation stability properties for palm biodiesel with additives using artificial neural network (ANN))
– Development of ANN using MATLAB (version R2023b).
Independent variables: Additive type (BHT, BHA, TBHQ, PG, PY, quercetin, α-T and curcumin), concentration (250, 500, 750, 1000 ppm).
Dependent variables: OSI, AV, IV, kinematic viscosity, linolenic acid content.

Figure 1.1. Project phases, research objectives and activities.

1.5 Thesis outline

The thesis has been structured into several chapters as described below.

Chapter 1, the introductory chapter, focuses firstly on providing an overview of biodiesel, and how the use of additives can mitigate the poorer oxidation stability of biodiesel. The problem statement is presented leading to the aim and objectives of this work. The project phases and research activities are also outlined.

Chapter 2 thoroughly discusses the oxidation process, from the properties related to biodiesel oxidation stability to the factors affecting the oxidation process and the use of additives to preserve oxidation stability. A critical review of past studies on the effects of additives in biodiesel is included in this chapter, with the aim of bridging the current knowledge in the field to the findings of this thesis.

Subsequently, Chapter 3 assesses the influences of synthetic (BHT, BHA, TBHQ, PG, PY) and bio-based (quercetin, α-tocopherol (α-T), curcumin) additives at different concentration levels in palm biodiesel. Acquired experimental data including induction period (IP), acid value, iodine value and kinematic viscosity are presented, statistically analysed and discussed comprehensively. Ultimately, this chapter identifies the best performing additives for the subsequent phases of work.

Chapter 4 appraises the oxidation kinetics and thermodynamics of palm biodiesel with best performing additives based on previous chapters. It presents how experimental changes in conductivity with time can be regressed to several kinetic

models. Coupled with error functions analyses, the best fit kinetic model is identified, and kinetic parameters are determined. Thereafter, thermodynamics parameters are calculated and together with the kinetic parameters, the additives are appraised in terms of their kinetic and thermodynamics effects on the oxidation process of palm biodiesel.

Following that, Chapter 5 explores the long-term storage stability of palm biodiesel with best performing synthetic and bio-based additives at different concentration levels over a period of 26 weeks (6 months). The experimentally acquired IP (Rancimat and PetroOXY), acid value, iodine value, kinematic viscosity and water content of samples are statistically analysed and discussed. Furthermore, high-performance liquid chromatography (HPLC), Fourier transform infrared spectrometry (FTIR), gas chromatography-flame ionization detector (GC-FID) and gas chromatography-mass spectrometry (GC-MS) are used to determine oxidation byproducts of palm biodiesel and propose oxidation pathways.

Chapter 6 discusses the use of ANN to predict the OSI and related physicochemical properties including acid value, iodine value and kinematic viscosity of palm biodiesel with additives. The experimental data collected in Phase 1 of the project are used to train, validate and evaluate the networks with a randomised split between these three criteria. From there, the developed ANNs are evaluated based on error functions analyses of the actual and predicted data.

Finally, Chapter 7 summarises the conclusions obtained from this research project.

It also provides several recommendations for future extension of this work.

2. Literature Review

2.1 Introduction

This chapter aims to provide an understanding of the oxidation stability of biodiesel, from the properties related to biodiesel oxidation process to factors leading to biodiesel oxidation of biodiesel and the use of additives to preserve fuel oxidation stability. A comprehensive review of past studies on additives in biodiesel has been completed to provide insights into the current gaps in knowledge within this field, which this thesis is aiming to address.

2.2 Biodiesel development and standards

Fossil fuels are the primary source of energy around the world. While the world's dependence on fossil fuels has declined by 12 % from 93.38 % in 1965 to 81.79 % in 2022 with the introduction of renewable fuels, it is estimated that it will take another 200 years before fossil fuels consumption decreases to 0 %. (Rapier, 2023). Furthermore, fossil fuels are finite resources; for instance, the oil reserves to production ratio (R/P) for the 2020 was recorded at 52.9 years remaining (Sönnichsen, 2021). Against the contrast of heavy dependence on fossil fuels, primary energy consumption has been increasing yearly at roughly a rate of 1.1 % per annum, with a growth of 1.4 % from 2021 to 2022 (Energy Institute, 2023). As such, renewable energy sources are needed to sustain the growing energy demand. The consumption of renewable energy increased from 39.97 to 45.18 exajoule from 2021 to 2022 (Energy Institute, 2023).

Biodiesel is a renewable alternative to existing fossil diesel. However, it is naturally more prone to oxidation and contamination, as well as undesired reactions in the presence of metals, elevated temperature and air compared to its fossil counterpart. This is due to the presence of monounsaturated and polyunsaturated alkyl bonds in the fatty acid methyl esters (FAME) of biodiesel, whereby the more unsaturated the FAME are, the less stable the biodiesel becomes (Saluja *et al.*, 2016). The stability of biodiesel is a concern towards large-scale biodiesel adoption as the fuel may be stored in storage tanks for up to months before reaching consumers. It is extremely likely that the untreated biodiesel will be oxidized to a certain degree due to multiple factors that promote the oxidation process.

With the rapid expansion of biodiesel research and production over the years, standardisation and quality assurance is crucial to the market acceptance as more biodiesel is introduced as an alternative fuel for transport and heating (Bouaid *et al.*, 2009). Furthermore, fuels with varying standards of quality will also result in different fuel properties that subsequently affects the engine performance (Pullen and Saeed, 2012). Hence, standards are needed to ensure smooth running of engines with biodiesel without the need for engine modifications due to differences in fuel properties compared to not only fossil diesel, but also different biodiesel blends. For this purpose, biodiesel standards such as the American ATSM D6751 and the European EN 14214 and were established to ensure commercial biodiesel produced is of the right quality and stability for use by the consumers. Table 2.1 and 2.2 show the biodiesel fuel standards for the ASTM

D6751 and EN 14214, respectively.

Table 2.1. ASTM D6751 biodiesel fuel standard.

Property	Test method	Limits	Units
Flash point (closed cup)	ASTM D93	93 minimum	°C
Alcohol control One of the following must be met:			
1. Methanol content	EN 14110	0.2 maximum	% volume
2. Flash point	ASTM D93	130.0 minimum	°C
Water and sediment	ASTM D2709	0.050 maximum	% volume
Kinematic viscosity, 40 °C	ASTM D445	1.9–6.0	mm^2/s
Sulphated ash	ASTM D874	0.020 maximum	% mass
Sulphur	ASTM D5453	0.0015 maximum (S15); 0.05 maximum (S500)	% mass (ppm)
Copper strip corrosion	ASTM D130	No. 3 maximum	
Cetane number	ASTM D613	47 minimum	
Cloud point	ASTM D2500	report	°C
Cold soak filterability	Annex A1	360 maximum	s
Carbon residue	ASTM D4530	0.050 maximum	% mass
Acid value	ASTM D664	0.50 maximum	mg KOH/g
Free glycerin	ASTM D6584	0.020	% mass
Total glycerin	ASTM D6584	0.240	% mass
Oxidation stability	EN 14112	3.0 minimum	h
Phosphorus content	ASTM D4951	0.001 max	% mass
Sodium and potassium, combined	EN 14538	5 maximum	ppm
Calcium and magnesium, combined	EN 14538	5 maximum	ppm
Distillation temperature, Atmospheric equivalent temperature, 90 % recovered	ASTM D1160	360 maximum	°C

Table 2.2. EN 14214:2012+A2:2019 biodiesel fuel standard.

Property	Test method	Limits	Units
Ester content	EN 14103	96.5 minimum	% (mol/mol)
Density at 15 °C	EN ISO 3675, EN ISO 12185	860–900	kg/m^3
Viscosity at 40 °C	EN ISO 3104, ISO 3105	3.5–5.0	mm^2/s
Flash point	EN ISO 3679	101 minimum	°C
Sulphur content	EN ISO 20846, EN ISO 20884	10.0 maximum	mg/kg
Carbon residue (10 % distillation residue	EN ISO 10370	0.30 maximum	% (mol/mol)
Cetane number	EN ISO 5165	51 minimum	
Sulphated ash content	ISO 3987	0.02 maximum	% (mol/mol)
Water content	EN ISO 12937	500 maximum	mg/kg
Total contamination	EN 12662	24 maximum	mg/kg
Copper band corrosion (3 hours at 50 °C)	EN ISO 2160	1	Degree of corrosion
Oxidation stability 110 °C	EN 14112	8.0 minimum	h
Acid value	EN 14104	0.50 maximum	mg KOH/g
Iodine value	EN 14111	120 maximum	g I_2/100 g
Linolenic acid content	EN 14103	12.0 maximum	% (mol/mol)
Polyunsaturated (≥4 double bonds) methyl esters	EN 14103	1 maximum	% (mol/mol)
Methanol content	EN 14110	0.20 maximum	% (mol/mol)
MAG content	EN 14105	0.70 maximum	% (mol/mol)

DAG content	EN 14105	0.20 maximum	% (mol/mol)
TAG content	EN 14105	0.20 maximum	% (mol/mol)
Free glycerol	EN 14105 EN 14106	0.020 maximum	% (mol/mol)
Total glycerol	EN 14105	0.25 maximum	% (mol/mol)
Group I metals (Na, K)	EN 14108 EN 14109	5.0 maximum	mg/kg
Group II metals (Ca, Mg)	EN 14538	5.0 maximum	mg/kg
Phosphorous content	EN 14107	4.0 maximum	mg/kg

2.3 Properties related to fuel oxidation stability

2.3.1 Iodine value

Iodine value is used to measure the level of unsaturation in a sample. According to the EN 14111, the iodine value is measured by the mass of iodine (in grams) that can be added into 100 grams of sample. In short, iodine value is an indicator of the number of double bonds present in the sample, in which the greater the number of double bonds present, the higher the iodine value. A higher iodine value indicates that the biodiesel is more prone to oxidation. Theoretically, the iodine value of a pure compound, IV_{pure}, can be calculated using Eqn. 2.1.

$$IV_{pure} = \frac{253.81 \times db}{MW_f} \quad \text{(Eqn. 2.1)}$$

where *db* is the number of double bonds in the compound, MW_f is the molecular weight of the compound, while 253.81 is the atomic weight of two iodine atoms theoretically added to a double bond (Knothe, 2002). Similarly, the iodine value of a mixture of fatty compounds, $IV_{mixture}$, can be calculated using Eqn. 2.2.

$$IV_{mixture} = \sum 100 \times \frac{A_f \times 253.81 \times db}{MW_f} \quad \text{(Eqn. 2.2)}$$

where A_f is the amount (% weight) of a particular fatty compound in the mixture. Both the equations assume full iodination.

According to the EN 14214 standard, the maximum allowable IV is 120 g I_2 per 100 g of sample. As the iodine value depends only on the number of double bonds in the samples, disregarding the distribution of double bonds within the molecular structure, it cannot be

used to predict the oxidation stability of a particular sample (Knothe and Dunn, 2003). Two samples with the same iodine value can have different oxidation stabilities and properties. With the level of unsaturation unknown via the iodine value, it is insufficient to be used as the sole indicator of oxidation stability.

2.3.2 Linolenic acid content

Linolenic acid is a type of fatty acid that contains three double bonds in its 18-carbon long chain. As the level of unsaturation increases, the oxidation instability also increases. With this, it can be said that linolenic acid is more prone to oxidation in comparison with other fatty acids such as oleic acid (18:1) and linoleic acid (18:2). The EN 14214 states the highest limit for linolenic acid to be present in biodiesel as 12 %. The measurement of linolenic acid can be an alternative measurement to show the oxidation progress as the FAME content slowly diminishes as oxidation takes place (Yaakob *et al.*, 2014). Lacoste and Lagardere (2003) also demonstrated the decrease in ester content as time increases. The linolenic acid content can be measured according to test method described in the EN 14103.

2.3.3 Oxidation stability index (OSI)

As the unsaturated ester content in biodiesel promotes the attack of radicals, this results in the decrease of oxidation stability as the process goes on. As such, specific standards have been established to ensure the quality of the fuel. The minimum oxidation stability of biodiesel, measured as induction period (IP) is 3 h and 6 h for the ASTM D6751 and the EN 14214, respectively. In other words, the IP value can be referred as the time needed

for biodiesel to reach rapid oxidation. The Rancimat apparatus is used to measure the OSI of biodiesel samples, and the term “Rancimat’ and ‘OSI’ are often used interchangeable in the literature when referring to the test method (Waynick, 2005).

According to the test method EN 14112, the biodiesel sample is heated to 110 °C with air passing through it at a fixed rate (10 l/h). The air passing through will then carry secondary oxidation products containing short chain, water soluble carboxylic acids into a measuring vessel containing an absorption solution with distilled water. As the cell electrodes continue to monitor the conductivity of the measuring vessel, the surge of volatile acids content from the passing air will in turn raise the conductivity of the solution in the measuring vessel. To summarize, the oxidation process will release volatile acids which are measured by the increase in conductivity of the absorption solution. A higher oxidation instability indicates more volatile acids being released, leading to higher conductivity readings obtained. It has been reported that the main volatile acid formed during the process is formic acid, whereby the decomposition of hydroperoxides to formic acid has been studied (Waynick, 2005).

The IP value is calculated automatically by the Rancimat software, which is the maximum second derivative of conductivity with respect to time (Pullen and Saeed, 2012). The Rancimat method determines the OSI of the biodiesel sample by accelerating the oxidation process, via heating and exposing the sample to a controlled air flow. This standard method has become one of the important tests to study the oxidation stability of biodiesels, whereby the IP value is used to evaluate the effectiveness of antioxidants in enhancing the oxidation stability of biodiesel.

Other than that, there is another new test method called the PetroOXY method which can be used to determine the oxidation stability. Unlike the Rancimat method, the PetroOXY adheres to the ISO 7536 - ASTM D 525- IP 40 (Neumann, Jebens and Volkmar, 2008). 5 mL of test sample is brought in contact with oxygen at a pressure of 700 kPa and heated to 140 °C. The test method artificially ages the sample within the small hermetically sealed chamber, resulting in a drop in pressure measured by the test apparatus. The oxidation stability of the sample is measured by the time needed to achieve a fixed pressure drop. One of the major advantages of the PetroOXY method over the Rancimat one is that it greatly reduces the time needed to complete a test cycle, thus allowing replicates of experiments to be accomplished within a smaller time frame. Besides, it also reduces the volatilisation of compound during the measurement. Some studies in the past also proved that the results of the two methods could be correlated (Botella *et al*., 2014; Murta Valle *et al.*, 2014). However, the lower limit of PetroOXY has yet to be established, resulting in the drawback of adopting this test method as a test standard (Zhou *et al.*, 2016).

2.3.4 Acid value

Acid value can also be used to determine the oxidation stability of a biodiesel sample. It is used to determine the number of carboxylic acid groups present in the sample, which in turn reflects how much acid is present inside the fuel. During the oxidation process, hydroperoxide (ROOH) are usually formed from the attack of peroxide radical on the hydrocarbon chain. As the propagation process continues, hydroperoxides accumulate as time goes on. From there, the oxidation process will also allow the hydroperoxides to

undergo complex reactions to form aldehydes, which will then further be oxidised into acids (Yaakob *et al*., 2014).

An increasing acid value is often used to indicate the ongoing oxidation process. Also, by plotting the graph of acid value against time, the IP value of biodiesel can be determined as the concentration of acid increases exponentially when oxidation enters the propagation stage. As previously discussed in Section 2.3.3, the IP value of a biodiesel sample is the time needed for the sample to reach the point of rapid oxidation. Therefore, by knowing when the acid value starts to increase rapidly, the IP value of the sample can be known. In the event of oxidation, acid value is expected to increase over time in extended storage period as acid continues to form from oxidation processes. According to the test methods ASTM D664 and EN 14104 from the ASTM D6751 and EN 14214 biodiesel fuel standards, respectively, acid value is determined by the amount of base measured in milligrams of potassium hydroxide (KOH) needed to neutralize the acid content of 1 g of the sample. Both these standards specify a maximum of 0.50 mg KOH/g of acid value for biodiesel. Acid value is one of the important parameters used to study the quality of biodiesel as it increases as the biodiesel oxidises and deteriorates (Saluja *et al.*, 2016).

2.3.5 Kinematic viscosity

Another parameter that correlates with acid value is the kinematic viscosity. Both parameters are commonly used to assess the quality of fuel samples as both the AV and kinematic viscosity increase as oxidation progresses. Under normal circumstances, the acid value and kinematic viscosity will continue to increase until the IP of the sample

reaches zero. Thereafter, they will increase at a higher rate. There is also a direct correlation between the acid value and kinematic viscosity of the sample as the formation of acids in the system is directly related to the increase in sample viscosity (Waynick, 2005).

The viscosity of biodiesel is an important fuel property as it impacts the fuel injection system. Secondary oxidation products are the main reason the viscosity of fuel increases as oxidation progresses (Yaakob *et al*., 2014). The formation of insoluble, long chain saturated compounds, sediments, gum and polymers as a result of oxidation might plug fuel filters and injection systems when oxidation occurs (Kumar, 2017). To simplify, there are three factors which heavily affects the viscosity of a fuel sample: (1) number of carbon atoms, (2) degree of saturation, and (3) double bond configuration; *cis* or *trans* (Saluja *et al.*, 2016).

The increase in the number of carbon atoms in the hydrocarbon chain and the degree of saturation increases the viscosity of the fuel. Furthermore, it is proven that *trans* double bonds give higher viscosity than *cis* double bonds (Knothe and Steidley, 2005). Despite that, differences in the double bond position, *cis* and *trans*, are said to have little effect on viscosity. However, it is important to note that isomerisation of the double bond occurs during a rapid oxidation process. The double bond usually changes from *cis* to *trans*, contributing slightly to the increase in viscosity of the fuel.

Measurement of kinematic viscosity is usually performed according to the test methods prescribed in the biodiesel fuel standards. The ASTM D6751 biodiesel standard limits the viscosity determined via the test method ASTM D445 to within 1.9–6.0 mm^2/s.

Meanwhile, the test methods EN ISO 3104 and ISO 3105 are specified in the EN 14214 biodiesel standard, a stricter standard as it sets the viscosity range to within 3.5–5.0 mm^2/s.

2.4 Oxidation process

Oxidation is defined as the direct attack of oxygen on the unsaturated carbon bond, leading to the formation of acids, peroxides, aldehydes and polymers through a series of classical free radical chain reaction (Waynick, 2005; Christensen and McCormick, 2014). The chain reaction goes by three steps: initiation, propagation and termination. Each step can be overlapping or sequential (Pullen and Saeed, 2012). The following describes the generalised reaction scheme:

Step 1: Initiation

$$RH + I\cdot \rightarrow R\cdot + IH \qquad \text{(Reaction 2.1)}$$

This step is best described as the hydrogen atom removal from the unsaturated fatty acid (RH) to form the carbon-based radical (R·) and stable product (IH) (Kumar, 2017). These hydrocarbon radicals are formed from the attack of initial radical (I·) on the bisallylic carbon.

Step 2: Propagation

$$\begin{cases} R\cdot + O_2 \rightarrow ROO\cdot \\ ROO\cdot + RH \rightarrow ROOH + R\cdot \end{cases} \qquad \text{(Reaction 2.2)}$$

In this stage, the presence of diatomic oxygen together with the hydrocarbon radical (R·) promotes the formation of unstable peroxide radical (ROO·). These peroxide radicals, although not as reactive as the hydrocarbon radical will react with the original substrate

(RH). This results in the formation of another new hydrocarbon radical (Waynick, 2005). The self-sustaining chain reaction termed as the propagation stage promotes the formation and accumulation of alkyl hydroperoxide (ROOH).

Step 3: Termination

$$R\cdot + R\cdot \rightarrow R\text{-}R \qquad \text{(Reaction 2.3)}$$

$$ROO\cdot + ROO\cdot \rightarrow \text{Stable product} \qquad \text{(Reaction 2.4)}$$

As the alkyl hydroperoxide continues to accumulate and the original substrate is exhausted, the hydrocarbon radicals (R·) and peroxide radicals (ROO·) react with each other to form non radical species. This will only form when the concentrations of radicals are high enough for them to collide with each other (Pullen and Saeed, 2012).

During the start of the initiation phase of the oxidation process, the concentration of alkyl hydroperoxide (ROOH) is low. This holds true for a set length of time until the oxidation process starts to accelerate. This period is termed as the induction period (IP), which is used to determine the time needed for the concentration of alkyl hydroperoxide (ROOH) to reach the point of rapid oxidation process. In other words, a longer IP shows that it will take a longer time for the rapid oxidation process to occur, which also implies that the biodiesel is less susceptible to oxidation (Pullen and Saeed, 2012).

2.4.1 Factors affecting oxidation

2.4.1.1 Presence of double bonds (bisallylic sites) in fatty acid chain

In the three-step oxidation process described above, the formation of alkyl peroxides (ROOH) requires the extraction of hydrogen atom from the substrate (RH). The easiest

carbon to be attacked are the allylic carbons of the unsaturated fatty acid chain. Based on Waynick's report in 2005, this is due to the resonance stability offered by the pi electron system in the adjacent olefin group. Plant-based and vegetable oils which naturally contain these bisallylic methylene group are more susceptible to oxidation. This is also true with the increase in bisallylic sites on the fatty acid chain. The order of oxygen stability reduces from oleic acid (18:1) to linoleic acid (18:2) to linolenic acid (18:3), with linolenic acid being the least stable. The same work by Waynick also shows the rate of oxidation is proportional to the number of bisallylic sites present on the unsaturated fatty acid. This means that with the increase of linoleic acid (18:2) and linolenic acid (18:3) in the FAME, the susceptibility to oxidation increases as well.

2.4.1.2 Storage condition

Aside from the presence of bisallylic sites on the FAME, the storage condition will also affect the rate of oxidation. As discussed in Section 2.1, biodiesel will usually need to sit in the storage tanks for up to months before reaching the consumers. Briefly, there are three main aspects that will affect the oxidation stability of biodiesel: (1) airflow, (2) presence of light and (3) temperature.

As seen in the propagation stage of the oxidation process, the hydrocarbon radicals (R·) react with diatomic oxygen to form the unstable peroxide radicals (ROO·). The presence of airflow in the storage system means oxygen will be more readily available for the propagation step to proceed. In Argawal and Khurana's study (2013), they demonstrated the storage capabilities of Karanja oil methyl ester (KOME) under different circumstances. Most of the samples stored under open air had drastic decrease in their IP

value. For example, the IP of two samples stored under open air-metal and open air-without metal were nearly zero at day 60. Furthermore, they also concluded that the presence of air contact with the sample is one of the major reasons of the declining oxidation stability of the samples, thus demonstrating the impact of airflow on the biodiesel oxidation stability.

While airflow is one of the influencing factors of oxidation instability, the presence of light will also induce the oxidation process in biodiesel. This process is called photo-oxidation. Similar to auto-oxidation, the initial radical might form from the photo-oxidation process. The difference between auto-oxidation and photo-oxidation is the presence of light in the latter on top of oxygen. Unlike auto-oxidation, photo-oxidation relies on ultraviolet (UV) light to decompose the oxygen-containing compound in the biodiesel to generate radicals. These radicals, usually decomposed from peroxides, hydroperoxides, carbonyls etc., will facilitate the initial phase of the auto-oxidation process (Yaakob *et al*., 2014). There are two routes for photo-oxidation. The first one is similar to auto-oxidation process. The second one is the photo-catalysed ene reaction. In this reaction, the diatomic oxygen is excited to its electrophilic singlet state and reacts with the olefin carbon to form hydroperoxides. Figure 2.1 illustrates the general ene reaction.

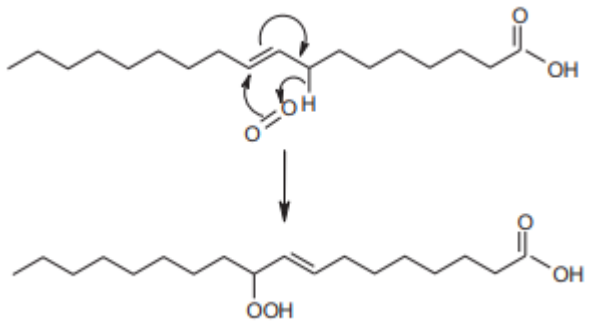

Figure 2.1. Ene reaction of photo-oxidation (Adapted from Yaakob *et al*., 2014).

However, photo-oxidation is rare in biodiesel storage as it relies heavily on UV light. As most biodiesel fuels are stored in opaque tanks, it is highly unlikely that this will contribute much to the oxidation instability of biodiesel (Pullen and Saeed, 2012).

Moving on to the third factor that will affect the oxidation stability of biodiesel in its storage, temperature is another major aspect that will influence the biodiesel oxidation stability. As discussed in previously, the oxidation process proceeds via a chain reaction initiated by the initial radical (I·). One of the formation pathways of the initial radical is through the thermo-dissociation of hydroperoxides (ROOH) present as impurities. The reaction of thermo-dissociation is shown by Reaction 2.5 as follows:

$$ROOH \rightarrow RO\cdot + OH\cdot \qquad \text{(Reaction 2.5)}$$

Under elevated temperature, the hydroperoxide dissociates to form lipid oxy radical (RO·) and hydroxyl radical (OH·). These radicals, formed from the stable hydroperoxide (ROOH) will act as the initial radicals (I·) for the oxidation process. Such process can also happen during the propagation step, where these newly formed radicals will continue to attack other stable substrates to continue the chain reaction. High temperature will also

initiate the isomerisation of methylene-separated polyunsatured olefin into a more conjugated structure. The newly formed diene group can react with a single olefinic group to form a cyclohexene ring. Such a process is called the Diels Alder reaction and the product of the reaction is referred as a dimer (Yaakob *et al*., 2014; Rashed *et al*., 2015). Figure 2.2 shows the general Diels Alder reaction.

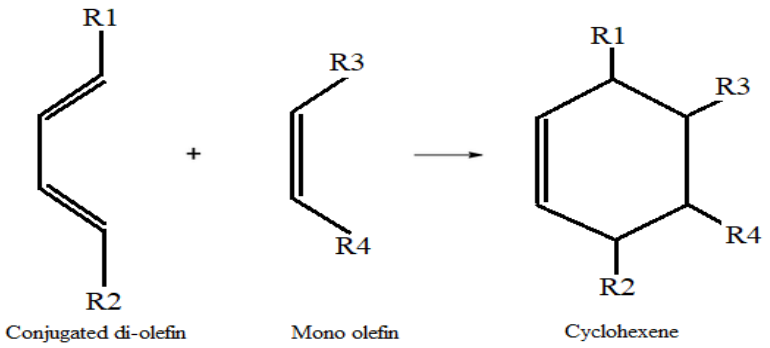

Figure 2.2. Diels Alder reaction.

While it is possible for the reaction to occur under high temperature of near 300 °C, it is only applicable for biodiesels obtained from cooking oil and animal fats (Waynick, 2005; Yaakob *et al*., 2014).

2.4.1.3 Presence of metal

Likewise to elevated temperature, the presence of metal will also promote the oxidation process via the decomposition of hydroperoxides (ROOH). These metal elements may come in the form of impurities during the production of biodiesel, in the storage tank and during contact with engine compartments (Endalew and Kiros, 2014). Trace metals such as copper, zinc, tin, lead and bronze may help in degrading the stable hydroperoxides (ROOH) into unstable radical species (Kumar, 2017). The reaction between the metal (M)

and hydroperoxides (ROOH) is described by the Reaction 2.6 and 2.7.

$$ROOH + M^{2+} \rightarrow RO\cdot + OH + M^{3+} \quad \text{(Reaction 2.6)}$$

$$ROOH + M^{3+} \rightarrow ROO\cdot + H^{+} + M^{2+} \quad \text{(Reaction 2.7)}$$

The metal catalysed reaction revolves around donation of an electron from the metal ion (usually a transition metal) to form a stable hydroxyl species while the metal itself is promoted to a higher charge species. To return to a lower charge species, the metal ion will then extract an electron from another stable substrate to form a peroxide radical and a free hydrogen ion. The process does not stop until the substrate is completely depleted because the metal ion itself is self-sufficient as a catalyst. Knothe and Dunn (2003) had investigated the effects of three transition metals, namely copper, nickel, iron on common FAME compounds. Their results showed that the IP value with copper (4.25 h for 1 mg) was the lowest out of all the three transition metals tested. Nickel and iron on the other hand were 11.40 h and 8.20 h, respectively.

2.5 Additives as a solution to oxidation instability

The oxidation process that occurs naturally in biodiesel due to these influencing factors will result in a decrease in fuel quality as well as affecting other fuel properties like kinematic viscosity, acid value, iodine value and peroxide value. These fuel properties will change drastically as the oxidation process goes on. To address this major disadvantage of biodiesel, antioxidant additives are introduced into biodiesel blends to improve their resistance towards oxidation, thus improving the stability of biodiesel. The most common type of antioxidants are the chain-inhibitors (peroxide radical quencher)

and hydroperoxide decomposers (reducing agent) (Yaakob *et al*., 2014).

Chain inhibitors function by reacting with free radicals to form a stable product that do not contribute to the oxidation process (McCormick *et al*., 2007). Phenolic and aminic type antioxidants usually belong to this group (Kumar, 2017). The stability of the chain inhibitor structure allows it to donate a hydrogen away while becoming a stable radical or further reacting with other radicals to form a stable product. The process prevents the propagation step from snowballing to produce unwanted by-products from the oxidation process. Meanwhile, hydroperoxide decomposers react with hydroperoxides (ROOH) and converts them into alcohol. The conversion will also prevent the propagation step from continuing as the hydroperoxide is less likely to be broken down again to form free radicals under the influence of temperature as discussed in Section 2.2.1. Furthermore, some antioxidants can also act as oxygen quencher or scavenger, where it involves the deactivation of excited singlet oxygen by either reversing the formation of singlet oxygen via energy transfer, or charge transfer via complex formation with electron deficient oxygen molecules (Fatima, Masood and Luqman, 2016). While the functionality of antioxidant appears to mitigate the oxidation of biodiesel, the naturally occurring oxidation process will slowly deplete the antioxidants added into biodiesel. Therefore, it can be concluded that the addition of antioxidant is to delay the attack of the initial radical on the bisallylic site of FAME. Table 2.3 lists examples of antioxidants used to improve fuel oxidation stability.

Table 2.3. Examples of antioxidants used to improve oxidation stability.

Type	Name	Abbreviation	Nature

Bio-based	α-tocopherol	α-T	Chain inhibitor
	β-carotene	β-C	Chain inhibitor
Synthetic	Butylated hydroxyanisole	BHA	Chain inhibitor
	Butylated hydroxytoluene	BHT	Chain inhibitor
	Tert-butylhydroquinone	TBHQ	Chain inhibitor
	Propyl gallate	PG	Chain inhibitor
	Pyrogallol	PY	Oxygen quencher
	Hydrogenated cardanol	HC	Oxygen quencher
	Alkyl hydrogenated cardanol	AHC	Oxygen quencher
	Gallic acid	GA	Reducing agent

2.5.1 Synthetic additives

Comparing with natural antioxidants, there are more studies on the effects of synthetic antioxidants due to their wide availability and high purity. Table 2.4 is a bibliographic compilation of studies on the effects of synthetic antioxidants on biodiesel fuels. As natural antioxidants usually come from plants, it is harder to conduct studies with just the extracts alone. Extracts of these natural antioxidants contain multiple compounds, and there might be synergistic effects that have yet to be elucidated to date (Sonam and Guleria. 2017). There are also studies that reported synthetic antioxidants are better at maintaining the oxidation stability of biodiesel for a longer period than natural ones. This could be seen in Yung *et al.*'s study (2006), where only 50 ppm of BHT and TBHQ was sufficient to raise the IP value of distilled palm oil methyl ester (DPOME) above 6 h. On the other hand, 1000 ppm of α-T was needed to raise the IP value of DPOME to 6.17 h. As discussed in Section 2.3.3, the IP value is used to evaluate the effectiveness of antioxidants in enhancing the oxidation stability of biodiesel. The measurement of IP is carried out by heating up the sample to produce volatile acids that are measured by

electrodes in the measuring vessel. The slower these volatile acids are detected implies a longer time is needed for the sample to oxidize, which corresponds to a higher oxidation stability of the sample. In other words, the increase in IP values in dosed samples as compared to those without additives meant that the antioxidants served their purpose of improving the oxidation stability of the sample.

Kleinberg *et al.*'s study (2019) on beef tallow using both natural and synthetic antioxidants also showed similar results. Cashew nut shell liquid (CNSL) samples were used in their study as the natural antioxidant. Under the same 5000 mg/kg concentration, both natural and technical CNSL were subpar compared to TBHQ and BHT. While the oxidation stability of beef tallow increased to 4.90 h and 8.24 h for natural CNSL and technical CNSL, respectively, TBHQ was able to improve the oxidation stability to 74.20 h, while the BHT one was 85.28 h. When comparing to the IP value of the control (0.55 h), it is evident that synthetic antioxidants showed a much larger increase in IP value. TBHQ, the weaker one among the two synthetic antioxidants tested, increased the IP value of the control by over 134 times, while the stronger natural antioxidant, technical CNSL, only increased the IP by a factor of near 15. The stark difference between the natural and synthetic antioxidants activities is perhaps the major factor in the popularity of synthetic antioxidants and the wider availability of studies on synthetic antioxidants.

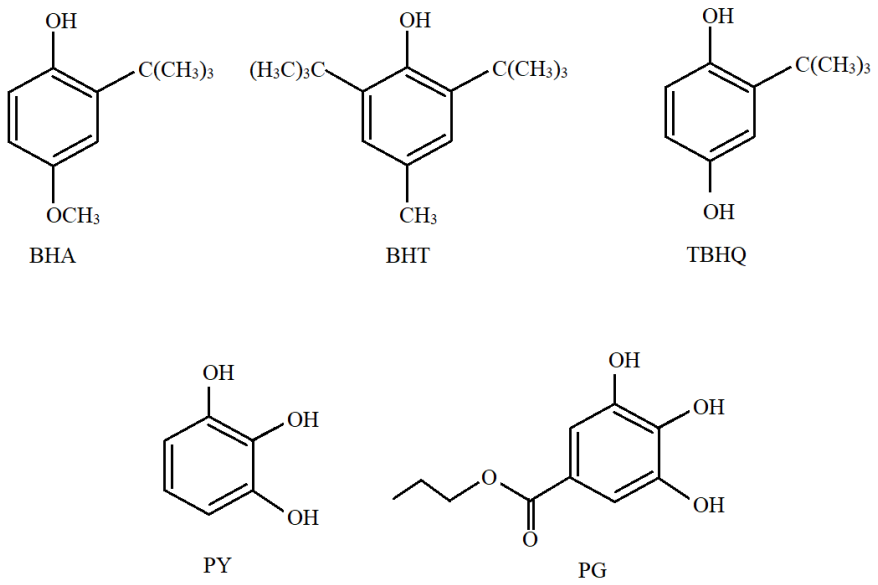

Figure 2.3. Chemical structures of BHT, BHA, TBHQ, PY and PG.

The molecular structures of antioxidants play an important role in their antioxidation effectiveness. The scavenging of free radicals usually occurs via hydrogen transfer (Lewandowski *et al.*, 2020). Therefore, the number of hydroxyl groups (-OH) usually correlates with the antioxidant capabilities of an antioxidant. Studies also demonstrated that the antioxidant capabilities of an antioxidant is directly proportional to the number of hydroxyl groups in its molecular structure (Baldim *et al.*, 2017; Sánchez-Marzo *et al.*, 2020). Furthermore, another important structural group that may influence the effectiveness of an antioxidant is the presence of methoxy group, as seen in the molecular structure of BHA. Becerra-Herrera *et al.* (2017) found that the effectiveness of the methoxyl group is comparable to that of the hydroxyl group, as it is able to donate electrons to stablise the phenoxy radicals formed after a phenolic antioxidant scavenges free radicals.

Yang *et al*. (2017) conducted a study on the usage of synthetic antioxidants in camelina biodiesel. The authors investigated the effects of BHA, BHT, PG and TBHQ on B100 camelina biodiesel. The results showed that TBHQ was the most effective out of the four, followed by PG, BHT and BHA as the least effective antioxidant. Furthermore, 2000 ppm BHT, 1000 ppm PG or 1000 ppm TBHQ was sufficient to raise the oxidation stability index from 2.3 h to 8.0 h. Additionally, the authors also concluded that 3000 ppm of TBHQ was required to stabilize the said biodiesel for one year storage. This study showed that the concentration of antioxidant plays a key role in the oxidation stability of biodiesel. With proper dosage of antioxidant, it can improve the biodiesel's resistance towards oxidation.

In another study, Karanja biodiesel samples were treated with different concentrations of antioxidants from 300 ppm to 1000 ppm (Agarwal and Khurana, 2013). In addition to the four synthetic antioxidants used in Yang *et al*.'s 2017 study, Argarwal and Khurana. also examined the effects of pyrogallol (PY) in their experiments. The antioxidant activity for PY was the highest, at which 500 ppm was able to retain the stability of biodiesel samples over 4 months storage. PG came in second at 700 ppm for the same period of time. However, in contrast with the results from Yang *et al*. (2017), the authors concluded that TBHQ, BHT and BHA were unable to reach the minimum stability at 6 h even at 1000 ppm, nor were they able to retain the samples for long periods of time. The difference seen between these two reported works demonstrate that even if the concentration of antioxidant remains the same, it might give different results. In the work by Agarwal *et al.* (2013), Karanja biodiesel recorded 72 % oleic acid (C18:1) and 12 % linoleic acid (C18:2), while Yang *et al*. (2017) stated that Camelina biodiesel had 14.4 % oleic acid

(C18:1), 19.1 % linoleic acid (C18:2) and 33.5 % linolenic acid (C18:3). The difference between the fatty acid compositions in both types of biodiesel samples could possibly be the reason why the results differed despite using the same synthetic antioxidants. Although this suggests that the same antioxidants impact various types of biodiesel samples differently, more detailed studies are needed to fully understand how these antioxidants work in biodiesel samples of different fatty acid composition.

Canha *et al.* (2018) investigated the effects of hydroquinone (HQ), BHT and BHA on soybean and rapeseed biodiesels. The effectiveness of the antioxidants studied decreased from HQ to BHT to BHA with BHA as the least effective. It was found that 114 ppm and 229 ppm of HQ were able to raise the IP values of soybean and rapeseed biodiesels, respectively to over 8 h. They had also deduced that such a difference in the HQ concentration was attributed due to the difficulties in the dissolution of HQ in biodiesel. A full dissolution could only be achieved at approximately 50 °C. Besides, both BHT and BHA required concentrations of nearly five times higher than HQ in soybean biodiesel, namely 568 ppm and 600 ppm, respectively. Meanwhile, around twice of the concentration of HQ was needed for the other two antioxidants to obtain the same results for rapeseed biodiesel, which were 453 ppm and 500 ppm for BHT and BHA, respectively. From their results, they concluded that HQ was the best antioxidant for both biodiesels, and it was perhaps due to its molecular structure with two OH groups and being less bulky compared to TBHQ, as illustrated in Figure 2.4. Steric hindrance can occur during the reaction between the antioxidant and FAME. Bulkier molecule structures may result in a weaker antioxidant activity compared to less bulky ones (Nagarajan *et al.*, 2020). The only downside for HQ was the solubility issue that occurred during the

addition of the said antioxidant into the fuel. Both HQ and TBHQ have similar molecular structures. While the antioxidants might not give the same exact results in terms of enhancing the IP value, this feature provides insights as to how TBHQ might impact the oxidation stability in a similar manner to HQ.

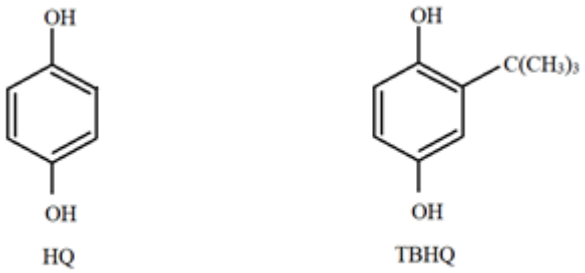

Figure 2.4. Molecular structures of HQ and TBHQ.

Zhou *et al.* (2017) carried out a study to compare the effectiveness of five synthetic antioxidants, namely PY, PG, TBHQ, BHT and BHA on cooking oil biodiesel. The main purpose of their study was to determine the better way to screen the antioxidants using both the Rancimat and pressure differential scanning calorimetry (PDSC) methods. Both the methods showed different rankings of antioxidants. For the Rancimat method, the effectiveness of the antioxidants studied could be ranked as TBHQ >PY >PG >BHA >BHT, while it was PY >PG >BHA, BHT >TBHQ for the PDSC method. From this, the authors explained the contrast in TBHQ's results with possibility of TBHQ reacting with excess oxygen in the PDSC test chamber and undergoing thermal decomposition by the high temperature and pressure involved. Meanwhile, BHT and BHA performed better in the PDSC method, possibly due to the high pressure in the PDSC thermoanalytical technique that reduced volatilization losses for these two

antioxidants. This explanation is considered viable as BHA and BHT have naturally high volatility (Hwang and Winkler-Moser, 2014). Furthermore, PY and PG performed better than BHA and BHT in both the methods. The authors also concluded that the molecular structures of PY and PG were the most likely factors contributing to the observed results. Moreover, Tang *et al.* (2009) also investigated the concentration of antioxidants added into soybean oil biodiesel and found that concentration decreased from 1000 ppm to 575 ppm for TBHQ, and 1000 ppm to <100 ppm for PG after storage time of 30 months. The authors also pointed out that the slower consumption of TBHQ signified that TBHQ was able to maintain the fuel properties better than PG.

The study of synthetic antioxidants including BHT, BHA, TBHQ, PY and gallic acid (GA) as shown in Figure 2.5 has also been carried out for Pongamia biodiesel (Obadiah *et al*., 2012). From their results, PY once again showed the highest effectiveness in improving the oxidation stability of Pongamia biodiesel with an IP of 25.02 h and 34.35 h for 2000 ppm and 3000 ppm, respectively. In their study, all five antioxidants, at 1000 ppm, were unable to raise the IP above 6 h, following EN 14214:2008. The best was still PY at 4.99 h. Out of the remaining four, only TBHQ was able to increase the IP to 6.19 h at 3000 ppm, while BHT and BHA sat at 4.88 h and 5.02 h, respectively at the same concentration. GA (Figure 2.5) was shown to be the weakest out of all five antioxidants. Even at 3000 ppm, its IP only reached 0.88 h even at 3000 ppm.

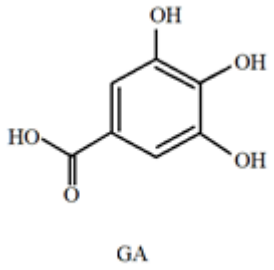

Figure 2.5. Molecular structure of GA.

The authors also explained their results according to the molecular structures of the antioxidants studied. They deduced that the antioxidant capabilities of these antioxidants related closely to the number of phenol group in 1, 2 or 1, 4 positions in its aromatic ring. Meanwhile, they also came to the same conclusion where the lower BHA and BHT IP values were related to their high volatility just like in Zhou *et al.* (2017)'s work. However, the low antioxidant effect of GA was not clearly explained.

Uğuz *et al.* (2019) discussed the possible use of Fourier transform infrared spectroscopy (FTIR) to evaluate the biodiesel stability after the addition of antioxidants. As discussed in Section 3, oxidation occurs when initial radical attacks the methyl and methylene bond to free a hydrogen atom from the fatty acid, thus creating an unstable carbon radical. Monitoring the absorption of these bonds will help in identifying the possibility of sample oxidation. Their work showed a decrease in the % transmittance for $\nu_{(C\text{-}H)}$: 3000 – 2700 cm^{-1} as the concentration of antioxidants increased. Such results could be interpreted as the increase in C-H bonds as the antioxidants' concentration increased. Hence, it was possible to conclude that the antioxidants were protecting the site of oxidation initiation as there would be lesser C-H bonds if the oxidation occurred rapidly. The absence of the band adjacent to $\nu_{(-O\text{-}C=O\text{-})}$ at > 1741 cm^{-1} also proved that there were no carboxylic acids

present in the biodiesel, which was a by-product of oxidation. Furthermore, the authors also reported that TBHQ reduced the crystal formation peak temperature (CFP) by 0.47 °C and the crystallisation peak temperature (CPT) by 0.78 °C via differential scanning calorimetry (DSC) method. It was concluded that both the FTIR and DSC were suitable alternative methods to replace the time consuming Rancimat method.

In addition, Zhou *et al.* (2017) also discussed the importance of monitoring the change in ester carbonyl band (~1740 cm^{-1}) for the degradation of biodiesel. The study reported the broadening and shifting of said band as biodiesel continued to degrade due to oxidation processes. Similar trend was also observed in another study on castor oil FAME (Araújo *et al.*, 2011). This was suggested to be due to the formation of aldehydes, ketones and carboxylic acid that during oxidation processes (Zhou *et al*, 2017).

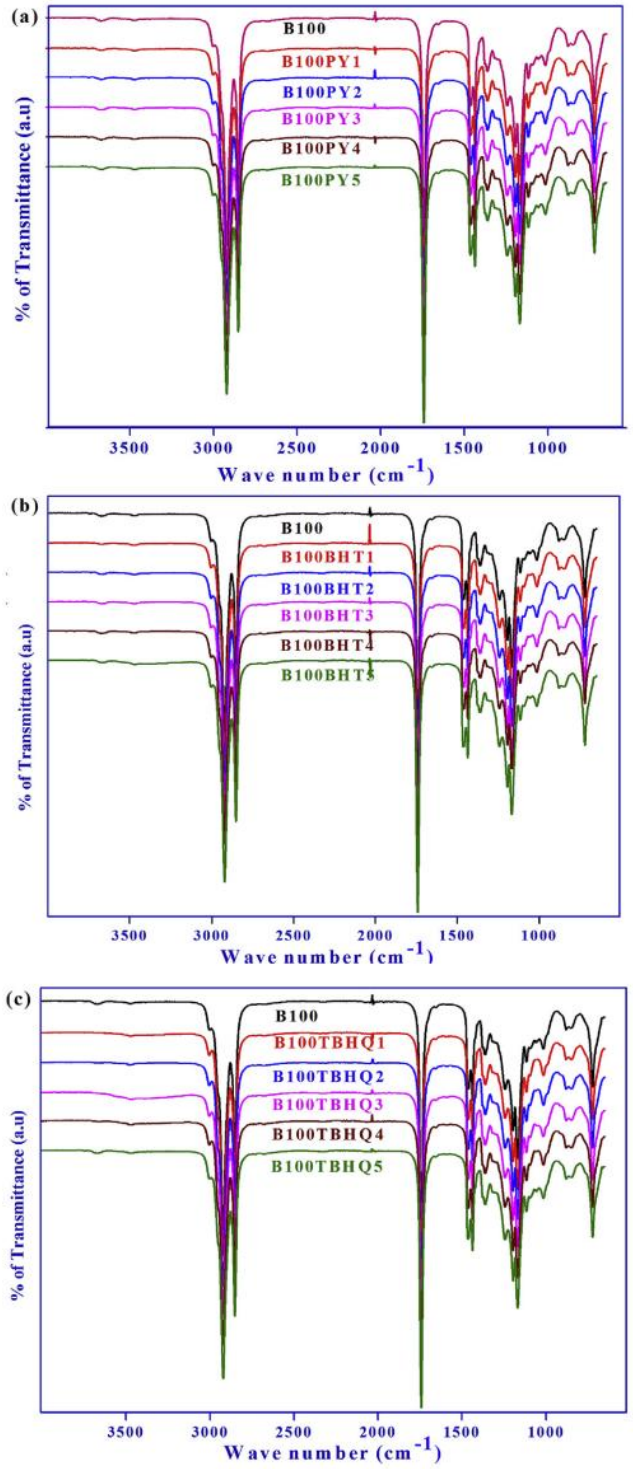

Figure 2.6. FTIR spectra of waste cooking oil methyl ester dosed with PY, BHT and TBHQ at 375, 750, 1000, 1125, 1500 ppm, respectively (Adapted from Uğuz *et al*., 2019).

Table 2.4. Compilation of studies on synthetic antioxidants in different biodiesels.

Type of biodiesel	Type of antioxidant and order	Method of evaluation	Results	Remarks	Reference
Palm	TBHQ>BHT >α-T	Rancimat	50 ppm of TBHQ and BHT sufficient to raise IP to 6h while 1000 ppm was required for α-T	Crude palm oil methyl ester can meet EN 14214	Yung *et al*., 2006
Croton *megalocarpus*	PY>PG>BHA	Rancimat	200 ppm of PY and PG are needed to satisfy said standard requirements	Untreated biodiesel was unable to reach 6 h IP	Kivivele *et al*., 2011
Sunflower	TBHQ>BHT	Rancimat	P-DSC is consistent with Rancimat method for TBHQ	BHT is unable to reach 6 h IP even at 2500 ppm	Tavares *et al*., 2011
Jatropha curcas	PY>PG>TBHQ > BHT> BHA	Rancimat and TGA	Thermal stability decreases with the decrease of oxidation stability	Only PY was able to maintain 6 h IP at 100 ppm	Jain and Sharma, 2012
Pongamia pinnata (Karanja)	PY>TBHQ >BHA>BHT >GA	Rancimat	Only PY and TBHQ were able to increase IP above 6 h at 3000 ppm. BHT and BHA were at 4.88 h and 5.04 h, respectively	All antioxidants were unable to raise IP above 6 h at 1000 ppm. 3000 ppm of GA only show IP of 0.88 h	Obadiah *et al*., 2012
Karanja oil	PY>PG>BHA> BHT>TBHQ	Rancimat	Only PY and PG were able to retain sample for over 4 months with 700 and 1000 ppm. None of the BHA, BHT, TBHQ samples were able to achieve 6 h IP.	Exposure to sunlight and air reduces the IP value drastically	Argawal and Khurana, 2013
Palm	PY >BHT	Rancimat	PY is better in controlling corrosion rate upon contact with copper for 60 days.	IP 6.17, 0.11, respectively for PY and BHT	Fazal *et al*., 2017

Calophyllum innophyllum	TBHQ	Rancimat	Increase in temperature decreases oxidation stability, dosage above 1000 ppm reduces oxidation stability	Highest IP recorded at 27.98 for 1000 ppm.	Mohammed Shameer and Ramesh, 2017
Camelina oil	TBHQ>PG >BHT>BHA	OSI-6, Oxidative Stability Instruments	2000 ppm of BHT, 1000 ppm of PG, 1000 ppm of TBHQ required to raise IP from 2.3 to 8.0 h	3000 ppm of TBHQ can ensure biodiesel storage up to 1 year	Yang *et al*., 2017
Waste cooking oil	TBHQ>PY>PG >BHA>BHT (Rancimat) PY>PG>BHA, BHT>TBHQ (P-DSC)	Rancimat, Pressure differential scanning calorimetry (P-DSC)	Possibility of thermal decomposition for TBHQ under Rancimat method and high pressure under P-DSC might reduce volatilisation loss	While P-DSC seems to be the better choice for screening antioxidants, more tests are needed	Zhou *et al.*, 2017
Soybean and rapeseed	HQ>BHT >BHA	Rancimat	Concentration for BHT and BHA were doubled of HQ in order to achieve the same IP for rapeseed biodiesel, and five times for soybean biodiesel	Exposure of sunlight, high temperature, oxygen availability reduces IP value	Canha *et al.*, 2018
Beef tallow	BHT>TBHQ	Rancimat	5000 ppm of TBHQ and BHT raise IP of biodiesel to 74.20 h and 85.28 h, respectively	Natural and technical CNSL were used as comparison	Kleinberg *et al*., 2019
Safflower seeds	TBHQ>BHA	Rancimat	IP value of BHA doped samples at 1000 ppm were unable to reach the standard that EN 14214 set. TBHQ on the other hand was able to at same concentration	Combined usage of both antioxidants did not seem to have synergistic effects	Nogales-Delgado *et al.*, 2019
Soybean	TMBP[c] = BHT	Rancimat	TMBP and BHT both showed near similar IP value at all temperature ranging from 110 °C to 125 °C	Rate constants and other thermodynamics	Schirmann *et al.*, 2019

				parameters were also similar for both antioxidants	
Waste cooking oil	TBHQ>PY >BHT	DSC, Fourier transform infrared spectroscopy (FT-IR)	TBHQ reduces the crystal formation peak temperature (CFP) by 0.47 °C and crystallisation peak temperature (CPT) by 0.78 °C	DSC is found to be a suitable alternate method to replace conventional Rancimat method	Uğuz *et al.*, 2019
Rapeseed oil, seed oil (sunflower & corn), used fried oil	BHA	Rancimat	BHA shows the best effectiveness in rapeseed biodiesel. Meanwhile, only above 1500 ppm, BHA can increase the IP of seed biodiesel and used fried biodiesel to over 8 h	Authors studied the effects of BHA on multiple biodiesel samples	Encinar *et al.*, 2020
Babassu	PDA[a] >IONOL >U-CDN[b]	Rancimat, DSC	At 10 ppm, IONOL raised the IP value of sample from around 10 h to roughly 25 h, while PDA increased to 70 h at the same concentration. Even at 1000 ppm, U-CDN was only reaching 20 h	PDA showed IP value above 180 h at 100 ppm	Figueredo *et al.*, 2020
Canola (CA), corn (C) and soybean (SB) oil	Best for each biodiesel: CA: oregano extract C: TBHQ SB: BHA,BHT	Electronic paramagnetic resonance (EPR)	Each type of biodiesel has its most suitable antioxidants that gives the best results in terms of enhancing the oxidation stability	Authors analysed about the electron trapping level for both synthetic and natural antioxidants	Mantovani *et al.*, 2020
High-oleic sunflower oil and corn oil	TBHQ>BHA	Rancimat	Original IP value for biodiesel from sunflower and corn oil (mixed) was 5.7 h. At 400 ppm of both antioxidants, they were able to reach the 8 h standard set by EN 14214	Kinematic viscosity of the biodiesel studied, under 1200 ppm of BHA exceeded the maximum standard	Nogalez-Delgado *et al.*, 2020

				of EN 14214	
Dairy waste scum (DWSME), *B. variegata* (BVME), *B. monosperma* (BMME)	BHT > *Eucalyptus* oil	Rancimat	4000 ppm of *Eucalyptus* oil is found to have similar antioxidation capabilities with 3000 ppm of BHT over the storage period of 90 days	Both antioxidants at the mentioned concentration fulfil the requirement of ATSM D6751 standard	Yatish *et al.*, 2020
Soybean and bovine tallow	Eugenol > TBHQ	Rancimat	While TBHQ gave a higher IP value from the start (13.5 h at 25 ppm), Eugenol maintained at around 11 h even until day 150 of storage.	Results also showed that Eugenol provided a lower AV value from compared to TBHQ and has higher potential	Ramos *et al.*, 2021
Used cooking oil	PG>BHT >curcumin >TBHQ	Rancimat	All antioxidants were able to increase the IP value to above 8 h at all concentration measured. When sample is introduced to metal strip corrosion, all antioxidants showed protection towards biodiesel corrosion	Corrision inhibition efficiency in for carbon steel was BHT>curcumin >PG>TBHQ while it was PG>BHT >TBHQ> curcumin for copper	Sequira *et al.*, 2021

[a]N,N'-disec-butyl-p-phenylenediamine
[b]Unsaturated cardanol
[c]3,3',5,5'-tetramethoxybiphenyl-4,4'-diol

2.5.2 Bio-based additives

Synthetic antioxidants are widely studied due to their availability and cheaper cost in terms of production. However, due to these synthetic antioxidants being petroleum-based products, there are health risks regarding the usage of these antioxidants in biodiesel (Lourenço *et al.*, 2019). Also, synthetic antioxidants may cause environmental problems after emission. To mitigate these problems, researchers started investigating bio-based antioxidants as alternative additives. These bio-based antioxidants usually originate from plants and have high phenolic contents that function as antioxidants. Some of the examples include tocopherols, tocotrienols, polyphenols, chlorophylls, ascorbates, lignin and carotenoids (Varatharajan and Pushparani, 2018). Some of these antioxidants already exist in the plant feedstock for biodiesel, but the biodiesel production processes, namely purification and distillation, break down these natural products. As a result, the produced biodiesel becomes prone to oxidation (Sharma *et al.*, 2008).

To date, most of the studies on bio-based antioxidants revolve around plant extracts. Table 2.5 is a bibliographic compilation of the literature on bio-based antioxidants. In one study, Fernandes *et al*. (2015) demonstrated that 98 % ethanol extract of *Moringa oleifera* leaves was better than TBHQ in terms of enhancing the oxidation stability of soybean biodiesel and residual methyl biodiesel. Their results also showed that all concentrations of *M. oleifera* leaves extract gave higher IP values compared to TBHQ at the same concentration. From Section 2.3.1, it is noted that TBHQ is one of the best synthetic antioxidants used to enhance biodiesel stability. The results of this study provided evidence that bio-based antioxidants are also viable in solving the oxidation issues in biodiesel.

In another study with *M. oleifera* leaves ethanol extract, however, the plant extract showed slightly lower antioxidant capabilities when compared to BHT (França *et al*., 2017). The samples dosed with 1000 ppm to 4000 ppm had very little increase in IP (7.75 h to 9.61 h). Meanwhile, BHT of the same concentration showed an increase from 8.01 h to 13.49 h. The results obtained from these two studies highlighted the complexity of extract studies. The difference between the measured oxidation stabilities might be linked to the different extraction processes. In Fernandes *et al*. (2015)'s study, the *M. oleifera* leaves were ground into powder before subjected to ethanol extraction for seven days. Conversely, França *et al*. (2017)'s extraction was carried out with an ultrasonic bath at a frequency of 40 kHz. The higher antioxidant capabilities of the former could probably be due to more antioxidants being extracted from the sample to be added into the biodiesel samples. The presence of multiple antioxidants and their synergistic effects could not also be ruled out, which again emphasises the challenges faced in extract studies. Nonetheless, this presents researchers with an opportunity to carry out in-depth studies on the plant extracts and their multiple natural antioxidants as additives to biodiesel.

Devi *et al.* (2017) have demonstrated that ginger extract extracted with 100 % alcohol showed promising antioxidant results. Pongamia biodiesel dosed with 250, 500, 1000 and 2000 ppm of ginger extract resulted in IP values of 8.01, 11.03, 17.24, 23.99 h, respectively. According their 2,2-diphenyl-1-picrylhydrazyl (DPPH) radical scavenging test, the ginger extract exhibited strong radical scavenging activities, at which even 250 ppm gave 57.21 % DPPH radical inhibition. A 2000 ppm concentration of ginger extract was the highest measurement, which was 93.5 % inhibition of DPPH radical. A subsequent study by the authors (Devi *et al.*, 2018) was carried out on potato peel extract

(PPE). The extraction process of this study was the same as the one for the ginger extract, where it was ground into powder before subjected to ethanol soaking. Instead of doing an assessment on the plant extract alone, the antioxidant activities of the PPE were compared to TBHQ of the same concentration. PPE showed similar level of antioxidant capabilities to TBHQ, both falling in the range of 5.9 h to 7.1 h for their IP values. Their results also showed that 150 ppm of PPE was sufficient to hit 6.21 h of IP to fulfil the EN 14214 biodiesel fuel standard.

Spacino *et al*. (2015) conducted a study using rosemary, oregano and basil extracts as antioxidants. While the focus of their study was more on the kinetic and thermodynamics of these natural extracts, their data showed promising results. They tested multiple formulations of the three said extracts at 7000 ppm concentration in total. Even by using the sole extract, they were able to increase the IP of B100 soybean biodiesel from 2.73 h to 9.40 h, 9.20 h and 8.04 h for rosemary, oregano and basil, respectively. A 50:50 mixture of rosemary and oregano extracts was notably the best performing one, with an IP of 10.18 h.

While Kleinberg *et al*.'s study (2019) of natural and technical CNSL on beef tallow showed inferior results compared to TBHQ and BHT, both samples of CNSL demonstrated potential antioxidant characteristics. Natural CNSL recorded an IP of 4.90 h at 5000 ppm while technical CNSL was 8.42 h at the same concentration. All these studies highlight the potential of plant extracts as future biodiesel antioxidants.

Other than naturally extracted antioxidants, commercially available bio-based antioxidants have also been studied throughout the years. For example, Chakraborty *et al.*

(2012) compared the effectiveness of α-T against existing synthetic antioxidants in *T. belerica* biodiesel, namely TBHQ, PY, PG, BHA and BHT. While α-T and BHA were unable to reach the expected 6 h IP borderline for EN 14214, the results for both antioxidants were comparable. This showed that α-T had the potential as a natural replacement for synthetic antioxidants. Another study also showed that α-T and other tocopherol variants were able to reach the stipulated IP limit of EN 14214 albeit at higher concentrations for sunflower oil methyl ester (SME), tallow methyl ester (TME) and rapeseed oil methyl ester (RME) (Fröhlich *et al.*, 2007).

de Souza *et al*. (2014) investigated the potential of β-carotene and curcumin on soybean biodiesel. The 2,2-diphenyl-1-picrylhydrazyl (DPPH) radical scavenging test result for curcumin was remarkable. Curcumin was able to scavenge the DPPH radicals by 30-90 % compared to the 30-94 % of TBHQ ranging from 25 to 200 μg/ml. β-carotene, on the other hand, was only able to reduce the DPPH radical by 15 %. Not only that, 500 ppm of curcumin could already attain the 6 h standard of EN 14214. In contrast, the authors also concluded that β-carotene showed no antioxidant activity suitable for soybean biodiesel.

Besides that, catechin, curcumin and quercetin were studied as alternative sources of antioxidants to replace synthetic ones (Freitas *et al*., 2019a). All three natural antioxidants showed higher antioxidant capabilities compared to BHA, which is a wide used synthetic antioxidant. While all four antioxidants tested reached 6 h of IP at 500 ppm, it is important to note that catechin, curcumin and quercetin showed higher increases to the original biodiesel without any additives. This also meant that it would require lesser concentration for these three antioxidants to maintain the standards set by authorities.

Freitas *et al*. (2019b) also conducted another study with catechin, curcumin and quercetin on cottonseed biodiesel. Unlike some of the examples discussed prior to this, the authors doped their biodiesel using a mixture of the three samples. A 50:50 mixture of catechin and curcumin was the weakest antioxidant mix in their study. But even so, it successfully raised the IP value of their sample to the acceptable standard of 6.29 h at 1000 ppm. Most of their samples doped with 1000 ppm of antioxidants fell within the range of 7-10 h, with 100 % catechin hitting 12 h at the same concentration. Their experiments also showed that catechin and quercetin have higher antioxidant activities than BHA, while curcumin is an equally strong antioxidant.

The potential of quercetin was also proven in de Souza *et al*.'s study in 2021 as it showed the highest radical scavenging activities among the antioxidants tested, using 2,2-azino-bis-3-ethylbenzothiazoline-6-sulphonic acid (ABTS) assay. Biodiesel samples were also doped with bilberry, oregano and basil extracts to compare against quercetin. At 3000 ppm, quercetin displayed an IP value of 12 h whereas the other three plant extracts were within 7-8 h. It is interesting to note that the authors also tested the synergistic effects of quercetin with these plant extracts with the same concentration. All the antioxidant samples mixed with quercetin showed higher results compared to quercetin alone, starting with 13 h and above, which showed that quercetin and the plant extracts studied had good synergistic effects.

While bio-based additives were proved to have comparable results with those of synthetic additives, application of bio-based additives were often obstructed by the tedious extracting and purification processes needed. Even if some widely known bio-based

additives such as tocopherol variants can be synthesised in laboratory, costs of these additives became another issue for its application in biodiesel. Production processes and cost issues of these antioxidants have to be solved before it can be implemented in the solving biodiesel stability on an industrial level.

Table 2.5. Compilation of studies on bio-based antioxidants in different biodiesels.

Type of biodiesel	Type of antioxidant and order	Method of evaluation	Results	Remarks	Reference
Sunflower oil biodiesel, rapeseed oil biodiesel, tallow biodiesel	α-T, δ-T	Rancimat	1000 ppm of antioxidant was sufficient to increase the initial IP to above 6 h for all antioxidants tested	Type of biodiesel heavily affects the effectiveness of antioxidants	Fröhlich *et al.*, 2007
T. belerica biodiesel	PG> PY> TBHQ> BHT> BHA> α-T	Rancimat	All antioxidants, except BHA and α-T's IP value did not exceed 6 h at 1500 ppm.	α-T showed to have comparable results with BHA	Chakraborty *et al.*, 2012
Soybean biodiesel	β-carotene and curcumin	Rancimat and PetroOXY	Curcumin showed up to 90 % DPPH radical scavenging activity at 200 μg/ml as compared TBHQ's 94 % on the concentration. IP value also exceeded 6 h at 500 ppm for curcumin.	β-carotene said to have no antioxidant activities on soybean biodiesel	de Sousa *et al.*, 2014
Residual cooking oil biodiesel, soybean biodiesel	*M. oleifera* leaves extract	Rancimat	IP value of 98 % ethanolic extract of *M. oleifera* was 10.3 h, 18.2 h and 21.2 h while TBHQ was 8.6 h, 11.0 h and 12.8 h for 100, 500, and 1000 ppm respectively.	70 % ethanolic extract however showed lower, but near similar IP compared to TBHQ	Fernandes *et al.*, 2015
Soybean biodiesel	Rosemary, oregano and basil extract	Rancimat	All combinations of extracts showed IP values around 9-10 h at 7000 ppm. Only basil extract's IP is 8.02 h	50:50 extract of rosemary and oregano was recorded at 10.18 h	Spacino *et al.*, 2015
Pongamia biodiesel	Ginger extract	Rancimat	250, 500, 1000 and 2000 ppm of ginger extract gives IP value of	DPPH radical scavenging activity	Devi *et al.*, 2017

			8.01, 11.03, 17.24, 23.99 h respectively.	for 250 ppm was 57.21 % and 2000 ppm at 93.5 %	
Commercial biodiesel (30 % soy, 30 % tallow, 40 % cotton)	*M. oleifera* leaves extract	Rancimat	IP value for 1000, 2000, 3000, 4000 ppm of *M. oleifera* leaves extract samples were 7.75 h, 8.67 h, 9.02 h, 9.61 h respectively. Meanwhile, it is 8.01 h, 9.38 h, 11.31 h, 13.49 h for BHT of same concentration.	Extraction of samples were done using ultrasonic water bath with frequency of 40 kHz.	França *et al*., 2017
Mesua ferra L. biodiesel	Potato peel extract	Rancimat	Both PPE and TBHQ showed similar IP value, ranging from 5.9 to 7.1 h for 100 to 250 ppm.	150 ppm of PPE extract is able to meet EN 14214 standard.	Devi *et al.*, 2018
Waste cooking oil biodiesel	*Thuja oreantalis* L. extract, TBHQ	Rancimat	While Thuja extract is able to increase the IP value of biodiesel to above 8 h at 500 ppm, only above 1000 ppm is able to maintain the IP value above 8 h for over 90 days	500 ppm of TBHQ is able to maintain 8 h of IP for over 90 days	Devi *et al.*, 2019
Cottonseed biodiesel	Catechin, curcumin, quercetin and BHA	Rancimat	All four antioxidants tested achieved IP value of 6 h at 500 ppm. But catechin, curcumin and quercetin showed higher antioxidants capabilities than BHA.	Catechin at 3000 ppm were able to reach IP value of 27 h.	Freitas *et al*., 2019a
Cottonseed biodiesel	Mixture of catechin, curcumin, and quercetin	Rancimat	50:50 mix of catechin and curcumin samples showed IP of 6.29 h on 1000 ppm, while the other samples mostly have IP values of 7-10 h on the same concentration.	1000 ppm of catechin alone were able to reach IP of 12 h.	Freitas *et al*., 2019b
Beef tallow	Natural and	Rancimat	IP value for 5000 ppm natural	5000 ppm TBHQ	Kleinberg *et al*.,

biodiesel	technical CSNL extract		CSNL was 4.90 h while technical CSNL was 8.42 h.	and BHT raise the IP of biodiesel to 74.20 and 85.28 respectively	2019
Commercial soybean biodiesel (CBSO) and soybean biodiesel with bovine tallow (SOBT)	Curcumin	Rancimat	Curcumin at 15000 ppm was able to increase IP of CBSO to 9.43 h and SOBT to 14.78 h. IP of any tested concentration below 15000 ppm for CBSO were below 8 h	Control samples of CBSO and SOBT biodiesel were 2.79 h and 8.79 h respectively	Santos *et al.*, 2019
Canolo oil biodiesel	*Larrea tridentata* extract	Rancimat	500 ppm of the extract studied increases the IP of biodiesel to 16.89 h, while 1000 ppm was able to hit 32.27 h	Comparing their results to previously existing studies, the extract showed potential as natural antioxidant	Sagaste *et al.*, 2019
Soybean biodiesel	Barley waste (BW) and *M. oleifera* (ML) leaves extract	Rancimat	Combination of both extracts (BW at 9000 ppm and ML at 13000 ppm) doubles the IP of soybean biodiesel from 4.04 h.	Biodiesel sample dosed with the same concentration is able to be stored for 6.5 months without deteriorating	Valenga *et al.*, 2019
Waste cooking oil biodiesel	Green tea *(Camilla asamica)* extract	Rancimat	Green tea extract showed 75.77 % of DPPH radical scavenging activity at 250 ppm as compared to 70.74 % of ascorbic acid at same concentration.	1000 ppm of green tea extract were only able to surpass 7 h of IP standard set by EN 14214	Bharti and Singh, 2020
Soybean	*Platymiscium*	Rancimat and	1000 ppm of $CHCl_3$ extract was	Both extracts at	Nogueira *et al.*,

biodiesel	*floribundum* ethanolic (EtOH) and chloroform ($CHCl_3$) extract	DSC	unable to surpass 8 h standard set by EN 14214 while EtOH extract at the same concentration were able to.	10000 ppm hits around 18 h of IP value	2020
Dairy waste scum (DWSME), *B. variegata* (BVME), *B. monosperma* (BMME)	BHT > *Eucalyptus* oil	Rancimat	4000 ppm of *Eucalyptus* oil is found to have similar antioxidation capabilities with 3000 ppm of BHT over the storage period of 90 days	Both antioxidants at the mentioned concentration fulfil the requirement of ATSM D6751 standard	Yatish *et al.*, 2020
Soybean biodiesel	Quercetin, basil, oregano and rosemary extracts	Rancimat and PetroOXY	IP value reached 12 h for quercetin, and the other three plants samples were recorded at 7-8 h.	Samples doped with mixture of quercetin and plant samples showed higher IP, signifying some synergistic effects.	de Sousa *et al*., 2021
Soybean and bovine tallow	Eugenol > TBHQ	Rancimat	While TBHQ gave a higher IP value from the start (13.5 h at 25 ppm), Eugenol maintained at around 11 h even until day 150 of storage.	Eugenol provided a lower AV value from compared to TBHQ.	Ramos *et al.*, 2021
Soybean biodiesel	Tannin extract >TBHQ	UV-vis absorption spectroscopy	Tannin extracts showed 90 % DPPH radical scavenging activities at 12.5 ppm.	When 350 ppm of tannin extracts added into biodiesel, it performs better than TBHQ	Schaumlöffel *et al*., 2021

2.6 Kinetics and thermodynamics of biodiesel oxidation with additives

Spacino *et al*. (2015) demonstrated that temperature affected the IP of B100 biodiesel samples. The results they obtained showed the decrease in IP with an increase in temperature of the Rancimat test. All the controls and antioxidant-dosed samples showed similar trends, whereby the logarithm of conductivity (ln *A*) versus time (*t*) in hours displayed a linear relationship. The graph plotted provided the values of the angular coefficients and intercepts in the Eyring equation and the Gibbs free energy equation to determine the thermodynamic parameters of the oxidation reaction. By obtaining the enthalpy (ΔH), entropy (ΔS) and the Gibbs free energy (ΔG) from the two equations, the authors were able to show that the reaction between the plant extract antioxidants and biodiesel was endothermic and non-spontaneous. This also proved that the use of natural antioxidants was very effective in stopping the oxidation process in biodiesel.

Using the linear adjustment of logarithm of conductivity (ln *A*) versus time (*t*), the reaction rate constant (*k*) can be determined using Eqn. 2.3 and 2.4 below.

$$\ln A = \ln A_0 - kt \qquad \text{(Eqn. 2.3)}$$

$$\ln k = \ln A - E_a/(RT) \qquad \text{(Eqn. 2.4)}$$

where k is the rate constant in s^{-1}, A is the pre-exponential factor, R is the ideal gas constant (8.314510 $JK^{-1}mol^{-1}$), T is temperature in Kelvin, E_a is the activation energy in $kJmol^{-1}$. The E_a is calculated using ln k versus the inverse of T (Romagnoli *et al*., 2018). The thermodynamics equations are represented by Eqn. 2.5 till 2.8.

$$\Delta G^{\ddagger} = -RT \ln K^{\ddagger} \qquad \text{(Eqn. 2.5)}$$

$$\Delta G^{\ddagger} = \Delta H^{\ddagger} - \mathrm{T}\,\Delta S^{\ddagger} \quad \text{(Eqn. 2.6)}$$

$$\ln K^{\ddagger} = -\Delta H^{\ddagger}/(RT) + \Delta S^{\ddagger}/R \quad \text{(Eqn. 2.7)}$$

$$\ln (k/T) = -\Delta H^{\ddagger}/(RT) + \ln (k_b/h) + \Delta S^{\ddagger}/R \quad \text{(Eqn. 2.8)}$$

where $K^{\ddagger}$ is thermodynamic equilibrium constant. By using the linear form of the Eyring equation, the $\Delta H^{\ddagger}$ and $\Delta S^{\ddagger}$ can be determined using ln (k/T) versus $1/T$ plot. The plot should have a negative slope of $-\Delta H^{\ddagger}/R$ and a y-intercept of $\Delta S^{\ddagger}/R$ + ln (k_b/h) where k_b is the Boltzmann constant (1.381×10^{-23} JK^{-1}) and h is Planck's constant (6.626×10^{-34}Js).

The thermodynamic study of synthetic antioxidants can be seen in Borsato *et al.*'s study (2014b), whereby TBHQ, BHT, BHA and PG were dosed into B100, then subjected to Rancimat tests under temperatures ranging from 110 °C to 125 °C. Positive $\Delta H^{\ddagger}$ value showed that the reaction between the antioxidants and biodiesel was endothermic. From Table 2.6, we can also see that the $\Delta S^{\ddagger}$ values from their study range from negative to positive. A negative $\Delta S^{\ddagger}$ value indicates that the reaction is non-spontaneous, and usually results in the formation of an activation complex where the degree of freedom is lost. A positive $\Delta S^{\ddagger}$ value on the other hand shows that the interaction between the antioxidants and FAME has a higher degree of freedom (Ong *et al*., 2013). Their study showed that PG was the only antioxidant that was spontaneous.

The effects of coffee and sage extracts have also been studied, and their thermodynamics parameters were elucidated (Gregório *et al.*, 2018). The authors found that all the reactions for the plant extracts in biodiesel were endothermic and non-spontaneous, which agreed with the findings of Spacino *et al.* (2015). Coffee and sage extracts had $\Delta H^{\ddagger}$ values of 79.02 $kJmol^{-1}$ and 75.05 $kJmol^{-1}$, respectively which were higher than the 63.41

kJmol^{-1} of the control. While coffee and sage extracts gave the expected less negative $\Delta S^{\ddagger}$ values, a mixture of coffee and sage extracts showed otherwise. The lower $\Delta H^{\ddagger}$ value (52.41 kJmol^{-1}) and more negative $\Delta S^{\ddagger}$ value (-115.47 JK^{-1}mol^{-1}) as compared to the control's, indicated that there might be some interactions between the extracts and biodiesel inside the system that caused the unexpected trend (Zhang *et al.,* 2019).

Similar trends can also be observed in de Sousa *et al.*'s study (2019). A synthetic antioxidant PY and natural antioxidants in the form of quercetin, bilberry extract, basil extract and oregano extract all followed the trends obtained in the different studies mentioned above. The antioxidants all showed positive $\Delta H^{\ddagger}$ values and negative $\Delta S^{\ddagger}$ values, indicating that they were endothermic and non-spontaneous. The best performing antioxidants in their study were PY and quercetin. These two antioxidants had the highest $\Delta H^{\ddagger}$ values and least negative $\Delta S^{\ddagger}$ value overall. The observed trend could possibly be due to the purity of the antioxidants themselves, as extracts contain multiple compounds with antioxidative effects. It is also noteworthy that the results for the three extracts studied were different when using different measuring instruments, namely the Rancimat and PetroOXY. The Rancimat showed an activation energy trend of bilberry > basil > oregano while a trend of bilberry > oregano > basil was obtained for the PetroOXY. Since the PetroOXY method analyses both volatile and non-volatile compounds in the system, it may contribute to this difference in the results (Botella *et al*., 2014; Bär *et al.*, 2021).

From Table 2.7, it is evident that the reaction constant, *k*, increases as the temperature increases. This could be viewed as the consumption rate of antioxidant increasing as the temperature increased, and that could be translated to lower IP value (Xin, *et al.,* 2009).

In Zhou *et al.*'s work (2016), the authors demonstrated that measurement of the lower *k* value indicated the lower consumption rate of antioxidant. Their experimental reaction constant increased in the order of TBHQ < PG < PY < BHA < BHT. Considering the IP value at 110 °C for PY and PG were 16.11 h and 10.07 h at 100 ppm, respectively, PY showed a faster rate of consumption compared to PG. Moreover, TBHQ, the best performing antioxidant in their study for 250 ppm onwards, had the highest critical condition. The authors also commented that TBHQ could be a radical producer on top of being a radial scavenger. The statement can also be backed with Bao et al.'s work (2020), whereby TBHQ increased the lipid radical formation during lipid oxidation. However, their results contradicted with Borsato *et al.*'s (2014b) study, where the authors found that PG was a better antioxidant compared to TBHQ.

Comparison of synthetic and natural antioxidants in terms of their kinetic parameters can also be seen in de Sousa et al.'s study (2020). Pure antioxidants, with PY as synthetic and quercetin as natural, together with three different plant extracts, namely bilberry, basil and oregano were studied. The results highlighted how pure antioxidants had a lower rate of consumption compared to the extracts. However, the rate of consumption for the two said antioxidants increased at a much higher rate compared to the extracts with elevated temperatures, whereby it was roughly 20-fold for PY, and 25-fold for quercetin from 90 °C to 140 °C. All three extracts however had increased by 10-fold each approximately. The observed trend could possibly be due to the sensitivity of the purer antioxidants to temperature (Alhaithloul, Galal and Seufi, 2021). A similar trend of reaction constant was also reported in a study of passionfruit extract (Jain *et al.*, 2021). However, it is noteworthy that the critical concentration (C_{cr}) for passionfruit extract studied was much

higher compared to those extracts in de Sousa et al.'s (2020). As the type of biodiesel used were different, namely waste cooking oil biodiesel in the former, and soybean biodiesel in the latter, more studies need to be conducted to further understand and screen for potential natural antioxidants to replace the synthetic ones.

Activation energy, E_a, is another important factor when it comes to assessing the effectiveness of an antioxidant as well as its dependence on temperature. Generally, a higher activation energy means that the reaction is temperature sensitive and vice versa (Hashemi *et al.*, 2014). Also, it can also be translated as lesser temperature increase is needed to affect the rate of oxidation if a reaction has a higher activation energy (Eryakai Nambi *et al.*, 2016). It is important to note that activation energy is the minimum energy threshold required for a reaction to surpass to get the final product. Since the presence of antioxidants inside the system prevents the formation of the final product, the activation energy usually increases after the addition of an antioxidant (Romagnoli et al., 2018). This behaviour can be observed in all the studies listed in Table 2.8. For instance, Borsato *et al.* (2014b) showed that the activation energy of increased after the addition of antioxidant as compared to the control. Meanwhile, TBHQ's activation energy was 85.65 $kJmol^{-1}$ while it was 78.48 $kJmol^{-1}$ for BHT followed by 70.68 $kJmol^{-1}$ for BHA. Rodrigues *et al.*'s work (2020) also reported similar trends. Furthermore, the authors also found that the zero order of reaction better described the reactions of BHA and PG, while the first order of reaction suited the BHT, TBHQ and ethanolic curcuminoid extract (ECE) reactions.

The addition of natural antioxidants into the system, specifically in extract form, will also

increase the activation energy of the oxidation degradation in the same manner as for the synthetic antioxidants. Extracts of pecan nut (Amaral *et al.*, 2019), *Platymiscium floribundum* (Nogueira *et al.*, 2020) and *Larrea tridentata* (Sagaste *et al.*, 2019) all showed increase in activation energy as compared to their respective control samples. In Amaral *et al.*'s study, the ethanolic extract of pecan nut was demonstrated to be the least effective in increasing the activation energy as compared to the methanolic and aqueous extracts. Also, *Platymiscium floribundum* chloroform extracts at 1000 ppm was found to obey 1.5 order of reaction kinetics according to the authors (Nogueira *et al.*, 2020). However, at 5000 ppm it followed the first order of reaction as extract studies are complicated due to the presence of multiple compounds extracted from a particular solvent. Since binary, tertiary and quartenary interaction of antioxidants have been reported (de Sousa *et al.*, 2020), there might be synergistic and antagonistic effects that impact the oxidation process at different temperature levels.

Table 2.6. Compilation of thermodynamics parameters for antioxidants.

Antioxidants	$\Delta H^{\ddagger}$ (kJmol^{-1})	$\Delta S^{\ddagger}$ (JK^{-1}mol^{-1})	$\Delta G^{\ddagger}$ (kJmol^{-1})	Reference
TBHQ	82.40	-36.20	96.54	Borsato *et al.*, 2014b
BHT	67.44	-71.22	95.26	
BHA	75.24	-54.42	96.50	
PG	128.32	71.00	100.58	
Coffee extract	79.02	-46.43	97.15	Gregório *et al.*, 2018
Sage extract	75.05	-56.19	97.00	
Coffee and sage extract	52.41	-115.47	97.49	
Control	63.41	-80.85	94.98	
Pyrogallol[a]	78.15	-125.04	115.43	de Sousa *et al.*, 2019
Quercetin[a]	74.49	-128.20	112.71	
Bilberry extract[a]	60.61	-157.97	107.71	
Oregano extract[a]	48.80	-190.14	105.49	
Basil extract[a]	58.86	-163.12	107.49	
Pyrogallol[b]	76.40	-121.63	112.66	
Quercetin[b]	66.93	-142.42	109.39	
Bilberry extract[b]	42.15	-194.21	110.05	
Oregano extract[b]	41.24	-197.12	100.01	
Basil extract[b]	38.74	-203.11	99.30	

[a]Rancimat test
[b]PetroOXY test

Table 2.7. Compilation of reaction constant (k) and critical concentration (C_{cr}) at different temperatures.

Temperature	Antioxidant, reaction constant (k) and critical concentration (C_{cr})										Reference
(°C)	k (h^{-1})	C_{cr} (ppm)	k (h^{-1})	C_{cr} (ppm)	k (h^{-1})	C_{cr} (ppm)	k (h^{-1})	C_{cr} (ppm)	k (h^{-1})	C_{cr} (ppm)	
	TBHQ				PG		BHA		BHT		Borsato *et*
110	0.5523	-			0.1271	-	0.5853	-	0.9251	-	*al.*, 2014b
115	0.9197	-			0.2245	-	0.9277	-	1.3400	-	
120	1.2180	-			0.3669	-	1.2910	-	1.8090	-	
125	1.5480	-			0.6078	-	1.4650	-	2.1120	-	
	TBHQ		PY		PG		BHA		BHT		
100							0.2044	38.72	0.1872	53.30	Zhou *et*
110	0.0606	79.03	0.2401	4.42	0.1574	33.66	0.3741	50.40	0.3622	68.20	*al.*, 2016
120	0.1351	81.14	0.4779	6.99	0.3353	40.61	0.7417	56.99	0.7984	73.02	
130	0.2720	90.17	0.8563	11.02	0.7029	43.76	1.3585	61.79	1.5982	71.86	
140	0.5607	91.69	1.5635	16.29	1.4305	48.11	2.4387	59.73	3.1981	79.95	
150	1.1210		2.8579		2.7720						
					PG						Xin *et al.*,
100					0.1203	101.00					2009
105					0.1883	105.00					
110					0.2739	100.00					

115					0.4031	103.00					
120					0.6015	109.00					
	Quercetin		PY		Bilberry extract		Oregano extract		Basil extract		de Sousa
90	0.1360	10.49	0.0424	34.81	0.3196	4.44	0.3659	2.10	0.3288	5.05	*et al.*,
100	0.1662	73.70	0.0671	87.36	0.5733	3.82	0.5351	3.42	0.5733	3.78	2019
110	0.3907	23.81	0.2849	2.48	0.5980	56.83	0.5762	42.52	0.5896	57.40	
120	0.7125	14.15	0.5422	3.25	1.6468	16.44	0.8546	79.04	1.1484	48.91	
130	1.0844	41.26	0.6601	35.16	2.3711	82.27	1.8706	99.48	2.3711	80.64	
140	3.0602	32.14	0.8533	34.47	3.9650	56.26	2.9951	64.72	4.0147	35.52	
	Passionfruit extract										Jain *et al.*, 2021
100	0.43	161.39									
110	0.79	170.51									
120	1.73	171.07									
130	4.67	175.68									
140	7.04	178.12									

Table 2.8. Compilation of activation energy (E_a) and reaction order (n) for antioxidants.

Antioxidant	E_a (kJmol^{-1})	n	Reference
Control	23.35	-	Borsato *et al*., 2014b
TBHQ (500 ppm)	85.65	-	
BHA (500 ppm)	70.68	-	
BHT (500 ppm)	78.48	-	
PG (500 ppm)	131.57	-	
Control	78.82	1	Rodrigues *et al*., 2020
BHA (500 ppm)	78.69	0	
BHT (500 ppm)	102.24	1	
PG (500 ppm)	119.43	0	
Ethanolic curcuminoid extract (ECE) (500 ppm)	100.43	1	
Control	103.00	1	Amaral *et al*., 2019
Aqueous pecan nut extract (ANE) (12000 ppm)	125.17	1	
Ethanolic pecan nut extract (ENE) (5000 ppm)	106.40	1	
Methanolic pecan nut extract (MNE)[a] (12000 ppm)	138.55	1	
Control	137.27	1	Nogueira *et al*., 2020
Platymiscium floribundum chloroform extract (PF-$CHCl_3$) (1000 ppm)	154.17	1.5	
Platymiscium floribundum chloroform extract (PF-$CHCl_3$) (5000 ppm)	188.12	1	
Platymiscium floribundum ethanolic extract (PF-EtOH) (1000 ppm)	163.23	1	
Platymiscium floribundum ethanolic extract (PF-EtOH) (5000 ppm)	170.65	1	
Control	70.32	-	Sagaste *et al*., 2019
Larrea tridentata extract (250 ppm)	102.23	-	
Larrea tridentata extract (500 ppm)	118.47	-	
Larrea tridentata extract (1000 ppm)	91.37	-	

[a]Extracted using methanol + water

2.7 Artificial Neural Network (ANN) modelling for biodiesels

Many studies on biodiesel have concentrated on measuring the changes in fuel properties prior to and after the introduction of additives since the doped fuel need to adhere to the standards of ASTM D6751 and EN 14214. Within this context, developing predictive models to measure the fuel oxidation stability depending on the type of additive and concentration remains unexplored for palm biodiesel. Hence, the development of artificial neural network (ANN) models will enable quantification and prediction of fuel properties relevant to oxidation stability. To date, ANN models for biodiesel production as well as emissions resulting from biodiesel combustion have been developed and tested, but not for biodiesel oxidation stability and related properties based on additive type and concentration.

Agu *et al.* (2024) explored three training methods, namely scaled conjugated gradient (SCG), bayesian regularization (BR) and levenberg maraquardt (LM) to predict biodiesel production from waste catfish oil and found that SCG produced predictions closest to the experimental data. The SCG method also produced the lowest mean squared error (*MSE*) and higher coefficient of determination (R^2) values which further justified the relevance of the ANN. Sultana *et al.* (2022) on the other hand compared support vector regression (SVR) with ANN and found that SVR performed better than ANN as the latter was able to predict closest to the experimental data. Besides SCG, Samuel *et al.* (2021) explored both Adaptive Neuro-Fuzzy Inference System (ANFIS) and ANN for the prediction of biodiesel production using tobacco seed oil and found that ANFIS was more suitable for the task. On the contrary, ANN was found to be better than Nelder-Mead (NM) simplex algorithm for the prediction of engine performance and combustion emission

characteristic (Esonye et al., 2019). The authors reported that while both ANN and NM were able to produce networks that fit the experimental data, NM was more restricted to second-order polynomial. Additionally, the assessments of ANN to predict biodiesel production highlighted its simplicity and predictability (Banerjee *et al*., 2017; Fangfang *et al*., 2021).

2.8 Storage time studies

Storage time studies are necessary if the fuel applications entail storing over a longer period, for example reservoir tanks for backup electricity generators. Investigating the protection offered by additives over an extended period allows researchers to understand the rate of depletion of antioxidants and enable the estimation of how long it takes before the biodiesel becomes fully oxidised.

Christensen *et al.* (2014) showed that addition of TBHQ and BHT into commercial biodiesel extended the storage time by 1 month before the IP values dropped below 3 h. However, 500 ppm of BHT was unable to increase the IP value of fresh commercial biodiesel to above 8 h stipulated in the EN 14214 standard. The authors also revealed that antioxidants addition to a pre-aged biodiesel did not aid in increasing the IP, which highlighted the importance of introducing antioxidants into the fuel before the propagation stage. Blending of doped biodiesels into B5 and B20 recorded much larger increases in IP values compared to B100. Overall, the IP values decreased over time as hypothesised from the nature of oxidation processes. The results were also supported by another study on Karanja biodiesel (Agarwal *et al.*, 2013) whereby PY and PG at both

700 and 1000 ppm were able to maintain the IP values above the required limit of the EN 14214 standard for 4 months. While increased IP values for BHT and TBHQ doped samples were observed, the increments were insufficient to reach the stipulated limit and decreased over time.

Changes in other fuel properties over extended periods have also been noted. For instance, the kinematic viscosity and acid value in antioxidant-doped Pongamia biodiesel increased in relation to the type and concentration of antioxidants, but the increments were comparatively lower compared to the neat fuel (Obadiah *et al*, 2012). This stresses the importance of antioxidants in the context of long-term storage since there are limits of 500 mm^2/s and 0.5 mg KOH/g for kinematic viscosity and acid value, respectively as specified in the EN 14214:2012 standard. The formation of oxidised polymeric compounds during storage increased the viscosity of the samples. These, if accumulated, can form gum and sediments that may damage the generator. Meanwhile, the increment in acid value over time can be elaborated by the hydrolysis of FAMEs to fatty acids during oxidation. Karavalakis *et al.*'s study (2011) also supported the findings of kinematic viscosity and acid value of doped commercial biodiesel increasing over time. TBHQ, PG and PY were found to be more effective than BHA and BHT in terms of maintaining the fuel properties over the course of 10 weeks. Although TBHQ was the best performing antioxidant, the authors reported its poor performance in biodiesel blends compared to B100.

In addition to IP, kinematic viscosity and acid value, Lin *et al.* (2009) also reported changes in water content and iodine value in palm biodiesel doped with BHT. The usage

of antioxidant was able to reduce the increment rate over time. Similar to water content, the sample with BHT was able to maintain the iodine value close to the initial value (50 g I_2/100 g) over the course of 5 months when the biodiesel was stored at 20 °C. Meanwhile, neat B100 recorded a slight drop as compared to the BHT-doped fuel.

2.9 Concluding remarks

A comprehensive review of the biodiesel oxidation stability issue, oxidation stability properties, oxidation factors and the proposed use of additives as a solution has been completed. Studies covering additives kinetics and thermodynamics, their effects in biodiesel under long-term storage and biodiesel modelling have been discussed. Naturally occurring oxidation process in biodiesel due to the unsaturation of its FAME content is a major disadvantage compared to petroleum diesel. Additives have thus been introduced to enhance the oxidation stability of biodiesel. Nonetheless, comprehensive comparative studies of both synthetic and bio-based additives for palm biodiesel, the fuel of interest in this study, are lacking. Furthermore, the oxidation kinetics and thermodynamics of palm biodiesel with additives, as well as fuel stability and oxidation pathways over long-term storage remains largely unexplored. The prediction of fuel oxidation stability properties via artificial neural network (ANN) modelling has not been attempted since most ANN modelling studies in this area focused on biodiesel production. This thesis aims to address these gaps in knowledge, in line with Malaysia's direction towards a more sustainable future with higher adoption of palm biodiesel in the transportation and industrial sectors.

3. Comparative assessment of the oxidation stability of palm biodiesel with additives

3.1 Introduction

This chapter focuses on the first phase of work aiming to assess the effects of synthetic and bio-based additives on the oxidation stability of palm biodiesel. In this phase, B100 palm biodiesel samples with and without additives were prepared. α-tocopherol (α-T), curcumin and quercetin were selected as natural or bio-additives, while BHT, BHA, THBQ, PY and PG were selected as synthetic additives. They were mixed with palm biodiesel at 4 different concentrations, namely 250, 500, 750 and 1000 ppm. The oxidation stability of the fuel samples was assessed by the test method EN 15751 (Rancimat test/oxidation stability index). The PetroOXY method described in the ASTM D7545 and EN 16091 standards, which is faster than the Rancimat test was also used to benchmark the results obtained. The purpose of the tests was to assess the samples against the specifications in the ASTM 6751 and EN 14214, which stipulate that a min of 3 h and 8 h induction period at 110 ºC, respectively must be met. Other fuel properties which link to oxidation stability such as acid value, iodine value, and kinematic viscosity were measured according to the EN 14104, EN 14111, EN ISO 3104 and EN 14103, respectively.

3.2 Materials

Butylated hydroxyanisole (BHA, ≥ 98.5 %), 2,6-di-tert-butyl-4-methylphenol (BHT, 99 %), tert-butylhydroquinone (TBHQ, 97 %), pyrogallol (PY, ≥ 98 %), propyl gallate

(PG, ≥ 98 %), curcumin (≥ 94 % curcuminoid, ≥ 80 % curcumin), α-tocopherol (α-T, 96 %), heptane (HPLC, 99 %) and ethyl acetate (HPLC, 99.8 %) were purchased from Sigma Aldrich (M) Sdn. Bhd. Quercetin (97 %) and 2,2-diphenyl-1-picrylhydrazyl (DPPH, 95%) were purchased from Alfa Aesar. Dimethyl sulphoxide (99.9 %) and potassium hydroxide were purchased from Fisher Chemicals. Ethanol (96 %), methanol, phenolphthalein, sodium thioslphate, Wijs solution, potassium iodide, methylnonadecanoate (≥ 98 %) were purchased from Merck. Gallic acid, Folin-Ciocalteu solution, sodium carbonate, toluene, acetic acid, cyclohexane and starch were purchased from Chemiz, UK. All reagents and chemicals were of analytical grade. Refined bleached deodorized B100 palm oil methyl ester (RPOME) was provided by Sime Darby Oils Biodiesel Sdn. Bhd.

3.3 Preparation and characterization of biodiesel samples

Refined bleached deodorized palm oil methyl ester (RPOME) was vacuum distilled at 210 °C and 720 rpm using a laboratory-scale distillation set up connected to a vacuum pump until 5–10 % of RPOME remained. The resulting distilled palm oil methyl ester (DPOME) was stored at –20 °C immediately after distillation and thawed when used in the experiments. The thawing temperatures were kept below 40 °C. Both the RPOME and DPOME were characterized for their fatty acid content (FAC), vitamin E content, free radical scavenging activity (DPPH), oxidation stability index (OSI) / induction period (IP) via Rancimat and PetroOXY, acid value, iodine value and kinematic viscosity following the procedures described in Section 3.5.

The assessment experiments were initiated once all the RPOME had been fully distilled.

The recovery rate for 10 L of sample was recorded at 82 % with the remaining 18 % being thick yellowish liquid with natural phytochemicals present in oil palm. All fractions of distilled samples were homogenised before splitting into aliquots of 900 mL for the respective antioxidants. All samples were stored in –20 °C, and only thawed prior to the experiments.

3.4 Effects of synthetic and bio-based additives

Eight antioxidants were tested to assess their effects on the oxidation stability of DPOME. They were BHT, BHA, TBHQ, PG, PY, α-tocopherol, quercetin and curcumin. Each antioxidant was added into DPOME at room temperature at four levels of concentrations, *i.e.*, 250, 500, 750, 1000 ppm. Thereafter, samples were extracted for analyses of free radical scavenging activity (DPPH), oxidation stability index (OSI) / induction period (IP) via Rancimat and PetroOXY, acid value, iodine value and kinematic viscosity according to the procedures in Section 3.5. The tests were conducted in triplicates.

3.5 Analytical methods

3.5.1 Free radical scavenging activity (DPPH)

A mixture of 5 mL of 0.1 mM DPPH in methanol and 5 mL of antioxidant was prepared. The two portions were mixed and kept in the dark for 30 min. A blank sample was prepared by replacing the DPPH portion with methanol. The absorbance was read at 517 nm using a Lambda 365 UV-Vis spectrophotometer (Perkin Elmer, UK). A control sample with no antioxidant was also prepared by replacing the antioxidant fraction with DPPH in methanol. Eqn. 2.1 was applied to determine the DPPH radical scavenging activity (%).

DPPH radical scavenging activity (%) = $(1 - [A_{sample}/A_{control}] \times 100$ (Eqn. 2.1)

where A_{sample} is absorbance of sample and $A_{control}$ is the absorbance of control.

3.5.2 Fatty acid composition (FAC)

Determination of FAC in palm biodiesel was carried out using a gas chromatograph-flame ionization detector (GC-FID, Perkin Elmer, UK). Prior to analysis, 2 g of sample was dissolved in 10 mL of heptane and the volume of sample injected was 1 µL. Two different analytical methods were tested to determine the FAC. The first method was conducted according to the EN 14103 standard for total FAME and linolenic acid using a Carbowax capillary column (30 m × 0.25 mm × 0.25 µm). The hydrogen carrier gas flow rate was set at 2 mL/min. The oven initial temperature was set at 60 °C for 2 min, followed by heating to 200 °C at a rate of 10 °C/min. It was then heated to a final temperature of 240 °C at a rate of 5 °C/min before remaining constant for 7 min. Meanwhile, the temperature of the injector and detector was set at 250 °C. The second analysis was an in-house procedure developed by the Malaysian Palm Oil Board (MPOB). A BPX70 capillary column (30 m × 0.25 mm × 0.25 µm) was used instead of the Carbowax column. The oven initial temperature was set at 140 °C, followed by heating to 220 °C at a rate of 8 °C/min. The final temperature was held for 2 min. The results from both methods were compared to the standard palm oil FAC for the identification of peaks. Results were expressed in % of the total FAC content.

3.5.3 Vitamin E concentration

High performance liquid chromatography (HPLC) was used to determine the vitamin E

concentration in palm biodiesel on an HPLC Agilent 1100 series (USA) equipped with a UV detector. The stationary phase was silica column (250 × 4.6 mm, 5 µm pore size) and the mobile phase was heptane with 3% ethyl acetate. The mobile phase was filtered with a 0.22 µm polytetrafluoroethylene membrane filter and degassed in an ultrasonic bath for 30 min. UV detection was accomplished by setting the excitation wavelength at 270 nm and emission wavelength at 315 nm. The flow rate was set at 1 mL/min. Qualification of the vitamin E variants was accomplished by comparing detected peaks with the corresponding peaks of a tocopherol standard. Standards of α-T (200, 400, 800 ppm), α-T3 (200, 450, 900 ppm), β-T3 (30, 50, 100 ppm), γ-T3 (300, 650, 1300 ppm) and δ-T3 (100, 250, 500 ppm) were prepared to serve as calibration curves for quantification.

3.5.4 Oxidation stability index (OSI)

3.5.4.1 Induction period (IP) using Rancimat

The Rancimat test was conducted to measure the oxidation stability following the test method EN14112 specified in the EN 14214:2012 biodiesel standard using an 892 Professional Rancimat (Metrohm, Switzerland). 7.5 g of sample was weighed and tested at 110 °C under a controlled air flow of 10 L/h. Volatile oxidation products were collected in the measuring vessel under accelerated oxidation, from which the electrical conductivity was constantly measured. The IP of each sample was measured by the apparatus automatically.

3.5.4.2 Induction period (IP) using PetroOXY

The PetroOXY test was carried out by using a PetroOXY Petrotest, Germany. 5 mL of

sample was heated to 140 °C inside a sealed chamber under increased oxygen pressure. The IP was measured automatically once the apparatus detected a fixed pressure drop that was directly related to the oxidation stability.

3.5.5 Acid value

Acid value was measured as described in the EN 14104 standard. 20 g of sample was weighed into a 250 mL conical flask. The test sample was dissolved in 100 mL of neutralized solvent mixture (toluene 50 % + ethanol 50 %). Five drops of phenolphthalein solution were added, and titration was initiated using potassium hydroxide as the titrant. Titration was continued until a single drop of potassium hydroxide produced a colour change persisting for at least 15 s.

3.5.6 Iodine value

Iodine value was measured as specified in the EN 14111 standard. 0.13 g to 0.15 g of test sample was weighed in a glass weighing scoop, while the blank contained no sample. The glass weighing scoop containing the test sample was placed in a 500 mL flask and then dissolved using 20 mL of solvent (cyclohexane 50 % + acetic acid 50 %). 25 mL of Wijs solution was added using a precision pipette. A stopper was inserted, and the flask was swirled carefully before sitting in the dark for 1 h. At the end of the reaction time, 20 mL of potassium iodide solution and 150 mL of water were added into the flask. The mixture was titrated with a standard sodium thiosulfate solution until the yellow colour almost disappeared. Five drops of starch solution were added, and titration was continued until the blue colour disappeared after vigorous shaking.

3.5.7 Kinematic viscosity

Kinematic viscosity was measured following the EN ISO 3104 standard. The sample was dispensed into a viscometer tube via the filling arm and left in the tube for 20–30 min. By applying suction on the tubing attached to the capillary arm using a syringe, the sample was moved up into the capillary part of the viscometer tube until its meniscus reached the overflow bulb over the timing lines. The air arm was then opened, and the syringe was removed from the capillary arm to ensure both arms were open to atmosphere. Timing was initiated when the sample reached the top timing line and stopped when sample reached the bottom timing line.

3.6 Results and discussion

3.6.1 DPPH radical scavenging activity of additives

Table 3.1 displays that the DPPH test results for all synthetic antioxidants showed high positive values at 1 mg/mL. A concentration of 1 mg/mL was found to be too high for all five antioxidants tested since the lowest reading was recorded at 92.685 % for PY, while the highest was 94.417 % for BHA. The similarity in the DPPH radical scavenging activities near the maximum value of 100% made it difficult to identify any significant trends and differences between the antioxidants. Therefore, a repeat was carried out by diluting the 1 mg/mL sample by 100-fold to 10 µg/mL. Obvious decreases in the DPPH radical scavenging activities were detected for BHT and BHA as a result while TBHQ, PY and PG remained above 90 % even after dilution (Table 3.1). Thus, a further 10-fold dilution of the antioxidant concentration to 1 µg/mL was decided for the next set of tests

which included the bio-additives to compare the potential effectiveness of all antioxidants in terms of their DPPH radical scavenging activities.

Table 3.1. DPPH test results for synthetic antioxidants.

Antioxidant	DPPH radical scavenging activity (%) at different concentrations[a]	
	1 mg/mL	10 µg/mL
BHA	94.417 ± 0.000	53.945 ± 0.213
BHT	93.414 ± 0.139	82.340 ± 0.426
TBHQ	93.740 ± 0.141	92.873 ± 0.000
PY	92.685 ± 0.144	90.789 ± 0.000
PG	94.221 ± 0.000	92.374 ± 0.000

[a]Average of triplicates ± standard deviation.

Table 3.2 shows that at 1 µg/mL concentration, the ranking of the antioxidants' radical scavenging activities in ascending order was BHT < BHA < α-T < curcumin < TBHQ < quercetin < PG < PY. The dilution of samples proved to be effective in depicting a clearer picture of the radical scavenging capabilities of these antioxidants as compared to the DPPH tests conducted at higher concentrations. The lowest radical scavenging activity was recorded at 1.0525 % for BHT, while the highest was PY at 48.3122 %. Quercetin, a bio-based antioxidant, showed promising antioxidation capability with its ability to scavenge DPPH radicals better than BHA, BHT and TBHQ, which are widely used in stabilizing biodiesel. Results of DPPH suggested a link with the amount of hydroxyl bonds in the molecular structure of each antioxidant. TBHQ, PY and PG which has more than 2 hydroxyl bonds were the highest, while BHA and BHT were lower as there is only 1 hydroxyl bond. Since oxidation of biodiesel is closely related to the formation and reactions of radicals as previously discussed in Section 2.4, the data acquired here would

provide context for discussion of subsequent results.

Table 3.2. DPPH test results for synthetic and bio-based antioxidants at 1 µg/mL.

Antioxidant	DPPH radical scavenging activity (%)[a]
BHA	2.2268 ± 0.1205
BHT	1.0525 ± 0.2105
TBHQ	7.5949 ± 0.2110
PY	48.3122 ± 0.0000
PG	28.9361 ± 0.0000
α-T	4.1135 ± 0.1228
Curcumin	4.5064 ± 0.3717
Quercetin	14.8465 ± 0.4458

[a]Average of triplicates ± standard deviation.

3.6.2 Fatty acid composition (FAC) of palm biodiesel

A B10 fuel sample provided by MPOB was initially tested following the EN14103 standard for total FAME and linolenic acid on a Carbowax GC column to determine the relevancy of the test method. However, as illustrated in Figure 3.1, there was only a minor peak at 17.5 min in the resulting chromatogram instead of multiple discernible peaks signifying the different carbon-chain fatty acids. Replicate tests resulted in the same chromatogram as Figure 3.1. A C17 standard was then tested to verify the feasibility of the EN14103 test method. With a concentration of 10-fold used for the test, a peak was finally obtained on the chromatogram at 15.23 min as shown in Figure 3.2. Even so, peak broadening was observed, implying that there was a possibility for compounds to be hidden from detection should they have a lower concentration than the concentration of the standard used. It was concluded that this method was unsuitable to be used to

determine both the FAC and concentration of linolenic acid in palm biodiesel samples.

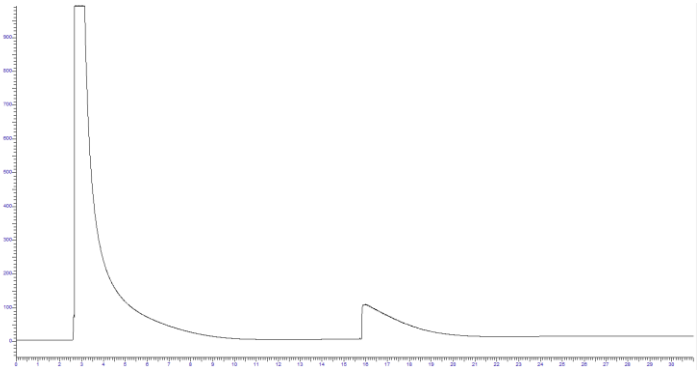

Figure 3.1. GC chromatogram of B10 fuel sample using EN 14103 method.

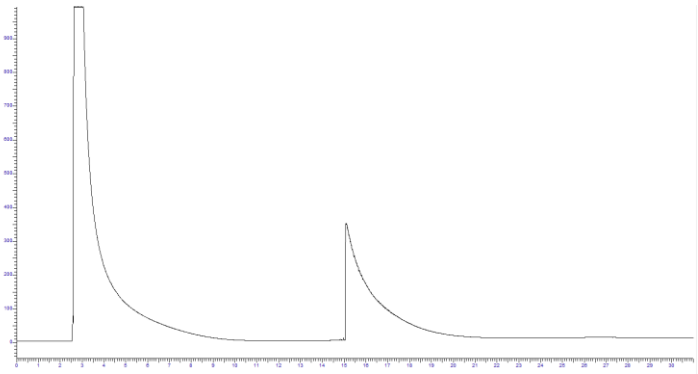

Figure 3.2. GC chromatogram of C17 standard using EN 14103 method.

The second analysis following the in-house procedure by MPOB was then tested using a BPX-70 GC column instead of the Carbowax column. Figure 3.3 and Figure 3.4 are the resulting chromatograms for the RPOME and DPOME samples, respectively. As shown, sharp peaks were obtained, thereby validating this analytical method as the superior protocol for analysing the FAC compared to the EN14103 method.

Based on Figure 3.3 and 3.4, similar peaks were recorded for both RPOME and DPOME. Major peaks were obtained for C16:0 and C18:1 fatty acid chains, which are the signature

peaks for palm oil (Zhang *et al.*, 2015; Japir *et al.*, 2017; Guerrero-Esperanza *et al.*, 2023). This confirms that the biodiesel indeed originated from palm oil and proves that the distillation of RPOME to remove natural antioxidants does not change the overall FAC profile. It can also be concluded that the fatty acid chains do not breakdown or react to form by-products as heat is introduced into the system during distillation. This is in line with other studies in the literature. For instance, Fournier *et al.* (2006) showed that fatty acid chains ranging from C14:0 to C22:1 in fish oil did not breakdown when subjected to deodorization at 180, 220 and 250 °C. Furthermore, Imahara *et al.* (2008) added that C16:0 and C18:0 fatty acids were stable and recoverable at temperatures below 300 °C while C18:1 and C18:2 were stable at 270 °C. Moreover, degradation of palm oil methyl ester (POME) was reported to be at 269.84 °C (Walvekar *et al.*, 2021). Another study concluded that neat palm oil, waste palm oil and waste palm oil methyl ester were stable till at least 330 °C (Awogbemi *et al.*, 2019). Overall, the main fatty acid chains, namely C16:0, C18:0, C18:1 and C18:2 were relatively stable under the distillation temperature of 210 °C in this study.

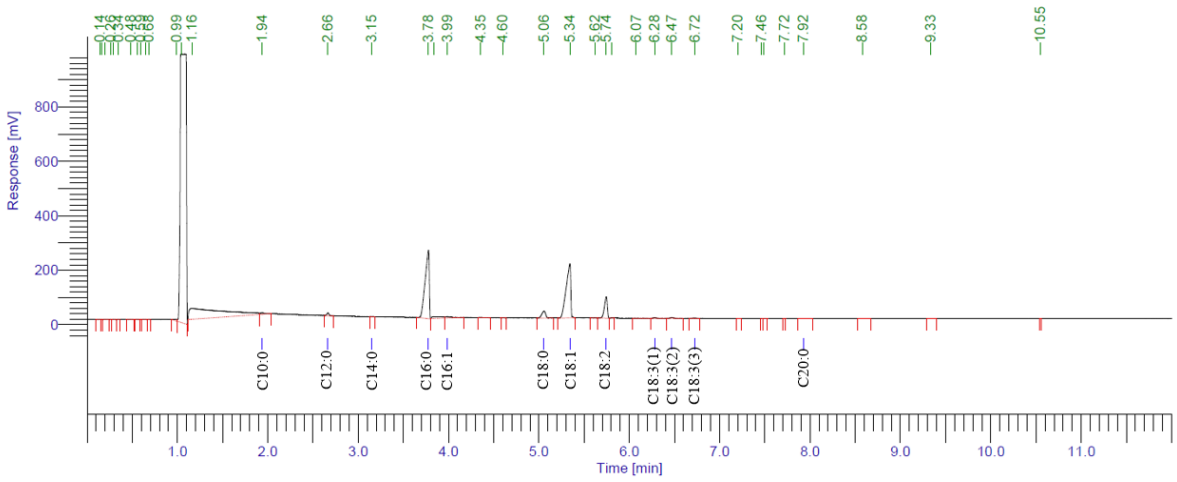

Figure 3.3. GC chromatogram of RPOME illustrating the fatty acid composition (FAC).

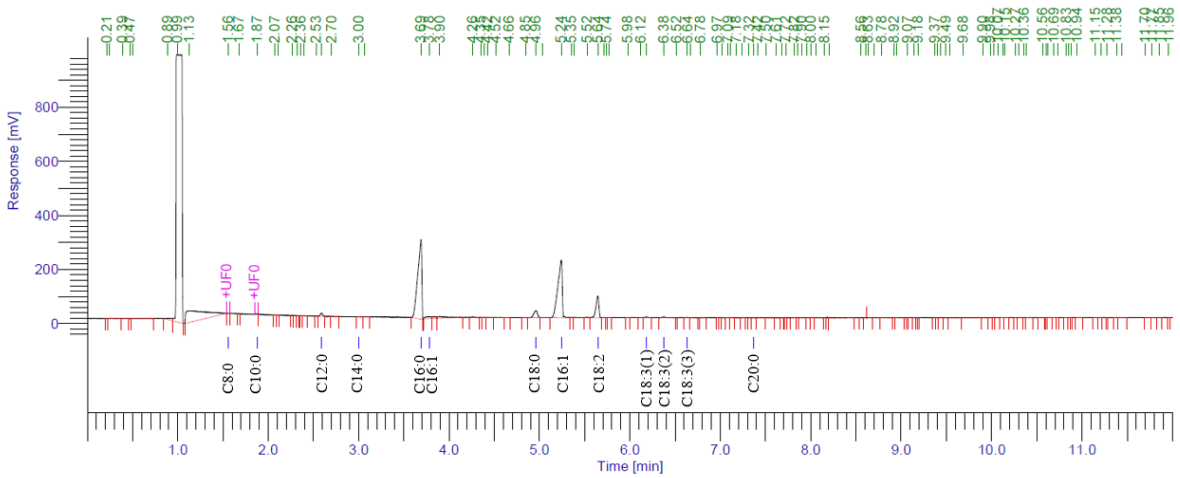

Figure 3.4. GC chromatogram of DPOME illustrating the fatty acid composition (FAC).

Table 3.3 lists the FAC of both RPOME and DPOME used in this study. The GC-FID analyses show that RPOME and DPOME have the highest C16:0 content, followed by C18:1, C18:2 and C18:0. Other fatty acid chains are negligible in composition, but they concur with other reported values (Monde *et al.*, 2009; Montoya *et al.*, 2014). It is noticeable that C8:0 is detected in DPOME but not in RPOME, possibly due to the masking of peak since the concentration is extremely low. The compositions of C16:0 and C18:1 are 43.59 wt% and 38.35 wt% for RPOME, and 46.89 wt% and 36.31 wt% for DPOME, respectively. This aligns with the FAC of palm oil as reported by Yung *et al.* (2006). The significant presence of methyl esters with low saturation (C16:0 and C18:1) implies that RPOME should be relatively stable. As previously discussed in Section 2.4.1.1, oxidation of methyl esters relates closely to the extraction of H atom to form alkyl peroxides. Since allylic carbon atoms are the easiest target to be attacked, methyl esters with higher double bond counts are more susceptible to oxidation hence rendering methyl esters with lower saturation much more stable in general.

Table 3.3. Fatty acid composition (FAC) of RPOME and DPOME.

Fatty acid chain	Composition (wt%)	
	RPOME	DPOME
Caprylic acid, ME (C8:0)	-	0.06
Capric acid, ME (C10:0)	1.14	0.14
Lauric acid, ME (C12:0)	0.91	1.08
Myristic acid, ME (C14:0)	0.05	0.06
Palmitic acid, ME (C16:0)	43.59	46.89
Palmitoleic acid, ME (C16:1)	1.35	1.67
Stearic acid, ME (C18:0)	4.07	3.77
Oleic acid, ME (C18:1)	38.35	36.31
Linoleic acid, ME (C18:2)	9.63	9.13
Linolenic acid, ME (C18:3)	0.80	0.80
Arachidic acid, ME (C20:0)	0.10	0.10

3.6.3 Vitamin E concentration in palm biodiesel

Table 3.4 records the concentrations of Vitamin E variants in RPOME and DPOME obtained via HPLC analyses. These serve as the baseline data for the later oxidation stability assessment tests. For RPOME, the concentration ranged from 1.927 to 20.080 ppm. The highest vitamin E variant was α-T3 at 20.080 ppm, followed by α-T at 14.947 ppm, γ-T3 at 11.938 ppm, δ-T3 at 2.674 ppm and lastly, β-T3 at 1.927 ppm. The total amount of Vitamin E was recorded at 51.566 ppm, in contrast to 644 ppm in Yung et al.'s study (2006). This difference lies in the use of crude palm oil methyl esters in the said study which contains more Vitamin E compared to the RPOME used here. Vitamin E content has been reported to decrease by roughly 20 % after the refining processes of palm oil, namely degumming, bleaching and deodorizing (Puah et al., 2007). The same could be observed for sunflower oil (15 %), rapeseed oil (25 %), corn oil (30 %), and

soybean oil (45 %) though these oils are also subjected to additional processes of neutralizing and wintering (Ergönüla and Köseoğlu, 2013).

Distillation of RPOME stripped off most of the vitamin E variants and thus the concentrations in DPOME fell to within a range of 0.101 to 0.348 ppm. The stark contrast between the appearance of peaks in Figure 3.5 and the absence of or diminished peaks in Figure 3.6 depicted that the removal of the said compounds was successful. The removal of these compounds via distillation was necessary to establish a baseline or control for comparison between different synthetic and bio-based antioxidants without interference from synergistic or antagonistic effects of these compounds (de Sousa et al., 2021).

Table 3.4. Vitamin E content in RPOME and DPOME.

Vitamin E variant	Concentration (ppm)	
	RPOME	DPOME
Alpha-tocopherol (α-T)	14.947	0.184
Alpha-tocotrienol (α-T3)	20.080	0.110
Beta-tocotrienol (β-T3)	1.927	0.101
Gamma-tocotrienol (γ-T3)	11.938	0.305
Delta-tocotrienol (δ-T3)	2.674	0.348

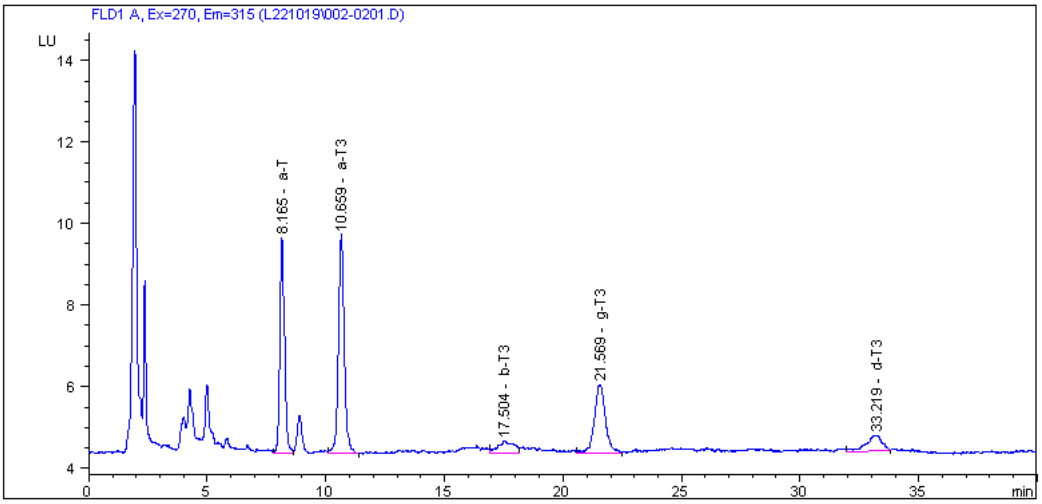

Figure 3.5. HPLC chromatogram of RPOME illustrating the vitamin E variants.

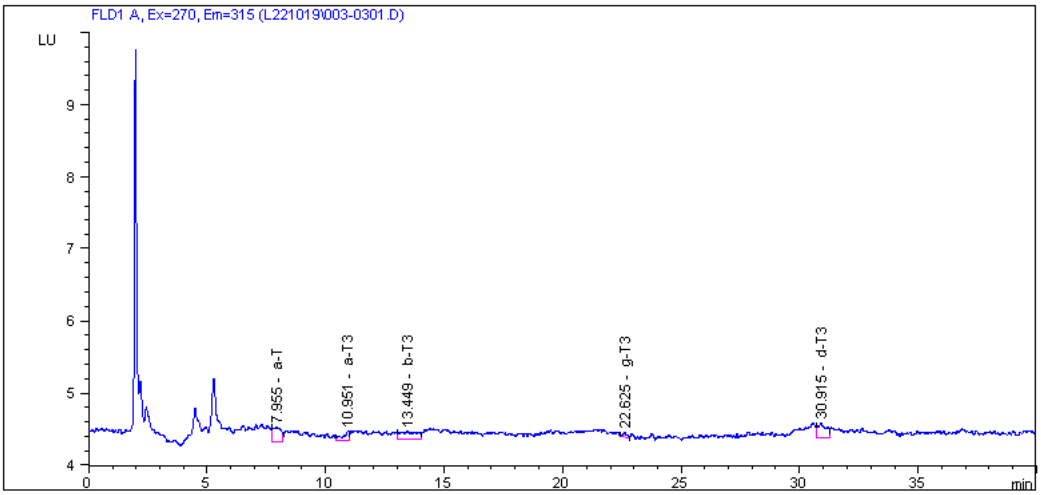

Figure 3.6. HPLC chromatogram of DPOME illustrating the Vitamin E variants.

3.6.4 Effects of synthetic and bio-based additives

3.6.4.1 Induction period (IP) using Rancimat

The IP value corresponds to the inflection point of the conductivity (µS/cm) versus time (h) curve. As an illustration, Figure 3.7 shows the conductivity and second derivative curves as well as the inflection point obtained from Rancimat test (Focke *et al.*, 2016) for

RPOME.

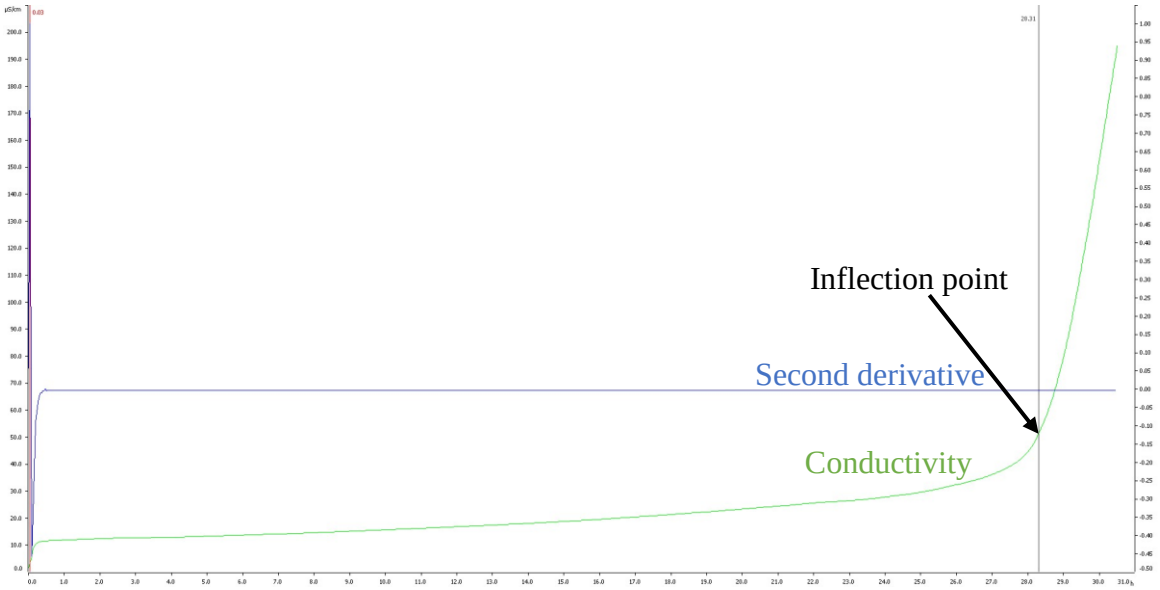

Figure 3.7. Rancimat conductivity and second derivative curves for RPOME.

As presented in Table 3.5, the IP value of RPOME determined via Rancimat was recorded at 28.41 h while DPOME was at 5.27 h. This could be explained by the presence of vitamin E variants in RPOME as discussed in Section 3.6.4.2 which act as antioxidants, thereby prolonging the duration whereby the fuel is resistant to oxidation (Lau *et al.*, 2008). Hence, RPOME is considered stable as it is, but guidelines for biodiesel handling highly recommend the use of antioxidant additives for B100 fuels, especially with longer-term storage (NREL, 2023).

The PetroOXY results also showed a similar decreasing trend from 81.02 min for RPOME to 16.94 min for DPOME. A major advantage of using the PetroOXY method for measuring the OSI is its ability to greatly reduce the long analysis times associated with Rancimat and thus increase the rate of sample analyses. As shown in Table 3.5, huge time reductions of 95.25 % and 94.64 % for RPOME and DPOME, respectively were

made possible with PetroOXY. While both test methods showed correlation in the obtained results, it has been highlighted that more studies are needed to properly understand the relationship between the two (Botella *et al.*, 2014; Murta Valle *et al.*, 2014).

Table 3.5. Induction period (IP) values of RPOME and DPOME.

Oxidation stability index test	Induction period (IP)[a]	
	RPOME	DPOME
Rancimat (h)	28.41 ± 0.13	5.27 ± 0.32
PetroOXY (min)	81.02 ± 6.09	16.94 ± 0.16

[a]Average of triplicates ± standard deviation.

Unlike fossil diesel, biodiesels such as DPOME naturally possess allylic carbon bonds that are prone to attacks from free radicals. These attacks will trigger the oxidation process, slowly stripping away the stability of biodiesel. Thus, antioxidants are necessary for biodiesel production as they act as chain inhibitor, oxygen quencher and at times reducing agent (Fatima et al., 2016; McCormick, 2017). The presence of antioxidants slows the propagating oxidation process and allows the fuel to last longer in storage.

Figure 3.8 shows the IP (h) of DPOME with the addition of bio-based and synthetic antioxidants at different concentration levels as measured using Rancimat (data in Table A.1). Each set of data was statistically analysed using one-way ANOVA and the p-values are recorded in Table 3.6. The data sets were also subjected to two-way ANOVA to determine whether there was any relationship between the type of antioxidant and the concentration of antioxidant, with the tabulated results displayed also in Table 3.6. Firstly, for all tested antioxidants, the IP value increased as the concentration of antioxidant

increased from 250 to 1000 ppm. Despite all antioxidants showing an increasing trend for IP with concentration, the effect of concentration was less pronounced for BHA, PG and α-tocopherol with their less steep lines compared to the rest of the antioxidants. The effect of concentration was most significant for TBHQ whereby every 250-ppm increment resulted in increased IP value by at least 15 % of the previous value. This contrasts starkly with α-T, where the IP increased by 8 % from 250 to 500 ppm, and by mere 1 % and 2 % for 500 to 750 ppm, and 750 to 1000 ppm, respectively. From Figure 3.9, TBHQ clearly had the highest IP values followed by PY with close tailing by PG, especially at 500 and 750 ppm. A t-test analysis indicated that PY and PG had no significant difference with a p value of 0.127 (>0.05). At the other end of the spectrum, curcumin and α-T produced the lowest IP values while BHA, BHT and quercetin were in the mid-range. Comparing curcumin to α-T, curcumin displayed a lower IP of 17.67 h at 250 ppm compared to 18.51 h recorded for α-T but higher IP values beyond 500 ppm. A similar trend could be noted for BHA and BHT, where at 1000 ppm, BHT outperformed BHA by 4.4 h at the highest concentration of 1000 ppm.

The ranking of antioxidant capability in extending the IP could be established from Figure 3.8. At 250 ppm concentration, the ranking in ascending order was: curcumin, α-T, BHT, PY, BHA, quercetin, PG, TBHQ. Meanwhile, at 1000 ppm concentration, it was: α-T, curcumin, BHA, BHT, quercetin, PG, PY, TBHQ. The trend also conforms with the results of Yung *et al.* (2006), where the authors reported that 50 ppm of TBHQ and BHT were enough to increase the initial IP of DPOME from an initial value of 3.52 h to 8.85 h and 6.42 h, respectively. As summarised in Table 3.6, all individual p-values were less than 0.05 with curcumin having the lowest value of 1.11E-08, thus indicating that there

was a statistically significant difference when the antioxidants were dosed at different concentration levels. The highest p-value was attained for PY at 2.04E-04, but it was still within the accepted range of $p \leq 0.05$. The two-way ANOVA p-values shown in Table 3.6 imply that each antioxidant was statistically significant from one another, as well as their concentrations. Additionally, the p-value obtained for the interaction between these two variables was extremely low (3.17E-31). The p-values highlighted that the results were dependent on both the individual variables as well as their interactions.

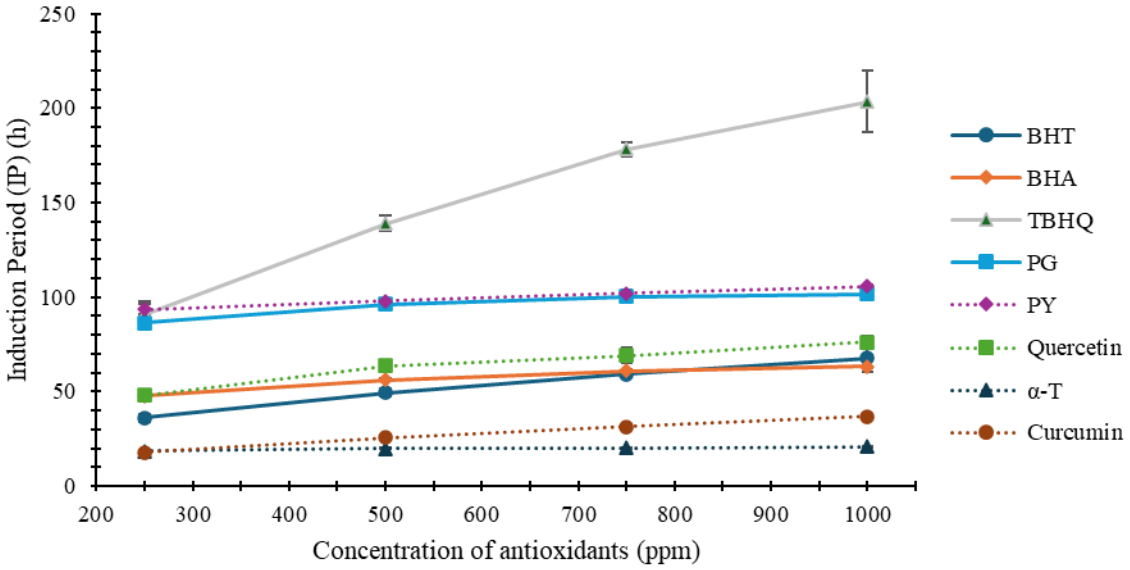

Figure 3.8. Induction periods (IP) of DPOME with synthetic and bio-based antioxidants at different concentrations measured using Rancimat.

Table 3.6. p-values of one-way and two-way ANOVA tests for IP of DPOME with synthetic and bio-based antioxidants (Rancimat).

One-way ANOVA		Two-way ANOVA	
Antioxidant	p-value	Source of variance	p-value
BHT	7.21E-06	Concentration	8.54E-37
BHA	2.49E-05	Antioxidant	3.55E-69
TBHQ	2.49E-06	Concentration × Antioxidant	3.17E-31
PG	4.79E-07		
PY	2.04E-04		
Quercetin	8.7E-06		
α-T	3.98E-05		
Curcumin	1.11E-08		

From the acquired IP data, the effectiveness factors of all antioxidants were calculated using Eqn. 3.1.

$$\text{Effectiveness factor} = IP_{sample} / IP_{DPOME} \quad \text{(Eqn. 3.1)}$$

where IP_{sample} is the IP value of sample dosed with a specific antioxidant at a specific concentration and IP_{DPOME} is the IP value of DPOME (Jemima Romola et al., 2021).

Figure 3.9 illustrates the effectiveness factors of DPOME with synthetic and bio-based antioxidants at different concentrations measured using Rancimat (data in Table A.2). Firstly, it could be observed that elevating the concentration increased the effectiveness factor of antioxidants. This effect was most prominent for TBHQ whereas concentration had the least impact on α-T. For TBHQ, the effectiveness factor increased from 17.21 to 38.62 while for α-T, it merely increased from 3.51 to 3.93. Like the trends obtained for IP, TBHQ had similar or higher effectiveness factors compared to PY and PG, while quercetin, BHA and BHT had overlapping ranges of values. Curcumin and α-T were the

least effective. At 1000 ppm concentration, the ranking of antioxidants in ascending order in terms of effectiveness factor was the same as for IP value: α-T, curcumin, BHA, BHT, quercetin, PG, PY, TBHQ.

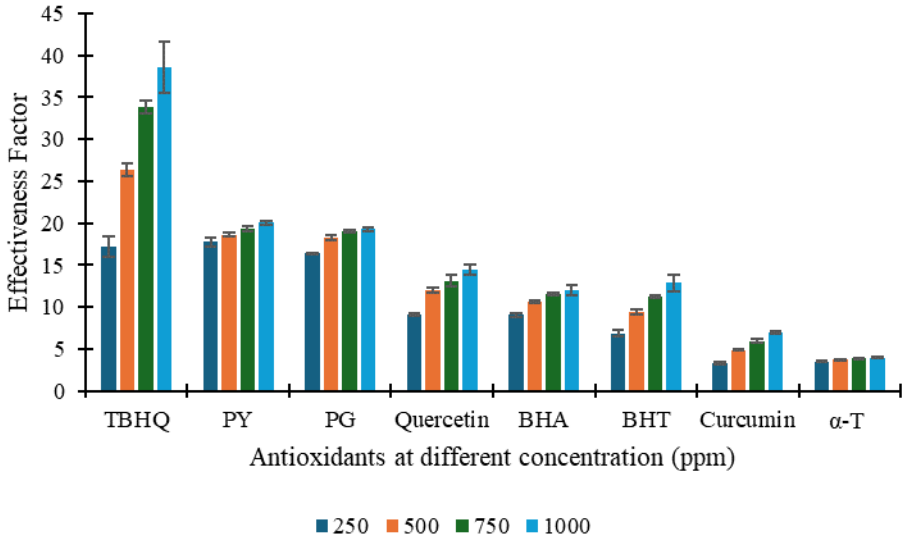

Figure 3.9. Effectiveness factors of synthetic and bio-based antioxidants in DPOME at different concentrations measured using Rancimat.

Overall, all antioxidants at all levels of concentrations were able to raise the initial IP of 5.27 h above the 8 h requirement of EN 14214. The lowest IP of 17.67 h was obtained using 250 ppm of curcumin while the highest IP was recorded at 203.54 h for 1000 ppm TBHQ. The strong effect of TBHQ in protecting DPOME from oxidising implies that lower concentration is sufficient to protection against oxidation during storage, which will reduce cost. Apart from TBHQ, quercetin also showed strong antioxidant capabilities despite being a bio-based antioxidant since it outperformed both BHA and BHT. Nonetheless, it should be noted that BHA, BHT and TBHQ were ranked lower under the DPPH radical scavenging activity tests. The differences in ranking might be due to the

chain inhibition properties of BHA, BHT and TBHQ. These antioxidants donate free hydrogen atoms to free radicals while forming stable radicals that does not continue the oxidation chain (Domingos et al., 2007). Although the literature in general reports a proportionate relationship between DPPH and OSI, these compared natural antioxidants and extracts instead of BHT, BHA and TBHQ (Tura et al., 2019; Roshanpour et al., 2020). Furthermore, the correlation may not always be straightforward as shown in one study whereby BHA dosed samples only had a slightly higher IP value of 6.1 h compared to microwave-assisted hydrodistillation (MAHD) samples with 5.345 h despite having much better IC_{50} value of 0.410 mg/mL compared to 26.973 mg/mL for MAHD (Ghazanfari et al., 2020). It should also be noted that solubility issues were faced during the doping of DPOME whereby curcumin, quercetin and PY were unable to be fully dissolved into the fuel sample leading to slight sediments at the bottom of the containers used. Fuel sampling was therefore problematic for the three antioxidants. The addition of a surfactant will aid in mitigating this. For example, a recent study by Yusri et al. (2020) experimented with the addition of a surfactant to promote the dispersion and solubility of PY in palm biodiesel. The surfactant improved the overall solubility of PY and enhanced its antioxidation ability across four weeks of storage time.

3.6.4.2 Induction period (IP) using PetroOXY

Figure 3.10 illustrates the IP of antioxidants at different concentrations measured using PetroOXY (data in Table A.3). Increasing the concentration of antioxidant extended the IP values, and the effect of concentration was clearly significant for BHA with its step line. Comparing this to the Rancimat results in Figure 3.8, a significant difference was TBHQ

being ranked first for Rancimat, but last for PetroOxy. The ascending order of antioxidant capability in extending IP at 250 ppm was: TBHQ, curcumin, α-T, BHT, PY, quercetin, PG and BHA. At the highest concentration of 1000 ppm, the order was: TBHQ, α-T, curcumin, PY, BHT, quercetin, PG and BHA. The opposite rankings of TBHQ under Rancimat and PetroOXY were also observed in Zhou et al.'s studies (2016, 2017). The authors discussed the thermal degradation of TBHQ under the influence of high temperature and pressure in PDSC. In the present study, the Rancimat test was conducted at 110 °C under atmospheric pressure while the conditions of the PetroOXY test were 140 °C and 700 kPa, representing increments of 27 % and 591 % in temperature and pressure, respectively. Hence, it is likely that degradation of TBHQ occurred under the more extreme conditions of PetroOXY.

Notably, BHA ranked first in terms of its capability in extending the IP of DPOME. The IP value of DPOME with BHA at 250 ppm reached 199.05 min, which was much higher than TBHQ, α-T, curcumin, PY and BHT even at 1000 ppm. The presence of high pressure in the PetroOXY reduced the volatilization losses of BHA which has naturally high volatility (Hwang and Winkler-Moser, 2014) resulting in its higher capability ranking for PetroOXY. When high pressure is present in a system, a higher temperature needs to be attained before volatilization of antioxidants occurs (de Jesus et al., 2020).

Figure 3.10 illustrates that PG, quercetin, BHT and PY had overlapping mid-range IP values over the tested concentrations while curcumin, α-T and TBHQ produced the low IP values, with TBHQ being the least. A point to note as well in the figure is the relatively high standard deviation of quercetin at 1000 ppm, which could be caused by the slight

solubility issue faced with quercetin as discussed previously.

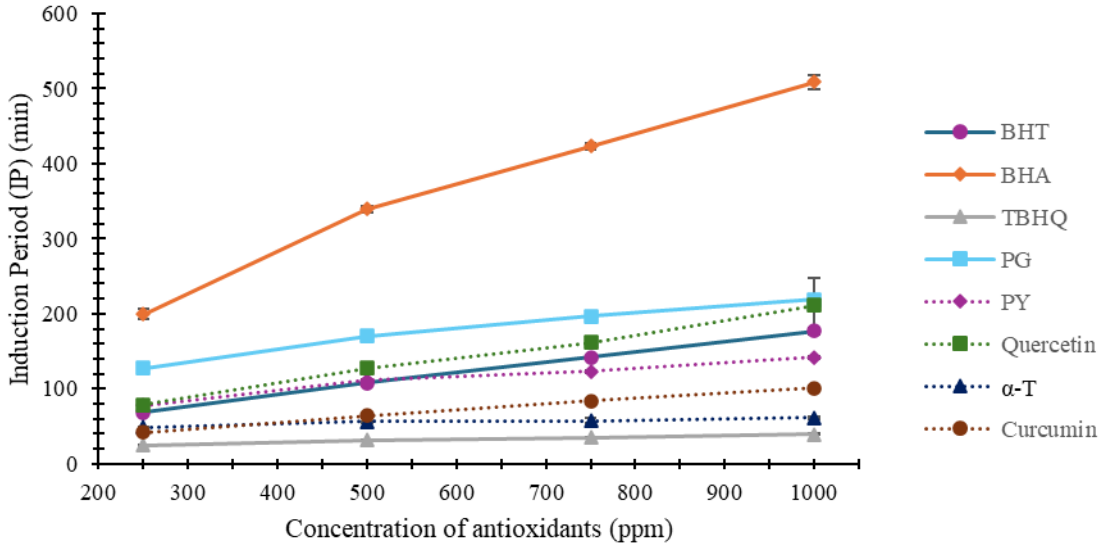

Figure 3.10. Induction periods (IP) of DPOME with synthetic and bio-based antioxidants at different concentrations measured using PetroOXY.

Table 3.7 displays the p-values of the data subjected to both one-way ANOVA and two-way ANOVA tests. The results for all antioxidants were statistically significant in terms of dependence on the concentration since all p-values were lower than 0.05. The highest p-value was recorded at 8.61E-05 for α-T while the lowest was 7.69E-12 for TBHQ. The two-way ANOVA results showed that each variable, namely the type of antioxidant and the concentration of antioxidant, together with the interaction of both variables had extremely low p-values. This indicated that each type of antioxidant was statistically different from one another, as well as the concentration of antioxidant tested. The IP values were also dependent on the interaction of both variables.

Table 3.7. p-values of one-way and two-way ANOVA tests for IP of DPOME with synthetic and bio-based antioxidants (PetroOXY).

One-way ANOVA		Two-way ANOVA	
Antioxidant	p-value	Source of variance	p-value
BHT	3.03E-11	Concentration	7.33E-58
BHA	4.94E-11	Antioxidant	9.08E-83
TBHQ	7.69E-12	Concentration × Antioxidant	4.45E-47
PG	4.72E-09		
PY	1.54E-10		
Quercetin	1.5E-05		
α-T	8.61E-05		
Curcumin	2.33E-09		

Subsequently, the effectiveness factors for DPOME with antioxidants at different concentrations were calculated and plotted as can be seen in Figure 3.11 (data in Table A.4). As for Rancimat, higher concentration resulted in increased effectiveness factor. The effect of concentration was strongest for BHA whereby the effectiveness factor displayed a 2.56-fold increase (155 %) from 11.75 to 30.03 when the concentration was raised from 250 to 1000 ppm. At the other end of the spectrum, α-T only displayed an increase of 25.64 % with the same concentration increment. As for the trends obtained for IP, BHA exerted the highest effectiveness factors while PG, quercetin, BHT and PY had overlapping ranges of effectiveness factors. Curcumin, α-T and TBHQ were the least effective. At 1000 ppm concentration, the ranking of antioxidants in ascending order in terms of effectiveness factor was the same as for IP value: TBHQ, α-T, curcumin, PY, BHT, quercetin, PG and BHA.

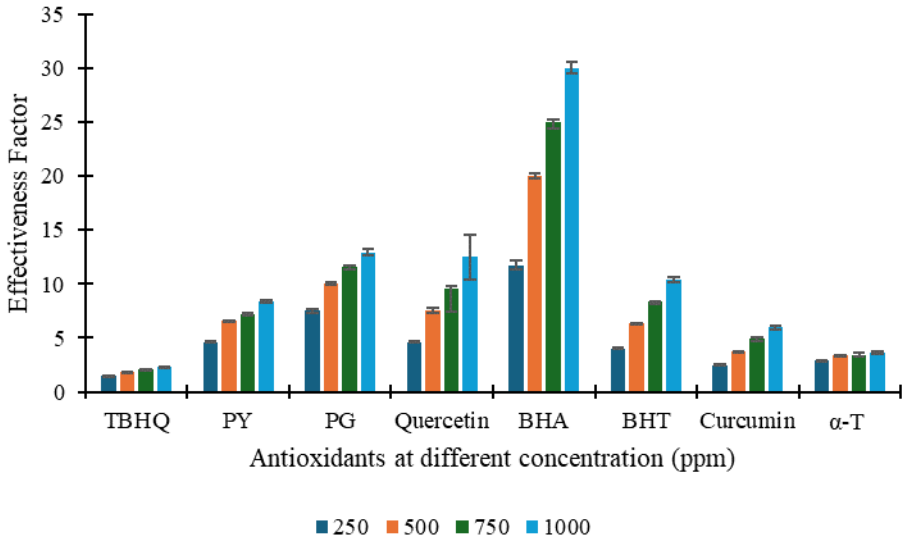

Figure 3.11. Effectiveness factors of synthetic and bio-based antioxidants in DPOME at different concentrations measured using PetroOXY.

3.6.4.3 Correlations between Rancimat and PetroOXY IP values

Overall, the IP values measured using Rancimat had significant correlation with the PetroOXY's IP results for all antioxidants except for PY. This can be seen in Table 3.8 where the p-values of two samples t-test for PY was 0.0770, which was greater than 0.05 while other antioxidants had p-values much lower than 0.05, with α-T having the lowest p-value of 1.03E-11.

Table 3.8. p-values of two samples t-test for DPOME with synthetic and bio-based antioxidants for correlation between Rancimat and PetroOXY results.

Antioxidant	p-value
BHT	8.79E-05
BHA	2.11E-06
TBHQ	1.83E-06
PG	4.66E-06
PY	0.0770
Quercetin	1.94E-04
α-T	1.03E-11
Curcumin	2.30E-05

As of now, there are no limits stated in the EN 14214 or ATSM D6751 standards for IP values measured using PetroOXY. Nonetheless, researchers or practitioners may only have access to PetroOXY instead of Rancimat for IP measurements. Thus, developing correlations between the two test methods is beneficial. Figure 3.12 shows the scatter plots of the Rancimat versus PetroOXY data. The hypothesis that a positive relationship existed between all the Rancimat and PetroOXY data was disproved since linear regression resulted in a low R^2 value of 0.0019 as well as a negative trendline. Hence, it could be said that the overall relationship between the Rancimat and PetroOXY results was statistically insignificant, likely due to the wide variety of antioxidants used in this study. However, linear regression was possible when applied to the same antioxidant at all concentrations, as shown by the regression lines in Figure 3.12. The regression equations or correlations and their R^2 values are tabulated in Table 3.9. The R^2 values ranged from 0.7922 for α-T to 0.9937 for curcumin. All synthetic antioxidants had R^2 values above 0.9 apart from PY at 0.8631. Meanwhile, for bio-based antioxidants, only

curcumin displayed an R^2 value above 0.9. These correlations can be used to predict the Rancimat IP values when one only has access to PetroOXY measurements.

In other words, this meant that it was impossible to relate Rancimat and PetroOXY data as a whole due the complexity of how each antioxidants function in the system, but it was possible to relate the results when sets of data were confined within each antioxidants pile. Application of the correlation between both experimental methods cannot be completed at this stage, unless a more in depth analysis on how each antioxidant works in the system has been conducted.

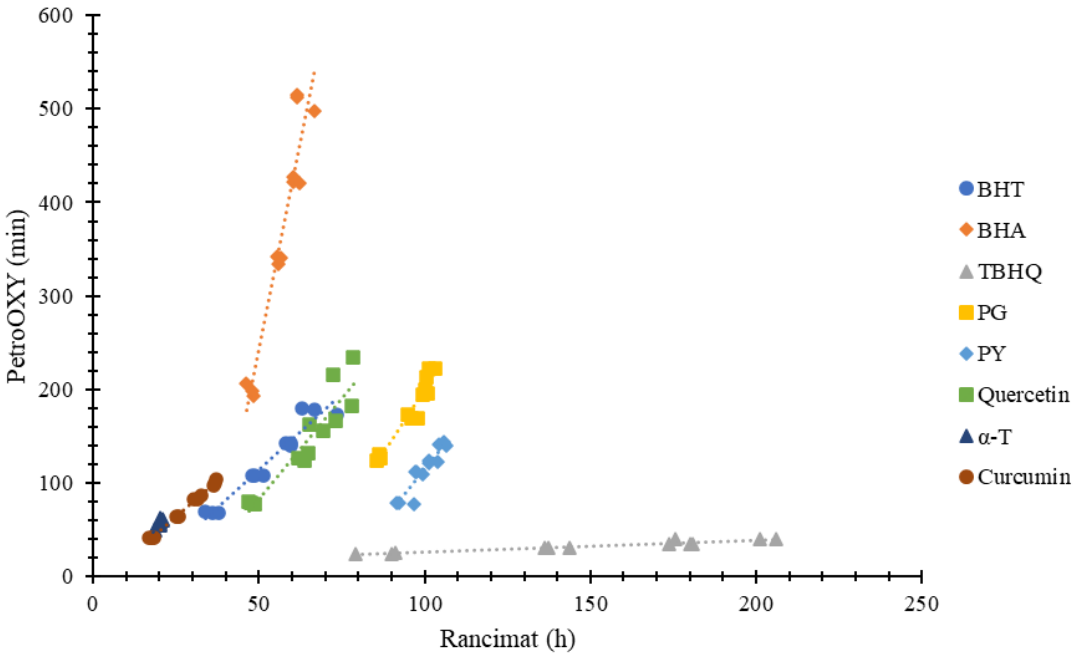

Figure 3.12. Scatter plots and regression lines of PetroOXY versus Rancimat data for individual antioxidants at all concentrations.

Table 3.9. Correlations and R^2 values for Rancimat versus PetroOXY data for individual antioxidants at all concentrations.

Antioxidant	Correlation[a]	R^2

BHT	*y = 3.2354 x – 47.769*	0.9364
BHA	*y = 17.592 x – 634.42*	0.9058
TBHQ	*y = 0.1231 x + 14.374*	0.9318
PG	*y = 5.4136 x – 341.98*	0.9319
PY	*y = 4.4943 x – 334.99*	0.8631
Quercetin	*y = 4.3188 x – 132.51*	0.8709
α-T	*y = 4.9662 x – 42.491*	0.7922
Curcumin	*y = 3.1001 x – 13.546*	0.9937

[a]*y* is the PetroOXY IP (min) and *x* is the Rancimat IP (h).

3.6.4.4 Acid value

Figure 3.13 depicts the acid value of DPOME with synthetic and bio-based antioxidants at different concentrations measured according to EN14104 standard (data in Table A.5). As acid value is used to depict the amount of free fatty acid (FFA) in the sample, their values are expected not to change significantly when compared to DPOME without antioxidants. The acid value of DPOME was 0.2803 mg KOH/g. All tested samples met the maximum limit of 0.50 mg KOH/g except for 1000 ppm of PG which resulted in 0.5044 mg KOH/g. Thus, PG applied at 1000 ppm should be excluded for the subsequent phases of study.

As observed in Figure 3.13, PG and quercetin clearly have increasing acid value trends with concentrations. There are published works investigating the effects of storage time for these two antioxidants but none to date on the relationship between the acid value and the concentration of PG and quercetin. For instance, Yuliarita et al. (2019) reported an acid value of 0.35 mg KOH/g for 500 ppm of PG in commercial biodiesel while 0.06 mg KOH/g acid value was obtained for 1000 ppm of PG in commercial biodiesel (50 %

rapeseed oil, 20 % sunflower oil, 30 % waste cooking oil) by Karavalakis et al. (2011). Here, a plausible explanation is that the natural acidity of these antioxidants affected the acid value thereby elevated readings were recorded for increased concentration levels. PG is a trihydroxybenzoic acid (Park, 2021) while quercetin is a weak pentabasic acid (Chebotarev & Snigur, 2014).

Table 3.10 lists the one-way and two-way ANOVA p-values for acid value. From the one-way ANOVA test, all antioxidants except PG and quercetin had p-values > 0.05. Thus, these results were not statistically different when the concentration increased and the null hypothesis of concentration having no effect on the acid value of DPOME was accepted for BHT, BHA, TBHQ, PY, α-T and curcumin. In contrast, the p-values of PG and quercetin indicated that the results were statistically different, which meant that the acid value increased when the concentration increased.

Meanwhile, the p-values of two-way ANOVA test highlighted that the results were statistically significant for each variable when all antioxidants were included. However, it is important to note that p-value for concentration of antioxidant after excluding PG and quercetin was 0.6002 whereas the p-value for the interaction between both variables was 0.3824. This confirmed that the results for all antioxidants except PG and quercetin were neither dependent on the concentration nor on the interaction between both variables. On the contrary, the results were shown to be statistically dependent on the type of antioxidant used.

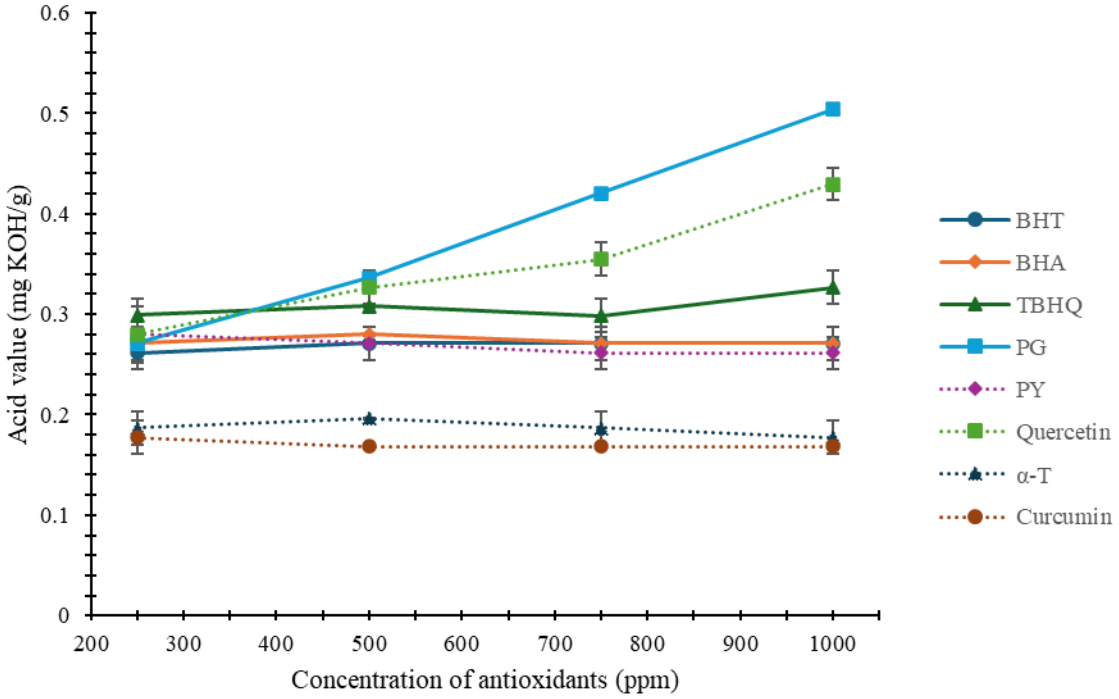

Figure 3.13. Acid values of DPOME with synthetic and bio-based antioxidants at different concentrations measured according to EN14104 test method.

Table 3.10. p-values of one-way and two-way ANOVA tests for acid value of DPOME with synthetic and bio-based antioxidants.

One-way ANOVA		Two-way ANOVA	
Antioxidant	p-value	Source of variance	p-value
BHT	0.8584	All antioxidants	
BHA	0.8043	Concentration	1.59E-16
TBHQ	0.1187	Antioxidant	2.52E-47
PG	2.3567E-09	Concentration × Antioxidant	4.23E-23
PY	0.3653	Excluding PG and quercetin	
Quercetin	1.0823E-04	Concentration	0.6002
α-T	0.4868	Antioxidant	1.66E-30
Curcumin	0.4378	Concentration × Antioxidant	0.3824

3.6.4.5 Iodine value

Figure 3.14 illustrates the iodine value of DPOME with synthetic and bio-based antioxidants at different concentrations measured according to EN14111 standard (data in Table A.6). The iodine value determines the level of unsaturation in the sample. Similar to the acid value, the iodine value is expected to remain approximately the same as DPOME which had a value of 49.9023 g I_2/100 g. From Figure 3.14, curcumin notably had the highest iodine value across all concentrations, which could be attributed to the presence of three allylic carbon bonds in its chemical structure as shown in Figure 3.15. Fluctuating trends could be observed across the concentration of antioxidants which could be due to constraints in incubation and sampling times. In the case of PY and quercetin, their lack of solubility could be a contributing factor. Nonetheless, all samples passed the standard maximum limit of 120 g I_2/100 g for iodine value.

From one-way ANOVA, all antioxidants except BHT had p-values higher than 0.05 as summarized in Table 3.11, with the highest p-value recorded at 0.9606 for PG and the lowest at 0.0121 for BHT. The p-values >0.05 showed that the concentrations of antioxidants had statistically insignificant effects on the measured iodine values of samples. Therefore, the null hypothesis of iodine value being independent of concentration of antioxidant was accepted for all tested antioxidants except BHT. In other words, the fluctuations seen in Figure 3.15 excluding BHT are not considered significant trends. It was also observed that the p-values of TBHQ, PG and curcumin were the highest among the eight tested antioxidants, which corresponded to relatively flat lines seen in Figure 3.15. Additionally, the two-way ANOVA test results seen in Table 3.11 also support the hypothesis that concentration has no significant effect on iodine value since

the p-value of concentration and interaction of concentration and type were 0.3908 and 0.1866, respectively. The p-value of 2.64E-11 for type of antioxidant implied that the iodine value was significantly dependent on the said variable.

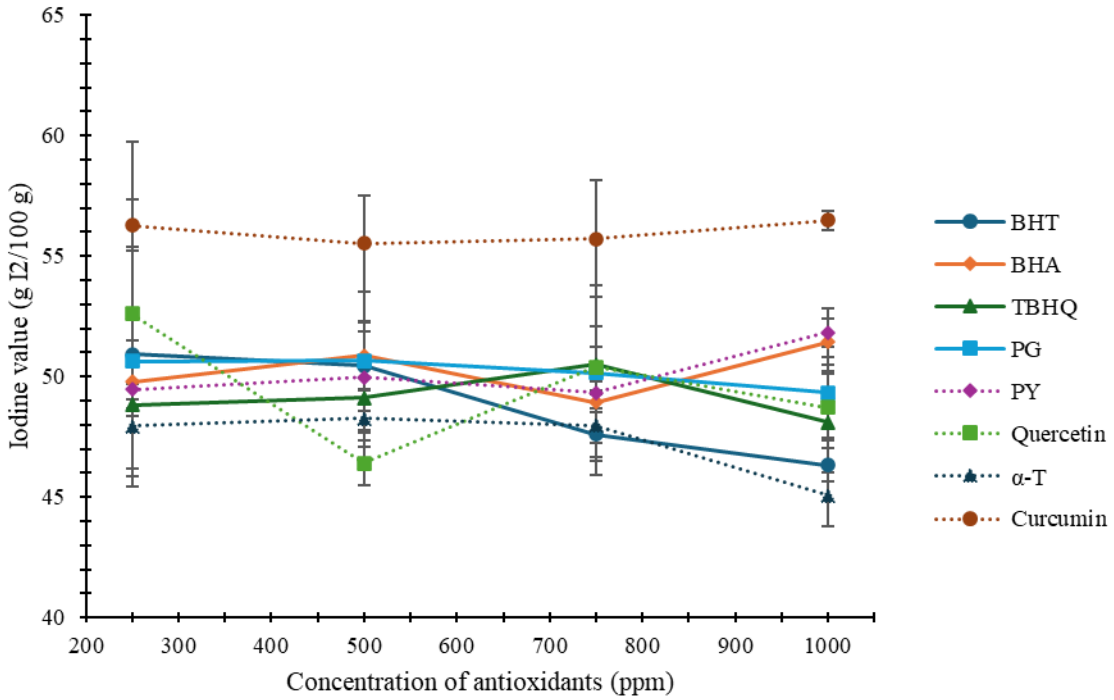

Figure 3.14. Iodine values of DPOME with synthetic and bio-based antioxidants at different concentrations measured according to EN14111 test method.

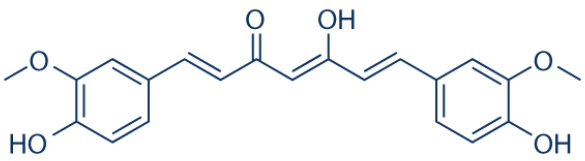

Figure 3.15. Chemical structure of curcumin.

Table 3.11. p-values of one-way and two-way ANOVA tests for iodine value of DPOME with synthetic and bio-based antioxidants.

One-way ANOVA		Two-way ANOVA	
Antioxidant	p-value	Source of variance	p-value
BHT	0.0121	Concentration	0.3908
BHA	0.1684	Antioxidant	2.64E-11
TBHQ	0.6240	Concentration × Antioxidant	0.1866
PG	0.9606		
PY	0.1735		
Quercetin	0.2991		
α-T	0.1259		
Curcumin	0.8818		

3.6.4.6 Kinematic viscosity

Figure 3.16 illustrates the kinematic viscosity of DPOME with bio-based and synthetic antioxidants at 40 °C for different concentrations measured according to EN ISO 3104 standard (data in Table A.7). The kinematic viscosity of DPOME was recorded at 4.3884 mm^2/s. Generally, as the concentration of antioxidant increases, the kinematic viscosity increases since the amount of solute per unit volume is higher which causes the sample to become more viscous. This effect is more prominent for TBHQ, PY, PG and curcumin. The exception to the trend was quercetin whereby the kinematic viscosity fell from 500 to 750 ppm, then rose again at 1000 ppm, which could be linked to its lack of solubility. The measured kinematic viscosities mostly ranged from 4.3900 to 4.3960 mm^2/s, but TBHQ, PY, PG and curcumin exceeded the 4.4000 mm^2/s at higher concentration levels. The results are in line with the findings of Kivevele and Huan (2013) which reported the increase in concentration of PY increased the kinematic viscosity of *M. oleifera* methyl

ester, *C. megalocarpus* methyl ester and *J. curcus* methyl ester. Conversely, increased kinematic viscosities were not observed for PY and BHA in another study (Goh et al., 2022). Hence, it was hypothesised that the changes in the initial kinematic viscosity upon addition of antioxidants were dependent on both the type of antioxidant and type of biodiesel. While the kinematic viscosity of all samples were within the permitted range of 3.5 to 5.0 mm^2/s as stipulated in EN 14214, the higher kinematic viscosities of TBHQ, PY, PG and curcumin at high concentrations may very well exceed the maximum limit during the long-term stability study when fuel oxidation or degradation occurs, forming compounds which increase fluid viscosity. Increased fuel viscosity will often lead to problems related engine performances. As such, lower concentration of these antioxidants should be considered if they were to be selected.

From Table 3.12, the one-way ANOVA test results implied that the kinematic viscosities for all antioxidants except BHT ($p=0.0887$) were significantly dependent on their concentrations. As for iodine value, antioxidants with higher p-values tend to have relatively flat lines and vice versa. The two-way ANOVA test results as listed in Table 3.25 also showed that the kinematic viscosity was statistically dependent on the concentration and type of antioxidant with extremely low p-values ($<<0.05$). Furthermore, the p-value of 2.91E-37 obtained for the interaction between concentration and type of antioxidant indicated that the results depended too on this factor.

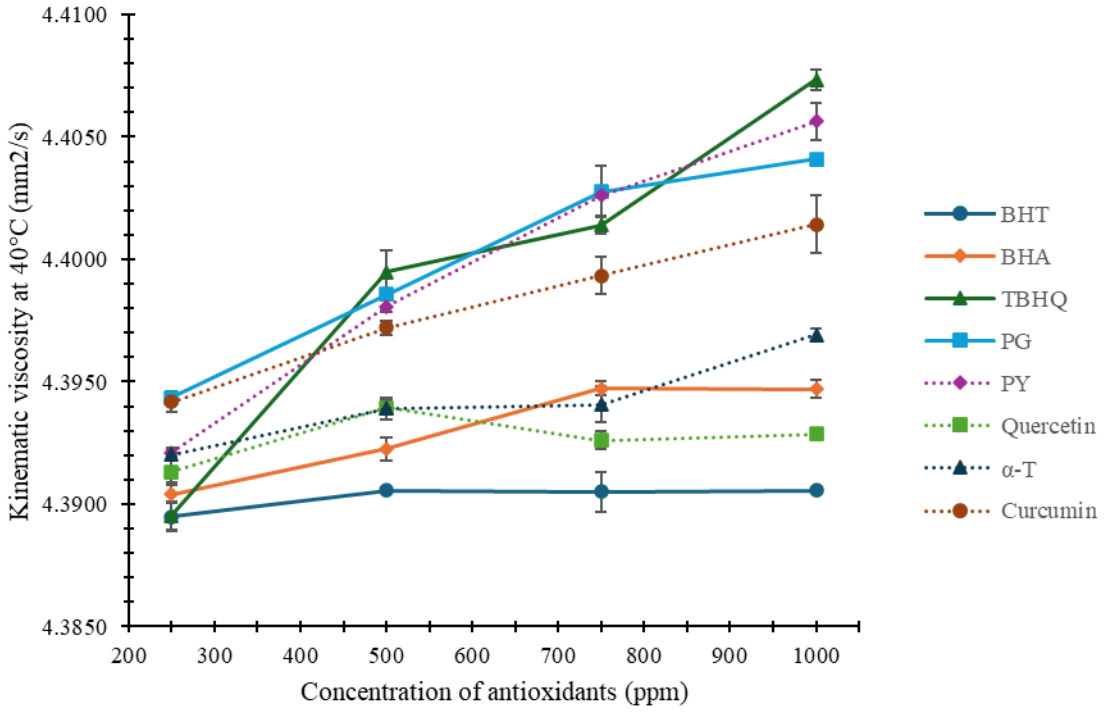

Figure 3.16. Kinematic viscosities of DPOME with synthetic and bio-based antioxidants at 40°C for different concentrations measured according to EN ISO 3104 test method.

Table 3.12. p-values of one-way and two-way ANOVA tests for kinematic viscosity of DPOME with synthetic and bio-based antioxidants.

One-way ANOVA		Two-way ANOVA	
Antioxidant	p-value	Source of variance	p-value
BHT	0.0887	Concentration	9.8E-53
BHA	1.37E-06	Antioxidant	5.99E-57
TBHQ	2.41E-09	Concentration × Antioxidant	2.91E-37
PG	9.09E-08		
PY	7.58E-10		
Quercetin	8.48E-05		
α-T	8.78E-06		
Curcumin	1.45E-05		

3.7 Concluding remarks

Assessment of the effects of synthetic and bio-based antioxidants on DPOME at different concentration levels has been completed. Table 3.13 compares the main results of this first phase of the study. The results of Rancimat IP and effectiveness factor, as well as acid value and iodine value, indicated that TBHQ was the most effective antioxidant. However, the kinematic viscosity of DPOME with TBHQ increased markedly above 500 ppm. Nevertheless, the application of TBHQ at 250 ppm increased the IP value significantly from 5.27 h to 90.71 h, which corresponded to an effectiveness factor of 17.21. Thus, a much lower concentration can be applied in the case of TBHQ, which will also mitigate the high viscosity. A notable finding was the reverse ranking of TBHQ in terms of IP when tested using PetroOXY, which was likely caused by its degradation under the more extreme conditions of PetroOXY.

PY, PG, BHT, BHA and quercetin demonstrated mid-range to high effectiveness in terms of IP under Rancimat and PetroOXY tests. Nevertheless, PY, quercetin and curcumin could not be dissolved fully in DPOME. In practice, solubility of antioxidants is vital as formation of sediments may lead to adverse engine performance during combustion of biodiesel. It was clear too that α-T and curcumin had the least effects on IP and effectiveness factor. Meanwhile, all measured oxidation stability and other physicochemical properties except acid value for 1000 ppm of PG met the limits of EN 14214 standard.

One-way and two-way ANOVA tests were carried out on the data acquired. The IP values for Rancimat as well as PetroOXY were significantly dependent on concentration of

antioxidant from one-way ANOVA while two-way ANOVA demonstrated the dependence on concentration of antioxidant, type of antioxidant and the interaction of both variables. The acid value was shown to be significantly dependent on concentration only for PG and quercetin from one-way ANOVA, which could be linked to their natural acidity. From two-way ANOVA, only the type of antioxidant had significant effect on acid value when PG and quercetin were excluded. Apart from that, the concentration had insignificant effect on iodine value except for BHT from one-way ANOVA while two-way ANOVA showed that only the antioxidant type impacted the iodine value. Lastly, kinematic viscosity significantly depended on the concentration of antioxidant except for BHT from one-way ANOVA whereas two-way ANOVA indicated significant dependence on concentration, type as well as the interaction of both variables.

Correlations based on linear regression were developed to predict the Rancimat IP values based on the IP values obtained by PetroOXY. The R^2 of the correlations ranged within 0.7922 (α-T) – 0.9937 (curcumin). These correlations would be beneficial if one only has access to PetroOXY equipment for IP measurements but needs to translate these so that they can be compared to biodiesel standards.

For the next phase of study, PY, quercetin and curcumin were excluded due to their lack of solubility. In addition, PG was ruled out for failing to meet the acid value limit of EN 14214:2012 at 1000 ppm. The contradictory IP rankings of TBHQ and BHA measured using Rancimat and PetroOXY were a point of interest in this study, which warranted further elucidation. Meanwhile, BHT produced good, mid-range results in all tests and can act as a good baseline. Although α-T and curcumin were the least effective, curcumin

had higher iodine value and kinematic viscosities. Hence, α-T was included in the next phase as well to represent a bio-based antioxidant. Despite being ranked low, the oxidation stability and other properties with α-T were still within the EN 14214:2012 limits. In summary, TBHQ, BHA, BHT and α-T were selected to be added to DPOME for the appraisal of oxidation kinetics and thermodynamics.

Table 3.13. Comparison of main results from Phase 1 of study.

IP and effectiveness factor		Acid value	Iodine value	Kinematic viscosity
Rancimat	PetroOXY			
High: TBHQ, PY, PG Mid-range: BHT, BHA, quercetin Low: α-tocopherol, curcumin All IP met EN 14214	High: BHA Mid-range: PG, quercetin, BHT and PY Low: α-tocopherol, curcumin, TBHQ	All except 1000 ppm PG met EN 14214	All met EN 14214; curcumin noticeably the highest	All met EN 14214; TBHQ increased markedly above 500 ppm
OWA[a]: Significant dependence on concentration	OWA: Significant dependence on concentration	OWA: Significant dependence on concentration only for PG and quercetin	OWA: Significant dependence on concentration only for BHT	OWA: Significant dependence on concentration (except BHT)
TWA[b]: Significant dependence on concentration, type, concentration × type	TWA: Significant dependence on concentration, type, concentration × type	TWA: Significant dependence on type. PG and quercetin had significant dependence on concentration, type, concentration × type	TWA: Significant dependence on type	TWA: Significant dependence on concentration, type, concentration × type
Solubility issues with curcumin, quercetin, PY				

[a]One-way ANOVA

[b]Two-way ANOVA

4. Oxidation kinetics and thermodynamics of palm biodiesel with additives

4.1 Introduction

This chapter focuses on the second phase of study aiming to appraise the oxidation kinetics and thermodynamics of palm biodiesel with the selected additives of TBHQ, BHA, BHT and α-tocopherol. The doped fuel samples were subjected to accelerated oxidation tests within the temperature range of 100 to 130 ºC. The acquired experimental IP data were regressed against different kinetic models and error functions were applied to statistically analyse the validity of the regression results and decide on the best model. Thereafter the rate constants, activation energies and pre-exponential factors under selected order of reaction were determined using the Arrhenius equation. Meanwhile, thermodynamics parameters such as the enthalpy and entropy of oxidation as well as the Gibbs free energy of activation were calculated based on thermodynamic principles and the Eyring equation or activation complex theory. Overall, this phase allowed the kinetics of oxidation of DPOME with and without antioxidants and the nature of the oxidation process such as endothermicity and spontaneity to be established.

4.2 Materials

Butylated hydroxyanisole (BHA, ≥ 98.5 %), 2,6-di-tert-butyl-4-methylphenol (BHT, 99 %), tert-butylhydroquinone (TBHQ, 97 %), and α-tocopherol (α-T, 96 %) were purchased from Sigma Aldrich (M) Sdn. Bhd. All reagents and chemicals were of analytical grade. Refined bleached deodorized B100 palm oil methyl ester (RPOME) was

provided by Sime Darby Oils Biodiesel Sdn. Bhd.

RPOME was vacuum distilled at 210 °C and 720 rpm using a laboratory-scale distillation set up connected to a vacuum pump until 5–10 % of RPOME remained. The resulting distilled palm oil methyl ester (DPOME) was stored at –20 °C immediately after distillation and thawed when used in the experiments. The thawing temperatures were kept below 40 °C. The recovery rate for 1.5 L of sample was recorded at 80% with a loss of 5% during vacuum suction and the remaining 15 % being thick yellowish liquid.

4.3 Accelerated oxidation of DPOME with additives

The antioxidants BHA, BHT, TBHQ and α-T were dosed into DPOME at a concentration level of 100 ppm based on results from previous chapter. All samples, including the control DPOME, were tested with an 892 Professional Rancimat (Metrohm, Switzerland) at temperatures of 100, 110, 120 and 130 °C. The conductivity (Λ) versus time (t) data were collected from the equipment for all runs for the kinetics modelling and thermodynamics analyses.

4.4 Kinetics modelling and thermodynamics analyses

The experimental data were regressed against the zeroth, first and second order of reaction models as expressed by Eqn. 4.1–Eqn. 4.3, respectively. From the regression, the reaction rate constants (k) were determined. Subsequently, the logarithmic form of the Arrhenius equation (Eqn. 4.4) was applied for the calculation of activation energy (E_a) where the value was determined from the gradient ($-E_a/R$) of the plot of ln k versus $1/T$, as shown in Eqn. 4.5.

0^{th} order: $A_t = -kt + A_0$ (Eqn. 4.1)

1^{st} order: $\ln A_t = kt + \ln A_0$ (Eqn. 4.2)

2^{nd} order: $1/A_t = kt + 1/A_0$ (Eqn. 4.3)

where A_t is the conductivity at t, k is the rate constant in $molL^{-1}h^{-1}$ (0^{th} order), h^{-1}(1^{st} order) and $Lmol^{-1}h^{-1}$ (2^{nd} order), t is time in h and A_0 is the initial conductivity.

$$k = A \exp(-E_a/(RT)) \quad \text{(Eqn. 4.4)}$$

$$\ln k = \ln A - E_a/(RT) \quad \text{(Eqn. 4.5)}$$

where k is the rate constant in $molL^{-1}h^{-1}$ (0^{th} order), h^{-1}(1^{st} order) and $Lmol^{-1}h^{-1}$ (2^{nd} order), A is the pre-exponential factor, R is the ideal gas constant (8.314510 $JK^{-1}mol^{-1}$), T is the temperature in Kelvin, E_a is the activation energy in $kJmol^{-1}$.

Meanwhile, the Gibbs free energy, $\Delta G^{\ddagger}$ ($kJmol^{-1}$) is related to the equilibrium constant, $K^{\ddagger}$, enthalpy change, $\Delta H^{\ddagger}$ ($kJmol^{-1}$) and entropy change, $\Delta S^{\ddagger}$ ($JK^{-1}mol^{-1}$) thermodynamically as shown in Eqn. 4.6 and 4.7. Combining Eqn. 4.6 and 4.7 results in Eqn. 4.8 as shown.

$$\Delta G^{\ddagger} = -RT \ln K^{\ddagger} \quad \text{(Eqn. 4.6)}$$

$$\Delta G^{\ddagger} = \Delta H^{\ddagger} - T\,\Delta S^{\ddagger} \quad \text{(Eqn. 4.7)}$$

$$\ln K^{\ddagger} = -\Delta H^{\ddagger}/(RT) + \Delta S^{\ddagger}/R \quad \text{(Eqn. 4.8)}$$

where R the ideal gas constant (8.314510 $JK^{-1}mol^{-1}$), T is the temperature in Kelvin k_b is the Boltzmann constant (1.381×10^{-23} JK^{-1}) and h is the Planck's constant (6.626×10^{-34} Js).

Since $K^{\ddagger}$ is also defined by Eqn. 4.9, the substitution of Eqn. 4.9 into Eqn. 4.8 results in the linear form of the Eyring Equation as expressed by Eqn. 4.10.

$$K^{\ddagger} = kh/k_bT \quad \text{(Eqn. 4.9)}$$

$$\ln (k/T) = -\Delta H^{\ddagger}/(RT) + \ln (k_b/h) + \Delta S^{\ddagger}/R \quad \text{(Eqn. 4.10)}$$

where k_b is the Boltzmann constant (1.381×10^{-23} JK^{-1}) and h is the Planck's constant (6.626×10^{-34}Js).

Using the plot of ln (k/T) versus $1/T$, $\Delta H^{\ddagger}$ and $\Delta S^{\ddagger}$ were calculated from the gradient ($-\Delta H^{\ddagger}/R$) and y-intercept ($\Delta S^{\ddagger}/R + \ln (k_b/h)$), respectively. Finally, $\Delta G^{\ddagger}$ was calculated using Eqn. 4.7 with the obtained $\Delta H^{\ddagger}$ and $\Delta S^{\ddagger}$ values.

4.5 Error functions

Error functions were applied jointly with the regression analyses to elucidate the best-fit kinetic model. As different error functions provide different insights to the regression analyses, five error functions were chosen, namely, the correlation (R), coefficient of determination (R^2), sum of squares errors (*ERRSQ/SSE*), sum of absolute errors (*SAE*) and chi-square test (χ^2). The error functions are defined in the following along with their mathematical equations (Eqn. 4.11–4.15) whereby t is time (h), t_{mean} is mean of time (h), and for zeroth order, A is the experimental conductivity (µS/cm), A_{mean} is the mean of conductivity (µS/cm) and A_{pred} is the predicted conductivity (µS/cm). For first and second order, A is substituted by ln A and $1/A$, respectively. This applies to all respective A, A_{mean} and A_{pred}.

4.5.1 Correlation (R)

Correlation determines the relationship between two variables, which in the case of this study, were conductivity and time. It measures the relationship between two variables,

without explaining how one variable affects the other variable. Correlation is the most basic error function that ranges from -1 to 1, whereby a negative value shows that both variables are inversely proportionate and vice versa. A value closer to 0 implies that the gradient of the plot is close to 0. Correlation is defined by the Eqn. 4.11.

$$R = \frac{\sum(t - t_{mean})(A - A_{mean})}{\sqrt{\sum(t - t_{mean})^2 \sum(A - A_{mean})^2}} \quad \text{(Eqn. 4.11)}$$

4.5.2 Coefficient of determination (R^2)

Coefficient of determination (R^2) is commonly used to validate the fitting of the line of best fit to the scatterplot. It also represents the variance of mean value (Serafin and Dziejarski, 2023). As R^2 is equal to the square of correlation, the closer the R^2 value is to 1, the more fitting the model is for the experimental data. The formula for R^2 is shown by Eqn. 4.12.

$$R^2 = \left(\frac{\sum(t - t_{mean})(A - A_{mean})}{\sqrt{\sum(t - t_{mean})^2 \sum(A - A_{mean})^2}}\right)^2 \quad \text{(Eqn. 4.12)}$$

4.5.3 Sum of squares errors (ERRSQ/SSE)

Sum of squares errors (*ERRSQ/SSE*) is expressed by the following Eqn. 4.13. A low *ERRSQ* value translates to smaller difference between the experimental and predicted results, thus implying that the results are highly accurate. However, in cases where the data is of a large number, the *ERRSQ* is not suitable to be used as an indicator for the accuracy of the data.

$$ERRSQ = \sum (A - A_{pred})^2 \quad \text{(Eqn. 4.13)}$$

4.5.4 Sum of absolute errors (SAE)

Sum of absolute errors (*SAE*) calculates the overall sum of error by using modulus. This way of calculation eliminates the need of squaring the errors in *ERRSQ* and provides a better understanding of the accuracy of data with larger numbers. The *SAE* is defined in Eqn. 4.14.

$$SAE = \sum |(A - A_{pred})| \quad \text{(Eqn. 4.14)}$$

4.5.5 Chi-square test (χ^2)

The chi-square test (χ^2) on the other hand calculates the squared difference of the predicted and experimental data, then divides that by the experimental data. Eqn. 4.15 shows the formula for χ^2:

$$\chi^2 = \sum \frac{(A_{pred} - A)^2}{A} \quad \text{(Eqn. 4.15)}$$

4.6 Results and discussion

4.6.1 Rancimat induction period (IP)

Table 4.1 lists the Rancimat IP values for all samples at all tested temperatures. All samples had the highest IP values when tested at the lowest temperature of 100 °C, with the highest being BHA. Overall, the IP values in decreasing order were BHA > TBHQ > BHT > α-T > DPOME. This trend held true for all temperatures except 130 °C, whereby

α-T had a higher IP value of 3.2800 h compared to BHT (3.0133 h). It was also observed that the IP values of all samples with antioxidants were nearly halved with every 10 °C increment in temperature. Contrastingly, for DPOME, the decreasing trend was less drastic.

Table 4.1. Rancimat induction periods (IP) for DPOME with and without antioxidants.

Temperature (°C)	Rancimat induction period (IP) (h)[a]				
	DPOME	BHA	BHT	TBHQ	α-T
100	3.8667 ± 0.0666	64.0067 ± 0.9184	30.0533 ± 0.5582	44.9500 ± 1.3859	24.9967 ± 0.6292
110	2.4733 ± 0.0416	28.8433 ± 0.3808	14.5933 ± 0.4572	19.6800 ± 0.3985	12.2367 ± 0.0751
120	1.7433 ± 0.0208	13.6067 ± 0.2468	6.2667 ± 0.0850	10.0300 ± 0.0608	6.2433 ± 0.0643
130	1.2233 ± 0.0208	6.6133 ± 0.0153	3.0133 ± 0.0351	5.1300 ± 0.0819	3.2800 ± 0.0436

[a]Average of triplicates ± standard deviation.

4.6.2 Error functions of zeroth, first and second order kinetic models

Table 4.2 tabulates the error functions, namely *R*, R^2, *ERRSQ*, *SAE* and χ^2 for the zeroth order, first order, and second order kinetic models for DPOME with and without antioxidants. The *R* values for the zeroth and first order models were positive while they were negative for the second order model, which corresponded to positive and negative slopes for the respective plots. As seen in Table 4.1, the *R* values were lower for the zeroth order (0.6033–0.9701) compared to the first order (0.8381–0.9908). Meanwhile, the *R* ranged from -0.5800 till -0.8584 for the second order model. The results suggested that the first order kinetic model was best suited to describe the experimental data.

All samples had the highest R^2 values when tested under the assumption of first order of reaction except DPOME at 130 °C. Nonetheless, the R^2 value for DPOME at 130 °C was still considered high at 0.9239 under the first order model. Overall, the first order model had best R^2 values ranging from 0.7024 to 0.9817 as compared to 0.3640 to 0.9411 for the zeroth order, and 0.3364 to 0.7368 for the second order. Ideally, the values of R^2 should be as close to 1 as possible since they indicate how close the data is to the mean. Like *R*, the R^2 also supports the first order model for the description of kinetic data.

As aforementioned, the *ERRSQ* was unsuitable for analysis of data with larger number. This was immediately reflected upon regression analysis under the zeroth order. The large range of values for conductivity greatly increased the squared errors in the calculations. This however was not present for the first and second order of reactions as the conductivity was expressed in ln *A* and *1/A*, both of which minimized the raw conductivity data for higher accuracy. Even so, the calculations were solely based on the errors of the experimental results compared to the predicted results. The scaling of data with natural log and inverse functions rendered the *ERRSQ* unsuitable to compare or draw any conclusions on the best fit order of reaction.

Compared to *ERRSQ*, *SAE* eliminated the squared errors which moderated the effect of the data with a large range of values for the zeroth order. However, the base concept of *SAE* is similar to *ERRSQ* with results scaled with the use of natural log and inverse functions for higher orders of reaction thus making it hard to draw any conclusions solely based on *SAE*.

Finally, the χ^2 is the ratio of the errors between predicted and experimental data divided

by the experimental data. This error function provided better grounds to compare between the models as the errors were scaled accordingly with the relative scales of the natural log and inverse functions. Nonetheless, the χ^2 values for the zeroth order model still ranged from 977.734 to 7967.504 due to the conductivity data which ranged from 0 to 300 µS/cm. Thus, the large difference between both ends with the overall mean led to the large χ^2 values. In contrast, the first order and second order models that used natural log and inverse functions greatly reduced the χ^2 values, with ranges of 1.4785 to 15.4118 and 20.7353 to 169.2339, respectively. Theoretically, χ^2 values would be close to 0 as the errors between the predicted and experimental data approach 0 for absolute fit. In this case, the first order kinetic model was the most suitable to be used to describe the dataset.

Summarily, the order of suitability of error functions used to determine the best fit model or in other words, the order of oxidation reaction, was: $\chi^2 > R^2 > SAE > ERRSQ > R$. Hence, the oxidations of all samples with different antioxidants and under different temperatures were concluded to follow first order reaction kinetics based on error functions analyses.

Table 4.2. Error functions of zeroth, first and second order kinetic models for DPOME with and without antioxidants.

Model	Zeroth order					First order					Second order				
130 °C	*R*	R^2	*ERRSQ*	*SAE*	χ^2	*R*	R^2	*ERRSQ*	*SAE*	χ^2	*R*	R^2	*ERRSQ*	*SAE*	χ^2
DPOME	0.9701	0.9411	23150.69	853.920	977.734	0.9612	0.9239	7.5267	15.1104	7.9285	-0.7025	0.4935	1.9242	7.7302	97.3922
BHA	0.8526	0.7269	123945.40	2576.461	7967.504	0.9720	0.9448	9.7340	22.3412	5.0461	-0.8395	0.7047	3.3738	13.3582	114.483
BHT	0.7398	0.5474	87075.35	1624.091	2818.008	0.9574	0.9164	7.2897	17.0822	3.9261	-0.7516	0.5649	3.0705	10.4016	85.0283
TBHQ	0.8656	0.7492	105944.50	2298.648	5297.900	0.9873	0.9747	3.8693	14.0380	2.1567	-0.8212	0.6744	2.2665	11.0435	84.5707
α-T	0.7652	0.5855	78836.76	1342.311	4237.210	0.9318	0.8682	11.0664	17.9101	4.8097	-0.8306	0.6900	0.9402	4.9002	19.7756
120 °C	*R*	R^2	*ERRSQ*	*SAE*	χ^2	*R*	R^2	*ERRSQ*	*SAE*	χ^2	*R*	R^2	*ERRSQ*	*SAE*	χ^2
DPOME	0.9496	0.9017	38533.42	1227.813	1470.203	0.9857	0.9715	3.0323	10.8653	1.4784	-0.7845	0.6155	1.1452	6.6534	56.8810
BHA	0.7621	0.5808	104712.60	1864.142	5902.544	0.9297	0.8643	14.4586	23.3924	6.4169	-0.8288	0.6869	1.7503	7.4848	45.3592
BHT	0.6919	0.4788	84526.49	1484.501	1937.915	0.9383	0.8804	8.0909	16.7807	4.6474	-0.7122	0.5072	1.4694	7.4232	35.8764
TBHQ	0.7744	0.5997	95615.30	1782.295	3951.654	0.9502	0.9028	8.8341	18.2978	3.3644	-0.8584	0.7368	0.8286	5.2691	24.6001
α-T	0.6943	0.4820	86274.65	1438.060	4258.658	0.8955	0.8019	14.5653	19.5913	5.6257	-0.8303	0.6894	0.9647	5.0226	20.7353
110 °C	*R*	R^2	*ERRSQ*	*SAE*	χ^2	*R*	R^2	*ERRSQ*	*SAE*	χ^2	*R*	R^2	*ERRSQ*	*SAE*	χ^2
DPOME	0.9329	0.8704	57446.57	1684.580	2243.289	0.9891	0.9782	3.1380	11.3501	4.1660	-0.7387	0.5456	4.1598	14.3523	169.234
BHA	0.6643	0.4413	78783.14	1352.654	2803.748	0.9086	0.8256	11.8747	18.5390	4.3737	-0.8101	0.6563	1.2906	6.3871	29.5457
BHT	0.6247	0.3902	203696.70	2220.744	3543.086	0.8977	0.8059	14.5680	22.7442	8.1566	-0.6544	0.4282	3.2419	10.8129	103.769
TBHQ	0.6729	0.4528	81564.26	1438.071	1684.332	0.9169	0.8408	9.5044	18.8721	3.8756	-0.7258	0.5268	1.3059	7.0446	32.0954
α-T	0.6721	0.4517	78834.41	1232.905	2149.265	0.9156	0.8382	9.5372	15.8278	4.3722	-0.7322	0.5361	1.7166	6.6913	44.8501
100 °C	*R*	R^2	*ERRSQ*	*SAE*	χ^2	*R*	R^2	*ERRSQ*	*SAE*	χ^2	*R*	R^2	*ERRSQ*	*SAE*	χ^2
DPOME	0.9195	0.8454	47030.85	1215.720	1776.094	0.9908	0.9817	1.8198	7.1533	3.0545	-0.7318	0.5355	2.5655	8.7957	102.219
BHA	0.6589	0.4342	103948.90	1551.869	2288.824	0.8948	0.8006	11.8919	18.9662	5.6452	-0.6796	0.4619	1.0811	6.1474	27.2564
BHT	0.6033	0.3640	591703.70	3662.579	7699.255	0.8381	0.7024	23.5489	28.2981	12.511	-0.5800	0.3364	2.8691	9.5641	155.495
TBHQ	0.6142	0.3772	172619.20	2052.040	3180.759	0.8885	0.7895	14.6963	22.6363	5.5520	-0.7092	0.5030	1.8090	8.3984	52.2863
α-T	0.6420	0.4122	343499.00	2864.365	7731.510	0.8549	0.7308	20.3268	36.5677	15.412	-0.6415	0.4115	1.8637	7.2413	74.8222

4.6.3 First order reaction rate constants

Table 4.3 presents the compiled first order reaction rate constants for DPOME with and without antioxidants. It could be observed that the rate constants increased as temperature increased from 100 to 130 °C. All values of *k* nearly doubled for every 10 °C increase in temperature. At higher temperatures, molecules have greater kinetic energy and thus collide with each other more frequently, thereby increasing the probability of reaction. In the context of this study, not only the oxidation of methyl esters is triggered, but also the reactions of antioxidants with radicals, oxidation intermediates as well as the methyl esters themselves. Therefore, it can be concluded that when the temperature increases, the consumption rate of antioxidants and substrates also increases.

Notably, the rate constants of all samples dosed with antioxidants were significantly lower compared to DPOME at fixed temperatures as depicted in Table 4.3. For instance, at 100 °C, the *k* value for DPOME was recorded at 0.8863 h^{-1} compared to the highest value for α-T at 0.1411 h^{-1}. The trend of rate constants for samples with antioxidants at all temperatures except 130 °C in descending order was: α-T > BHT > TBHQ > BHA. Overall, the *k* values of samples with antioxidants at all temperature levels were lower than *k* value of DPOME at 110 °C (1.3584) h^{-1}. The lower *k* values of samples with antioxidants showed their potential in maintaining the stability of DPOME. However, α-T was less effective compared to TBHQ and BHA. The rate constants for TBHQ and BHA have been reported by other researchers. Zhou et al. (2016) reported *k* values for TBHQ at 0.0606 to 0.5607 $h^{-1}$from 110 °C to 140 °C, and 0.3741 to 2.4387 h^{-1} for BHA for the same temperature range. Conversely, Borsato et al. (2014) showed comparable *k* values for TBHQ and BHA at 110 °C to 125 °C. TBHQ performed slightly better than BHA with

k values of 0.5523 and 0.5853 h^{-1}, respectively at 110 °C, but BHA was better at 125 °C instead. Another study showed that the presence of Cu^{2+}, Fe^{2+} and Fe^{3+} ions will greatly increase the *k* value of raw commercial biodiesel (Clemente *et al.*, 2023), while the presence of antioxidants reduced the *k* values across all temperature tested. This highlighted the potency of using antioxidants to preserve the oxidation stability of biodiesel, as well as using *k* values as an indicator of fuel stability under certain storage condition. The range of values obtained in this study overlap with the reported literature values and discrepancies arise due to factors such as fuel type and concentration of antioxidants. A two-way ANOVA test showed that temperature had a p-value of 1.04E-05 while type of antioxidant had a p-value of 5.41E-07. Both the p-values highlighted that *k* was significantly dependant on both temperature and type of antioxidant.

Table 4.3. First order reaction rate constants for DPOME with and without antioxidants.

Temperature (°C)	First order reaction rate constant, *k* (h^{-1})[a]				
	DPOME	BHA	BHT	TBHQ	α-T
100	0.8863 ± 0.0277	0.0692 ± 0.0048	0.1220 ± 0.0028	0.0897 ± 0.0065	0.1411 ± 0.0191
110	1.3584 ± 0.0439	0.1412 ± 0.0038	0.2370 ± 0.0115	0.1916 ± 0.0111	0.2734 ± 0.0066
120	1.6521 ± 0.0180	0.2681 ± 0.0274	0.5229 ± 0.0110	0.3303 ± 0.0139	0.5520 ± 0.0186
130	2.3121 ± 0.1998	0.5790 ± 0.0059	1.1427 ± 0.0642	0.6419 ± 0.0417	1.0678 ± 0.0151

[a]Average of triplicates ± standard deviation.

4.6.4 Activation energies and thermodynamic parameters

Table 4.4 summarises the activation energies and thermodynamics parameters for

DPOME with and without antioxidants. As shown, the addition of antioxidants into DPOME increased the activation energy, $E_{a,}$. All tested antioxidants raised the E_a by at least 80 kJmol^{-1} from the initial value of 38.4737 kJmol^{-1}. The higher E_a upon doping DPOME implied that the threshold for oxidation reaction to be initiated is higher, hence making it harder for oxidation to occur and form products (Romagnoli et al., 2018). The highest E_a value was recorded for BHT (93.7210 kJmol^{-1}), followed by BHA (87.5267 kJmol^{-1}), α-T (84.7248 kJmol^{-1}) and lastly, TBHQ (80.7271 kJmol^{-1}). Typically, high E_a values are associated with higher antioxidation capabilities. Despite BHT having higher E_a values compared to BHA, the IP values of BHA were doubled of BHT at all temperatures from 100 °C to 130 °C (64.01 h vs 30.05 h at 100 °C, 28.84 h vs 14.59 h at 110 °C, 13.59 h vs 6.27 h at 120 °C and 6.61 h vs 3.16 h at 130 °C), which concurred with the obtained *k* values. This phenomenon was also observed in Rodrigues et al.'s work (2020). Their ethanolic curcuminoid extract (ECE) was reported to have an IP value of 10.90 h compared to 10.18 h for PG, but PG had a higher E_a value than ECE. The authors did not discuss further on the reason behind this phenomenon. This could probably be related to formation of stable compounds in the BHA-doped samples as compared to the BHT ones. Jain *et al.* (2012) discussed the increment of E_a value from 39.39 kJmol^{-1} of B100 *Jatropha curcas* biodiesel (JCB) to 41.06, 42.96 and 47.21 kJmol^{-1} when 100 ppm of BHA, BHT and TBHQ were added into JCB respectively. Compared to the results collected in this chapter, the increments were minute and far inferior compared to their antioxidation capabilities in DPOME. However, the increments were evident at 600 ppm where BHA, BHT and TBHQ increased the E_a by at least 50 %. This was most probably due to the instability of JCB as compared to DPOME, and needed a larger

amount of antioxidants to stabilise the fuel properties. Clemente *et al*. (2023) reported the presence of metal ions in storage will greatly reduce the E_a of biodiesel. Jabuticaba peel extracts were able to improve E_a of commercial biodiesel even if Fe^{2+} and Fe^{3+} ions were present, but not with Cu^{2+}. Meanwhile, thermodynamics of synthetic antioxidants under influence of metal ions had yet to be elucidated.

Positive $\Delta H^{\ddagger}$ values were recorded for all samples tested as listed in Table 4.4. This indicated that the oxidation reactions were endothermic. The $\Delta H^{\ddagger}$ values of DPOME, and DPOME with BHA, BHT, TBHQ and α-T were 35.2503 $kJmol^{-1}$, 84.4380 $kJmol^{-1}$, 90.5063 $kJmol^{-1}$, 77.4643 $kJmol^{-1}$, and 81.4758 $kJmol^{-1}$, respectively. Meanwhile, the negative $\Delta S^{\ddagger}$ values for all samples (-59.0494 – -22.1861 $JK^{-1}mol^{-1}$) also showed that the reactions were non-spontaneous, meaning that it was likely that activation complexes formed during the oxidation process (Ong *et al*., 2013). The ranking of $\Delta S^{\ddagger}$ values from the least negative to the most negative was BHT, BHA, α-T, TBHQ, DPOME. Comparing the $\Delta H^{\ddagger}$ and $\Delta S^{\ddagger}$ values, it was noticeable that the $\Delta H^{\ddagger}$ values in samples with antioxidants increased, while their $\Delta S^{\ddagger}$ values were less negative. The findings in this study agree with those reported in the literature. Borsato *et al.* (2014) reported $\Delta H^{\ddagger}$ values of 75.24 $kJmol^{-1}$, 67.44 $kJmol^{-1}$ and 82.40 $kJmol^{-1}$ for BHA, BHT and TBHQ respectively in soybean-based biodiesel, which all were comparable to the findings in this study. The difference with $\Delta H^{\ddagger}$ values of BHT to this study were evident, but the reason was most probably due to the biodiesel type used. Furthermore $\Delta H^{\ddagger}$ values of 79.02 $kJmol^{-1}$ and 75.05 $kJmol^{-1}$ for coffee and sage extract in soybean biodiesel from Gregório *et al.*'s work (2018) also supported the increase of $\Delta H^{\ddagger}$ values upon the addition of antioxidants into biodiesel. To add, $\Delta S^{\ddagger}$ values reported from both works were also higher than the control samples

(Borsato *et al.*,2014: -36.20 – -72.11 $JK^{-1}mol^{-1}$; Gregório *et al.*, 2018: -46.43 – -56.19 $JK^{-1}mol^{-1}$). Finally, the positive values of $\Delta G^{\ddagger}$ (98.9037 – 101.0857 $kJmol^{-1}$) explained that all reactions were endergonic, whereby energy was required for the reaction to take place. Other studies also suggested minor increase of $\Delta G^{\ddagger}$ values from control samples upon the addition of antioxidants (Spacino *et al.*, 2015; de Souza *et al.*, 2019; de Souza *et al.*, 2020). $\Delta G^{\ddagger}$ values from these works were between 96 – 100 $kJmol^{-1}$ as compared to 93 – 94 $kJmol^{-1}$ of the control sample. Nonetheless, both positive $\Delta H^{\ddagger}$ and $\Delta G^{\ddagger}$ values also proved that these antioxidants do not promote the formation of products in the oxidation process. De Souza *et al.*'s work (2019) added that the thermodynamic analyses of B100 soybean-derived biodiesel using data from Rancimat and PetroOXY yielded different $\Delta H^{\ddagger}$ $\Delta S^{\ddagger}$ and $\Delta G^{\ddagger}$ values. The difference was much evident in samples with extract additives where ranking of additive effectiveness for Rancimat and PetroOXY were different. The authors also noted the complexity of to relate both instruments despite both being reliable methods to quantify the oxidation stability of biodiesel.

Table 4.4. Activation energies and thermodynamics parameters for DPOME with and without antioxidants[a].

Sample	E_a ($kJmol^{-1}$)	$\Delta H^{\ddagger}$ ($kJmol^{-1}$)	$\Delta S^{\ddagger}$ ($JK^{-1}mol^{-1}$)	$\Delta G^{\ddagger}$ ($kJmol^{-1}$)[b]
DPOME	38.4737	35.2502	-153.0550	94.7549
	± 4.1655	± 3.9268	± 0.0108	± 0.3977
BHA	87.6598	84.4380	-42.8899	101.0857
	± 3.4020	± 3.4021	± 0.0089	± 0.0494
BHT	93.7294	90.5063	-22.1861	99.1178
	± 3.0077	± 3.0107	± 0.0078	± 0.0539
TBHQ	80.6881	77.4642	-59.0494	100.3843
	± 5.1773	± 5.1789	± 0.0132	± 0.0520

α-T	84.6998 ± 4.7440	81.4758 ± 4.7469	-44.8999 ± 0.0120	98.9037 ± 0.1163

[a]Average of triplicates ± standard deviation.

[b]$\Delta G^{\ddagger}$ calculated as average of 373.15, 383.15, 393.15 and 403.15 K.

4.7 Concluding remarks

This chapter has appraised the oxidation kinetics and thermodynamics of DPOME with selected antioxidants. Regression analyses coupled with a combination of error functions demonstrated that DPOME dosed with BHA, BHT, TBHQ and α-T followed the first order kinetic model. This was supported by the high R and R^2 values and low χ^2 values.

The first order rate constants increased as temperature increased from 100 to 130 °C, indicating increased reaction rates with elevated kinetic energy of the molecules. Significantly, the k values of all samples dosed with antioxidants were lower compared to DPOME at fixed temperatures which showed the potential of antioxidants in maintaining the stability of DPOME. The E_a of all samples were shown to increase upon the addition of antioxidants. All samples showed positive $\Delta H^{\ddagger}$ values (74.4642 – 90.5063 $kJmol^{-1}$) and negative $\Delta S^{\ddagger}$ values (-59.0494 – -22.1861 $JK^{-1}mol^{-1}$). This indicated that the reactions were endothermic and non-spontaneous. Furthermore, the positive $\Delta G^{\ddagger}$ values (98.9037 – 101.0857 $kJmol^{-1}$) described the reactions as endergonic reactions.

By appraising the rate constants, it was clear that TBHQ and BHA were the most effective. This agreed with the results from Phase 1 whereby TBHQ and BHA emerged as the most effective antioxidants from the determined IPs under Rancimat and PetroOXY test, respectively. Although BHT had the highest E_a values, its IP values were lower

compared to TBHQ and BHA. In agreement with Phase 1, α-T was less effective compared to TBHQ and BHA. Nonetheless, for evaluation of the long-term palm biodiesel storage stability and formulation of oxidation pathways, TBHQ and BHA from the synthetic category and α-T from the bio-based one were chosen. This would allow long-term differences, if any, to be elucidated for the additives.

5. Long-term storage stability of palm biodiesel with additives

5.1 Introduction

This chapter reports on the final phase of the study on long-term storage stability and oxidation pathways. Following the conclusions obtained from the second phase, TBHQ, BHA and α-T at 100 and 500 ppm were chosen as additives for palm biodiesel to be stored and tested for a duration of 6 months (26 weeks). Fortnightly fuel sampling was carried out to determine the IPs (Rancimat and PetroOXY following EN 15751 and ASTM D7545, and EN 16091, respectively), acid value, iodine value, kinematic viscosity and water content according to EN 14104, EN 14111, EN ISO 3104 and EN ISO 12937 test methods, respectively. In addition, the additives concentration, esters composition, functional groups and compounds of the doped biodiesels were analysed using HPLC, GC-FID, FTIR and GC-MS, respectively every 4 weeks.

5.2. Materials

Butylated hydroxyanisole (BHA, ≥ 98.5 %), tert-butylhydroquinone (TBHQ, 97 %), α-tocopherol (α-T, 96 %), heptane (HPLC, 99 %) and ethyl acetate (HPLC, 99.8 %) were purchased from Sigma Aldrich (M) Sdn. Bhd. Ethanol (96 %), methanol, phenolphthalein, sodium thioslphate, Wijs solution, potassium iodide, methylnonadecanoate (≥ 98 %) were purchased from Merck. Toluene, acetic acid, cyclohexane and starch were purchased from Chemiz, UK. Potassium hydroxide, acetonitrile (ACN, HPLC, ≥99.9%), isopropanol (HPLC, ≥99.9 %) and glacial acetic acid (HPLC, ≥99.7 %) were purchased from Fisher Chemicals. Deionized water was used for HPLC assays. All reagents and

chemicals were of analytical grade. Distilled palm oil methyl ester (DPOME) was prepared according to the procedures described in Section 3.3 for this final phase.

5.3 Long-term storage stability study

The long-term storage stability of DPOME with three additives, *i.e.*, BHA, TBHQ and α-T, was evaluated. They were added into DPOME at two levels of concentrations, *i.e.*, 100 ppm (samples BHA_{100}, $TBHQ_{100}$, $\alpha\text{-}T_{100}$) and 500 ppm (samples BHA_{500}, $TBHQ_{500}$, $\alpha\text{-}T_{500}$), thereby forming six fuel samples in total. The doped fuels were stored in tin-plated canisters under the shade outdoors over the course of 26 weeks. The ambient temperature and humidity of the storage area were recorded automatically using a digital hygrometer (Xiaomi Mijia, China). Every fortnightly, samples were extracted for analyses of oxidation stability index (OSI) / induction period (IP) via Rancimat and PetroOXY, acid value, iodine value, kinematic viscosity and water content. The tests were conducted in triplicates. Additional sampling every 4 weeks and at the end of the study was carried out for HPLC, FTIR, GC-FID and GC-MS analyses.

5.4 Analytical methods

5.4.1 Oxidation stability properties

The IP of each sample was measured using both Rancimat and PetroOXY following the procedures described in Section 3.5.4. Meanwhile, the acid value, iodine value and kinematic viscosity of samples were determined as outlined in Section 3.5.5–3.5.7. The water content was measured using an 831 KF Coulometer (Metrohm, Switzerland) according to EN ISO 12937. Approximately 0.1 g of sample was weighed using a manual

GC syringe before injection into a mixture of hydranal:xylene with a ratio of 60:40 (v/v). The injection of sample was conducted when the drift was stabilised at below 20 µL/min. The syringe was rinsed with heptane thrice, and sample twice before the next sample was analysed.

5.4.2 High performance liquid chromatography (HPLC)

5.4.2.1 Preparation of standards

1 mg/mL stock solution of each antioxidant (TBHQ and BHA) were prepared by carefully weighted and dissolved in 1:1 (v/v) isopropanol/ACN. Afterwards, 10, 20, 30, 40 and 50 µg/mL of each antioxidant were prepared from the stock solution and injected into the HPLC. Meanwhile, α-T standards were prepared by dissolving α-T in 1:1 (v/v) heptane. Subsequently, 20, 40 and 80 µg/mL standards were prepared and injected into HPLC. From there, individual calibration curves for the respective antioxidants were constructed based on the peaks observed. All stock solutions were covered with aluminium foils, if not in amber containers, and stored at −20 °C.

5.4.2.2 Preparation of fuel samples

The biodiesel samples with TBHQ and BHA were first dissolved at 1 g sample to 4.5 mL of 1:1 (v/v) isopropanol/ACN ratio. The dissolved samples were ultrasonicated in an ultrasonic bath for 15 min, followed by vortexing at 1000 rpm for 1 min. Then, the sample mixtures were centrifuged at 3500 rpm for 10 min. The upper layer of each sample was then injected into the HPLC for analysis. Meanwhile, 2 g of fuel sample with α-T was weighed in a 10 mL volumetric flask. Each sample was dissolved and diluted to

10 mL with heptane before injection into the HPLC.

5.4.2.3 High performance liquid chromatography (HPLC) analyses

For TBHQ and BHA, chromatographic analyses were carried out using an Agilent HPLC 1290 series (USA) equipped with UV detector. A reversed-phase C_{18} column (250 × 4.6 mm, 5 µm pore size) was used as the stationary phase. The mobile phases used were distilled water with 5 % acetic acid (solvent A) and ACN with 5% acetic acid (solvent B). They were first filtered using a 0.45 µm polytetrafluoroethylene membrane filter and degassed using an ultrasonic bath for 30 min. To the instrument, a gradient mode was performed by setting to 70 % solvent A and 30 % solvent B for the first 14 min, 100 % solvent B for the next 8 min, and 100% solvent A for the last 4 min. UV detection was accomplished at 280 nm and the flow rate was maintained at 1 mL/min. Quantification of antioxidant concentration was accomplished by using the calibration curves of the corresponding standards prepared in Section 6.4.2.1.

To determine the α-T concentration in the fuel samples, an Agilent HPLC 1100 series (USA) equipped with a UV detector was used. The stationary phase was silica column (250 × 4.6 mm, 5 µm pore size) and the mobile phase was heptane with 3% ethyl acetate. The mobile phase was filtered with a 0.22 µm polytetrafluoroethylene membrane filter and degassed in an ultrasonic bath for 30 min. UV detection was accomplished by setting the excitation wavelength at 270 nm and emission wavelength at 315 nm. The flow rate was set at 1 mL/min. Quantification of the α-T concentration was executed by using the calibration curve of the α-T standards prepared in Section 5.5.2.1.

5.4.3 Fourier transform infrared spectroscopy (FTIR)

FTIR analysis allows the identification of functional groups based on the absorption frequency of targeted compounds in the biodiesel samples. FTIR analyses of all fuel samples were carried out using an Agilent Cary 630 FTIR spectrometer equipped with Diamond ATR-1 Bounce sampling tech (USA) in the range 4000-600 cm^{-1}. Using a dropper, 2–3 drops of sample were carefully placed on the crystal and the crystal was thoroughly cleaned using a 1:1:1 ratio of acetone:ethanol:toluene solution.

5.4.4 Gas chromatography-flame ionisation detector (GC-FID)

A C19 standard was prepared by mixing 0.1 g of methyl nonadecanoate with 50 mL of heptane. Next, 0.1 g of fuel sample was measured and mixed thoroughly with 2.5 mL of C19 standard solution. Then, 1 µL of the sample was injected into a Clarus 680 GC-FID (Perkin Elmer, USA). Helium (He) was used as a carrier gas, and its flow rate was set to 2 mL/min constant flow.

Chromatographic separation of compounds was carried out with an Elite-5MS capillary column (5 % diphenyl/95 % dimethyl polysiloxane) with a length of 30.0 m, an inner diameter of 0.25 mm, and a film thickness of 0.1 µm. The initial temperature of oven was set to 50 °C held for 2 min, followed by a heating rate of 10 °C/min up to 300 °C, which was then held for 10 min. The temperature of the injector and detector was set at 250 °C. The individual ester content was determined using Eqn. 5.1.

$$Ester\ content = \frac{\frac{A_{target} \times R_{target}}{A_{C19}} \times \frac{W_{C19}}{W_{sample}} \times 100}{\sum(\frac{A_{target} \times R_{target}}{A_{C19}} \times \frac{W_{C19}}{W_{sample}}) \times 100} \times 100 \qquad \text{(Eqn 5.1)}$$

where A_{target} is the area of the peak of targeted ester, R_{target} is the theoretical flame ionization detector correction factor (TCF) for the targeted ester relative to C19:0 standard, A_{C19} is the area of the peak of C19:0 standard, W_{C19} is the weight of C19:0 standard in mg, and W_{sample} is the weight of the test sample in mg. For the case of linolenic acid esters (C18:3), the result was expressed as the summation of three relevant peaks. The TCF values relative to the C19:0 standard are listed in Table 5.1.

Table 5.1. TCF values of esters relative to C19:0 standard.

Ester	TCF
C8:0	1.2024
C10:0	1.1325
C12:0	1.0859
C14:0	1.0526
C16:0	1.0276
C16:1	1.0200
C18:0	1.0082
C18:1	1.0013
C18:2	0.9946
C18:3	0.9877
C20:0	0.9926

5.4.5 Gas chromatography-mass spectrometry (GC-MS)

Qualitative chemical analyses of the fuel samples were conducted using a Clarus 680 Gas Chromatograph (Perkin Elmer, USA), coupled with Clarus SQ 8S GC/Mass Spectrometer (Perkin Elmer, USA). All test samples were first diluted to 2.5 % (v/v) with heptane prior to filtration with a 0.45 µm syringe filter. A 0.5 µL of sample was injected into the programmable temperature vaporisation (PTV) injector set at 300 °C with a split ratio of

1:10. Helium (He) was used as a carrier gas, and its flow rate was set to 2 mL/min constant flow.

An Elite-5MS capillary column (5 % diphenyl/95 % dimethyl polysiloxane) with a length of 30.0 m, an inner diameter of 0.25 mm, and a film thickness of 0.1 µm was used to separate the compounds. The initial temperature of oven was set to 50 °C held for 2 min, followed by a heating rate of 10 °C/min up to 300 °C, which was then held for 10 min.

The transfer line from the GC to MS was maintained at 250 °C, and the effluent was ionised by electron impact (EI) ionisation (70 eV) with a source temperature of 200 °C. The mass analyser was run under a full scan mode between 36 and 640 mass-to-charge (*m/z*) range. The acquired data was processed using Turbomass software. Peaks were identified based on a National Institute of Standards and Technilogy (NIST) library search.

5.5 Results and discussion

5.5.1 Temperature and humidity

The hourly temperature and humidity data recorded was processed to produce the highest and lowest weekly readings as shown in Figure 5.1. Observation of the daily temperatures and humidities (data not shown) showed higher temperatures during the day and lower temperatures at night, as expected. This resulted in higher humidities at night and lower humidities during the day.

The average maximum temperature was recorded on Week 22 at 35.48 °C, approximately 2 °C higher than the end of the storage period. The monthly average maximum

temperature was determined to be 33 °C while the average minimum was 25 °C. Since Malaysia has a tropical climate with no seasonal changes, no drastic changes in temperature were noted throughout the 26 weeks of storage. Meanwhile, the average weekly maximum humidity was recorded at 95 % while the average minimum humidity was 58 %. As higher temperatures were observed nearing the end of the storage period, this resulted in lower humidities on those weeks. This was most probably due to the lack of rain in February – March 2024. Nevertheless, it was evident that no extreme changes in humidity were detected over the duration of study. These stability of storage conditions were important to note as Malaysia does not have seasonal changes like other non-tropical countries. Both temperature and humidity were expected to have little to no changes over the storage time. These trends then further proved that temperature and humidity changes has little to no impact on the changes of fuel properties over time.

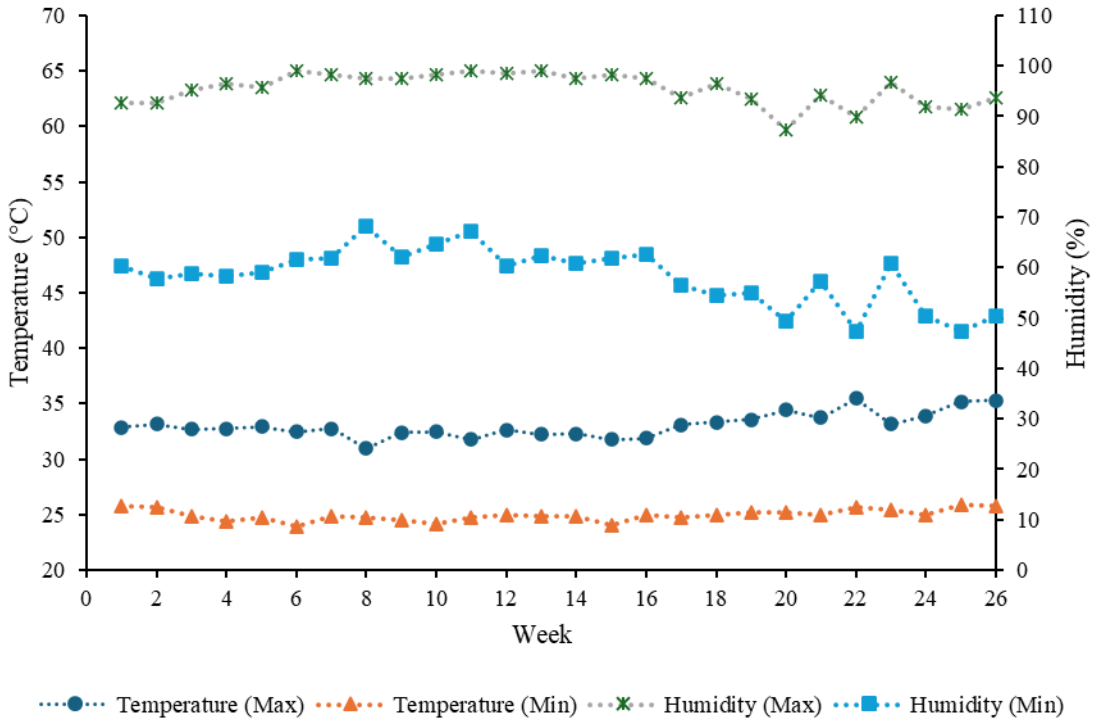

Figure 5.1. Weekly maximum and minimum temperatures and humidities of storage area (Oct 2023 – March 2024).

5.5.2 Rancimat induction period (IP)

All antioxidants were dosed in 100 ppm and 500 ppm to highlight the difference in fuel stability over storage period. From chapter 3, it was evident that 250 ppm was sufficient for all antioxidant types to maintain the fuel properties according to EN14214. 100 ppm was selected to determine if it was sufficient to maintain the fuel properties for 26 weeks, while 500 ppm was selected to show a more significant trend compared to the lower one. The initial IP value of the DPOME used for the long-term storage stability study determined via Rancimat was 2.82 h. All doped fuel samples were subjected to Rancimat analysis every fortnight. The collected IP data were subjected to linear regression as shown in Figure 5.2 and the minimum IP required according to EN14214 was labelled threshold. Statistical analyses were conducted to determine whether the trends observed over the course of 26 weeks were significant. Table 5.2 lists the coefficients of the linear regression lines shown in Figure 5.2 as well as the corresponding p-values. From Table 6.2, α-T_{100}, α-T_{500}, BHA_{100} and BHA_{500} have negative coefficients, which indicate that decreasing IP trends were observed across the storage time. The coefficients had p-values of 1E-06, 3E-09, 9E-06 and 0.0011, respectively, highlighting that the observed trends were significant. The higher p-value for BHA_{500} compared to the other samples could be linked to 2 outliers obtained in Week 14 and 20. After 26 weeks of storage, BHA_{500} still had a relatively high IP value of 35.75 h. The decrement in IP values over time could be expected since oxidation slowly converts the methyl esters into oxidised compounds. The presence of additives merely reduced the rate of the oxidation but did not halt the process

entirely.

Both α-T_{100} and α-T_{500} samples had initial IP values above 10 h, but these eventually dropped below the minimum requirement of 8 h as specified by the EN 14214:2012 standard. For α-T_{100}, an IP of 7.91 h was recorded on Week 4, meaning that 100 ppm of α-T was only able to extend the storage time of DPOME by slightly less than a month. Meanwhile, the IP of α-T_{500} fell below the limit to 7.74 h on Week 14. This demonstrated that although increasing the concentration of α-T in DPOME aided in stabilizing the fuel for a longer period, the additive is not a good choice if a much longer storage time is needed.

In contrast, opposite trends for $TBHQ_{100}$ and $TBHQ_{500}$ were obtained. The positive coefficient values listed in Table 5.2 showed that both samples had increasing IP values over the storage time. To elaborate further, the IP values for $TBHQ_{100}$ were much closer to the trendline compared to the scattered points of $TBHQ_{500}$ as seen in Figure 5.2. This corresponded to the higher p-value of $TBHQ_{500}$ (0.9389) compared that of $TBHQ_{100}$ (0.3104) though both values pointed to the insignificance of the trends. Statistical analyses aside, $TBHQ_{100}$ remained relatively stable across the entire storage period whereby the IP values were maintained close to 20 h for the whole study. Conversely, $TBHQ_{500}$ had a relatively high IP value of 71.87 h from the start and increased to 82.86 h in Week 26. As the analysis time for $TBHQ_{500}$ samples took approximately 70 – 80 h per run, samples were collected and froze prior to analysis. Therefore, the opposing trends obtained for $TBHQ_{500}$ might possibly be due to repeated sample freezing and thawing because of the unavailability of the Rancimat equipment. Such practices ended up

affecting the accuracy of the results from each sampling date, resulting in the fluctuating readings across weeks as shown in Figure 5.2. To reduce such inaccuracies of data, samples should be analysed as soon as it was collected.

The IP values of TBHQ were sufficiently high to justify it as the best performing antioxidant, followed by BHA and α-T. BHA was reasonably effective while α-T was not suitable for long-term storage stability of DPOME at the two concentrations tested. Since all trends highlighted that higher concentration led to higher IP, it might be possible for α-T to perform better at concentrations above 500 ppm. Summarily, the order of OSI as indicated by the Rancimat IP was $TBHQ_{500} > BHA_{500} > TBHQ_{100} \geq BHA_{100} > \alpha\text{-}T_{500} > \alpha\text{-}T_{100}$.

Decreasing trends of IP values were also observed in past literature. Nambiraj and Kumar's (2024) findings showed decreasing trends for samples doped with TBHQ and essential oil derived from *Citrus Aurantifolia* L (CA), *Curcuma longa* L (CL) and *Eucalyptus camaldulensis* Dehn (EC). The authors reported higher IP values for Prosopis juliflora methyl ester (PJME) sample with CA compared to TBHQ across 90 days of storage time, which were 11.2 to 5.8 h in CA vs 9.9 to 4.3 h in TBHQ. Higher IP values of bio-based antioxidants compared to synthetic ones were shown whereas synthetic ones worked better in this study. Furthermore, the low IP values reported for all samples in the study were mainly due to the high concentration of C18:1 (17.02 %) and C18:2 (53.91 %) in PJME as compared to lower concentrations in POME. Other studies on POME also supported the stability of POME even without addition of antioxidants (*Chrysikou et al.*, 2022). IP values of POME remained about 8 h even after 3 months of storage time in

stainless steel bottle outdoor, which is similar to the storage conditions implemented in this study. POME's IP value decreased to approximately 7 h on the 4th month and finished at 6 h at the end of the experiment. Soybean methyl ester (SME) which was studied in the same work also showed comparable results with POME. This phenomenon was further justified by Fathurrahman *et al.*'s work (2024) as it reported that no oxidation degradation was found during 6 months of storage period. IP values remained at a very high value, which were ~ 67 h and ~ 50 h for B30 and B40 respectively. A polynomial fitting of oxidation stability versus biodiesel content were also discussed.

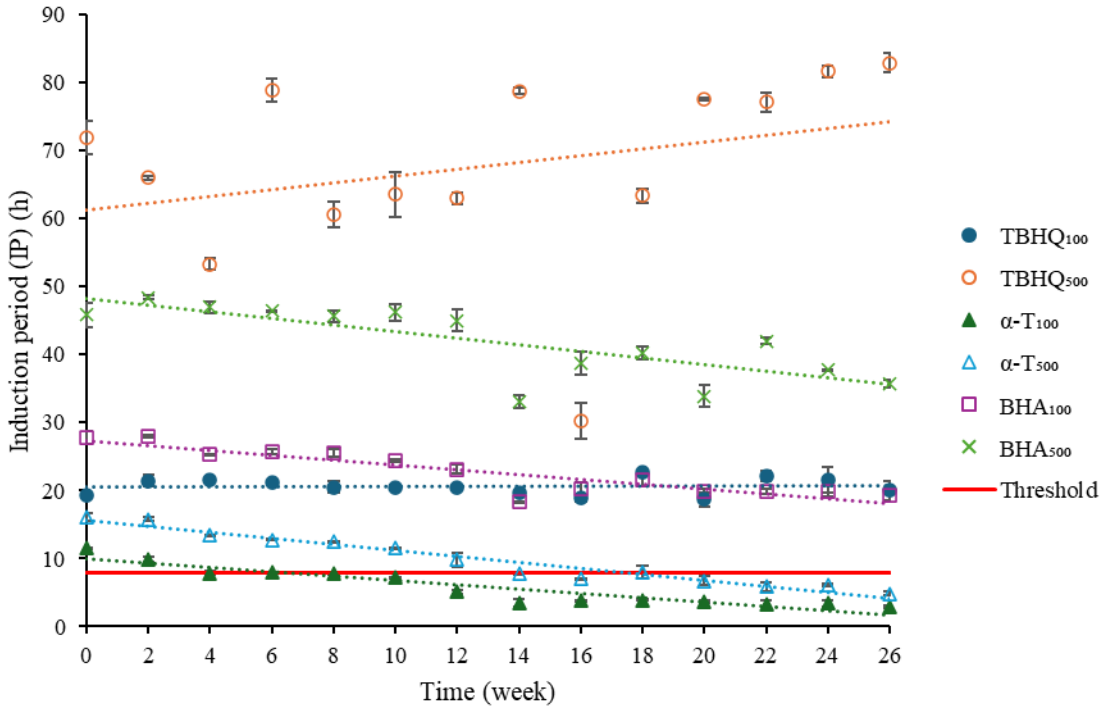

Figure 5.2. Rancimat induction periods (IP) of fuel samples over 26 weeks.

Table 5.2. Coefficients and p-values for regression analyses of Rancimat IP data.

Sample	Coefficient	p-value
$TBHQ_{100}$	0.0033	0.9389

$TBHQ_{500}$	0.4941	0.3104
$\alpha\text{-}T_{100}$	-0.3143	1E-06
$\alpha\text{-}T_{500}$	-0.4390	3E-09
BHA_{100}	-0.3566	9E-06
BHA_{500}	-0.4859	0.0011

5.5.3 PetroOXY induction period (IP)

Figure 5.3 illustrates the IP values of fuel samples measured using PetroOXY with regresssed trendlines. The initial PetroOXY IP value of DPOME was 13.86 min. Decreasing trends could be seen for all additives except $TBHQ_{500}$, with the regression coefficients and p-values summarised in Table 5.3. The regression plots displaying decreasing trends were all statistically significant, in line with the expected decline in IP over time due to fuel oxidation. Conversely, $TBHQ_{500}$ showed a weak increasing IP trend over the storage time with its positive coefficient (0.0269) and p-value > 0.05, which again could be due to repeated sample freezing and thawing.

Similar to the results reported in Chapter 3, fuel samples with BHA had much higher IP values compared to those doped with TBHQ. Most of the IP values of $TBHQ_{100}$ and $TBHQ_{500}$ were even lower than those of $\alpha\text{-}T_{100}$ and $\alpha\text{-}T_{500}$, respectively. The opposing PetroOXY IP values for BHA and TBHQ might be attributed to the thermal degradation of TBHQ under high temperature and pressure (Zhou et al., 2016; Zhou et al., 2017). The operating temperature and pressure of PetroOXY are higher compared to Rancimat (140 °C versus 110 °C and 700 kPa versus atmospheric).

Among all additives, BHA_{500} had the highest IPs, close to 300 min for the first 12 weeks, before slowly decreasing towards the end of the study. This was followed by BHA_{100}

where its IP decreased from 70.77 min to 52.48 min over the course of 26 weeks. Subsequently, α-T_{500} ranked third followed by α-T_{100} and finally, $TBHQ_{500}$ and $TBHQ_{100}$ had the least IP values. The final IP value of α-T_{100} at Week 26 (16.25 min) was close to that of DPOME (13.86 min), which indicated that α-T_{100} was approaching the oxidation stability of DPOME. The findings agreed with the IPs measured using Rancimat (2.91 h and 2.82 h, respectively).

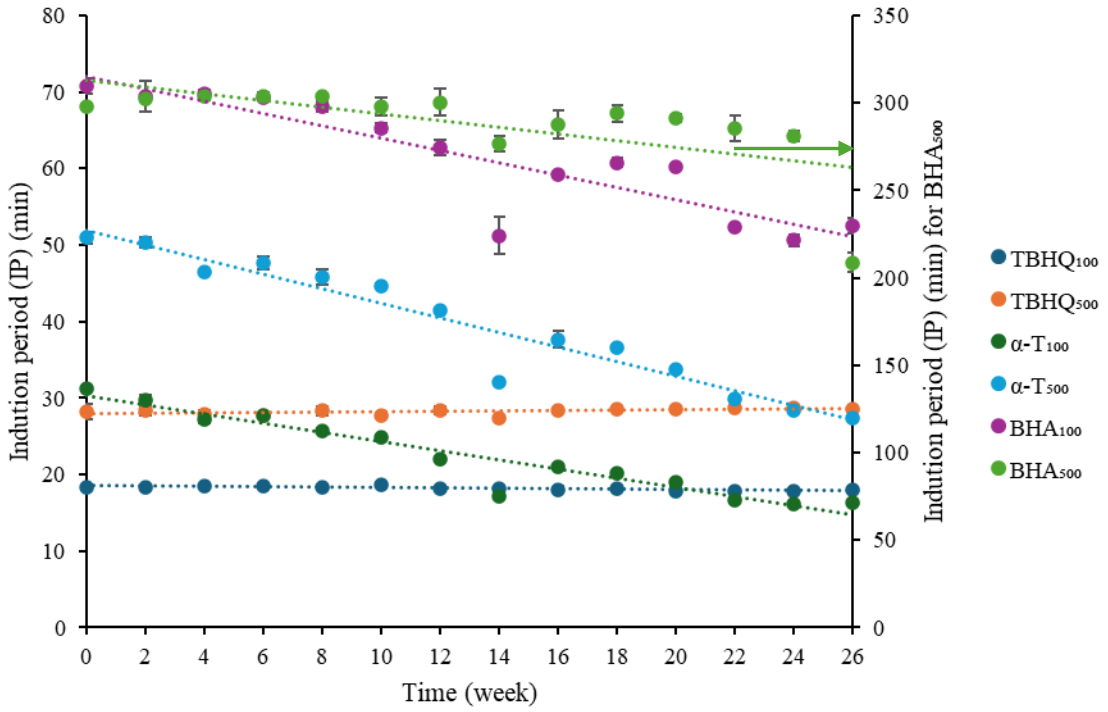

Figure 5.3. PetroOXY induction periods (IP) of fuel samples over 26 weeks.

Table 5.3. Coefficients and p-values for regression analyses of PetroOXY IP data.

Sample	Coefficient	p-value
$TBHQ_{100}$	-0.0246	0.0015
$TBHQ_{500}$	0.0269	0.0513
α-T_{100}	-0.5974	9.32E-08

α-T_{500}	-0.9546	2.83E-08
BHA_{100}	-0.8037	1.50E-05
BHA_{500}	-1.9207	0.0108

5.5.4 Acid value

Figure 5.4 displays the measured acid values in accordance with the EN 14104 test method. The maximum limit stipulated in the EN 14214 standard is 0.5 mg KOH/g, and all samples did not exceed this threshold. The initial acid value for DPOME was 0.15 mg KOH/g. All samples except $TBHQ_{500}$ maintained acid values within the range of 0.14 – 0.16 mg KOH/g for the whole storage period, while $TBHQ_{100}$ had an average of 0.21 mg KOH/g. This was most likely due to the presence of an extra hydroxyl (-OH) group in TBHQ compared to BHA and α-T as seen in Figure 5.5. More hydroxyl groups was reported to have an increased effect on acidity of carbon-chained acids (Gebresas *et al.*, 2023). As all three antioxidants comprised of phenol rings and carbon-chains, it was likely that an increase in TBHQ concentration would have an increase in acid value due to the increased number of hydroxyl groups. However, no discernible difference could be seen for $TBHQ_{100}$ against α-T_{100} and BHA_{100}. This could be explained with the range of 0.14–0.16 mg KOH/g being close to the lower limit of the auto-titrator used for the analysis. A clearer difference should be observable with an instrument of higher accuracy and lower limit.

The acid value data for all sample showed weakly increasing relationship with storage time. As shown in Table 5.4, the p-values obtained for the positive coefficients were above 0.05, indicating statistically insignificant trends, or in other words, the acidity

could be concluded to remain relatively stable over time. This meant that there was little increase in acidic by-products such as carboxylic acid from oxidation, proving all three antioxidants were able to prevent rapid oxidation of fuel by mitigating the formation of peroxides, the precursors for the formation of carboxylic acid.

Literatures also reported increase in AV over storage time due to the formation of acids during oxidation processes. CA and TBHQ showed good performance in slowing down the increase in AV, which were 1.28 and 1.23 mg KOH/g at 4% respectively compared to 2.02 mg KOH/g of control at day 90, but still unable to maintain it under the stipulated limit of 0.5 mg KOH/g of EN14214 (Nambiraj and Kumar, 2024). Another study also showed similar trend where natural leaf extract additive (LEA) was able to reduce the increment of AV for *Calophyllum inophyllum* methyl ester (CIME) compared to control sample over 90 days of storage time. The same study also highlighted the stability of AV across all biodiesel blends (B20 – B100) (Govindasamy *et al.*, 2022). Chrysikou *et al.* (2022) also reported the stability of POME's AV even without the usage of antioxidants during storage time of 6 months. POME was shown to have a much slower increase in AV over time compared to SME. Also, results obtained from that study were comparable to the results obtained in this study, further suggested that POME has lower initial AV values compared to fuels derived from other feedstocks. In addition, recent study on the stability of POME also further confirmed that AV of POME changes very little even without the addition of antioxidants to slow down the oxidation process. B30 and B40 from highland and coastal area saw little to no difference in terms of AV even after 6 months of storage (Fathurrahman *et al*., 2024). These studies highlighted the relevancy of the data collected in this study.

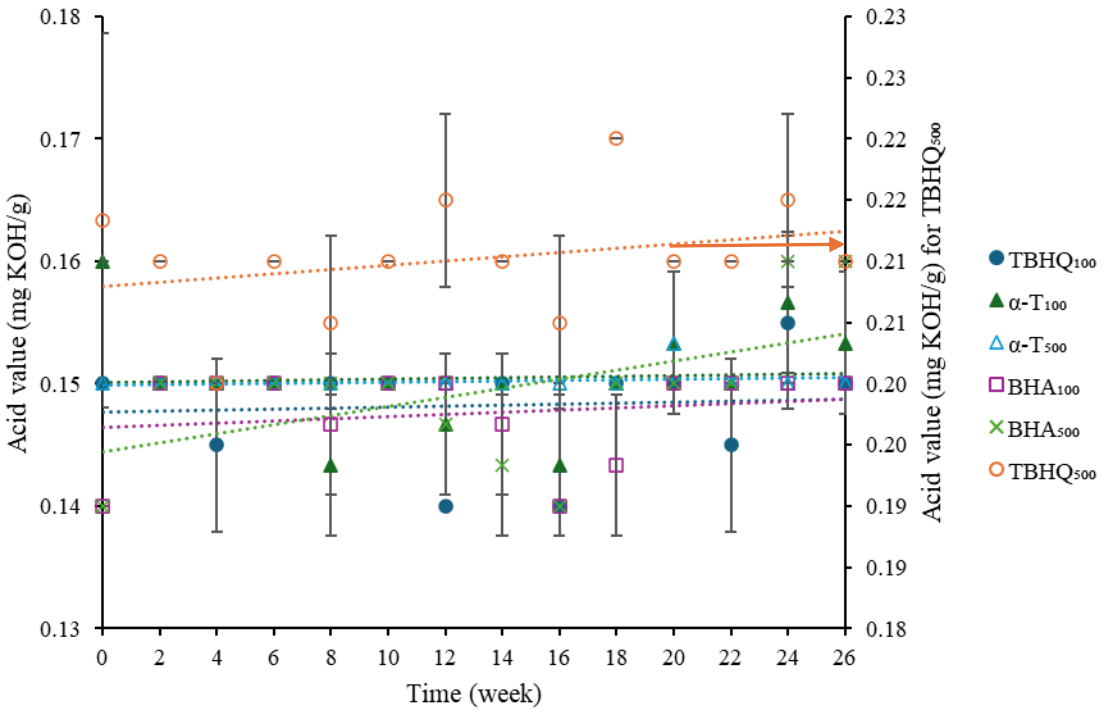

Figure 5.4. Acid values of fuel samples over 26 weeks (EN 14104 test method).

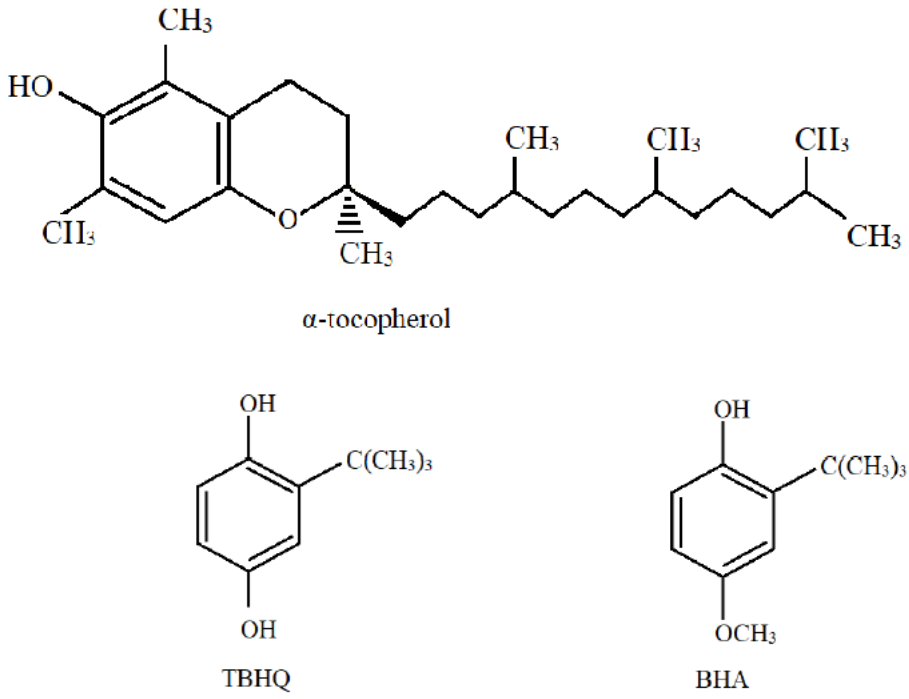

Figure 5.5. Chemical structures of α-T, TBHQ and BHA.

Table 5.4. Coefficients and p-values for regression analyses of acid value data.

Sample	Coefficient	p-value
$TBHQ_{100}$	3.85E-05	0.7951
$TBHQ_{500}$	0.000172	0.3062
$\alpha\text{-}T_{100}$	2.93E-05	0.8533
$\alpha\text{-}T_{500}$	2.56E-05	0.4069
BHA_{100}	8.79E-05	0.5068
BHA_{500}	0.000370	0.0528

5.5.5 Iodine value

According to the EN 14214 standard, a maximum iodine value of 120 g I_2/100 g is permitted. From Figure 5.6, all fuel samples had much lower iodine values compared to allowable limit, approximately 50 g I_2/100 g for the entire storage period. Moreover, the acquired data were also close to the initial iodine value of DPOME at 47.8980 g I_2/100 g. The highest values were reported for $TBHQ_{100}$ in Week 4 at 54.6750 g I_2/100 g, followed by $TBHQ_{500}$ in Week 2 at 54.1739 g I_2/100 g. As iodine value served as a basis for the number of double bonds in the sample, both values were considered to outliers since the values were expected not to differ much from the initial iodine value of DPOME. However, past study had shown that IV of POME decreased over storage time (Lin *et al.*, 2009). The authors also discussed that antioxidants helped in slowing the drop if IV over time, while higher storage temperature accelerated the drop compared to the ones stored under ambient temperature.

Table 5.5 records the coefficients and p-values of the regression plots. The TBHQ samples had negative coefficients indicating declining trends over time. On the contrary, the α-T and BHA samples showed increasing trends with time by their positive

coefficients. Nonetheless, it should be noted that these correlations were statistically insignificant, which corresponded to the fluctuations in data due to constraints in incubation and sampling times of the test method.

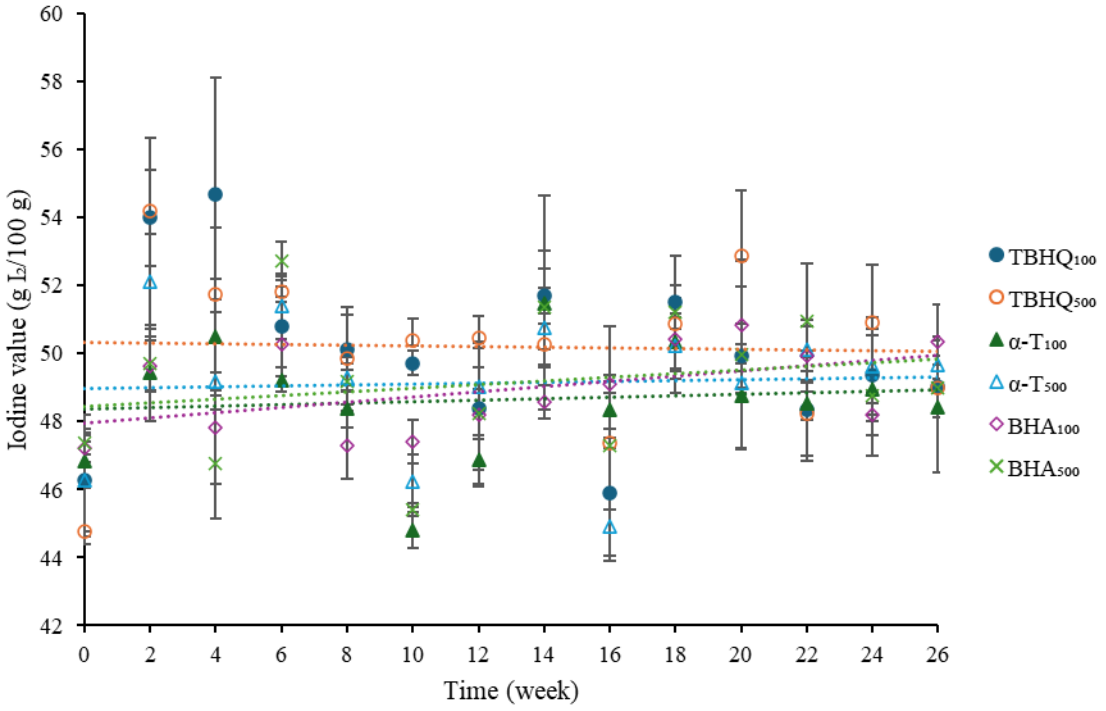

Figure 5.6. Iodine values of fuel samples over 26 weeks (EN 14111 test method).

Table 5.5. Coefficients and p-values for regression analyses of iodine value data.

Sample	Coefficient	p-value
$TBHQ_{100}$	-0.0868	0.3127
$TBHQ_{500}$	-0.0103	0.9014
$\alpha\text{-}T_{100}$	0.0218	0.7114
$\alpha\text{-}T_{500}$	0.0174	0.8104
BHA_{100}	0.0758	0.0736
BHA_{500}	0.0531	0.4516

5.5.6 Kinematic viscosity

The fuel samples were subjected to kinematic viscosity measured at 40 °C following the EN ISO 3104 test procedures. The initial kinematic viscosity of DPOME was recorded at 4.3875 mm^2/s. Upon the addition of antioxidants into DPOME, all samples had elevated kinematic viscosities in the order of BHA_{100} < α-T_{100} < $TBHQ_{100}$ < BHA_{500} < α-T_{500} < $TBHQ_{500}$. As shown in Figure 5.7, it was evident that all samples had increasing kinematic viscosities over the storage period. The positive coefficients obtained from regression analyses correlated to the increasing trends while the corresponding p-values highlighted the trends were statistically significant.

The samples with α-T had steeper gradients compared to samples with BHA, and samples with TBHQ had the least steep gradient. At the end of Week 26, the order of kinematic viscosity was $TBHQ_{100}$ < BHA_{100} < BHA_{500} < $TBHQ_{500}$ < α-T_{100} < α-T_{500}, with α-T_{500} reaching 4.4360 mm^2/s. Taking into account the results here as well as those obtained for IP, it could be inferred that more oxidation by-products were formed in samples with α-T due to its less effective protection against oxidation compared to BHA and TBHQ. These by-products increased the viscosity of the fuel samples by a larger margin. Nevertheless, it could be observed that none of the samples exceeded the maximum limit of 5 mm^2/s as regulated in the EN 14214:2012 standard.

Other studies showed similar increasing trends over storage time. At day 45, lower concentrations of TBHQ, CA, EC and CL samples were unable maintain the kinematic viscosity of PJME below 5 mm^2/s limit of EN14214 (Nambiraj and Kumar, 2024). The authors showed that only CA samples were able to maintain below 5 mm^2/s for all

concentrations (1 – 4 %), while all except 1 % of CL and TBHQ, 1 – 3 % of EC failed to protect the kinematic viscosity of B100 PJME tested. LEA on the other hand was shown to be able to maintain the kinematic viscosity of CIME below 5 mm^2/s for all concentrations tested (5 – 20 mL) and all biodiesel blends (B20 – B100). Despite so, increase trends over storage time was observed, suggesting that oxidation still occurs and the presence of antioxidants was only delaying the oxidation process (Govindasamy *et al*., 2022).

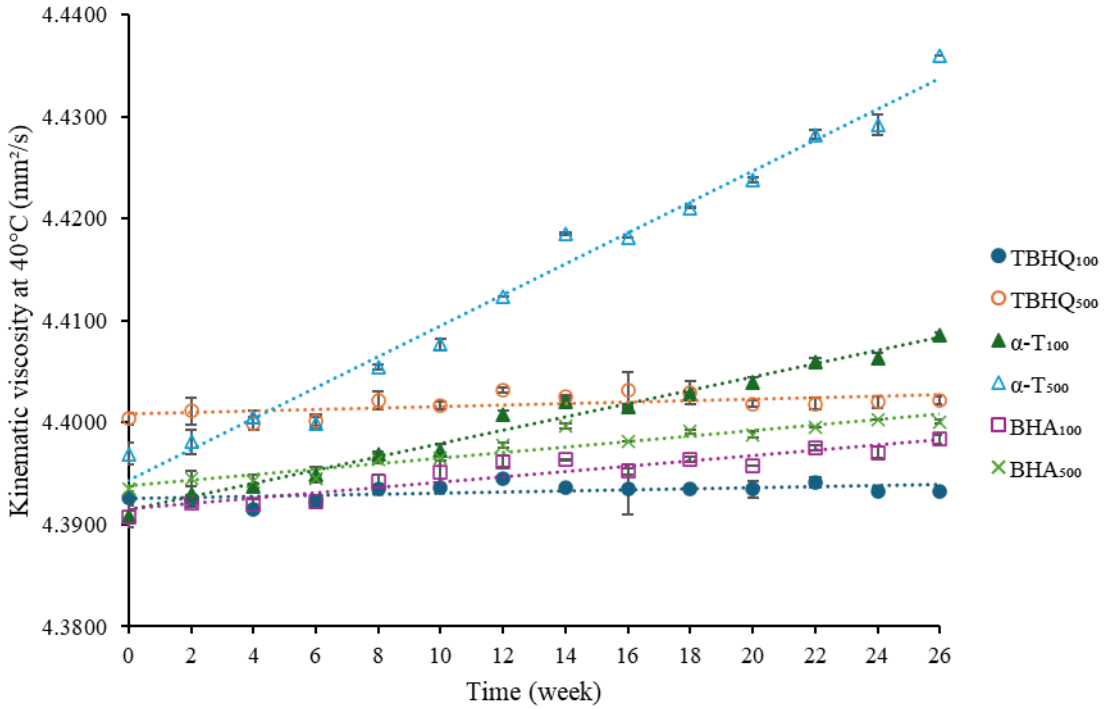

Figure 5.7. Kinematic viscosities at 40 °C of fuel samples over 26 weeks (EN ISO 3104 test method).

Table 5.6. Coefficients and p-values for regression analyses of kinematic viscosity data.

Sample	Coefficient	p-value
$TBHQ_{100}$	5.37E-05	0.0320

$TBHQ_{500}$	7.64E-05	0.0225
$\alpha\text{-}T_{100}$	0.000651	5.01E-12
$\alpha\text{-}T_{500}$	0.001518	1.16E-11
BHA_{100}	0.000262	5.79E-07
BHA_{500}	0.000271	2.13E-07

5.5.7 Water content

Water content in biodiesel must be maintained as the presence of water in storage tanks may jeopardise the performance of biodiesel over long periods. This is particularly important in stored biodiesel as presence of water in fuel will lead to problems such as machine stopping and even damages the operating machines (Hasan & Rahman, 2017). Moreover, study also discussed the modification of fungal community in biodiesel at higher water content that affects the chemical and biological stability of stored biodiesel (Cazarolli *et al.*,2021). According to the EN 14214:2012 standard, the maximum limit of water content is 500 mg/kg. As depicted in Figure 5.8, none of the samples crossed this threshold. The highest value recorded was for $TBHQ_{100}$ in Week 24 at 469.9967 mg/kg while the lowest was attained for BHA_{100} in Week 14 at 310.2167 mg/kg. In contrast, the water content for DPOME was 396.3200 mg/kg. The regressed coefficients listed in Table 6.7 showed that $TBHQ_{100}$, $\alpha\text{-}T_{100}$ and $\alpha\text{-}T_{500}$ had decreasing trends, while $TBHQ_{500}$, BHA_{100} and BHA_{500} had increasing trends. However, the regressed trends were deemed statistically insignificant based on the p-values obtained, which corresponded to the fluctuations in data. Theoretically, the water content in samples was expected to increase over time due to the formation of water molecules from hydrolysis of fatty acids during oxidation processes (Lin *et al.*, 2009). Chrysikou *et al.*'s work also supported the same

theory, as water content of POME increased over time even without the addition of antioxidants. Compared to SME (220 – 400 mg/kg) in the same study, water content was higher at all measuring intervals for POME (300 – 500 mg/kg). A different study on the effects of humidity on water content shed insights as similar fluctuating trends were observed for all biodiesel blends (B5 – B20) at both low and high humidity storage condition, namely tropic region (Brazil) and moist tropical region (Amazon) respectively (Amaral *et al*., 2020). The main highlight of the work was the increasing in fluctuations for higher biodiesel blends whereby B20 showed a more aggressive changes in water content (100 – 275 mg/kg) over 6 months of storage time compared to B5 (30 – 80 mg/kg) that has a higher fossil diesel ratio. The study also suggested that higher biodiesel blends were more prone to be affected by humidity of storage conditions.

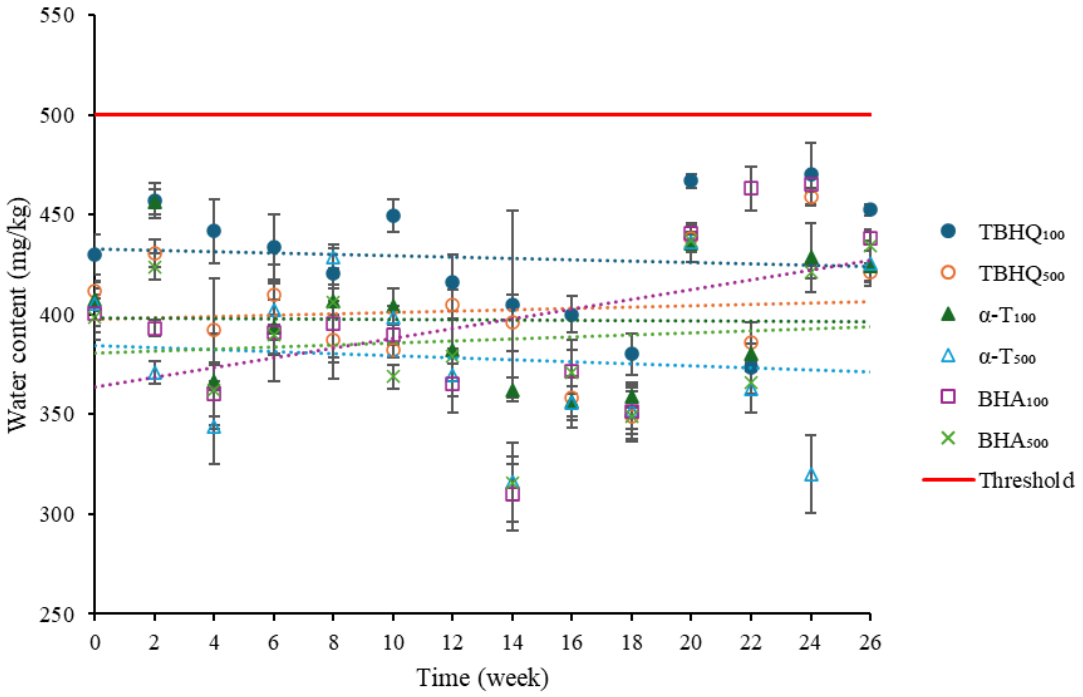

Figure 5.8. Water content of fuel samples over 26 weeks (EN ISO 12937 test method).

Table 5.7. Coefficients and p-values for regression analyses of water content data.

Sample	Coefficient	p-value
$TBHQ_{100}$	-0.3428	0.7500
$TBHQ_{500}$	0.3335	0.7514
$\alpha\text{-}T_{100}$	-0.0706	0.9490
$\alpha\text{-}T_{500}$	-0.4979	0.7169
BHA_{100}	2.4448	0.0946
BHA_{500}	0.4955	0.6870

5.5.8 High performance liquid chromatography (HPLC) analyses

The analyses of TBHQ and BHA were conducted based on Rashidi et al.'s work (2016) with minor modifications. Standards ranging from 20 to 100 ppm of the respective antioxidants were used to produce the calibration curves. The retention time of TBHQ was reported to be at 7.3 min while BHA was at 10.7 min. Elution of both antioxidants were slightly later compared to the retention time of Rashidi et al.'s work (TBHQ: ~7 min, BHA: ~9.8 min). Conversely, α-T was analysed using a different test method specifically for tocopherol variants present in palm oil. Standards ranging from 20 to 80 ppm were used to produce the calibration curve. Figure 5.9 and Figure 5.10 are the initial HPLC chromatograms of $\alpha\text{-}T_{100}$ and $\alpha\text{-}T_{500}$, respectively. They proved that only α-T was present in the fuel and other naturally existing tocopherols (α-T3, β-T3, γ-T3 and δ-T3) were removed during the fuel preparation step via distillation. All three calibration curves constructed showed high linearity ($R^2 \geq 0.999$) as depicted in Figure 5.11, indicating their reliability to be used for the analyses of TBHQ, α-T and BHA in the samples studied.

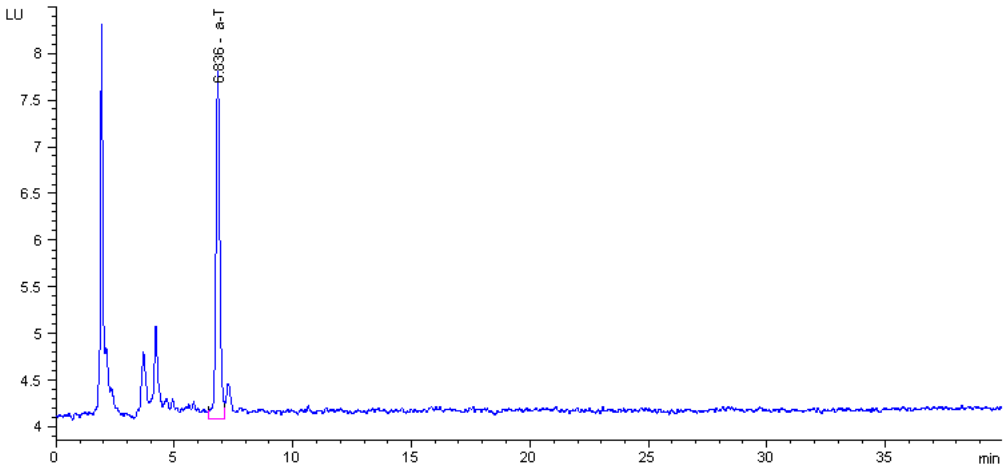

Figure 5.9. Initial chromatogram of α-T_{100}.

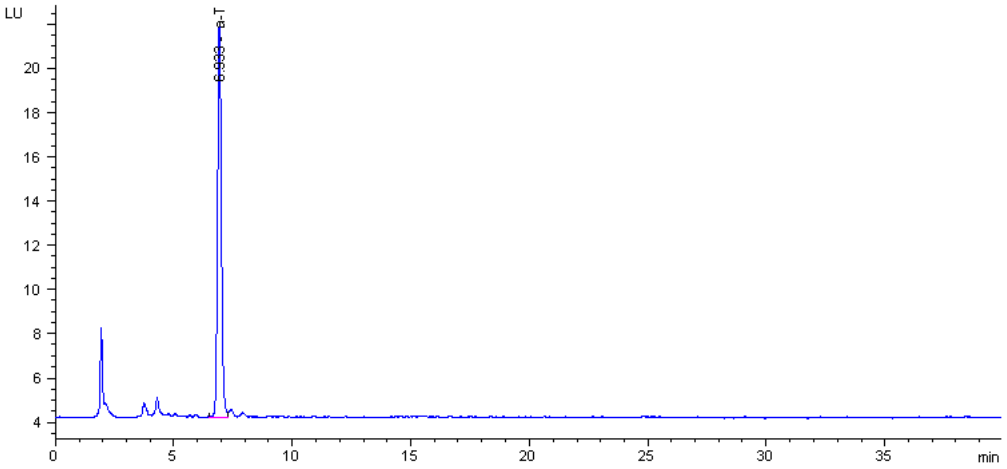

Figure 5.10. Initial chromatogram of α-T_{500}.

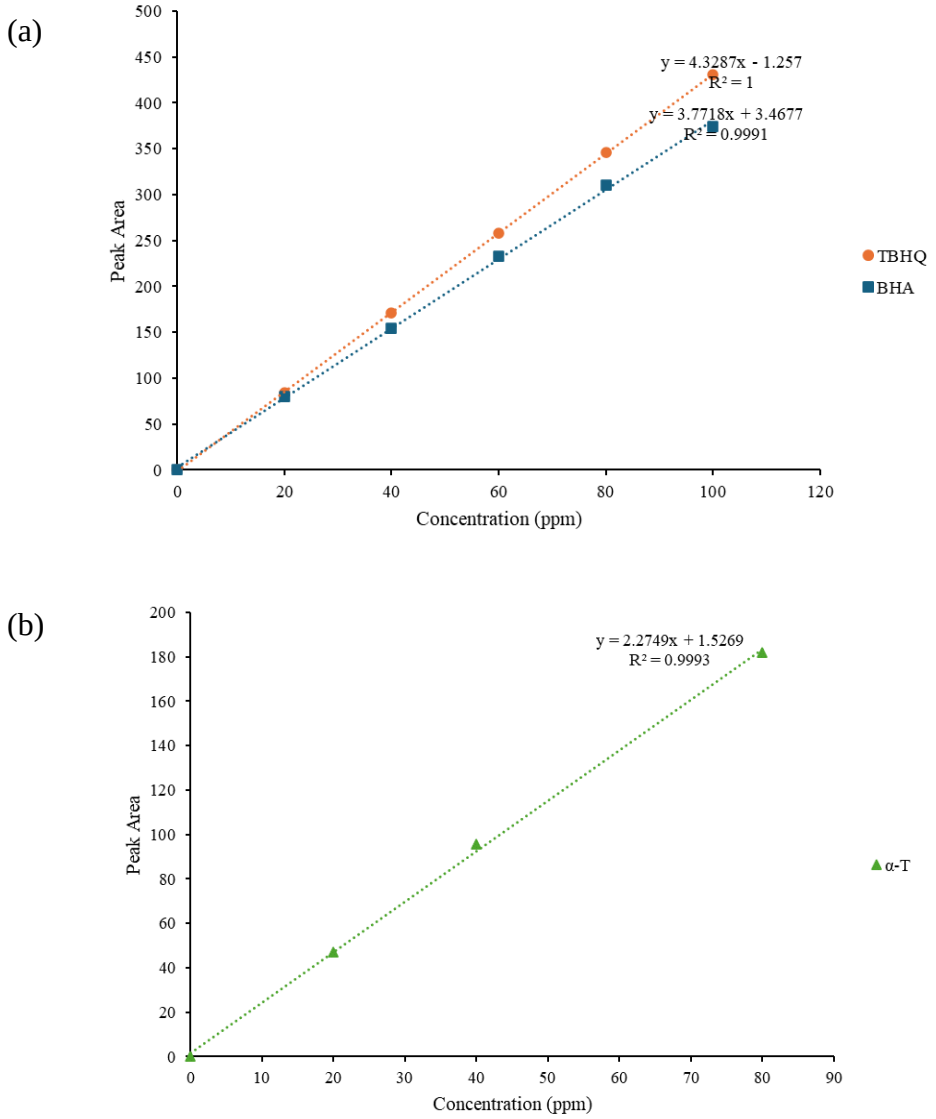

Figure 5.11. Calibration curves of (a) TBHQ and BHA and (b) α-T.

Figure 5.12 illustrates the consumption rates of the antioxidants. The consumption rate of antioxidants at the end of the study in increasing order was BHA_{500} (81.6 %) < $TBHQ_{500}$ (83.2 %) < $TBHQ_{100}$ (83.6 %) < BHA_{100} (84.7 %) < α-T_{500} (94.4 %) < α-T_{100} (95.1 %). Such consumption rates are closely tied to the sustainability of these antioxidants in long-term storage of palm biodiesel. The high consumption rate of α-T_{100} and α-T_{500} translated

to the non-suitability of α-T in stabilising palm biodiesel for a long period of time. Furthermore, the Rancimat IP values fell below the threshold for these samples. Regression analyses of the data resulted in positive cofficient values which were statistically significant for all samples (p-value < 0.05) as shown in Table 5.8, signifying that the increasing trends for the consumption rate were definitive. This could be expected as the antioxidants reacted over time, thus protecting the fuel.

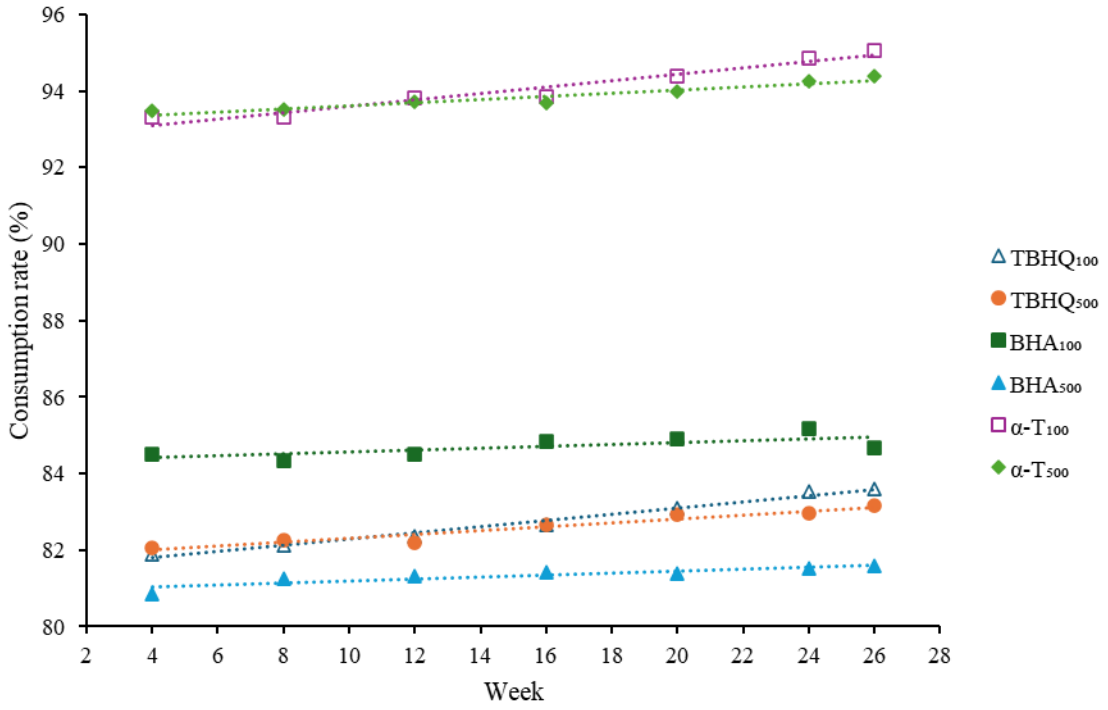

Figure 5.12. Consumption rates of antioxidants in fuel samples over 26 weeks.

Table 5.8. Coefficients and p-values for regression analyses of consumption rate data.

Sample	Coefficient	p-value
$TBHQ_{100}$	0.08278	3.27E-07
$TBHQ_{500}$	0.04819	5.68E-05
$\alpha\text{-}T_{100}$	0.08026	2.43E-05
$\alpha\text{-}T_{500}$	0.03532	0.0006
BHA_{100}	0.02464	0.0180
BHA_{500}	0.02167	0.0039

5.5.9 Fourier transform infrared (FTIR) spectroscopy

The FTIR spectra of samples with TBHQ, α-T and BHA are shown in Figure 6.13. The major peaks identified from the spectra for the samples according to their wavelengths are listed in Table 5.9.

The oxidation process is split into 3 phases: initiation, propagation, and termination. During initiation phase, the initial radical (I·) attacks the bisallylic carbon of methyl ester to form a stable product (IH) and unstable carbon-based radical (R·) (Figure 5.14). Upon the introduction of oxygen (O_2), carbon-based radicals are then converted into peroxyl radicals to start the propagation phase, where peroxyl radicals indefinitely attack the bisallylic carbon until all methyl esters are exhausted (Lau *et al.,* 2022). Finally, the termination phase occurs where the unstable radicals from the propagation phase react with one another to form stable oxidation by-products such as ketones, aldehydes, carboxylic acids, epoxides, and oligomers. These by-products that contain carbonyl group, or cyclic ether ring in the case of epoxide, can change the intensity of the carbonyl band at 1740 cm^{-1} (Zhou *et al*., 2017). Furthermore, Araújo *et al.* (2011) also discussed the increase in the carbonyl group's intensity at 1740 cm^{-1} during oxidation of castor oil

FAME using the PetroOXY and Rancimat methods. Similar observations were noted with B20 biodiesel (Zhou *et al*., 2017). Therefore, the carbonyl group (C=O) peak at ~1740 cm^{-1} was of particular interest in the analyses of the FTIR spectra.

It was noticeable that there were little to no changes in the bands at 1740 cm^{-1} for all samples throughout the 26 weeks. This implied that the oxidation did not proceed past the propagation phase, where by-products started forming. As illustrated in Figure 5.14, the antioxidants donate hydrogen atoms from their hydroxyl (-OH) group to stabilise the peroxyl radicals, thus preventing the peroxyl radicals from attacking the methyl esters. While BHA was used as an example in the said figure, the same theory can be applied to TBHQ and α-T as well since they all contain a hydroxyl group next to a conjugated double bond. The reason why these antioxidants remained stable even after being converted into radicals was due to the delocalisation of electron from the oxygen atom to the adjacent aromatic ring (Sánchez-Marzo *et al*., 2019).

Additionally, the % transmittance of the doped samples were compared to DPOME. The % transmittance at 1740 cm^{-1} of DPOME was recorded at 53.7430 % as opposed to the average 48.0047 – 49.7723 % of all samples. This further proved the capabilities of TBHQ, BHA and α-T in preventing or delaying the oxidation from propagating further in biodiesel. Past study on biodiesel stability using FTIR also illustrated the differences between spectra of control and samples with antioxidants (de Menezes *et al.*, 2022). It was reported that control chicken fat biodiesel has an extra band between 3200 and 3500 cm^{-1}. However, the same band was not observed in the other control samples in that study, which were Babassu biodiesel and corn biodiesel, nor it was observed in DPOME of this

study. These phenomena can be explained by the types of biodiesels studied as some biodiesels were more prone to oxidation due to higher concentrations of unsaturated and polyunsaturated methyl esters.

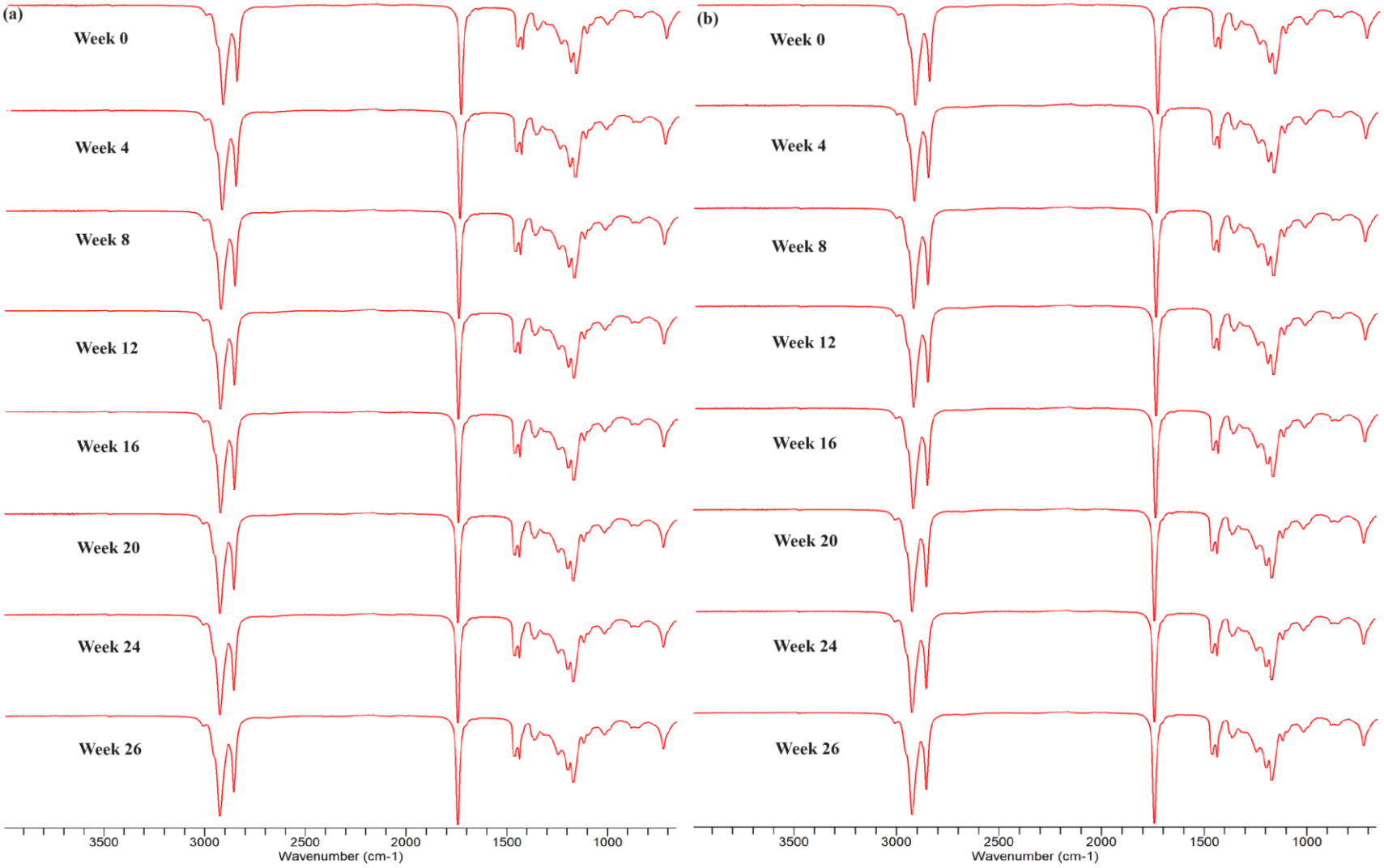
(a)
Week 0
Week 4
Week 8
Week 12
Week 16
Week 20
Week 24
Week 26
3500
3000
2500
2000
1500
1000
Wavenumber (cm-1)
(b)
Week 0
Week 4
Week 8
Week 12
Week 16
Week 20
Week 24
Week 26
3500
3000
2500
2000
1500
1000
Wavenumber (cm-1)

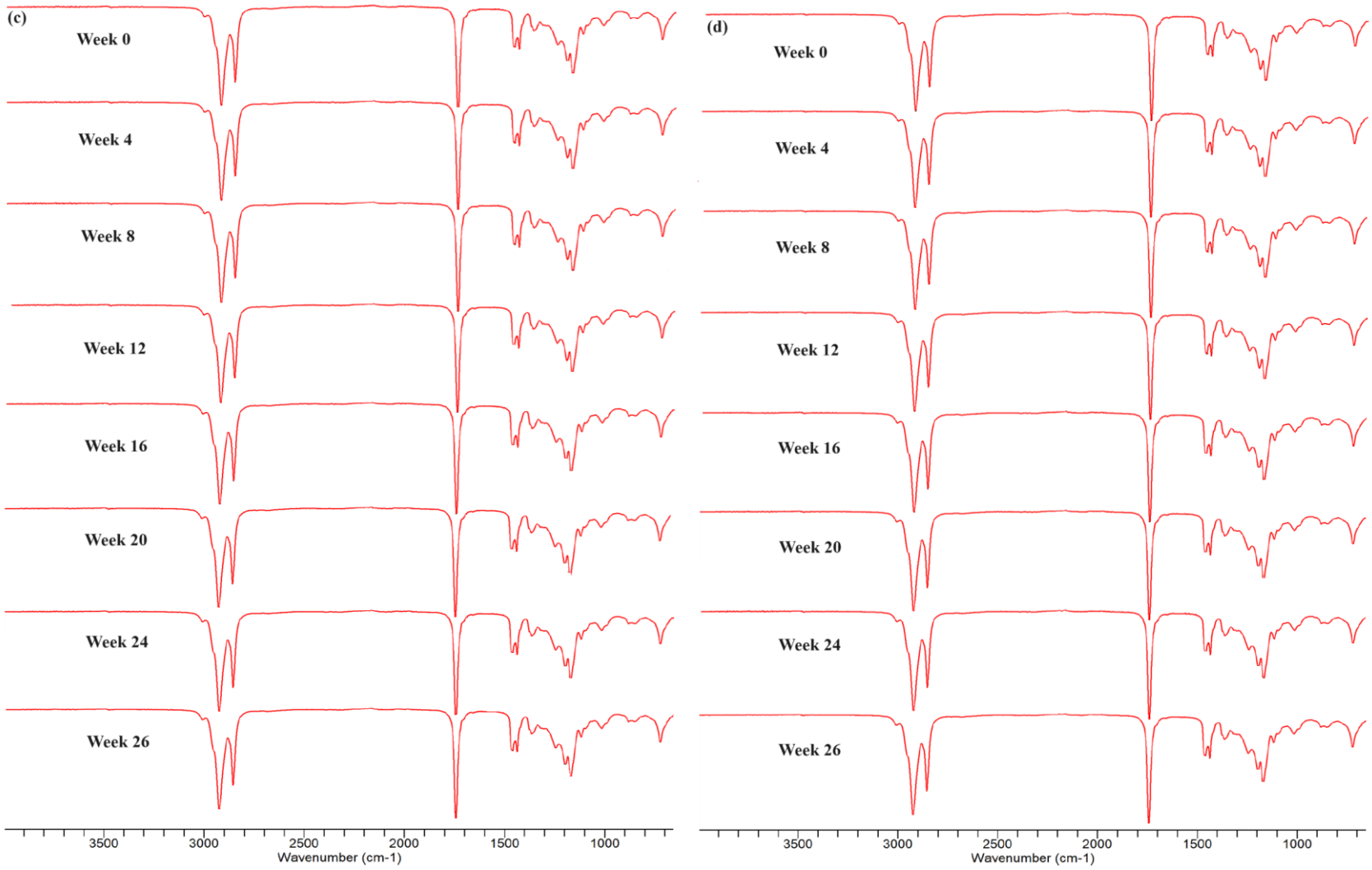
(c)
Week 0
Week 4
Week 8
Week 12
Week 16
Week 20
Week 24
Week 26
3500
3000
2500
2000
1500
1000
Wavenumber (cm-1)
(d)
Week 0
Week 4
Week 8
Week 12
Week 16
Week 20
Week 24
Week 26
3500
3000
2500
2000
1500
1000
Wavenumber (cm-1)

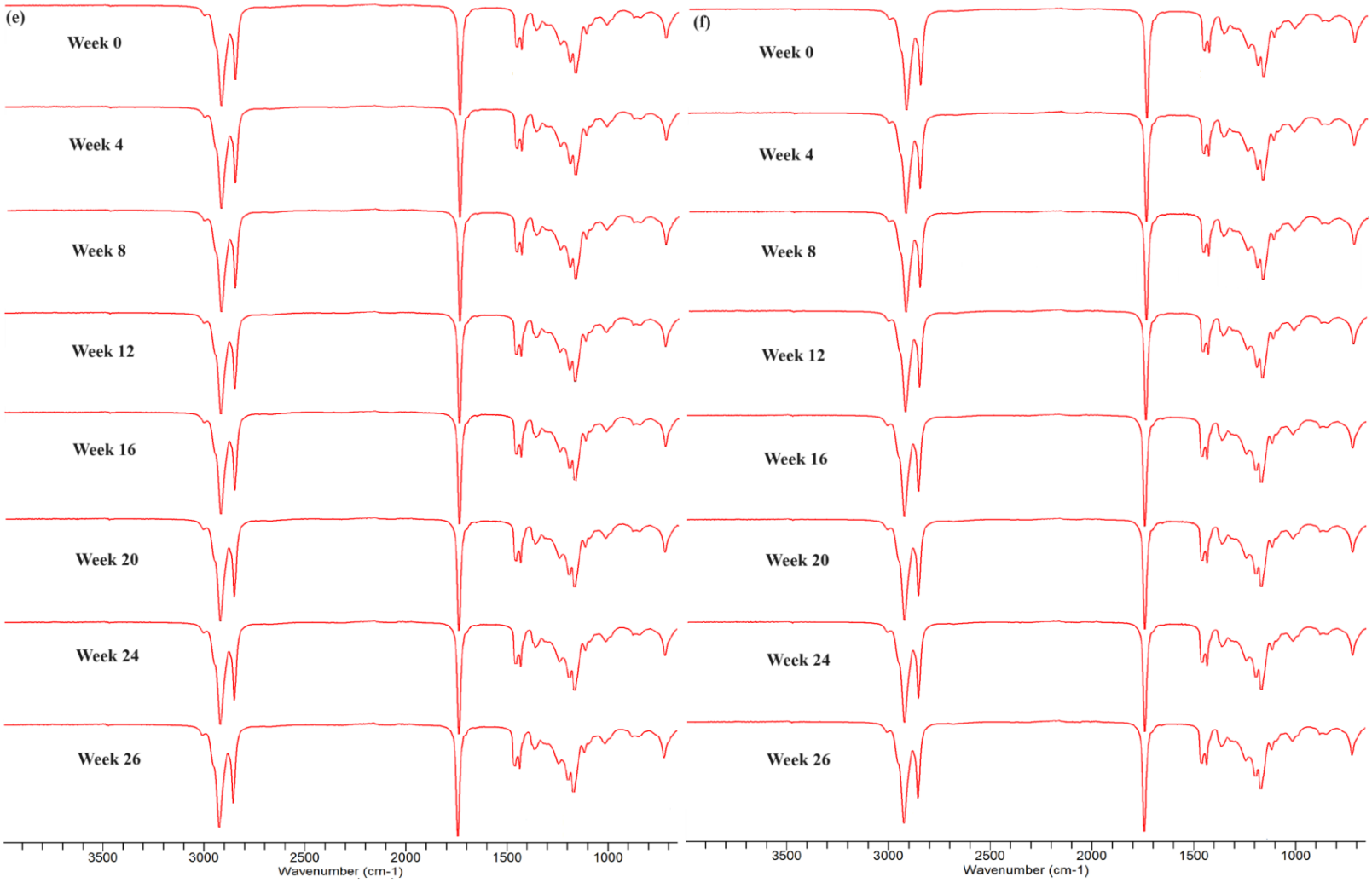

Figure 5.13. FTIR spectra of DPOME with (a) $TBHQ_{100}$, (b) $TBHQ_{500}$, (c) $\alpha\text{-}T_{100}$, (d) $\alpha\text{-}T_{500}$, (e) BHA_{100}, (f) BHA_{500} over 26 weeks.

Table 5.9. Wavelengths and corresponding functional groups (Thermo Fisher Scientific, 2015).

Wavelength (cm^{-1})	Functional group
723	C=C alkene
1170	C-O ester/tert alcohol
1436	C-H methyl
1459	C-H methylene
1742	C=O esters
2855	C-H alkane
2924	C-H alkane

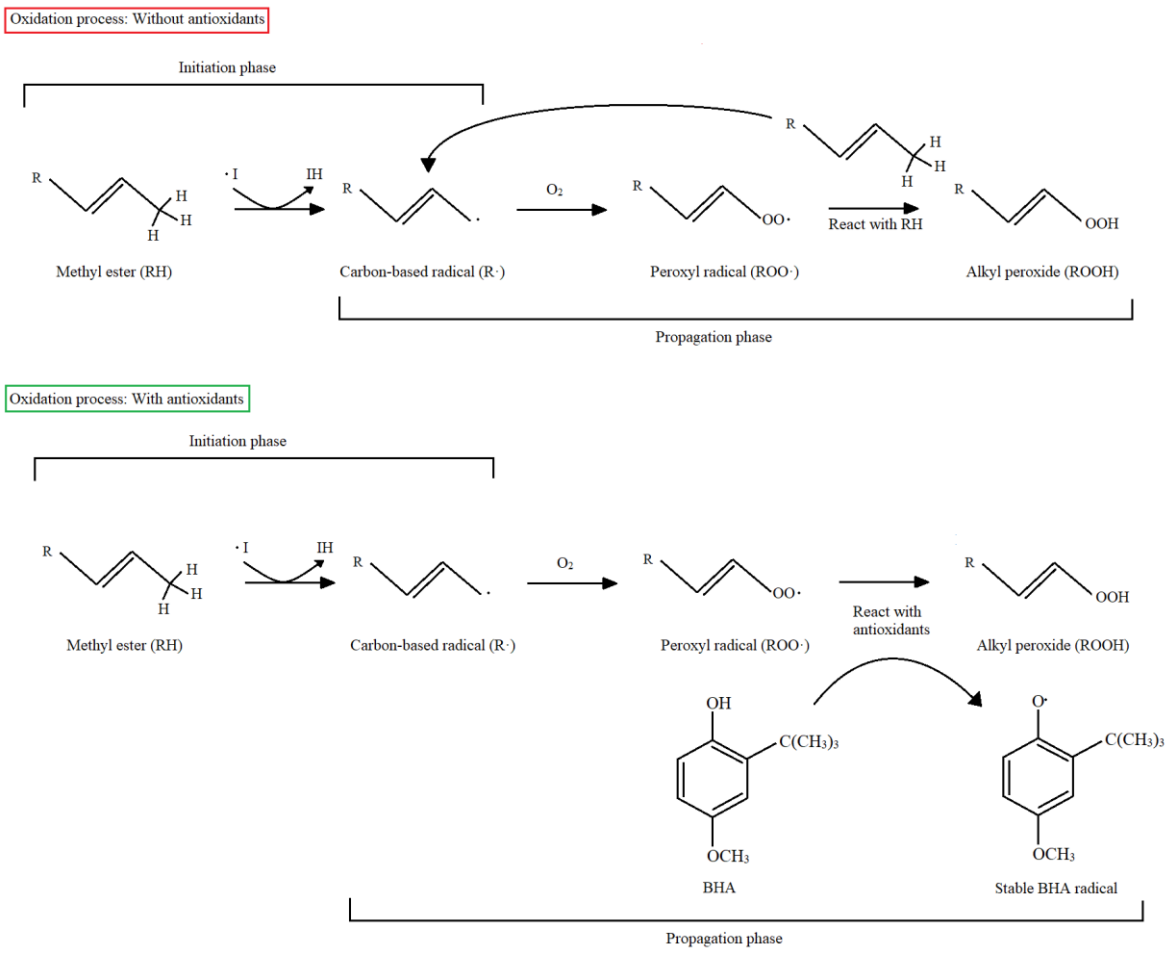

Figure 5.14. Oxidation mechanism with and without antioxidants (eg: BHA).

5.5.10 Gas chromatography-flame ionisation detector (GC-FID) analyses

Figure 5.15 and Figure 5.16 illustrate the concentrations of the major and minor esters, respectively as well as the regression lines. All samples reported high C16:0 and C18:1 which are the major esters naturally present inside palm biodiesel (Yung *et al*., 2006). The minor esters analysed ranged from C8 till C20.

Of all the esters present in palm biodiesel, linolenic acid methyl ester (C18:3) was the one of particular interest. As discussed in Chapter 2, oxidation occurs when radicals attack the double bonds of ester molecules due to the ease of electron transfer for the stabilisation of radicals. Hence, compounds with more double bonds are more prone to oxidation due to the increased number of sites for radical attacks. This is the reason why linolenic acid methyl ester content is one of the criteria stated in the EN 14214:2012 standard. The maximum permitted level is 12.0 %. As shown in Figure 6.16, none of the C18:3 for all fuel samples throughout 26 weeks had values above 0.13 %.

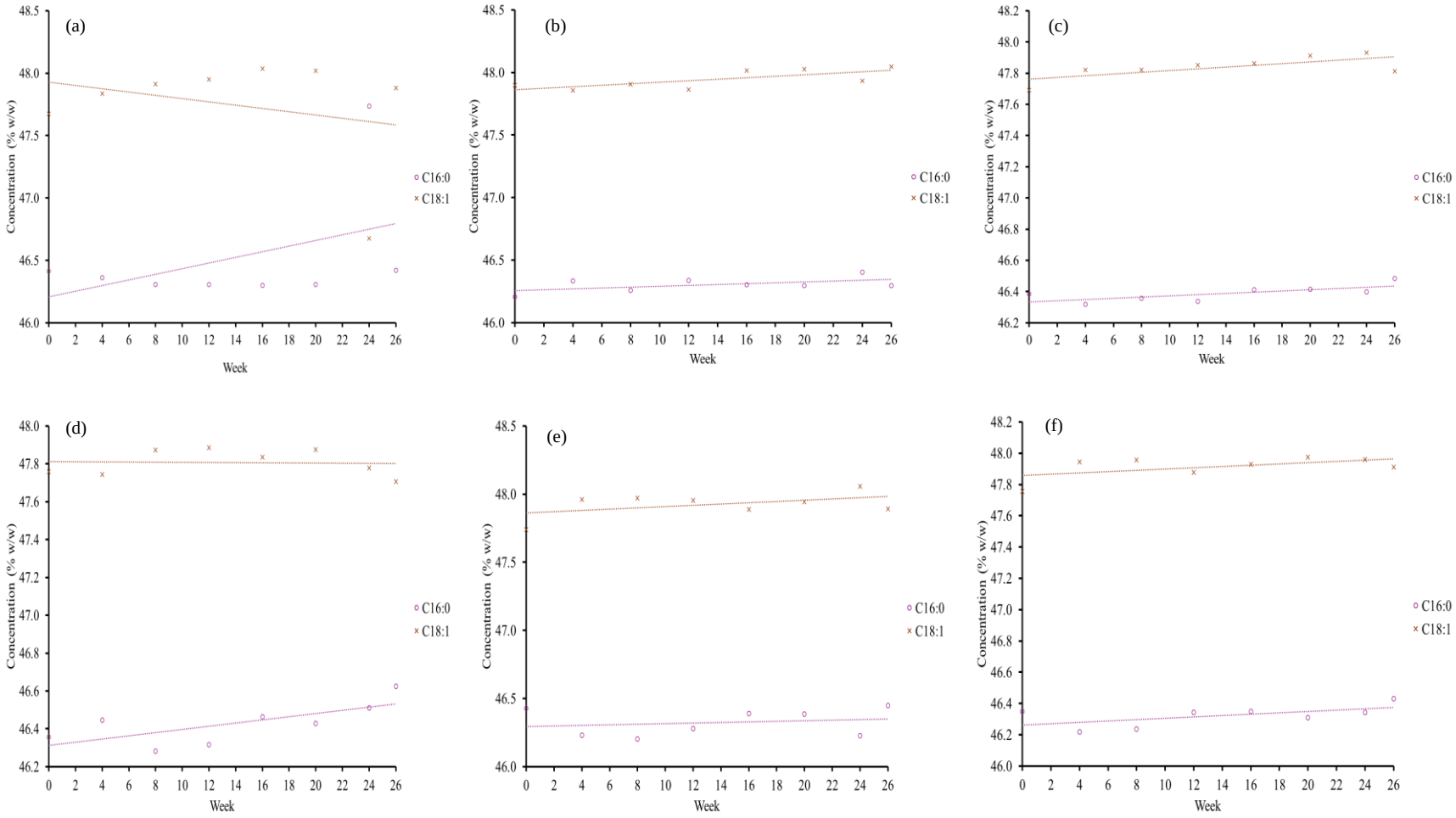

Figure 5.15. Concentration of major esters in DPOME with (a) $TBHQ_{100}$, (b) $TBHQ_{500}$, (c) $\alpha\text{-}T_{100}$, (d) $\alpha\text{-}T_{500}$, (e) BHA_{100}, (f) BHA_{500} over 26 weeks.

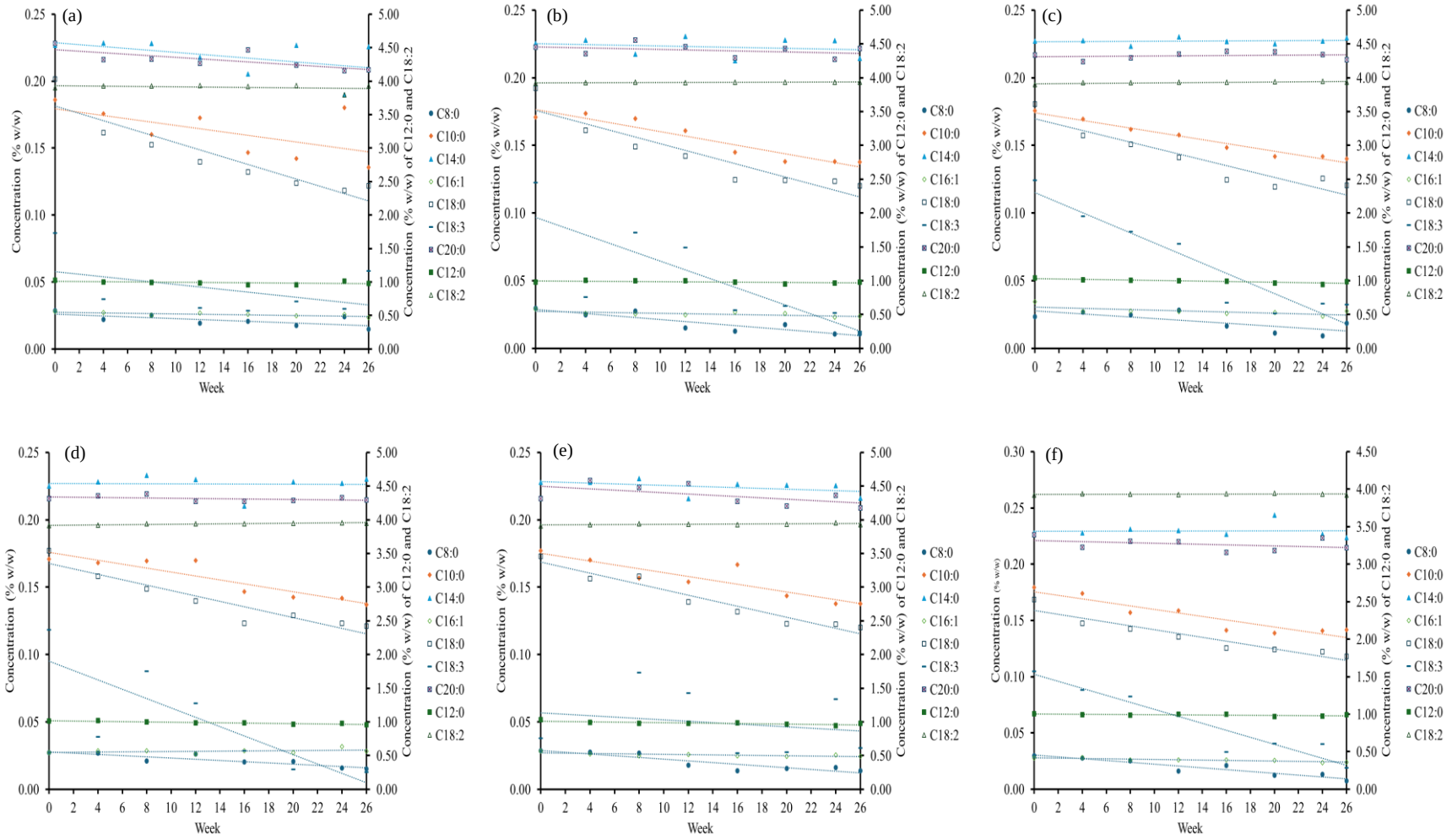

Figure 5.16. Concentration of minor esters in DPOME with (a) $TBHQ_{100}$, (b) $TBHQ_{500}$, (c) $\alpha\text{-}T_{100}$, (d) $\alpha\text{-}T_{500}$, (e) BHA_{100}, (f) BHA_{500} over 26 weeks.

Table 5.10 lists the coefficients and their corresponding p-values of the regressed plots. Significant decreasing trends in C18:3 (p-value < 0.05) were obtained for $TBHQ_{100}$, $TBHQ_{500}$, $\alpha\text{-}T_{100}$, $\alpha\text{-}T_{500}$ and BHA_{500} due to oxidation. However, BHA_{100} reported a p-value of 0.6096 which implied a weak decreasing trend over the storage period. Meanwhile, other ester chains with double bonds such as C18:1 and C18:2 had no significant declining trends as indicated by the large p-values for all samples. Here, it can be deduced that the radicals favoured attacking the carbon chains with the highest amount of double bonds first before moving to the ones with lower double bonds. In other words, palm biodiesel was relatively stable not only due to low amount of C18:3 which was the prime target for radical attacks during oxidation, but also due to the high amount of stable C16:0 and C18:1. It was noted that C8:0, C10:0, C18:0 and C16:1 had significant decreasing trends for all samples despite having no double bonds or a single double bond in the case of C16:1. However, all of these esters were present in extremely low concentrations and the declines might not necessarily be linked to the oxidation, but the analytical limitations at low concentrations. Literatures also suggested that no distinguished change was observed in B30 and B40 POME's ester content over storage period of 6 months (Fathurrahman *et al*., 2024). Such observations were due to the low concentration of the aforementioned C18:2 and C18:3 in POME, which were the main targets of oxidation processes. Since those methyl esters were minor esters in POME, oxidation will not occur as frequent as it was for biodiesel derived from feedstocks with high concentrations of the said methyl esters.

Table 5.10. Coefficients and p-values for regression analyses of ester concentrations data.

Ester	Parameter	$TBHQ_{100}$	$TBHQ_{500}$	$\alpha\text{-}T_{100}$	$\alpha\text{-}T_{500}$	BHA_{100}	BHA_{500}

C8:0	Coefficient	-0.0034	-0.0071	-0.0055	-0.0044	-0.0060	-0.0079
	p-value	0.0254	0.0020	0.0290	0.0036	0.0016	0.0003
C10:0	Coefficient	-0.0142	-0.0163	-0.0139	-0.0144	-0.0139	-0.0155
	p-value	0.0278	0.0002	0.0000	0.0008	0.0033	0.0011
C12:0	Coefficient	-0.0262	-0.0165	-0.0276	-0.0214	-0.0212	-0.0108
	p-value	0.0014	0.0756	0.0278	0.0063	0.0472	0.2629
C14:0	Coefficient	-0.0096	-0.0029	2.63E-05	-0.0008	-0.0030	-0.0004
	p-value	0.1910	0.3632	0.9893	0.7623	0.1515	0.8373
C16:0	Coefficient	-0.4241	-0.2152	-0.0434	-0.0402	-0.0314	-0.0684
	p-value	0.1646	0.3677	0.9101	0.8544	0.8551	0.7699
C16:1	Coefficient	-0.0015	-0.0015	-0.0022	0.0006	-0.0010	-0.0016
	p-value	0.0048	0.0250	0.0458	0.3455	0.0434	0.0003
C18:0	Coefficient	-0.0278	-0.0241	-0.0210	-0.0195	-0.0196	-0.0167
	p-value	0.0006	0.0007	0.0003	0.0005	0.0001	0.0004
C18:1	Coefficient	-0.7590	-0.2013	-0.0300	-0.1270	-0.0090	-0.0739
	p-value	0.2555	0.3866	0.9404	0.5347	0.9476	0.7278
C18:2	Coefficient	-0.0656	-0.0175	0.00476	0.0040	0.0033	-0.0085
	p-value	0.2650	0.3709	0.8843	0.7991	0.7717	0.5922
C18:3	Coefficient	-0.0656	-0.0175	0.0048	0.0040	0.0033	-0.0085
	p-value	0.0256	0.0167	0.0004	0.0091	0.6096	0.0002
C20:0	Coefficient	-0.0241	-0.0030	0.0002	-0.0015	-0.0048	-0.0027
	p-value	0.0007	0.1075	0.9400	0.0316	0.0954	0.3201

5.5.11 Gas chromatography-mass spectrometry (GC-MS) analyses

To elucidate the evolution of oxidation products, the GC-MS chromatograms of all samples doped with antioxidants were analysed. It was found that there little to no changes to the chromatograms over 26 weeks. As such, it can be concluded that BHA, TBHQ and α-T prevented or slowed the fuel oxidation process during storage for 26 weeks. The observations made concur with the rest of the results obtained for this last

phase of study. To further support this conclusion, the DPOME sample that was stored under the same conditions were analysed using GC-MS as well. The resulting gas chromatogram of DPOME is presented in Figure 5.17.

From Figure 5.17, a few observations were noted. First, in the chromatogram of DPOME, shorter peaks were detected at regions that were otherwise not found in other samples. This can be deduced as the detection of oxidation by-products forming in DPOME sample, which does not contain any additives. Second, a large peak at 22.52 min was detected, which was likely the major oxidation by-product. Lastly, for DPOME, the % transmittance at ~21 min region (C18 methyl esters (MEs)) was lower than those at ~19 min region (C16 MEs) in contrast to other samples. The lower % transmittance at the C18 ME region was the absolute evidence of C18 MEs, specifically methyl oleate (C18:1), methyl linoleate (C18:2) and methyl linolenate (C18:3) being consumed to the point where their concentrations fell below the C16 MEs. The DPOME chromatogram proved that the presence of antioxidants in the fuel samples correlated to the absence of significant changes in the doped samples' chromatograms over the storage period of 26 weeks. Since no significant changes were observed in the chromatograms across the weeks, the detected compounds are summarised as a whole in Table 5.11.

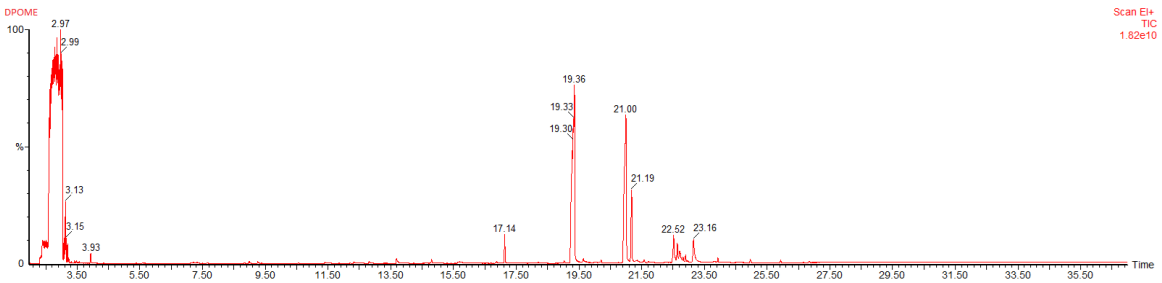

Figure 5.17. Gas chromatogram of DPOME.

For all fuel samples including DPOME, the standard palm oil FAME profile ranging from C10 to C20 were detected. The major compounds detected were C16:0, C18:1 and C18:2, which were the highest in concentrations. No oxidation by-products were detected according to the MS scans for all doped samples. Contrastingly, for DPOME, a range of oxidation by-products were detected. Traces of acetal, carboxylic acid, oxirane and alkylnoic acid were found in DPOME. The compound at 22.52 min was 3-octyl-oxiraneoctanoic acid ME. Additionally, 17-octadecynoic acid ME were also detected at the region close to 22.72 min. Furthermore, 9-oxo-nonanoic acid ME was also present in DPOME at trace level, which has been previously reported to be a possible oxidation precursor (Besser *et al*., 2017).

Figure 5.18 illustrates the proposed oxidation mechanisms for the formation of oxiraneoctanoic acid, 3-octyl-, trans- and 9-oxononanoic acid. First, the hydroxyl radical initiates the attack on the double bond of C18:1 ME and bonds itself onto the molecule. This then turns one of the C from the double bond into an electronegative state and attacks the hydroxyl group adjacent to it. As a result, oxiraneoctanoic acid, 3-octyl-, trans- is formed. The oxidation then propagates by further attack of hydroxyl radical on the epixode carbon atom. The attack of the second hydroxyl radical frees the epoxide ring and converts the unattached oxygen atom into a radical. Another attack from the electronegative oxygen atom on the adjacent carbon then splits the original C18:1 chain into two molecules. By absorbing an electron from nearby H^+ to stabilise the newly formed carbonyl radical, this finally leads to the formation of 9-oxononanoic acid as well as nonanol.

In addition, the proposed formation of 17-octadecynoic acid is visualised in Figure 6.19. Here, it is proposed that the hydroxyl radical initiates the attack on the hydrogen atom on the C18:1 ME, which results in the formation of an alkene radical and water. The alkene radical then stabilises itself by obtaining an electron from H^+ to form stable 17-octadecynoic acid, ME. However, the compound is expected to further oxidise given sufficient time due to the presence of its alkyne bond.

The main reason these compounds were not found in all samples with antioxidants was because the antioxidants aided to scavenge the initial radical as shown in Figure 5.14. Without these radicals, the fuel oxidation process was delayed until all the antioxidants were consumed thereby preventing the propagation of oxidation and formation of oxidation by-products. In future studies, isotope labelling can be considered in future studies to further investigate the actual points of radical attacks and the possibility of formation of intermediates/transition state during the oxidation process. This will enable more detailed oxidation pathways for each of the detected compounds to be developed.

Table 5.11. Compounds detected by gas chromatography-mass spectrometry (GC-MS) for fuel samples.

Compounds	$TBHQ_{100}$	$TBHQ_{500}$	$\alpha\text{-}T_{100}$	$\alpha\text{-}T_{500}$	BHA_{100}	BHA_{500}	DPOME
Duodecanoic acid, ME (12:0)	Trace	Trace	Trace	Trace	Trace	Trace	Trace
Tetradecanoic acid, ME (14:0)	○	○	○	○	○	○	○
Hexadecenoic acid, ME (16:1)	Trace	Trace	Trace	Trace	Trace	Trace	Trace
Hexadecanoic acid, ME (16:0)	○	○	○	○	○	○	○
Octadecadienoic acid, ME (18:2)	○	○	○	○	○	○	○
Octadecenoic acid, ME (18:1)	○	○	○	○	○	○	○
Octadecanoic acid, ME (18:0)	○	○	○	○	○	○	○
Eicosanoic acid, ME (20:0)	Trace	Trace	Trace	Trace	Trace	Trace	Trace
Eicosenoic acid, ME (20:1)	Trace	Trace	Trace	Trace	Trace	Trace	Trace
Ethanol	×	×	×	×	×	×	Trace
Octanal	×	×	×	×	×	×	Trace
Nonanal	×	×	×	×	×	×	Trace
Decenal	×	×	×	×	×	×	Trace
Undecenal	×	×	×	×	×	×	Trace
9,12-octadecadienal, dimethyl acetal	×	×	×	×	×	×	Trace
Pentanoic acid	×	×	×	×	×	×	Trace
Octanoic acid, ME (C8:0)	×	×	×	×	×	×	Trace
Nonanoic acid, 9-oxo, ME (C9:0)	×	×	×	×	×	×	Trace
Duodecanoic acid, -OH (C12:0)	×	×	×	×	×	×	Trace
16-OH, octadecane, 1-(ethenyloxy)-	×	×	×	×	×	×	Trace
17-octadecynoic acid, ME	×	×	×	×	×	×	○
13,16-octadecadiynoic acid, ME	×	×	×	×	×	×	Trace
Oxiraneoctanoic acid, 3-octyl-, ME	×	×	×	×	×	×	○
Oxiraneundecanoic acid, 3-pentyl-, ME	×	×	×	×	×	×	Trace
Methyl-8-oxooctanoate	×	×	×	×	×	×	Trace

○ = present, × = absent, ME = methyl ester.

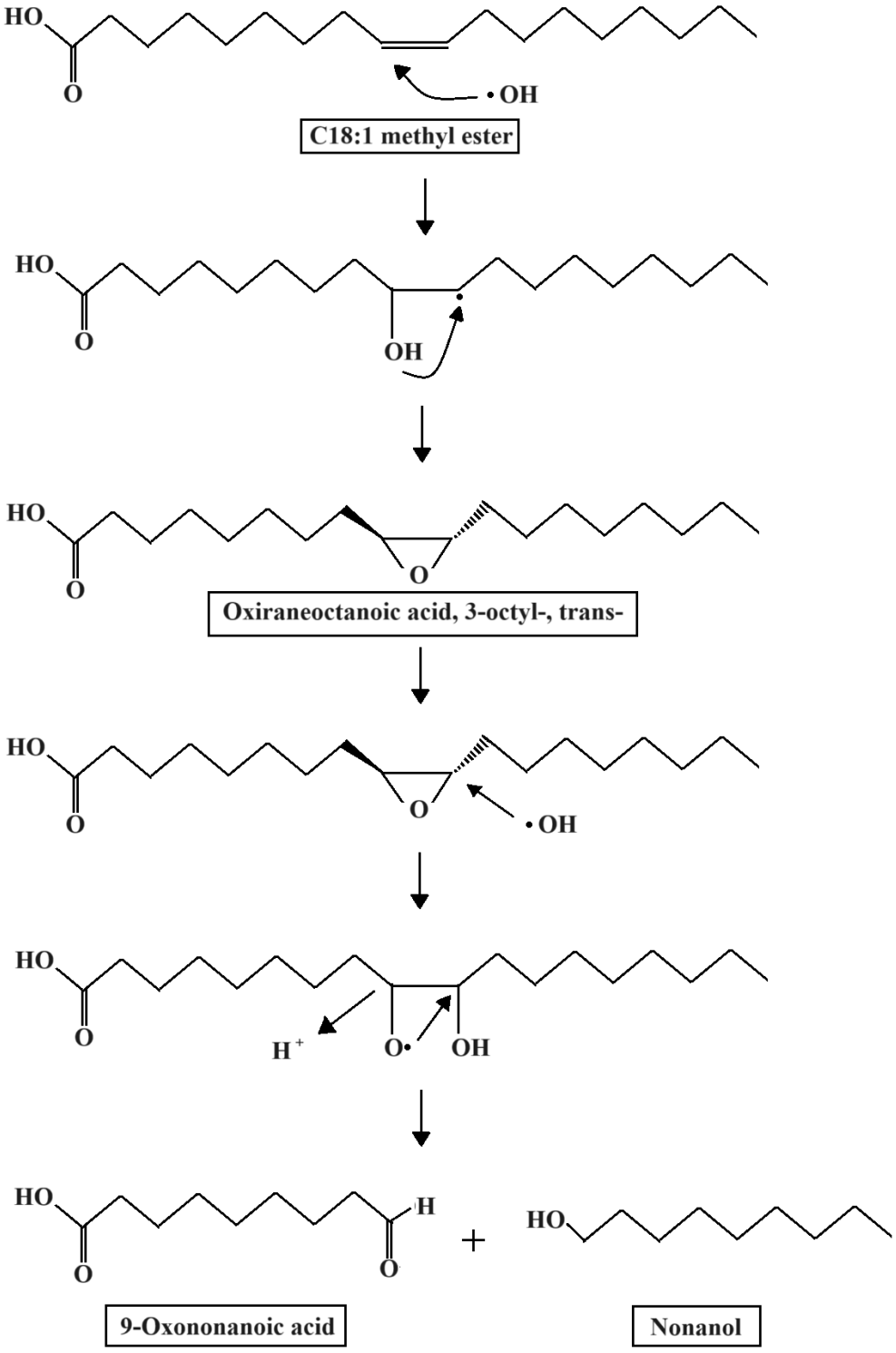

Figure 5.18. Proposed formation mechanisms of oxiraneoctanoic acid, 3-octyl-, trans- and 9-oxononanoic acid.

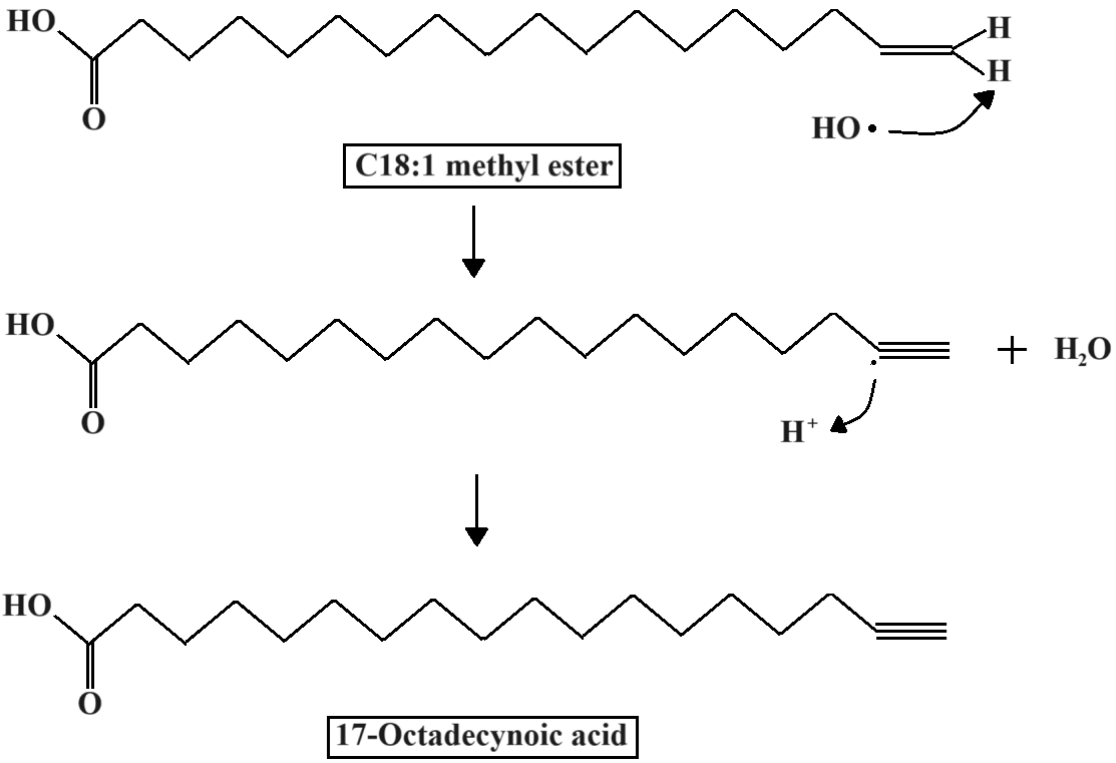

Figure 5.19. Proposed formation mechanism of 17-octadecynoic acid, ME.

5.6 Concluding remarks

In this final phase of project, the long-term storage stability of palm biodiesel with additives has been assessed through comprehensive analyses. Table 6.17 summarises the key findings from this phase. The Rancimat analyses found that TBHQ was the most effective antioxidant, followed by BHA and α-T. α-T was deemed not suitable for long-term storage of palm biodiesel due to the IP falling below the minimum limit stipulated in the EN 14214 standard. Using the PetroOXY test method, TBHQ had much lower IP values compared to BHA which concurred with the results obtained in the first phase and suggested that TBHQ thermal degradation might have occurred.

The acid values for all samples were maintained for the whole course of study, and the

higher concentration of $TBHQ_{500}$ correlated to increased acid value. Both acid value and iodine value had no significant trends based on regression analyses. The kinematic viscosities for all samples had significant increasing trends but were within the limit by the end of the storage period. Finally, the water contents of all samples were maintained below the EN 14214 limit throughout the storage and no significant trends were obtained.

The HPLC analyses indicated that there were significant increasing consumption rate trends for all samples. The consumption rate of antioxidants in increasing order was $BHA_{500} < TBHQ_{100} < TBHQ_{500} < BHA_{100} < \alpha\text{-}T_{100} < \alpha\text{-}T_{500}$. The high consumption rate of both α-T doped samples highlighted once again that α-T was not a feasible additive compared to TBHQ and BHA. From the FTIR spectra, no significant changes in the band at ~1740 cm^{-1} corresponding to the carbonyl group of oxidation by-products were detected for all doped samples showing that the additives aided in preventing or delaying oxidation. The increase in the ~1740 cm^{-1} band size for DPOME further justified this.

Analysis of the ester content via GC-FID showed that C18:3 had significant decreasing trends except for BHA_{100}. This could be attributed to the radicals favouring attacks on the carbon chains with the highest amount of double bonds first before moving to the ones with lower double bonds. The GC-MS results revealed that the two major oxidation products were 3-octyl-oxiraneoctanoic acid ME and 17-octadecynoic acid ME for palm biodiesel. Furthermore, traces of carboxylic acid, acetal, oxirane and alkylnoic acid were also found. Oxidation pathways for 3-octyl-oxiraneoctanoic acid ME, and 17-octadecynoic acid ME have been proposed based on the obtained results.

Table 5.12. Comparison of main results from Phase 4 of study.

Analytical test	Main results	Regression analysis
Rancimat IP	TBHQ > BHA > α-T Only α-T samples dropped below 8 h (α-T_{100} Week 4, α-T_{100} on Week 14)	Only $TBHQ_{100}$ and $TBHQ_{500}$ not significant
PetroOXY IP	BHA > α-T > TBHQ	Only $TBHQ_{500}$ not significant
Acid value	All samples met EN 14214	All not significant
Iodine value	All samples met EN 14214	All not significant
Kinematic viscosity	All samples met EN 14214	All significant
Water content	All samples met EN 14214	All not significant
HPLC	Increasing consumption rate trends observed for all samples	All significant
FTIR	Little to no changes in the bands at 1740 cm^{-1} for all doped samples. DPOME had increased % transmittance at 1740 cm^{-1}.	–
GC-FID	Decreasing C18:3 ester content observed for most samples.	All C18:3 decreasing trends significant except BHA_{100}
GC-MS	No obvious changes detected on chromatograms of doped samples. DPOME had oxidation by-products peaks which were detected by MS.	–

6. Modelling of oxidation stability properties for palm biodiesel with additives using artificial neural network (ANN)

6.1 Introduction

This chapter focuses on the third phase of work on developing artificial neural network (ANN) models to predict fuel stability properties for palm biodiesel based on the additive type and concentration. Using the MATLAB (version R2023b) software, ANN models for Rancimat and PetroOXY induction periods (IP), acid value, iodine value and kinematic viscosity were developed. A split of 70:15:15 (70 % training, 15 % validation, 15 % testing) from the data collected from the first phase of work were fed into the networks in randomised order for the development of the ANN models. The mean squared error (*MSE*) and correlation (R^2) values were used to validate the accuracy of the models. This chapter also discusses the potential of using the developed models to reduce experimental costs and time.

6.2 Experimental data input

The experimental results from the first phase as reported in Chapter 3 were used for the development of the ANN models. The ANN models were developed individually for Rancimat and PetroOXY IP, acid value, iodine value and kinematic viscosity. A total of 96 sets of data (Table A.1, A.3, A.5–A.7 in Appendix A) were utilised in the ANN model development.

6.3 Artificial neural network (ANN) modelling

The development of the ANN was accomplished using MATLAB version R2023b's Neural Net Fitting application. An example of an ANN architecture is shown in Figure 6.1. In general, artificial neurons are grouped together in different layers to process the data fed in the input layers. These data are then assigned with a weightage (*w*) and summed with a bias (*b*) (Ghasemzadeh *et al.*, 2018). The presence of weightage and bias enables the neural network to exert a distinguished behaviour during training thus lowering the errors of the developed ANN (Agu *et al.*, 2024). The general formula of data processing with ANN is shown as Eqn. 6.1.

$$y = wx + b \qquad \text{(Eqn. 6.1)}$$

where y is the output, x is the input, w is the weightage and b is the bias. A single output based on multiple inputs can also be expressed as the summation of each individual input multiplied by its respective weightages, then summed with the bias value. The equation for multiple inputs is shown as Eqn. 6.2.

$$y = w_1x_1 + w_2x_2 + w_3x_3 \ldots + \mathrm{b} \qquad \text{(Eqn. 6.2)}$$

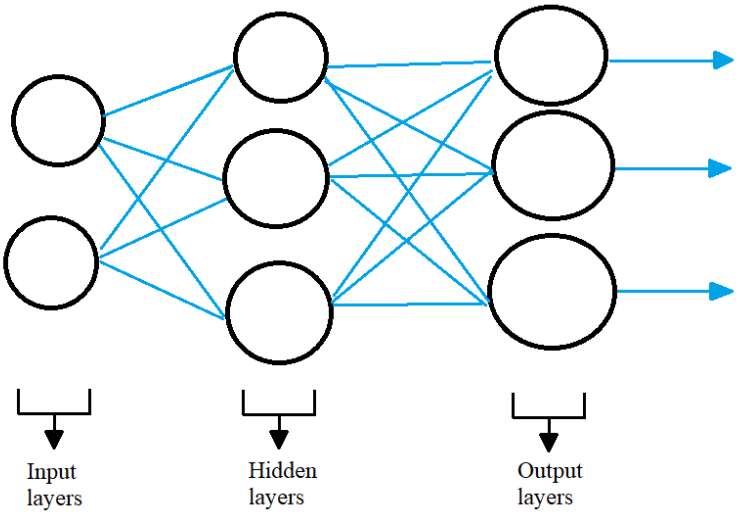

Figure 6.1. Example of an ANN design architecture.

The architecture of the ANN for this study consisted of 2 input variables, namely the type of additive and the additive concentration; and 1 output variable at a time (Rancimat IP, PetroOXY IP, acid value, iodine value and kinematic viscosity). As the inputs were only possible in numbers, all types of additives were assigned with individual code numbers as depicted in Table 6.1.

Table 6.1. Types of additives and their respective codes for ANN inputs.

Type of additive	Code
BHT	1
BHA	2
TBHQ	3
PG	4
PY	5
Quercetin	6
α-T	7
Curcumin	8

The ANNs were trained individually for each tests using the Levenberg-Marquardt training algorithm. Levenberg-Marquardt training algorithm was chosen because it has a fast convergence speed to solve non-linear least square problems (Che *et al.*, 2021). This method is also capable of finding a solution even if it is initiated far from the final minimum (Hemmati-Sarapardeh *et al.*, 2018). The 96 sets of raw data were split into 3 parts: training, validation, and testing. Default values of 70 % training (68 sets), 15 % validation (14 sets) and 15 % testing (14 sets) were randomly selected for the development of the ANNs. This was the same for all fuel oxidation stability properties (Rancimat IP, PetroOXY IP, acid value, iodine value and kinematic viscosity). It needs to be noted that the total of 28 sets from the validation and testing had no effect on the training phase and existed only to validate and test the performance of the ANN. The mean squared error (*MSE*) and correlation (R^2) were the error functions used to evaluate the performance of all 3 phases of the development.

6.4 Results and discussion

Past studies had highlighted the competency of ANN modelling compared to other existing modelling methods. ANN had shown higher accuracy compared to general regression neural network (GRNN) and response surface methodology (RSM) in the context of soybean biodiesel transesterification (Taib *et al.*, 2024). In addition, models of diesel engine performance also showed that ANN performed better than Nelder-Mead simplex algorithm (NM) as NM was more restricted to second-order polynomial (Esonye *et al.*, 2019). These were further supported by the superiority of ANN models in predicting oxidation stability of biodiesel with fruit peel waste extract (Bello *et al.*, 2024).

RSM models had lower R^2 values (0.9428 & 0.8091) compared to ANN (0.9710 & 0.9462). While most modelling studies focused on the biodiesel production and diesel performance, comparison studies of machine learning on biodiesel discussed the high accuracy of ANN compared to other conventional methods. Thus, the potentiality of ANN models for biodiesel stability should be further assessed.

Aside from setting the data split parameter for the development of the ANN models, the number of neurons present in the hidden layer is another variable that will impact the accuracy of the models. Table 6.2 shows that works on ANN modelling have reported the optimal neuron count to be within the range of 5–15. Values that are too low or too high are to be avoided as it is possible to underfit or overfit the data to the model. Based on that, the number of neurons for the hidden layer in this study were tested iteratively and the final values recorded in Table 6.3. Additionally, to discuss the accuracy of the model, *MSE* and *R* values were also recorded upon the completion of the development. The R^2 values were calculated by squaring the *R* values produced by the software.

Table 6.2. Number of neurons in reported ANN models.

ANN model	No of neurons	Reference
Pd-Ag membrane reactor (MR) system	10	Ghasemzadeh *et al*., 2018
Biodiesel production from waste catfish oil using heterogenous catalyst	10	Agu et al., 2024
Biodiesel production from microalgal oil	4	Sultana et al., 2022
Biodiesel production from castor oil	12	Banerjee et al., 2017
Biodiesel production from Nicotiana Tabacum L. oil	10	Samuel et al., 2021
Biodiesel production from waste cooking oil	11	Fangfang et al., 2021
Engine performance and combustion	3 and double	Esonye et al., 2019

emission characteristic of fuel blends	layered 3 (total 6)	
Combustion emission characteristic of COME biodiesel	4	Thulasiram et al., 2021
Biodiesel-emitted nitrogen oxides	10	Sayyed et al., 2023

From Figure 6.2, the Rancimat IP model yielded promising results using the default 10 neurons from the system. The *MSE* values of validation and testing were 6.7261 and 64.9252, respectively, which were much higher than the *MSE* of the training set. The R^2 value of testing set was also the lowest at 0.9801, indicating that the data used for testing were the least fitting compared to the other 2 sets. Nevertheless, the R^2 values of training and validation sets were high enough to be considered significant (0.9980 and 0.9973, respectively). Furthermore, from Table 6.3, the R^2 value of all data combined was calculated to be at 0.9966. As all R^2 values of Rancimat IP model were near to 1, this showed that Rancimat IP model was accurate to be used. Recent study on ANN modelling for biodiesel stability with plant extract also showcased high R^2 value (Bello *et al.*, 2024). The authors discussed 10 neurons were the best for Rancimat IP where the R^2 value were 0.9998, 0.9999 and 0.9999 for training, validation and testing set respectively.

Table 6.3. Summary of the number of neurons, *MSE* and R^2 values of all ANN models.

Property	No of neurons	Training		Validation		Testing	
		MSE	R^2	*MSE*	R^2	*MSE*	R^2
Rancimat IP	10	3.6540	0.9980	6.7261	0.9973	64.9252	0.9801
PetroOXY IP	7	90.8383	0.9916	76.6204	0.9951	100.4854	0.9943
Acid value	7	1.45E-04	0.9742	2.39E-04	0.9712	2.65E-04	0.9713
Iodine value	8	0.3921	0.8898	5.1206	0.9829	1.4054	0.9176
Kinematic	8	2.74E-07	0.9875	9.46E-07	0.9855	4.62E-07	0.9850

viscosity

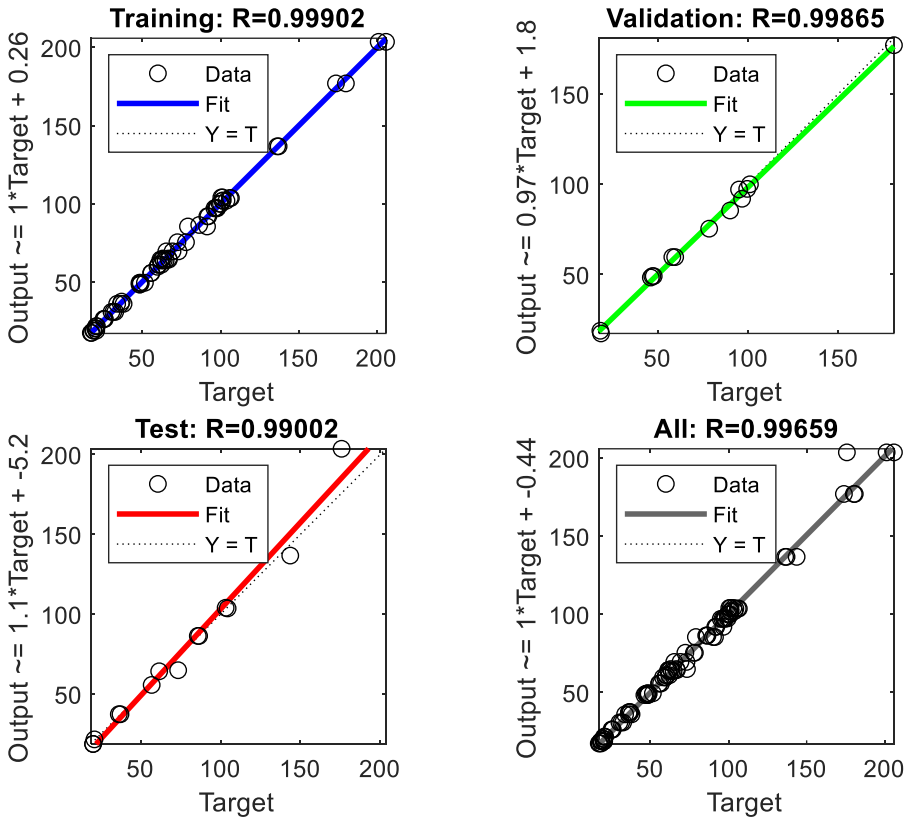

Figure 6.2. Diagnostic plots for Rancimat IP ANN.

To pursue a model of higher accuracy, the neuron count was iteratively adjusted for the PetroOXY IP model. The initial build went from 10 to 50 with increment of 10 per training session, but quickly proved to be not useful as the ANN was not learning the pattern of the data accurately enough to yield good *MSE* and R^2 values. This was most probably due to the overfitting of data during machine learning. The final trial for neuron count ended up at 7 as Figure 5.3 resulted after 5 min of relearning. The *MSE* of testing for the PetroOXY IP (100.4854) was the highest among the 3 phases of ANN development. This was the same as the Rancimat IP model. However, the R^2 values for

the PetroOXY oxidation stability model were 0.9916 (training), 0.9951 (validation), 0.9943 (testing) and 0.9927 (all), which were comparable to Rancimat's.

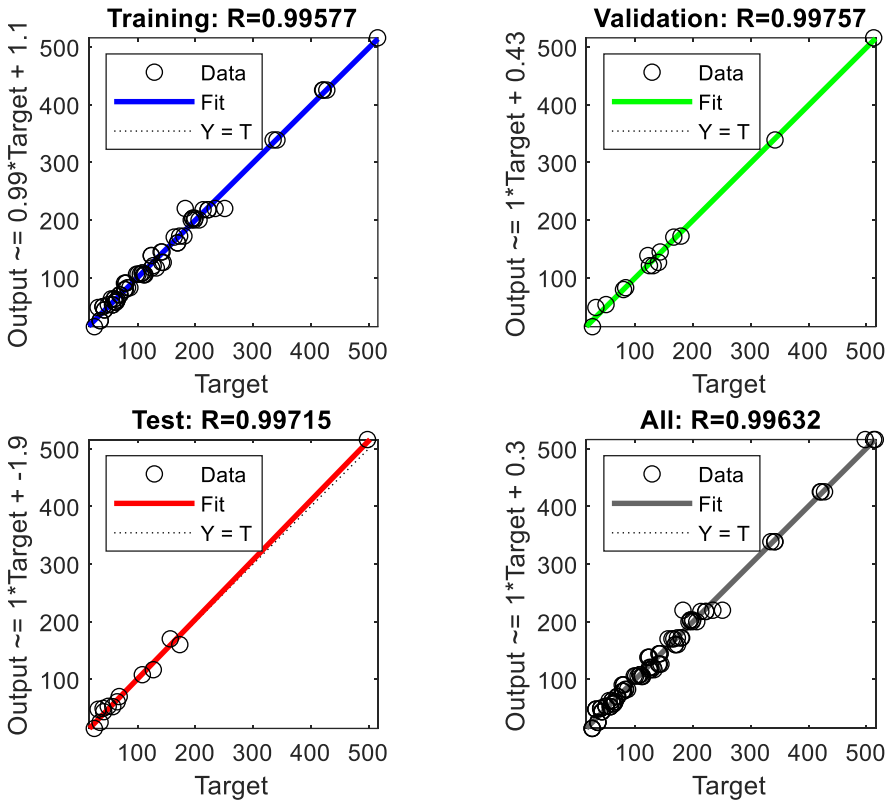

Figure 6.3. Diagnostic plots for PetroOXY IP ANN.

Following the PetroOXY IP model, the same neuron count of 7 was employed for developing the acid value model. The *MSE* values showed similar trends to the Rancimat and PetroOXY IPs whereby the highest value was recorded for the test set. This showed that the data for testing set were the least accurate among the 3 data sets. Furthermore, the R^2 value of the acid value testing set (0.9713) was also the lowest among all testing sets for all models developed. As the data were split randomly into 3 portions, it was hard to judge whether the testing of acid value model was the least convincing compared to the other models. Moreover, the R^2 values of the training and testing sets for acid value were

also the lowest recorded, which were 0.9742 for the training set and 0.9712 for the validation set. In addition, the R^2 value of all data for the acid value model was 0.9714, making it the least accurate model. It was also noticeable that the points fitted the best fit line well in Figure 6.4. Therefore, a neuron count of 7 was a better choice for the PetroOXY IP model compared to the acid value one. Nevertheless, the developed acid value model was deemed within the acceptable range ($p < 0.05$).

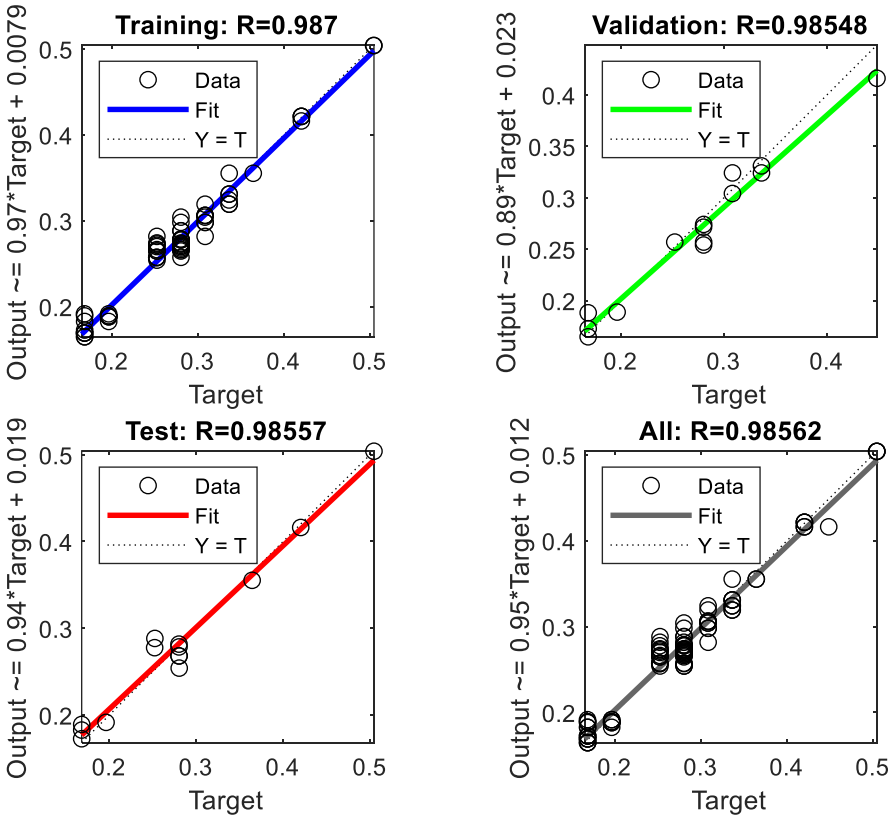

Figure 6.4. Diagnostic plots for acid value ANN.

Development of the iodine value model took the longest time to retrain compared to the other models due to the lack of significant trends as discussed in Chapter 3. The overall time taken for retraining to complete was approximately 3 h compared to the rest of the models that completed within 10–15 min each. Neuron counts within the range of 5 – 10

were tested to improve the accuracy of the model. The *MSE* and *R* values were monitored during the training process and 8 neurons was finalised at the end of the development. The *MSE* value of validation was highest at 5.1206, followed by testing at 1.4054, and finally training at 0.3921. The R^2 value of the validation set (0.9829) was the highest compared to the other sets. The R^2 value for the training set was only 0.8898, while it was 0.9176 for the testing set. The R^2 value for all data was even lower at 0.8387 which showed that the iodine value model was the least accurate. Compared to Figure 6.4, the points in Figure 6.5 tend to be scattered around the best fit line instead. To summarise, the lack of trends in the data set proved it hard even for machine learning, though such problems might be mitigated if the tests were conducted using instruments with higher accuracy.

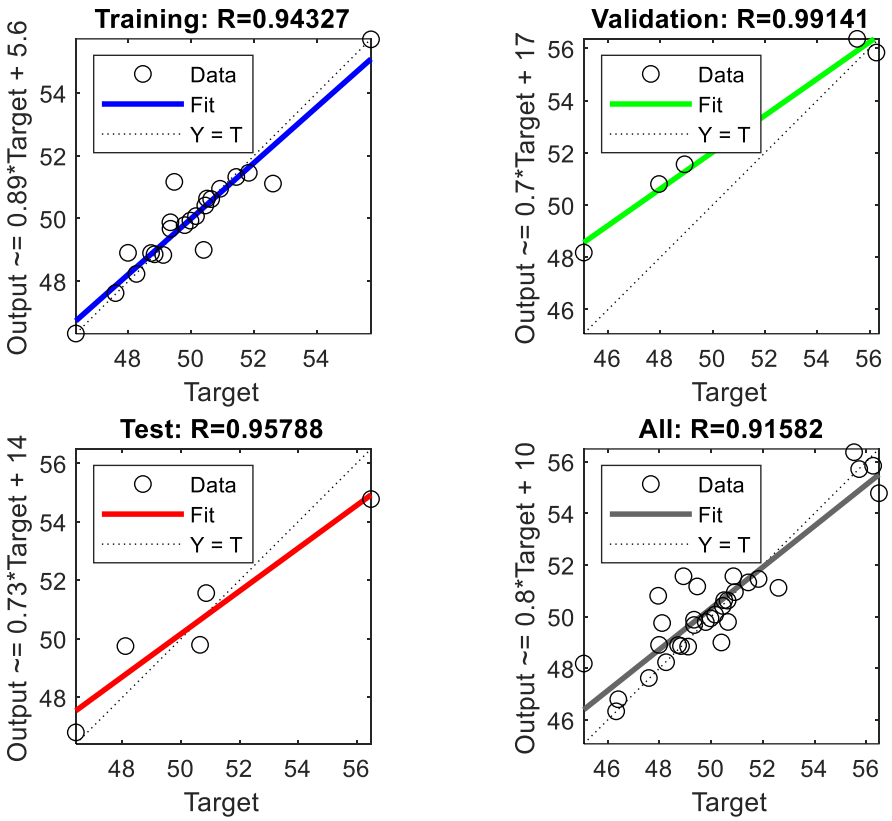

Figure 6.5. Diagnostic plots for iodine value ANN.

The neuron count was increased to 8 for the development of the kinematic viscosity model following the decrease of R^2 values obtained with the acid value model. Unlike the iodine value data set, the kinematic viscosity data set had a clearer trend. It was first hypothesised that the error functions values would be similar to those for the acid value, but the R^2 values of all sets were actually higher. All R^2 values were significantly valid (training: 0.9875, validation: 0.9855, testing: 0.9850), but still lower compared to the Rancimat and PetroOXY IP models ($p < 0.05$). Additionally, the R^2 value of all data was 0.9848, which was the second lowest after the acid value model. Unlike Figure 6.4, Figure 5.6 displays less scattered points especially in the plot for all data. This showed

that kinematic viscosity model was more accurate compared to the acid value model and highlighted that a neuron count of 7 – 8 was optimal for the number of neurons in the hidden layer for the modelling architecture developed in this study.

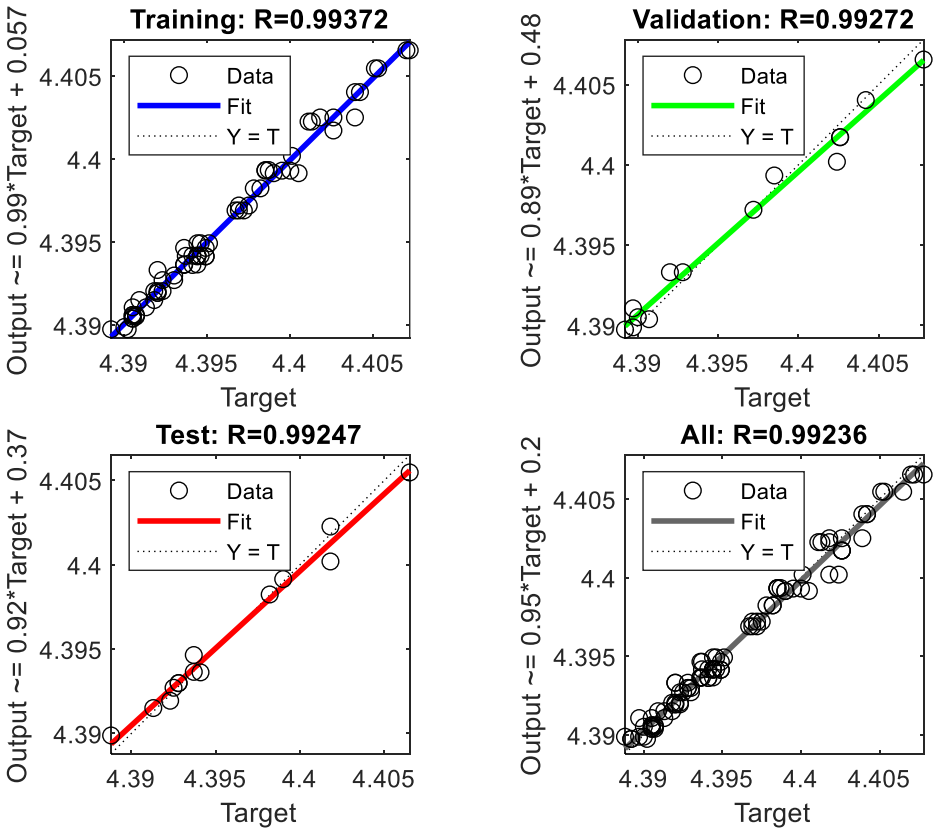

Figure 6.6. Diagnostic plots for kinematic viscosity ANN.

Overall, all the models developed were satisfactory, with the iodine value model being the least accurate. The models will allow predictions of the oxidation properties of palm biodiesel containing additives within the range of 250–1000 ppm, which will greatly reduce the analyses time and cost. Taking TBHQ at 250 ppm as an example in Table 5.4, the estimated total analysis time for this sample is extremely long at 2365 min, and samples with higher stability than $TBHQ_{250}$ will require an even longer analysis time on the Rancimat and PetroOXY equipment. By utilising the developed ANN models, the

prediction of highly accurate oxidation properties test can be done almost instantaneously. This eliminates time consuming process of repeated samples analyses.

Table 6.4 highlights the analysis time and cost needed for a single run of tests using $TBHQ_{250}$ as an example. It was noticeable that Rancimat was the most time-consuming test. The same was true for the cost of consumables, mainly due to the costly reaction vessels and air tubes needed for the Rancimat analysis. These are single-use accessories. The acid value and iodine value are more costly compared to the PetroOXY and kinematic viscosity due to the need for chemicals. With the developed ANNs having the ability to accurately predict the oxidation stability properties, this not only saves time and cost, but also reduces chemical wastes. Going forward, it might be possible to tackle the modelling of oxidation stability properties over storage time given the accuracy of the models developed in this chapter. Extra inputs such as storage time, biodiesel type and biodiesel blend can be included for a much higher accuracy in the ANN models developed. This will not only greatly reduce the time and cost for analysing said fuel for a long period of time, but also significantly boost the development for a much greener fuel for the future. Downside of this would be a large amount of data had to be analysed in order to produce a model that can fit multiple types of biodiesel and additives.

Table 6.4. Estimated analysis time and consumables cost for $TBHQ_{250}$.

Oxidation properties test	Analysis time (min)[a]	Consumables cost (RM)[b]
Rancimat	2100	34.20
PetroOXY	70	0.33
Acid value	15	3.38
Iodine value	150	3.21

Kinematic viscosity	30	0.15
Total	2365	41.27

[a]Analysis time includes the time needed for instruments to restabilise for subsequent sample analysis.
[b]Consumables cost are estimations, which includes utility costs and consumables. Prices are subjected to changes based on supplier's stock availability.

6.5 Concluding remarks

ANN models for Rancimat and PetroOXY IP, acid value, iodine value and kinematic viscosity for palm biodiesel with additives were developed using the Levernberg-Marquardt training method and validated with error functions. The *MSE* and R^2 values were used to discuss the accuracy of the model. Out of the 5 models, the Rancimat IP and PetroOXY IP were the most accurate with R^2 values (all) of 0.9932 and 0.9927, respectively. The accuracy of models in decreasing order of R^2 values (all) was Rancimat IP > PetroOXY IP > kinematic viscosity > acid value > iodine value. Acid value and iodine value were based on data sets with insignificant trends that might be the main reason behind the lower accuracy of the plots compared to the Rancimat and PetroOXY IPs. In addition, a neuron counts of 7 – 8 was found to be the most suitable for the development of ANN in this study. ANN also has the potential to greatly reduce the experimental analysis time and consumables cost. Also, ANN modelling of biodiesel stability over storage time can be developed given the accuracy of ANN models discussed. Such development will greatly help in the successful rollout of a more sustainable green fuel.

7. Conclusions and future work

7.1 Conclusions

This thesis has documented the results of a PhD study to evaluate synthetic and bio-based additives as oxidation stability enhancers in palm biodiesel. Comparative assessment of the effects of synthetic and bio-based additives on the oxidation stability of palm biodiesel was carried out in the first phase. Subsequently, the second phase focused on the appraisal of the oxidation kinetics and thermodynamics of palm biodiesel with selected additives. In the third phase, ANN models were developed to correlate the fuel oxidation stability with the additive type and concentration. Finally, the long-term storage stability of palm biodiesel with additives was evaluated and oxidation pathways of palm biodiesel under long-term storage was formulated. The following conclusions have been obtained from this study:

Comparative assessment of the effects of additives showed that TBHQ was the most effective antioxidant based on the results of Rancimat IP and effectiveness factor, as well as acid value and iodine value. A notable finding from this phase of study was the reverse ranking of TBHQ in terms of IP when tested using the PetroOXY, which was likely caused by its degradation under the high temperature and pressure of the PetroOXY system. PY, PG, BHT, BHA and quercetin demonstrated mid-range to high effectiveness in terms of IP under both the Rancimat and PetroOXY tests. Nevertheless, PY, quercetin and curcumin could not be dissolved fully in DPOME. Although α-T and curcumin had the least effects on IP and effectiveness factor, the assessment found that the oxidation stability, acid value, iodine value and kinematic viscosity of all samples met the limits of the EN 14214 standard except for the acid value of 1000 ppm PG. ANOVA tests yielded

significant dependence of IP and kinematic viscosity on the concentration, type and the interaction of both variables. Linear correlations were developed to predict the Rancimat IP values based on the IP values obtained by PetroOXY. The R^2 of the correlations ranged within 0.7922 (α-T) – 0.9937 (curcumin). These correlations would prove useful in the case of availability of only the PetroOXY equipment for IP measurements. Not only that, said correlation also highlighted the importance to study how different antioxidants work in palm biodiesel, in order to fully elucidate the proper relationship between Rancimat and PetroOXY results. Overall, TBHQ, BHA, BHT and α-T were assessed as the best additives for in-depth evaluation as oxidation stability enhancers.

In the appraisal of the oxidation kinetics and thermodynamics, it was found that DPOME dosed with BHA, BHT, TBHQ and α-T followed the first order kinetic model. This was supported by the high R and R^2 values and low χ^2 values. The first order rate constants (k) increased as the temperature increased, indicating increased reaction rates with higher molecular kinetic energy. Notably, the k values of all samples dosed with antioxidants were lower compared to DPOME at fixed temperatures which showed the potential of antioxidants in maintaining the stability of DPOME. The E_a of all samples also increased upon the addition of antioxidants. All samples demonstrated positive $\Delta H^{\ddagger}$ values (74.4642 – 90.5063 $kJmol^{-1}$) and negative $\Delta S^{\ddagger}$ values (-59.0494 – -22.1861 $JK^{-1}mol^{-1}$), highlighting that the reactions were endothermic and non-spontaneous. Furthermore, the positive $\Delta G^{\ddagger}$ values (98.9037 – 101.0857 $kJmol^{-1}$) described the reactions as endergonic reactions. This phase concluded that TBHQ, BHA and α-T should be included for evaluation of the long-term palm biodiesel storage stability and formulation of oxidation pathways.

Under long-term storage of 26 weeks, the results of Rancimat IP analyses determined that TBHQ was the most effective antioxidant, followed by BHA and α-T. The IP of α-T fell below the EN 14214 limit and hence, it was evaluated as not suitable for long-term storage of palm biodiesel. Interestingly, TBHQ had much lower IP values compared to BHA using the PetroOXY test method, which agreed with the results obtained in the first phase and suggested that TBHQ thermal degradation might have occurred. The acid values, iodine values, kinematic viscosities and water contents for all samples did not breach the limits of the EN 14214 standard by the end of the storage period. Significant increasing trends were noted for the kinematic viscosities of all samples. To briefly summarise, synthetic antioxidants still worked better than bio-based antioxidants in the context of palm biodiesel.

Over the course of 26 weeks, the consumption rate of antioxidants in increasing order was BHA_{500} < $TBHQ_{100}$ < $TBHQ_{500}$ < BHA_{100} < $\alpha\text{-}T_{100}$ < $\alpha\text{-}T_{500}$. The high consumption rate of both α-T samples reiterated that α-T was not a feasible additive compared to TBHQ and BHA for long-term fuel protection. The FTIR analyses highlighted no significant changes in the band at ~1740 cm^{-1} (carbonyl group of oxidation by-products) for all samples showing that the additives aided in preventing or delaying oxidation. The increase in the ~1740 cm^{-1} band size for DPOME further justified this. Additionally, GC-FID analyses indicated that the decreasing C18:3 trends could be attributed to the radicals favouring attacks on the carbon chains with the highest amount of double bonds first. The two major oxidation products of palm biodiesel over long-term storage were 3-octyl-oxiraneoctanoic acid ME and 17-octadecynoic acid ME as elucidated via GC-MS analyses. Traces of carboxylic acid, acetal, oxirane and alkylnoic acid were also detected.

It was postulated that 9-oxononanoic acid and nonanol were formed through multi-stepped hydroxyl radical attacks on the double bond of C18:1 ME, with 3-octyl-oxiraneoctanoic acid ME being the intermediate from the first hydroxyl radical attack that forms oxirane ring on the said bond. Meanwhile, 17-octadecynoic acid ME was postulated to form from the loss of H^+ from bisallylic site during radical attack. The discovery of these oxidation products enables subsequent study on a more detailed level, which will in turn elucidates the full oxidation pathways of palm biodiesel.

ANN models for Rancimat and PetroOXY IP, acid value, iodine value and kinematic viscosity for palm biodiesel with additives were successfully developed using the Levernberg-Marquardt training method and validated with the *MSE* and R^2 error functions. The accuracy of models in decreasing order of R^2 values (all sets) was Rancimat IP > PetroOXY IP > kinematic viscosity > acid value > iodine value. Acid value and iodine value were based on data sets with insignificant trends that might be the main reason behind the lower accuracy of the plots compared to the Rancimat and PetroOXY IPs. A neuron counts of 7–8 was found to be the most suitable for the development of ANN in this study. Furthermore, the potential of the developed ANN to reduce the experimental analysis time and consumables cost has been demonstrated. Usage of high accuracy ANN model can significantly speed up the biodiesel stability research for a much viable renewable fuel option to replace existing fossil diesel.

7.2 Future Work

Following the findings of this study, there were a few areas worthy of future investigation

as discussed below.

First, the contradictory IP results of TBHQ and BHA using Rancimat and PetroOXY can be further explored. Studies investigating the thermal degradation of TBHQ under high temperature and pressure will be useful in this respect. Additionally, more depth studies comparing the two IP analytical methods will enhance the understanding and applicability of PetroOXY as a viable substitute for the time-consuming Rancimat method. Also, an in-depth study on how each antioxidant worked in the context of palm biodiesel can also be studied. This will allow the deeper understanding of the correlation between Rancimat and PetroOXY data, which may further impact the relevancy of both tests under EN 14214 and ATSM D6751 limit regulations.

Next, the formulation of oxidation pathways for palm biodiesel can be further improved by using the isotope labelling approach which facilitates the identification of the point of attacks by the radicals. This can be accomplished by using nuclear magnetic resonance (NMR) spectroscopy, which was not possible in this study due to the unavailability of equipment and high analytical cost.

Lastly, other machine learning algorithms such as Bayesian regularization and scaled conjugated gradient can be employed to further compare and discuss the viability of the developed ANN models. The R^2 and *MSE* values from different training algorithms can be compared to evaluate which method is most suited for the prediction of palm biodiesel oxidation stability properties.

References

Agarwal, A.K., Khurana, D., 2013. Long-term storage oxidation stability of Karanja biodiesel with the use of antioxidants. Fuel Processing Technology 106, 447–452. https://doi.org/10.1016/j.fuproc.2012.09.011

Aghbashlo, M., Peng, W., Tabatabaei, M., Kalogirou, S.A., Soltanian, S., Hosseinzadeh-Bandbafha, H., Mahian, O., Lam, S.S., 2021. Machine learning technology in biodiesel research: A review. Prog Energy Combust Sci. https://doi.org/10.1016/j.pecs.2021.100904

Alhaithloul, H.A.S., Galal, F.H., Seufi, A.E.M., 2021. Effect of extreme temperature changes on phenolic, flavonoid contents and antioxidant activity of tomato seedlings (Solanum lycopersicum L.). PeerJ 9. https://doi.org/10.7717/peerj.11193

Amaral, A.A. do, Schuster, G.C., Boschen, N.L., Benvegnú, D.M., Wyzykowski, J., Pinto Rodrigues, P.R., Gallina, A.L., 2019. Antioxidant evaluation of extracts of pecan nutshell (Carya illinoensis) in soybean biodiesel B100 . Global Challenges 3, 1900001. https://doi.org/10.1002/gch2.201900001

Agu, C. M., Ani, K. A., Abiazieije, P. O., Omeje, J. A., Ekuma, J. C., Umelo, U. E., Omukwu, O. H., Nwankwo, E. D., & Chinedu, M. P., 2024. Biodiesel production from waste cat fish oil using heterogeneous catalyst from cat fish born: A viable waste management approach, and ANN modeling of biodiesel yield. Waste Management Bulletin, 1(4), 172–181. https://doi.org/10.1016/j.wmb.2023.11.002

Araújo, S. v., Rocha, B. S., Luna, F. M. T., Rola, E. M., Azevedo, D. C. S., & Cavalcante, C. L., 2011. FTIR assessment of the oxidation process of castor oil FAME submitted to PetroOXY and Rancimat methods. Fuel Processing Technology, 92(5), 1152–1155. https://doi.org/10.1016/j.fuproc.2010.12.026

Awalludin, M.F., Sulaiman, O., Hashim, R., Nadhari, W.N.A.W., 2015. An overview of the oil palm industry in Malaysia and its waste utilization through thermochemical

conversion, specifically via liquefaction. Renewable and Sustainable Energy Reviews. https://doi.org/10.1016/j.rser.2015.05.085

Baldim, J.L., Alcantara, B.G.V. de, Domingos, O.D.S., Soares, M.G., Caldas, I.S., Novaes, R.D., Oliveira, T.B., Lago, J.H.G., Chagas-Paula, D.A., 2017. The correlation between chemical structures and antioxidant, prooxidant, and antitrypanosomatid properties of flavonoids. Oxid Med Cell Longev 2017. https://doi.org/10.1155/2017/3789856

Bao, Y., Ren, X., Zhu, Y., Zhang, Y., Peng, Z., Zhou, G., 2020. Comparison of lipid radical scavenging capacity of spice extract in situ in roast beef with DPPH and peroxy radical scavenging capacities in vitro models. LWT 130. https://doi.org/10.1016/j.lwt.2020.109626

Bär, F., Knorr, M., Schröder, O., Hopf, H., Garbe, T., Krahl, J., 2021. Rancimat vs. rapid small scale oxidation test (RSSOT) correlation analysis, based on a comprehensive study of literature. Fuel. https://doi.org/10.1016/j.fuel.2021.120160

Becerra-Herrera, M., Sayago, A., Beltrán, R., 2017. Exploring antioxidant reactivity and molecular structure of phenols by means of two coupled assays using fluorescence probe (2,3-diazabicyclo[2.2.2]oct-2-ene, DBO) and free radical (2,2-diphenyl-1-picrylhydrazyl, DPPH ·). Journal of Chemical Sciences 129, 1381–1390. https://doi.org/10.1007/s12039-017-1331-1

Banerjee, A., Varshney, D., Kumar, S., Chaudhary, P., & Gupta, V. K., 2017. Biodiesel production from castor oil: ANN modeling and kinetic parameter estimation. International Journal of Industrial Chemistry, 8(3), 253–262. https://doi.org/10.1007/s40090-017-0122-3

Bello, U., Amran, N. A., Hazwan Ruslan, M. S., Yáñez, E. H., Suparmaniam, U., Adamu, H., Abba, S. I., Tafida, U. I., & Mahmoud, A. A., 2024. Enhancing oxidative stability of biodiesel using fruit peel waste extracts blend: Comparison of predictive modelling via RSM and ANN techniques. Results in Engineering, 21, 1-15. https://doi.org/10.1016/j.rineng.2024.101853

Bernama, 2021. Malaysia's biodiesel mandate to be delayed by 6 months. Star. URL https://www.thestar.com.my/business/business-news/2021/01/07/malaysia039s-biodiesel-mandate-to-be-delayed-by-6-months

Bernama, 2016. Malaysia re-pledges to achieve 45 per cent CO2 emission by 2030. News Straits Time. URL https://www.nst.com.my/news/2016/04/140725/malaysia-re-pledges-achieve-45-cent-co2-emission-2030

Besser, C., Pisarova, L., Frauscher, M., Hunger, H., Litzow, U., Orfaniotis, A., & Dörr, N., 2017. Oxidation products of biodiesel in diesel fuel generated by artificial alteration and identified by mass spectrometry. Fuel, 206, 524–533. https://doi.org/10.1016/j.fuel.2017.06.038

Bharti, R., Singh, B., 2020. Green tea (Camellia assamica) extract as an antioxidant additive to enhance the oxidation stability of biodiesel synthesized from waste cooking oil. Fuel 262. https://doi.org/10.1016/j.fuel.2019.116658

Bradley M., 2015. FTIR basic organic functional group reference chart. Thermo Fisher Scientific. URL https://www.thermofisher.com/blog/materials/a-gift-for-you-an-ftir-basic-organic-functional-group-reference-chart/

Borsato, D., Cini, J.R.D.M., Silva, H.C. da, Coppo, R.L., Angilelli, K.G., Moreira, I., Maia, E.C.R., 2014a. Oxidation kinetics of biodiesel from soybean mixed with synthetic antioxidants BHA, BHT and TBHQ: Determination of activation energy. Fuel Processing Technology 127, 111–116. https://doi.org/10.1016/j.fuproc.2014.05.033

Borsato, D., Galvan, D., Pereira, J.L., Orives, J.R., Angilelli, K.G., Coppo, R.L., 2014b. Kinetic and thermodynamic parameters of biodiesel oxidation with synthetic antioxidants: Simplex centroid mixture design. J Braz Chem Soc 25, 1984–1992. https://doi.org/10.5935/0103-5053.20140182

Botella, L., Bimbela, F., Martín, L., Arauzo, J., Sánchez, J.L., 2014. Oxidation stability of biodiesel fuels and blends using the Rancimat and PetroOXY methods. Effect of 4-allyl-

2,6-dimethoxyphenol and catechol as biodiesel additives on oxidation stability. Front Chem 2. https://doi.org/10.3389/fchem.2014.00043

Bouaid, A., Martinez, M., Aracil, J., 2009. Production of biodiesel from bioethanol and Brassica carinata oil: Oxidation stability study. Bioresour Technol 100, 2234–2239. https://doi.org/10.1016/j.biortech.2008.10.045

Canha, N., Felizardo, P., Correia, M.J.N., 2018. Controlling the oxidative stability of biodiesel using oils or biodiesel blending or antioxidants addition. Environ Prog Sustain Energy 37, 1031–1040. https://doi.org/10.1002/ep.12778

Chakraborty, M., & Baruah, D. C., 2012. Investigation of oxidation stability of Terminalia belerica biodiesel and its blends with petrodiesel. Fuel Processing Technology, 98, 51–58. https://doi.org/10.1016/j.fuproc.2012.01.029

Che, T. C., Duan, H. F., & Lee, P. J., 2021. Transient wave-based methods for anomaly detection in fluid pipes: A review. Mechanical Systems and Signal Processing 160. Academic Press. https://doi.org/10.1016/j.ymssp.2021.107874

Chebotarev, A.N., Snigur, D. V., 2015. Study of the acid-base properties of quercetin in aqueous solutions by color measurements. Journal of Analytical Chemistry 70, 55–59. https://doi.org/10.1134/S1061934815010062

Christensen, E., McCormick, R.L., 2014. Long-term storage stability of biodiesel and biodiesel blends. Fuel Processing Technology 128, 339–348. https://doi.org/10.1016/j.fuproc.2014.07.045

Clemente, M. A. J., Marcheafave, G. G., Silva, H. H. P., Branco, I. G., Canesin, E. A., Mantovani, A. C. G., Chendynski, L. T., & Borsato, D., 2023. Addition of jabuticaba peel extract with antioxidant properties in biodiesel. Fuel Processing Technology, 243, 1-5. https://doi.org/10.1016/j.fuproc.2023.107678

de Sousa, L.S., de Moura, C.V.R., de Oliveira, J.E., de Moura, E.M., 2014. Use of natural antioxidants in soybean biodiesel. Fuel 134, 420–428. https://doi.org/10.1016/j.fuel.2014.06.007

de Sousa, L.S., Garcia, M.A.S., Santos, E.C.P., do Nascimento Silva, J., de Castro, A.G., de Moura, C.V.R., de Moura, E.M., 2019. Study of the kinetic and thermodynamic parameters of the oxidative degradation process of biodiesel by the action of antioxidants using the Rancimat and PetroOXY methods. Fuel 238, 198–207. https://doi.org/10.1016/j.fuel.2018.10.082

de Torres, C., Díaz-Maroto, M.C., Hermosín-Gutiérrez, I., Pérez-Coello, M.S., 2010. Effect of freeze-drying and oven-drying on volatiles and phenolics composition of grape skin. Anal Chim Acta 660, 177–182. https://doi.org/10.1016/j.aca.2009.10.005

Deng, X., Han, J., Yin, F., 2012. Net energy, CO2 emission and land-based cost-benefit analyses of Jatropha biodiesel: A case study of the Panzhihua region of Sichuan Province in China. Energies (Basel) 5, 2150–2164. https://doi.org/10.3390/en5072150

Devi, A., Das, V.K., Deka, D., 2019. A green approach for enhancing oxidation stability including long storage periods of biodiesel via Thuja oreantalis L. as an antioxidant additive. Fuel 253, 1264–1273. https://doi.org/10.1016/j.fuel.2019.05.127

Devi, A., Das, V.K., Deka, D., 2018. Evaluation of the effectiveness of potato peel extract as a natural antioxidant on biodiesel oxidation stability. Ind Crops Prod 123, 454–460. https://doi.org/10.1016/j.indcrop.2018.07.022

Devi, A., Das, V.K., Deka, D., 2017. Ginger extract as a nature based robust additive and its influence on the oxidation stability of biodiesel synthesized from non-edible oil. Fuel 187, 306–314. https://doi.org/10.1016/j.fuel.2016.09.063

Elsayed, M., Wang, J., Wang, H., Zhou, Z., Osman, A. I., Almutairi, A. W., Faisal, S., & Abomohra, A., 2024. Conversion of protein-rich waste into biodiesel by Hermetia illucens: Enhanced energy recovery and reduced greenhouse gas emissions. Sustainable

Energy Technologies and Assessments, 66. https://doi.org/10.1016/j.seta.2024.103825

Encinar, J.M., Nogales, S., González, J.F., 2020. The effect of BHA on oxidative stability of biodiesel from different sources. Greenhouse Gases: Science and Technology 10, 1193–1201. https://doi.org/10.1002/ghg.2038

Endalew, A.K., Kiros, Y., 2014. Catalytic Autoxidation of Fatty Acid Methyl Esters from Jatropha Oil. Journal of Fuels 2014, 1–6. https://doi.org/10.1155/2014/470790

Energy Institute 2023, 2023. Statistical Review of World Energy 2023 | 72nd edition.

Esonye, C., Onukwuli, O. D., Ofoefule, A. U., & Ogah, E. O., 2019. Multi-input multi-output (MIMO) ANN and Nelder-Mead's simplex based modeling of engine performance and combustion emission characteristics of biodiesel-diesel blend in CI diesel engine. Applied Thermal Engineering, 151, 100–114. https://doi.org/10.1016/j.applthermaleng.2019.01.101

Eyarkai Nambi, V., Gupta, R.K., Kumar, S., Sharma, P.C., 2016. Degradation kinetics of bioactive components, antioxidant activity, colour and textural properties of selected vegetables during blanching. J Food Sci Technol 53, 3073–3082. https://doi.org/10.1007/s13197-016-2280-2

Fan, P., Huber, D.J., Su, Z., Hu, M., Gao, Z., Li, M., Shi, X., Zhang, Z., 2018. Effect of postharvest spray of apple polyphenols on the quality of fresh-cut red pitaya fruit during shelf life. Food Chem 243, 19–25. https://doi.org/10.1016/j.foodchem.2017.09.103

Fangfang, F., Alagumalai, A., & Mahian, O., 2021. Sustainable biodiesel production from waste cooking oil: ANN modeling and environmental factor assessment. Sustainable Energy Technologies and Assessments, *46*. https://doi.org/10.1016/j.seta.2021.101265

Fathordoobady, F., Mirhosseini, H., Selamat, J., Manap, M.Y.A., 2016. Effect of solvent type and ratio on betacyanins and antioxidant activity of extracts from Hylocereus polyrhizus flesh and peel by supercritical fluid extraction and solvent extraction. Food

Chem 202, 70–80. https://doi.org/10.1016/j.foodchem.2016.01.121

Fatima, K., Masood, N., Luqman, S., 2016. Quenching of singlet oxygen by natural and synthetic antioxidants and assessment of electronic UV/Visible absorption spectra for alleviating or enhancing the efficacy of photodynamic therapy. Biomedical Research and Therapy 3. https://doi.org/10.7603/s40730-016-0008-6

Fazal, M.A., Jakeria, M.R., Haseeb, A.S.M.A., Rubaiee, S., 2017. Effect of antioxidants on the stability and corrosiveness of palm biodiesel upon exposure of different metals. Energy 135, 220–226. https://doi.org/10.1016/j.energy.2017.06.128

Fernandes, D.M., Sousa, R.M.F., de Oliveira, A., Morais, S.A.L., Richter, E.M., Muñoz, R.A.A., 2015. Moringa oleifera: A potential source for production of biodiesel and antioxidant additives. Fuel 146, 75–80. https://doi.org/10.1016/j.fuel.2014.12.081

Figueredo, I.D.M., Rios, M.A.D.S., Cavalcante, C.L., Luna, F.M.T., 2020. Effects of amine and phenolic based antioxidants on the stability of babassu biodiesel using Rancimat and differential scanning calorimetry techniques. Ind Eng Chem Res 59, 18–24. https://doi.org/10.1021/acs.iecr.9b05209

Focke, W.W., Westhuizen, I. Van Der, Oosthuysen, X., 2016. Biodiesel oxidative stability from Rancimat data. Thermochim Acta 633, 116–121. https://doi.org/10.1016/j.tca.2016.03.023

França, F.R.M., dos Santos Freitas, L., Ramos, A.L.D., da Silva, G.F., Brandão, S.T., 2017. Storage and oxidation stability of commercial biodiesel using Moringa oleifera Lam as an antioxidant additive. Fuel 203, 627–632. https://doi.org/10.1016/j.fuel.2017.03.020

Freitas, João P.A., França, F.R.M., Silva, M.S., Toms, R.J., da Silva, G.F., 2019. Evaluation of antioxidant activity of natural extracts on the oxidative stability of cottonseed biodiesel. Brazilian Journal of Chemical Engineering 36, 905–911. https://doi.org/10.1590/0104-6632.20190362s20180308

Freitas, João Paulo Almeida, França, F.R.M., Silva, M.S., Toms, R.J., Silva, G.F. da, 2019. Cottonseed biodiesel oxidative stability in mixture with natural antioxidants. Korean Journal of Chemical Engineering 36, 1298–1304. https://doi.org/10.1007/s11814-019-0287-x

Fröhlich, A., & Schober, S., 2007. The influence of tocopherols on the oxidation stability of methyl esters. JAOCS, Journal of the American Oil Chemists' Society, 84(6), 579–585. https://doi.org/10.1007/s11746-007-1075-z

García, M., Botella, L., Gil-Lalaguna, N., Arauzo, J., Gonzalo, A., Sánchez, J.L., 2017. Antioxidants for biodiesel: Additives prepared from extracted fractions of bio-oil. Fuel Processing Technology 156, 407–414. https://doi.org/10.1016/j.fuproc.2016.10.001

Gebresas, G. A., Szabó, T., & Marossy, K., 2023. Effects of acidity, number of hydroxyl group, and carbon chain length of carboxylic acids on starch cross-linking. Current Research in Green and Sustainable Chemistry, 6. https://doi.org/10.1016/j.crgsc.2022.100354

Ghasemzadeh, K., Ahmadnejad, F., Aghaeinejad-Meybodi, A., & Basile, A., 2018. Hydrogen production by a Pd–Ag membrane reactor during glycerol steam reforming: ANN modeling study. International Journal of Hydrogen Energy, 43(15), 7722–7730. https://doi.org/10.1016/j.ijhydene.2017.09.120

Ginanjar, K., Kuntolaksono, S., Widya Iskandar, A., Joelianingsih, Zaelani, R., Abdurrojaq, N., Anggarani, R., Setyo Wibowo, C., & Allif Fathurrahman, N., 2024. Experimental analysis of palm-oil biodiesel oxidation stability on the aging characteristics of diesel-biodiesel Blends. IOP Conference Series: Earth and Environmental Science, 1354(1). https://doi.org/10.1088/1755-1315/1354/1/012008

Gonçalves-Filho, D., & de Souza, D., 2022. Detection of synthetic antioxidants: what factors affect the efficiency in the chromatographic analysis and in the electrochemical analysis? Molecules 27(20). MDPI. https://doi.org/10.3390/molecules27207137

Goh, B.H.H., Chong, C.T., Ong, H.C., Milano, J., Shamsuddin, A.H., Lee, X.J., Ng, J.H., 2022. Strategies for fuel property enhancement for second-generation multi-feedstock biodiesel. Fuel 315. https://doi.org/10.1016/j.fuel.2022.123178

Gregório, A.P.H., Romagnoli, É.S., Borsato, D., Galvan, D., Spacino, K.R., 2018. Kinetic and thermodynamic parameters in biodiesel oxidation reaction in the presence of coffee leaves and sage extracts. Sustainable Energy Technologies and Assessments 28, 60–64. https://doi.org/10.1016/j.seta.2018.06.008

Hashemi, S.M.B., Brewer, M.S., Safari, J., Nowroozi, M., Abadi Sherahi, M.H., Sadeghi, B., Ghafoori, M., 2016. Antioxidant activity, reaction mechanisms, and kinetics of Matricaria recutita extract in commercial blended oil oxidation. Int J Food Prop 19, 257–271. https://doi.org/10.1080/10942912.2015.1020438

Hemmati-Sarapardeh, A., Varamesh, A., Husein, M. M., & Karan, K., 2018. On the evaluation of the viscosity of nanofluid systems: Modeling and data assessment. Renewable and Sustainable Energy Reviews 81, 313–329 https://doi.org/10.1016/j.rser.2017.07.049

Ho, 2020. Malaysia Introduces B20 Palm Biodiesel. Autoworld.com. URL http://autoworld.com.my/news/2020/02/24/malaysia-introduces-b20-palm-biodiesel/

Hosseinzadeh-Bandbafha, H., Tabatabaei, M., Aghbashlo, M., Khanali, M., & Demirbas, A., 2018. A comprehensive review on the environmental impacts of diesel/biodiesel additives. Energy Conversion and Management 174, 579–614 https://doi.org/10.1016/j.enconman.2018.08.050

Hwang, H.S., Winkler-Moser, J.K., 2014. Food additives reducing volatility of antioxidants at frying temperature. JAOCS, Journal of the American Oil Chemists' Society 91, 1745–1761. https://doi.org/10.1007/s11746-014-2525-z

Jahirul, M.I., Brown, R.J., Senadeera, W., Ashwath, N., Rasul, M.G., Rahman, M.M., Hossain, F.M., Moghaddam, L., Islam, M.A., O'Hara, I.M., 2015. Physio-chemical

assessment of beauty leaf (Calophyllum inophyllum) as second-generation biodiesel feedstock. Energy Reports 1, 204–215. https://doi.org/10.1016/j.egyr.2015.10.003

Jain, S., Purohit, S., Kumar, D., Goud, V. v., 2021. Passion fruit seed extract as an antioxidant additive for biodiesel; shelf life and consumption kinetics. Fuel 289. https://doi.org/10.1016/j.fuel.2020.119906

Jain, S., Sharma, M.P., 2012. Application of thermogravimetric analysis for thermal stability of Jatropha curcas biodiesel. Fuel 93, 252–257. https://doi.org/10.1016/j.fuel.2011.09.002

Jeong, S.M., Kim, S.Y., Kim, D.R., Jo, S.C., Nam, K.C., Ahn, D.U., Lee, S.C., 2004. Effect of heat treatment on the antioxidant activity of extracts from citrus peels. J Agric Food Chem 52, 3389–3393. https://doi.org/10.1021/jf049899k

Ji, X., Liang, J., Wang, Y., Liu, X., Li, Y., Liu, Q., & Liu, R., 2023. Synthetic Antioxidants as Contaminants of Emerging Concern in Indoor Environments: Knowns and Unknowns. Environmental Science and Technology 57 (51), 21550–21557. https://doi.org/10.1021/acs.est.3c06487

Jin, B., Liu, X., Liang, W., Li, Q., Yan, J.K., Han, Z., 2022. Preparation, physicochemical characteristics and bioactivity evaluation of pitaya peel extract/soy protein nanocomposite film containing zinc oxide nanoparticles by photocatalysis. J Food Process Preserv 46. https://doi.org/10.1111/jfpp.16584

Khoo, H.E., He, X., Tang, Y., Li, Z., Li, C., Zeng, Y., Tang, J., Sun, J., 2022. Betacyanins and anthocyanins in pulp and peel of red pitaya (Hylocereus polyrhizus cv. Jindu), inhibition of oxidative stress, lipid reducing, and cytotoxic effects. Front Nutr 9. https://doi.org/10.3389/fnut.2022.894438

Kivevele, T.T., Mbarawa, M.M., Bereczky, A., Laza, T., Madarasz, J., 2011. Impact of antioxidant additives on the oxidation stability of biodiesel produced from Croton Megalocarpus oil. Fuel Processing Technology 92, 1244–1248.

https://doi.org/10.1016/j.fuproc.2011.02.009

Kleinberg, M.N., Rios, M.A.S., Buarque, H.L.B., Parente, M.M.V., Cavalcante, C.L., Luna, F.M.T., 2019. Influence of synthetic and natural antioxidants on the oxidation stability of beef tallow before biodiesel production. Waste Biomass Valorization 10, 797–803. https://doi.org/10.1007/s12649-017-0120-x

Knothe, G., 2002. Structure indices in FA chemistry. How relevant is the iodine value? JAOCS 79, 847–854. https://doi.org/10.1007/s11746-002-0569-4

Knothe, G., Dunn, Robert.O., 2003. Dependence of oil stability index of fatty compounds on their structure and concentration and presence of metals. JAOCS 80, 1021–1026. https://doi.org/10.1007/s11746-003-0814-x

Knothe, G., Razon, L.F., 2017. Biodiesel fuels. Prog Energy Combust Sci. https://doi.org/10.1016/j.pecs.2016.08.001

Knothe, G., Steidley, K.R., 2005. Kinematic viscosity of biodiesel fuel components and related compounds. Influence of compound structure and comparison to petrodiesel fuel components. Fuel 84, 1059–1065. https://doi.org/10.1016/j.fuel.2005.01.016

Kumar, N., 2017. Oxidative stability of biodiesel: Causes, effects and prevention. Fuel. https://doi.org/10.1016/j.fuel.2016.11.001

Lacoste, F., Lagardere, L., 2003. Quality parameters evolution during biodiesel oxidation using Rancimat test. European Journal of Lipid Science and Technology 105, 149–155. https://doi.org/10.1002/ejlt.200390030

Lapuerta, M., Rodríguez-Fernández, J., Ramos, A., Álvarez, B., 2012. Effect of the test temperature and anti-oxidant addition on the oxidation stability of commercial biodiesel fuels. Fuel 93, 391–396. https://doi.org/10.1016/j.fuel.2011.09.011

Lau, C. H., Gan, S., Lau, H. L. N., Lee, L. Y., Thangalazhy-Gopakumar, S., & Ng, H. K., 2022. Insights into the effectiveness of synthetic and natural additives in improving

biodiesel oxidation stability. Sustainable Energy Technologies and Assessments, 52. https://doi.org/10.1016/j.seta.2022.102296

Lawan, I., Zhou, W., Garba, Z.N., Zhang, M., Yuan, Z., Chen, L., 2019. Critical insights into the effects of bio-based additives on biodiesels properties. Renewable and Sustainable Energy Reviews. https://doi.org/10.1016/j.rser.2018.12.008

Lewandowski, W., Lewandowska, H., Golonko, A., Świderski, G., Świsłocka, R., Kalinowska, M., 2020. Correlations between molecular structure and biological activity in "logical series" of dietary chromone derivatives. PLoS One 15. https://doi.org/10.1371/journal.pone.0229477

Li, J., Li, W., Deng, Z., Li, H., Yu, Y., Zhang, B., 2021. Comparison of free, conjugated, and insoluble-bound phenolics and their antioxidant activities in oven-drying and freeze-drying bamboo (Phyllostachys edulis) shoot tips. J Food Sci 86, 4223–4243. https://doi.org/10.1111/1750-3841.15881

Lik Nang Lau, H., Choo, Y.M., Ma, A.N., Chuah, C.H., 2008. Selective extraction of palm carotene and vitamin E from fresh palm-pressed mesocarp fiber (Elaeis guineensis) using supercritical CO2. J Food Eng 84, 289–296. https://doi.org/10.1016/j.jfoodeng.2007.05.018

Lourenço, S.C., Moldão-Martins, M., Alves, V.D., 2019. Antioxidants of natural plant origins: From sources to food industry applications. Molecules. https://doi.org/10.3390/molecules24224132

Mantovani, A.C.G., Chendynski, L.T., Santana, V.T., Borsato, D., di Mauro, E., 2021. Influence of antioxidants in biodiesel degradation: Electronic paramagnetic resonance tracking of free radicals. Fuel 287. https://doi.org/10.1016/j.fuel.2020.119531

Maroušek, J., Maroušková, A., Gavurová, B., Tuček, D., & Strunecký, O., 2023. Competitive algae biodiesel depends on advances in mass algae cultivation. Bioresource Technology 374. https://doi.org/10.1016/j.biortech.2023.128802

McCormick, R.L., Ratcliff, M., Moens, L., Lawrence, R., 2007. Several factors affecting the stability of biodiesel in standard accelerated tests. Fuel Processing Technology 88, 651–657. https://doi.org/10.1016/j.fuproc.2007.01.006

Mohamed Shameer, P., Ramesh, K., 2017. FTIR assessment and investigation of synthetic antioxidant on the fuel stability of Calophyllum inophyllum biodiesel. Fuel 209, 411–416. https://doi.org/10.1016/j.fuel.2017.08.006

Monde, A.A., Michel, F., Carbonneau, M.A., Tiahou, G., Vernet, M.H., Eymard-Duvernay, S., Badiou, S., Adon, B., Konan, E., Sess, D., Cristol, J.P., 2009. Comparative study of fatty acid composition, vitamin E and carotenoid contents of palm oils from four varieties of oil palm from Côte d'Ivoire. J Sci Food Agric 89, 2535–2540. https://doi.org/10.1002/jsfa.3740

Montoya, C., Cochard, B., Flori, A., Cros, D., Lopes, R., Cuellar, T., Espeout, S., Syaputra, I., Villeneuve, P., Pina, M., Ritter, E., Leroy, T., Billotte, N., 2014. Genetic architecture of palm oil fatty acid composition in cultivated oil palm (Elaeis guineensis Jacq.) compared to its wild relative E. oleifera (H.B.K) Cortés. PLoS One 9. https://doi.org/10.1371/journal.pone.0095412

MPOB, 2023. OVERVIEW OF MALAYSIAN OIL PALM INDUSTRY 2023.

Murta Valle, M.L., Leonardo, R.S., Dweck, J., 2014. Comparative study of biodiesel oxidation stability using Rancimat, PetroOXY, and low P-DSC. J Therm Anal Calorim 116, 113–118. https://doi.org/10.1007/s10973-014-3706-6

Nagarajan, S., Nagarajan, R., Kumar, J., Salemme, A., Togna, A.R., Saso, L., Bruno, F., 2020. Antioxidant activity of synthetic polymers of phenolic compounds. Polymers (Basel). https://doi.org/10.3390/POLYM12081646

Neumann, A., Jebens, T., Volkmar, W., 2008. A Method for Determining Oxidation

Stability of Petrodiesel, Biodiesel and Blended Fuels [WWW Document]. Am Lab. URL https://www.americanlaboratory.com/914-Application-Notes/34716-A-Method-for-Determining-Oxidation-Stability-of-Petrodiesel-Biodiesel-and-Blended-Fuels/

Neupane, D., Bhattarai, D., Ahmed, Z., Das, B., Pandey, S., Solomon, J.K.Q., Qin, R., Adhikari, P., 2021. Growing jatropha (Jatropha curcas l.) as a potential second-generation biodiesel feedstock. Inventions. https://doi.org/10.3390/inventions6040060

Nogales-Delgado, S., Encinar, J.M., González, J.F., 2019. Safflower biodiesel: Improvement of its oxidative stability by using BHA and TBHQ. Energies (Basel) 12. https://doi.org/10.3390/en12101940

Nogales-Delgado, S., Encinar, J.M., Guiberteau, A., Márquez, S., 2020. The effect of antioxidants on corn and sunflower biodiesel properties under extreme oxidation conditions. JAOCS, Journal of the American Oil Chemists' Society 97, 201–212. https://doi.org/10.1002/aocs.12288

Nogueira, T.R., de Mesquita Figueredo, I., Tavares Luna, F.M., Cavalcante, C.L., Evangelista de Ávila dos Santos, J., Sousa Lima, M.A., Josino da Silva, T.S., Almeida Moreira Leal, L.K., Nunes, F.M., Alexsandra de Sousa Rios, M., Ávila Pimenta, A.T., 2020. Evaluation of oxidative stability of soybean biodiesel using ethanolic and chloroform extracts of Platymiscium floribundum as antioxidant. Renew Energy 159, 767–774. https://doi.org/10.1016/j.renene.2020.06.062

Nunes, J.C., Lago, M.G., Castelo-Branco, V.N., Oliveira, F.R., Torres, A.G., Perrone, D., Monteiro, M., 2016. Effect of drying method on volatile compounds, phenolic profile and antioxidant capacity of guava powders. Food Chem 197, 881–890. https://doi.org/10.1016/j.foodchem.2015.11.050

Obadiah, A., Kannan, R., Ramasubbu, A., Kumar, S.V., 2012. Studies on the effect of antioxidants on the long-term storage and oxidation stability of Pongamia pinnata (L.) Pierre biodiesel. Fuel Processing Technology 99, 56–63. https://doi.org/10.1016/j.fuproc.2012.01.032

Ong, L.K., Kurniawan, A., Suwandi, A.C., Lin, C.X., Zhao, X.S., Ismadji, S., 2013. Transesterification of leather tanning waste to biodiesel at supercritical condition: Kinetics and thermodynamics studies. Journal of Supercritical Fluids 75, 11–20. https://doi.org/10.1016/j.supflu.2012.12.018

Park, W.H., 2022. Propyl gallate decreases the proliferation of Calu-6 and A549 lung cancer cells via affecting reactive oxygen species and glutathione levels. Journal of Applied Toxicology 42, 436–449. https://doi.org/10.1002/jat.4231

Pico, J., Xu, K., Guo, M., Mohamedshah, Z., Ferruzzi, M.G., Martinez, M.M., 2019. Manufacturing the ultimate green banana flour: Impact of drying and extrusion on phenolic profile and starch bioaccessibility. Food Chem 297. https://doi.org/10.1016/j.foodchem.2019.124990

Pullen, J., Saeed, K., 2012. An overview of biodiesel oxidation stability. Renewable and Sustainable Energy Reviews. https://doi.org/10.1016/j.rser.2012.06.024

Rajendran, S., 2020. Effect of antioxidant additives on oxides of nitrogen (NOx) emission reduction from Annona biodiesel operated diesel engine. Renew Energy 148, 1321–1326. https://doi.org/10.1016/j.renene.2019.10.104

Ramos, T.C.P.M., Santos, E.P.S., Ventura, M., Pina, J.C., Cavalheiro, A.A., Fiorucci, A.R., Silva, M.S., 2021. Eugenol and TBHQ antioxidant actions in commercial biodiesel obtained by soybean oil and animal fat. Fuel 286. https://doi.org/10.1016/j.fuel.2020.119374

Rapier, R., 2023. Global energy trends: Insights from the 2023 statistical review of world energy. Forbes. URL https://www.forbes.com/sites/rrapier/2023/08/06/global-energy-trends-insights-from-the-2023-statistical-review-of-world-energy/

Rashed, M.M., Kalam, M.A., Masjuki, H.H., Rashedul, H.K., Ashraful, A.M., Shancita, I., Ruhul, A.M., 2015. Stability of biodiesel, its improvement and the effect of antioxidant treated blends on engine performance and emission. RSC Adv.

https://doi.org/10.1039/c4ra14977g

Rashidi, L., Gholami, Z., Nanvazadeh, S., & Shabani, Z., 2016. Rapid Method for Extracting and Quantifying Synthetic Antioxidants in All Edible Fats and Oils. Food Analytical Methods, 9(9), 2682–2690. https://doi.org/10.1007/s12161-016-0443-4

Reuters, 2020. Govt to implement B30 biodiesel mandate in transport sector before 2025. News Straits Time. URL https://www.nst.com.my/news/nation/2020/02/567546/govt-implement-b30-biodiesel-mandate-transport-sector-2025

Reuters, 2024. Malaysian 2024 biofuel output seen rising if B20 biodiesel usage expanded. News Straits Time. URL https://www.reuters.com/business/energy/malaysian-2024-biofuel-output-seen-rising-if-b20-biodiesel-usage-expanded-2024-03-05/

Ritchie, H., Roser, M., 2020. Malaysia: Energy Country Profile [WWW Document]. Our World in Data. URL https://ourworldindata.org/energy/country/malaysia.

Ritchie, H., Rosado. P., 2022. Fossil Fuels [WWW Document]. Our World in Data. URL https://ourworldindata.org/fossil-fuels

Robert De Mello, F., Claudia, I., Ii, B., Odebrecht, C., Ii, D., Gonzaga, L., Regina, E., Ii, A., Fett, R., Lys, I.I., Bileski, M., Iii, C., 2015. Antioxidant properties, quantification and stability of betalains from pitaya (Hylocereus undatus) peel Propriedades antioxidantes, quantificação e estabilidade das betalaínas da casca da pitaya (Hylocereus undatus). fev 45, 323–328. https://doi.org/10.1590/0103-8478cr20140582

Rodrigues, J.S., do Valle, C.P., Uchoa, A.F.J., Ramos, D.M., da Ponte, F.A.F., Rios, M.A. de S., de Queiroz Malveira, J., Pontes Silva Ricardo, N.M., 2020. Comparative study of synthetic and natural antioxidants on the oxidative stability of biodiesel from Tilapia oil. Renew Energy 156, 1100–1106. https://doi.org/10.1016/j.renene.2020.04.153

Romagnoli, É.S., Borsato, D., Silva, L.R.C., Chendynski, L.T., Angilelli, K.G., Canesin, E.A., 2018. Kinetic parameters of the oxidation reaction of commercial biodiesel with

natural antioxidant additives. Ind Crops Prod 125, 59–64. https://doi.org/10.1016/j.indcrop.2018.08.077

Roshanak, S., Rahimmalek, M., Goli, S.A.H., 2016. Evaluation of seven different drying treatments in respect to total flavonoid, phenolic, vitamin C content, chlorophyll, antioxidant activity and color of green tea (Camellia sinensis or C. assamica) leaves. J Food Sci Technol 53, 721–729. https://doi.org/10.1007/s13197-015-2030-x

Sagaste, C.A., Montero, G., Coronado, M.A., Ayala, J.R., León, J., García, C., Rojano, B.A., Rosales, S., Montes, D.G., 2019. Creosote bush (larrea tridentata) extract assessment as a green antioxidant for biodiesel. Molecules 24. https://doi.org/10.3390/molecules24091786

Saluja, R.K., Kumar, V., Sham, R., 2016. Stability of biodiesel – A review. Renewable and Sustainable Energy Reviews. https://doi.org/10.1016/j.rser.2016.05.001

Samuel, O. D., Okwu, M. O., Tartibu, L. K., Giwa, S. O., Sharifpur, M., & Jagun, Z. O. O., 2021. Modelling of Nicotiana tabacum L. oil biodiesel production: comparison of ANN and ANFIS. Frontiers in Energy Research, 8. https://doi.org/10.3389/fenrg.2020.612165

Sánchez-Marzo, N., Lozano-Sánchez, J., Cádiz-Gurrea, M. de la L., Herranz-López, M., Micol, V., Segura-Carretero, A., 2019. Relationships between chemical structure and antioxidant activity of isolated phytocompounds from lemon verbena. Antioxidants 8. https://doi.org/10.3390/antiox8080324

Santos, M.N., de Souza, E.F., Moreira Ramos, T.C.P., Cavalheiro, A.A., Fiorucci, A.R., Silva, M.S. da, 2019. Effect of curcumin natural antioxidant on oxidative stability of commercial biodiesels from different raw materials. Orbital 11, 239–245. https://doi.org/10.17807/orbital.v11i4.1225

Sayyed, S., Kumar Das, R., Ahmed, S. F., Kulkarni, K., Alam, T., & Eldin, S. M., 2023. Modelling of multiple biodiesel-emitted nitrogen oxides using ANN approach. Alexandria

Engineering Journal, 79, 116–125. https://doi.org/10.1016/j.aej.2023.08.005

Sultana, N., Hossain, S. M. Z., Abusaad, M., Alanbar, N., Senan, Y., & Razzak, S. A., 2022. Prediction of biodiesel production from microalgal oil using Bayesian optimization algorithm-based machine learning approaches. Fuel, 309. https://doi.org/10.1016/j.fuel.2021.122184

Schaumlöffel, L.S., Fontoura, L.A.M., Santos, S.J., Pontes, L.F., Gutterres, M., 2021. Vegetable tannins-based additive as antioxidant for biodiesel. Fuel 292. https://doi.org/10.1016/j.fuel.2021.120198

Schirmann, J.G., Angilelli, K.G., Dekker, R.F.H., Borsato, D., Barbosa-Dekker, A.M., 2019. 3,3″,5,5″-Tetramethoxybiphenyl-4,4″-diol: A new antioxidant enhancing oxidative stability of soybean biodiesel. Fuel 237, 593–596. https://doi.org/10.1016/j.fuel.2018.10.044

Serqueira, D.S., Pereira, J.F.S., Squissato, A.L., Rodrigues, M.A., Lima, R.C., Faria, A.M., Richter, E.M., Munoz, R.A.A., 2021. Oxidative stability and corrosivity of biodiesel produced from residual cooking oil exposed to copper and carbon steel under simulated storage conditions: Dual effect of antioxidants. Renew Energy 164, 1485–1495. https://doi.org/10.1016/j.renene.2020.10.097

Sharma, Y.C., Singh, B., Upadhyay, S.N., 2008. Advancements in development and characterization of biodiesel: A review. Fuel. https://doi.org/10.1016/j.fuel.2008.01.014

Shi, F., Jiang, Z.B., Xu, J., Bai, X.P., Liang, Q.Y., Fu, Z.H., 2022. Optimized extraction of phenolic antioxidants from red pitaya (Hylocereus polyrhizus) seeds by subcritical water extraction using response surface methodology. Journal of Food Measurement and Characterization 16, 2240–2258. https://doi.org/10.1007/s11694-021-01212-1

Silva de Sousa, L., de Moura, C.V.R., de Moura, E.M., 2020. Influence of binary, ternary and quaternary mixtures on oxidative stability and study of kinetics and thermodynamic parameters of the degradation process of soybean biodiesel. Fuel 259.

https://doi.org/10.1016/j.fuel.2019.116235

Silva de Sousa, L., Verônica Rodarte de Moura, C., Miranda de Moura, E., 2021. Action of natural antioxidants on the oxidative stability of soy biodiesel during storage. Fuel 288. https://doi.org/10.1016/j.fuel.2020.119632

Singh, D., Sharma, D., Soni, S.L., Sharma, S., Kumar Sharma, P., Jhalani, A., 2020. A review on feedstocks, production processes, and yield for different generations of biodiesel. Fuel. https://doi.org/10.1016/j.fuel.2019.116553

Sonam, S. K., & Guleria, S., 2017. Synergistic Antioxidant Activity of Natural Products. Annals of Pharmacology and Pharmaceutics, 2(8).

Sönnichsen, N., 2021. Global oil reserves to production ratio 1980-2019 [WWW Document]. Statista. URL https://www.statista.com/statistics/682098/oil-reserves-to-production-ratio-worldwide/.

Spacino, K.R., Borsato, D., Buosi, G.M., Chendynski, L.T., 2015. Determination of kinetic and thermodynamic parameters of the B100 biodiesel oxidation process in mixtures with natural antioxidants. Fuel Processing Technology 137, 366–370. https://doi.org/10.1016/j.fuproc.2015.05.006

Tabatabaei, M., Aghbashlo, M., Dehhaghi, M., Panahi, H.K.S., Mollahosseini, A., Hosseini, M., Soufiyan, M.M., 2019. Reactor technologies for biodiesel production and processing: A review. Prog Energy Combust Sci. https://doi.org/10.1016/j.pecs.2019.06.001

Taib, L. A., 2024. RSM and ANN methodologies in modeling the enhanced biodiesel production using novel protic ionic liquid anchored on g-C3N4@Fe3O4 nanohybrid. Chemosphere, 360, 1–10. https://doi.org/10.1016/j.chemosphere.2024.142399

Tan, S., Tang, J., Shi, W., Wang, Z., Xiang, Y., Deng, T., Gao, X., Li, W., Shi, S., 2020. Effects of three drying methods on polyphenol composition and antioxidant activities of

Litchi chinensis Sonn. Food Sci Biotechnol 29, 351–358. https://doi.org/10.1007/s10068-019-00674-w

Tavares, M.L.A., Queiroz, N., Santos, I.M.G., Souza, A.L., Cavalcanti, E.H.S., Barros, A.K.D., Rosenhaim, R., Soledade, L.E.B., Souza, A.G., 2011. Sunflower biodiesel: Use of P-DSC in the evaluation of antioxidant efficiency, in: Journal of Thermal Analysis and Calorimetry. pp. 575–579. https://doi.org/10.1007/s10973-011-1357-4

Thulasiram, R., Murugan, S., Ramasamy, D., & Sundaramoorthy, S., 2021. Modelling and evaluation of combustion emission characteristics of COME biodiesel using RSM and ANN-a lead for pollution reduction. Environmental Science and Pollution Research, 28, 34730–34741. https://doi.org/10.1007/s11356-021-12757-5/Published

Uğuz, G., Atabani, A.E., Mohammed, M.N., Shobana, S., Uğuz, S., Kumar, G., Al-Muhtaseb, A.H., 2019. Fuel stability of biodiesel from waste cooking oil: A comparative evaluation with various antioxidants using FT-IR and DSC techniques. Biocatal Agric Biotechnol 21. https://doi.org/10.1016/j.bcab.2019.101283

Valenga, M.G.P., Boschen, N.L., Rodrigues, P.R.P., Maia, G.A.R., 2019. Agro-industrial waste and Moringa oleifera leaves as antioxidants for biodiesel. Ind Crops Prod 128, 331–337. https://doi.org/10.1016/j.indcrop.2018.11.031

Varatharajan, K., Pushparani, D.S., 2018. Screening of antioxidant additives for biodiesel fuels. Renewable and Sustainable Energy Reviews. https://doi.org/10.1016/j.rser.2017.07.020

Wahdaningsih, S., Wahyuono, S., Riyanto, S., Murwanti, R., 2018. Antioxidant activity of red dragon fruit peel (Hylocereus polyrhizus (F.A.C. weber) britton and rose) isolates using 2,2-diphenyl-1-picrylhydrazyl method. Asian Journal of Pharmaceutical and Clinical Research 11, 124–128. https://doi.org/10.22159/ajpcr.2018.v11i1.21519

Waynick, J.A., 2005. Characterization of biodiesel oxidation and oxidation products. National Renewable Energy Laboratory (NREL).

Wu, L.C., Hsu, H.W., Chen, Y.C., Chiu, C.C., Lin, Y.I., Ho, J.A.A., 2006. Antioxidant and antiproliferative activities of red pitaya. Food Chem 95, 319–327. https://doi.org/10.1016/j.foodchem.2005.01.002

Wu, Q., Gao, H., Zhang, Z., Li, T., Qu, H., Jiang, Y., Yun, Z., 2020a. Deciphering the metabolic pathways of pitaya peel after postharvest red light irradiation. Metabolites 10. https://doi.org/10.3390/metabo10030108

Wu, Q., Zhou, Y., Zhang, Z., Li, T., Jiang, Y., Gao, H., Yun, Z., 2020b. Effect of blue light on primary metabolite and volatile compound profiling in the peel of red pitaya. Postharvest Biol Technol 160. https://doi.org/10.1016/j.postharvbio.2019.111059

Xin, J., Imahara, H., Saka, S., 2009. Kinetics on the oxidation of biodiesel stabilized with antioxidant. Fuel 88, 282–286. https://doi.org/10.1016/j.fuel.2008.08.018

Xue, J., Grift, T.E., Hansen, A.C., 2011. Effect of biodiesel on engine performances and emissions. Renewable and Sustainable Energy Reviews. https://doi.org/10.1016/j.rser.2010.11.016

Yaakob, Z., Narayanan, B.N., Padikkaparambil, S., Unni K., S., Akbar P., M., 2014. A review on the oxidation stability of biodiesel. Renewable and Sustainable Energy Reviews. https://doi.org/10.1016/j.rser.2014.03.055

Yang, J., He, Q.S., Corscadden, K., Caldwell, C., 2017. Improvement on oxidation and storage stability of biodiesel derived from an emerging feedstock camelina. Fuel Processing Technology 157, 90–98. https://doi.org/10.1016/j.fuproc.2016.12.005

Yatish, K. v., Lalithamba, H.S., Sakar, M., Balakrishna, G.R., Omkaresh, B.R., Arun, S.B., 2020. Parametric studies on the storage stability and aging effect of biodiesel treated with Eucalyptus oil as a cost-effective green-antioxidant additive. Int J Energy Res 44, 11711–11724. https://doi.org/10.1002/er.5800

Yeh, W.J., Tsai, C.C., Ko, J., Yang, H.Y., 2020. Hylocereus polyrhizus peel extract retards

alcoholic liver disease progression by modulating oxidative stress and inflammatory responses in C57Bl/6 mice. Nutrients 12, 1–12. https://doi.org/10.3390/nu12123884

Yi, J.Y., Lyu, J., Bi, J.F., Zhou, L.Y., Zhou, M., 2017. Hot air drying and freeze drying pre-treatments coupled to explosion puffing drying in terms of quality attributes of mango, pitaya, and papaya fruit chips. J Food Process Preserv 41. https://doi.org/10.1111/jfpp.13300

Yung, C.L., Choo, Y.M., Cheng, S.F., Ma, A.N., Chuah, C.H., Basiron, Y., 2006. The effect of natural and synthetic antioxidants on the oxidative stability of palm diesel. Fuel 85, 867–870. https://doi.org/10.1016/j.fuel.2005.09.003

Zhang, B., Xia, T., Duan, W., Zhang, Z., Li, Y., Fang, B., Xia, M., Wang, M., 2019. Effects of organic acids, amino acids and phenolic compounds on antioxidant characteristic of Zhenjiang aromatic vinegar. Molecules 24. https://doi.org/10.3390/molecules24203799

Zhou, J., Xiong, Y., Liu, X., 2017. Evaluation of the oxidation stability of biodiesel stabilized with antioxidants using the Rancimat and PDSC methods. Fuel 188, 61–68. https://doi.org/10.1016/j.fuel.2016.10.026

Zhou, J., Xiong, Y., Shi, Y., 2016a. Antioxidant consumption kinetics and shelf-life prediction for biodiesel stabilized with antioxidants using the Rancimat Method. Energy and Fuels 30, 10534–10542. https://doi.org/10.1021/acs.energyfuels.6b02199

Zhou, J., Xiong, Y., Xu, S., 2016b. Evaluation of the oxidation stability of biodiesel stabilized with antioxidants using the PetroOXY method. Fuel 184, 808–814. https://doi.org/10.1016/j.fuel.2016.07.080

Zhuang, Y., Zhang, Y., Sun, L., 2012. Characteristics of fibre-rich powder and antioxidant activity of pitaya (Hylocereus undatus) peels. Int J Food Sci Technol 47, 1279–1285. https://doi.org/10.1111/j.1365-2621.2012.02971.x

Zulqarnain, Yusoff, M.H.M., Ayoub, M., Jusoh, N., Abdullah, A.Z., 2020. The challenges of a biodiesel implementation program in Malaysia. Processes. https://doi.org/10.3390/pr8101244

Appendix A

Table A.1. Induction periods (IP) of DPOME with synthetic and bio-based antioxidants at different concentrations measured using Rancimat.

Antioxidant	Induction period (IP) at different concentrations (h)[a]			
	250 ppm	500 ppm	750 ppm	1000 ppm
BHT	35.97 ± 2.07	49.45 ± 1.86	59.10 ± 0.89	67.71 ± 5.26
BHA	47.58 ± 1.24	56.05 ± 0.68	60.88 + 1.08	63.31 + 3.14
TBHQ	90.71 ± 6.72	136.69 ± 4.02	177.02 ± 3.85	203.54 ± 16.21
PG	86.51 ± 0.42	96.96 ± 1.42	99.86 ± 0.81	101.82 ± 1.36
PY	46.64 ± 6.82	79.05 ± 2.59	102.52 ± 3.76	123.50 ± 1.14
Quercetin	47.89 ± 0.97	63.46 ± 1.50	76.04 ± 3.92	81.82 ± 3.36
α-T	18.51 ± 0.33	20.02 ± 0.11	20.23 ± 0.17	20.72 ± 0.36
Curcumin	17.67 ± 0.80	25.54 ± 0.44	31.38 ± 1.18	36.74 ± 0.53

[a]Average of triplicates ± standard deviation.

Table A.2. Effectiveness factors for synthetic and bio-based antioxidants in DPOME at different concentrations measured using Rancimat.

Antioxidant	Effectiveness factor at different concentrations (-)[a]			
	250 ppm	500 ppm	750 ppm	1000 ppm
BHT	6.8248	9.3827	11.2151	12.8476
	± 0.3922	± 0.3538	± 0.1698	± 0.9974
BHA	9.0285	10.6357	11.5522	12.0133
	±0.2347	± 0.1287	± 0.2040	± 0.5965
TBHQ	17.2125	26.3738	33.8299	38.6214
	± 1.2743	± 0.7625	± 0.7309	± 3.0750
PG	16.3561	18.2758	19.0234	19.2878
	± 0.0800	± 0.2703	± 0.1528	± 0.2587
PY	17.7356	18.6028	19.3713	20.0455
	±0.5365	± 0.2533	± 0.2766	± 0.2169
Quercetin	9.0867	12.0417	13.1322	14.4655
	± 0.1833	± 0.2854	± 0.7429	± 0.6377
α-T	3.5130	3.7982	3.8387	3.9311
	± 0.0621	± 0.0199	± 0.0329	± 0.0681
Curcumin	3.3523	4.8463	5.9551	6.9715
	± 0.1518	± 0.0830	± 0.2230	± 0.1000

[a]Average of triplicates ± standard deviation.

Table A.3. Induction periods (IP) of DPOME with synthetic and bio-based antioxidants at different concentrations measured using PetroOXY.

Antioxidant	Induction period (IP) at different concentrations (min)[a]			
	250 ppm	500 ppm	750 ppm	1000 ppm
BHT	68.57 ± 0.79	107.98 ± 0.34	141.82 ± 1.20	177.19 ± 4.01
BHA	199.05 ± 6.79	339.20 ± 4.00	423.07 ± 3.94	508.78 ± 9.42
TBHQ	25.08 ± 0.37	31.40 ± 0.06	34.87 ± 0.25	39.83 ± 0.15
PG	127.24 ± 3.27	170.31 ± 2.25	196.56 ± 2.37	219.03 ± 5.02
PY	78.34 ± 1.03	111.29 ± 1.38	122.82 ± 1.18	141.85 ± 2.16
Quercetin	78.63 ± 1.43	124.58 ± 18.86	162.00 ± 5.11	211.72 ± 36.11
α-T	48.95 ± 0.09	56.67 ± 0.22	57.72 ± 3.00	61.50 ± 1.20
Curcumin	41.85 ± 0.67	64.28 ± 0.13	83.90 ± 2.18	100.93 ± 3.33

[a]Average of triplicates ± standard deviation.

Table A.4. Effectiveness factors of synthetic and bio-based antioxidants in DPOME at different concentrations measured using PetroOXY.

Antioxidant	Effectiveness factor at different concentrations (-)[a]			
	250 ppm	500 ppm	750 ppm	1000 ppm
BHT	4.0470	6.3728	8.3705	10.4578
	± 0.0468	± 0.0201	± 0.0706	± 0.2365
BHA	11.7480	20.0199	24.9699	30.0286
	± 0.4006	± 0.2359	± 0.2323	± 0.5558
TBHQ	1.4802	1.8530	2.0580	2.3508
	± 0.0221	± 0.0034	± 0.0149	± 0.0089
PG	7.5098	10.0518	11.6012	12.9272
	± 0.1931	± 0.1330	± 0.1398	± 0.2965
PY	4.6235	6.5682	7.2491	8.3722
	± 0.0611	± 0.0817	± 0.0695	± 0.1273
Quercetin	4.6406	7.5418	9.5615	12.4956
	± 0.0843	± 0.2415	± 0.3015	± 2.1061
α-T	2.8890	3.3384	3.4067	3.6298
	± 0.0051	± 0.0127	± 0.1769	± 0.0708
Curcumin	2.4700	3.7936	4.9516	5.9569
	± 0.0394	± 0.0074	± 0.1286	± 0.1964

[a]Average of triplicates ± standard deviation.

Table A.5. Acid value of DPOME with synthetic and bio-based antioxidants at different concentrations measured according to EN14104 standard.

Antioxidant	Acid value at different concentrations (mg KOH/g)[a]			
	250 ppm	500 ppm	750 ppm	1000 ppm
BHT	0.2616 ± 0.0160	0.2709 ± 0.0161	0.2709 ± 0.0161	0.2709 ± 0.0162
BHA	0.2710 ± 0.0161	0.2802 ± 0.0001	0.2710 ± 0.0162	0.2709 ± 0.0163
TBHQ	0.2989 ± 0.0163	0.3082 ± 0.0001	0.2988 ± 0.0162	0.3270 ± 0.0162
PG	0.2710 ± 0.0161	0.3363 ± 0.0001	0.4203 ± 0.0001	0.5044 ± 0.0002
PY	0.2801 ± 0.0001	0.2709 ± 0.0162	0.2615 ± 0.0162	0.2616 ± 0.0162
Quercetin	0.2802 ± 0.0280	0.3270 ± 0.0162	0.3550 ± 0.0162	0.4296 ± 0.0164
α-T	0.1868 ± 0.0163	0.1962 ± 0.0000	0.1869 ± 0.0162	0.1775 ± 0.0161
Curcumin	0.1776 ± 0.0161	0.1682 ± 0.0000	0.1682 ± 0.0000	0.1682 ± 0.0001

[a]Average of triplicates ± standard deviation.

Table A.6. Iodine value of DPOME with synthetic and bio-based antioxidants at different concentrations measured according to EN14111 standard.

Antioxidant	Iodine value at different concentrations (g I_2/100 g)[a]			
	250 ppm	500 ppm	750 ppm	1000 ppm
BHT	50.9163 ± 1.8750	50.4468 ± 1.8675	47.5884 ± 0.9232	46.3242 ± 0.6876
BHA	49.7904 ± 1.0984	50.8596 ± 1.3947	48.9278 ± 1.6765	51.4332 ± 0.9427
TBHQ	48.8325 ± 2.6727	49.1088 ± 2.7553	50.5023 ± 0.7211	48.1013 ± 2.1064
PG	50.6346 ± 4.7560	50.6493 ± 2.8958	50.1515 ± 3.6274	49.3399 ± 1.8732
PY	49.4598 ± 1.1173	49.9737 ± 2.2815	49.3366 ± 0.0843	51.8314 ± 1.0079
Quercetin	52.6025 ± 7.1510	46.4071 ± 0.9201	50.3954 ± 1.7034	48.7203 ± 1.3917
α-T	47.9494 ± 1.7542	48.2546 ± 1.1899	47.9850 ± 2.0671	45.0723 ± 1.3070
Curcumin	56.2629 ± 1.0676	55.5253 ± 2.0027	55.7240 ± 2.4259	56.4872 ± 0.4053

[a]Average of triplicates ± standard deviation.

Table A.7. Kinematic viscosity of DPOME with synthetic and bio-based antioxidants at 40°C for different concentrations measured according to EN ISO 3104 standard.

Antioxidant	Kinematic viscosity at 40°C (mm^2/s)[a]			
	250 ppm	500 ppm	750 ppm	1000 ppm
BHT	4.3895 ± 0.0006	4.3906 ± 0.0001	4.3905 ± 0.0008	4.3906 ± 0.0001
BHA	4.3904 ± 0.0004	4.3924 ± 0.0003	4.3947 ± 0.0003	4.3947 ± 0.0004
TBHQ	4.3955 ± 0.0006	4.3955 ± 0.0009	4.4014 ± 0.0004	4.4073 ± 0.0004
PG	4.3944 ± 0.0003	4.3986 ± 0.0001	4.4028 ± 0.0011	4.4041 ± 0.0002
PY	4.3921 ± 0.0002	4.3947 ± 0.0002	4.4026 ± 0.0000	4.4056 ± 0.0008
Quercetin	4.3913 ± 0.0005	4.3939 ± 0.0003	4.3926 ± 0.0004	4.3929 ± 0.0001
α-T	4.3920 ± 0.0003	4.3939 ± 0.0004	4.3941 ± 0.0007	4.3969 ± 0.0003
Curcumin	4.3942 ± 0.0004	4.3972 ± 0.0003	4.3993 ± 0.0008	4.4014 ± 0.0012

[a]Average of triplicates ± standard deviation.